



## REDESIGNING CHEMICAL ANALYSIS: TRANSDUCING INFORMATION FROM CHEMICAL INTO DIGITAL

Rafael Wytze Fenwick Hoekstra

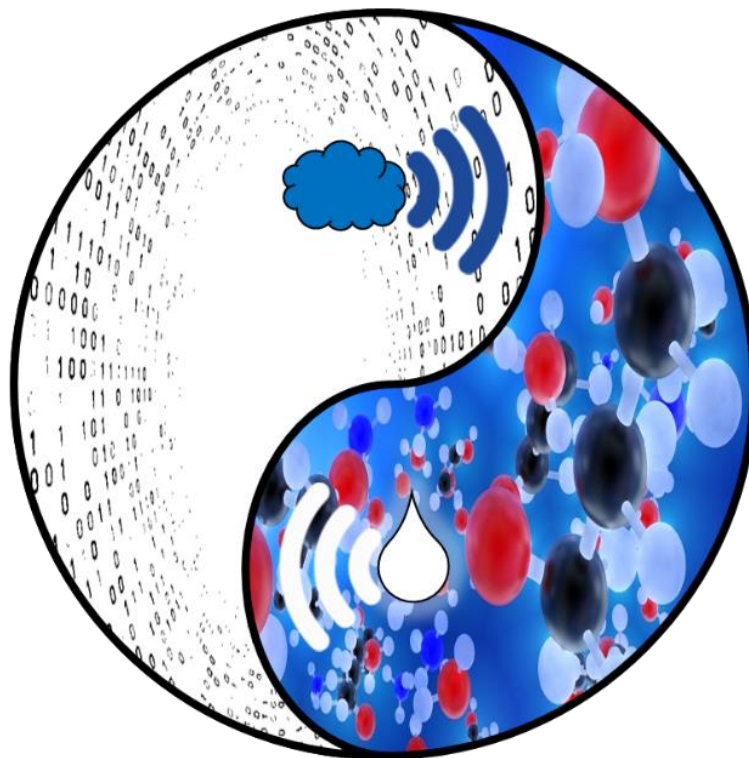
**ADVERTIMENT.** L'accés als continguts d'aquesta tesi doctoral i la seva utilització ha de respectar els drets de la persona autora. Pot ser utilitzada per a consulta o estudi personal, així com en activitats o materials d'investigació i docència en els termes establerts a l'art. 32 del Text Refós de la Llei de Propietat Intel·lectual (RDL 1/1996). Per altres utilitzacions es requereix l'autorització prèvia i expressa de la persona autora. En qualsevol cas, en la utilització dels seus continguts caldrà indicar de forma clara el nom i cognoms de la persona autora i el títol de la tesi doctoral. No s'autoritza la seva reproducció o altres formes d'explotació efectuades amb finalitats de lucre ni la seva comunicació pública des d'un lloc aliè al servei TDX. Tampoc s'autoritza la presentació del seu contingut en una finestra o marc aliè a TDX (framing). Aquesta reserva de drets afecta tant als continguts de la tesi com als seus resums i índexs.

**ADVERTENCIA.** El acceso a los contenidos de esta tesis doctoral y su utilización debe respetar los derechos de la persona autora. Puede ser utilizada para consulta o estudio personal, así como en actividades o materiales de investigación y docencia en los términos establecidos en el art. 32 del Texto Refundido de la Ley de Propiedad Intelectual (RDL 1/1996). Para otros usos se requiere la autorización previa y expresa de la persona autora. En cualquier caso, en la utilización de sus contenidos se deberá indicar de forma clara el nombre y apellidos de la persona autora y el título de la tesis doctoral. No se autoriza su reproducción u otras formas de explotación efectuadas con fines lucrativos ni su comunicación pública desde un sitio ajeno al servicio TDR. Tampoco se autoriza la presentación de su contenido en una ventana o marco ajeno a TDR (framing). Esta reserva de derechos afecta tanto al contenido de la tesis como a sus resúmenes e índices.

**WARNING.** Access to the contents of this doctoral thesis and its use must respect the rights of the author. It can be used for reference or private study, as well as research and learning activities or materials in the terms established by the 32nd article of the Spanish Consolidated Copyright Act (RDL 1/1996). Express and previous authorization of the author is required for any other uses. In any case, when using its content, full name of the author and title of the thesis must be clearly indicated. Reproduction or other forms of for profit use or public communication from outside TDX service is not allowed. Presentation of its content in a window or frame external to TDX (framing) is not authorized either. These rights affect both the content of the thesis and its abstracts and indexes.

# REDESIGNING CHEMICAL ANALYSIS:

*Transducing information from chemical into digital*



**Rafael Wytze Fenwick Hoekstra**



UNIVERSITAT  
ROVIRA i VIRGILI

DOCTORAL THESIS

2018



# REDESIGNING CHEMICAL ANALYSIS:

---

*Transducing information from chemical into digital*

RAFAEL WYTZE FENWICK HOEKSTRA  
DOCTORAL THESIS

Supervised by

Dr. FRANCISCO J. ANDRADE

and

Dr. PASCAL BLONDEAU



UNIVERSITAT  
ROVIRA i VIRGILI

Department of Analytical Chemistry and Organic Chemistry

Laboratory of Nanosensors

**Tarragona, June 2018**



## REDESIGNING CHEMICAL ANALYSIS:

---

*Transducing information from chemical into digital*

RAFAEL WYTZE FENWICK HOEKSTRA

*Tribunal members:*

**Professor Luis Fermín Capitán Vallvey** - Universidad de Granada, Spain

**Professor F. Xavier Rius** - Universitat Rovira i Virgili, Spain

**Dr. Devin Daems** - KU Leuven, Belgium

*External examiners:*

**Professor Dermot Diamond** – Dublin City University, Ireland

**Professor Mabel Tudino** – Universidad de Buenos Aires, Argentina



UNIVERSITAT  
ROVIRA i VIRGILI



UNIVERSITAT



ROVIRA I VIRGILI

DEPARTAMENT DE QUÍMICA ANALÍTICA I QUÍMICA ORGÀNICA

Campus Sescelades

Marcel·lí Domingo, 1

43007 Tarragona

Tel.: +34 977559562

Fax.: +34 977558446

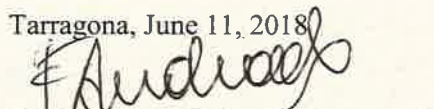
e-mail: [franciscojavier.andrade@urv.cat](mailto:franciscojavier.andrade@urv.cat)


[pascal.blondeau@urv.cat](mailto:pascal.blondeau@urv.cat)

*Francisco J. Andrade*, Ramón y Cajal researcher at the Department of Analytical Chemistry and Organic Chemistry at the Universitat Rovira i Virgili; and *Pascal Blondeau*:

I STATE, that the Doctoral thesis entitled: “*Redesigning chemical analysis: transducing information from chemical into digital*”, submitted by *Rafael Wytze Fenwick Hoekstra* to obtain the degree of Doctor within the Universitat Rovira i Virgili, has been carried out under my supervision in the Department of analytical and organic chemistry at the Universitat Rovira i Virgili. Furthermore, I state the stated thesis qualifies for the International Doctorate Mención.

Tarragona, June 11, 2018

  
Dr. Francisco J. Andrade

  
Dr. Pascal Blondeau





## ACKNOWLEDGEMENTS

---

While this book may bear my name, it is the fruit of many inspirations and supports.

Foremost, I offer my warm appreciation to Dr. Francisco Andrade. I will always be grateful for him accepting me into the Nanosensors research group, providing vision, training and guidance, and building a great team culture. Francisco, thank you for taking a chance on me- you have inspired me with your warm heart of a humanist, and sharp mind of a scientist.

Dr. Pascal Blondeau has been an amazing support (asombroso), offering patient assistance and endless good humour.

My deep appreciation goes to Professor F. Xavier Rius, who has guided the Nanosensors group, the chemistry department, and the Nanotechnology Master program.

I have been fortunate to share the company of many fine colleagues within this research group. In particular I wish to acknowledge the camaraderie of my fellow doctoral students, many now graduated. Among them Dra. Marta Novell, Dr. Marc Parrilla, Dra. Rocío Cánovas, and Marta Borràs, It has also been a joy to work with Dr. Santiago Macho, Adrià Maceira, Mohamed Bouri, Amelie Marcon, and Pär Blanking, and all of the Nanosensors group.

I enjoyed a wonderful research stay at Dublin City University. For this, I am grateful to Professor Dermot Diamond, and all of his research group for their warm welcome and support.

On a personal note, I offer my warmest gratitude to the encouragement and inspiration of Lama Mark Webber. The vision he imparts, transforms the world into a laboratory rich in opportunities for exploration.

My parents Dianne and Wytze have given me many gifts in life, more than can ever be expressed. Thank you Mum and Dad- for life, and much of it.

The strong friendships of Duncan Gray, Marc Isan, Dina Brodsky, Jamie van Dam, Stela Zarija, Pär Blanking and Rossella Rita Rocco have been incredible blessings. They have been sources of support in challenging times and joy in fair weather. Thank you all.



# TABLE OF CONTENTS

---

1	INTRODUCTION.....	4
1.1	Technology in context.....	5
1.2	Sensors and chemical sensors.....	6
1.3	Defining performance for distributed analysis in the information age.....	9
1.4	Design, analysis, and simplicity.....	11
1.4.1	Design.....	11
1.4.2	Analysis.....	12
1.4.3	Simplicity.....	12
1.5	The <i>Maker</i> movement.....	13
1.6	A revolution in chemical sensing?.....	14
1.7	References.....	16
2	SCIENTIFIC FOUNDATIONS.....	18
2.1	Fundamentals of electricity.....	19
2.2	Electrochemical techniques.....	19
2.2.1	Conductimetry.....	19
2.2.2	Potentiometry.....	22
2.3	Electrochemical potential.....	23
2.3.1	Phase-boundary potential.....	24
2.3.2	Donnan potential.....	26
2.3.3	Redox potential.....	27
2.4	Potentiometric electrodes.....	28
2.4.1	Indicator electrodes.....	28
2.4.2	Reference electrodes.....	31
2.5	Flow injection analysis.....	35
2.6	Calibration of potentiometric sensors.....	37
2.6.1	The challenge of calibration.....	37
2.6.2	Approaches to meeting the challenge.....	38

2.6.3	Approaches in this thesis .....	39
2.7	References .....	40
3	EXPERIMENTAL INFORMATION.....	42
3.1	Reagents .....	43
3.2	Materials.....	43
3.2.1	Paper-based electrodes .....	44
3.3	Instrumentation.....	44
3.4	Software .....	45
3.5	Ion-selective membrane preparation .....	45
3.6	References .....	47
4	CRITICAL REVIEW: Distributed electrochemical sensors: recent advances and barriers to market adoption.....	48
4.1	Introduction .....	49
4.1.1	Scope .....	49
4.1.2	Fields of need .....	51
4.2	Challenges and advances in the field of distributed sensors .....	53
4.2.1	Challenges and advances in the analytical performance of distributed sensors .....	53
4.2.2	Challenges and advances in the usability of decentralized sensors .....	57
4.2.3	Challenges and advances in the affordability of decentralized sensors.....	60
4.3	Summary and outlook .....	61
4.4	References .....	64
5	LAB-IN-A-BOX: A device for user-friendly potentiometric analysis.....	70
5.1	Introduction .....	71
5.1.1	The realities of externalities .....	71
5.1.2	The dry problem .....	72
5.1.3	The wet problem.....	73
5.1.4	The value proposition of the Lab-in-box.....	73
5.1.5	Lab-in-a-box prototypes .....	74
5.2	Lab-in-a-box: Mark I.....	74

5.2.1	Mark I: experimental .....	74
5.2.2	Mark I: Results .....	76
5.3	Lab-in-a-box: Mark II .....	78
5.3.1	Mark II: Integration of a miniature potentiometer.....	78
5.3.2	Mark II: Integration of paper-based electrodes and automation of calculations .....	80
5.3.3	Mark II: Incorporation of a miniature pump .....	82
5.3.4	Mark II: The relationship between baseline potential and standard potential .....	82
5.4	Lab-in-a-box: Mark III .....	91
5.4.1	Mark III: Experimental.....	92
5.4.2	Mark III: Results .....	95
5.5	Conclusions .....	101
5.6	References .....	103
6	HYDROGEL CAPPING MEMBRANES: A strategy for the dry <i>in situ</i> calibration of potentiometric sensors .....	106
6.1	Introduction .....	107
6.2	Experimental .....	109
6.2.1	Materials.....	109
6.2.2	Instrumentation.....	110
6.2.3	Membrane preparation.....	110
6.2.4	Preparation of capping membranes .....	110
6.2.5	Sensor preparation.....	111
6.3	Results and discussion.....	112
6.3.1	Sodium sensing.....	112
6.3.2	The relationship of baseline potential to standard potential .....	113
6.3.3	Screening of capping membranes.....	114
6.3.4	Poly(vinyl alcohol) capping membranes .....	116
6.4	Conclusions .....	121
6.5	References .....	122
7	POTENTIOMETRIC DETERMINATION OF CREATININE BY FLOW INJECTION ANALYSIS	

7.1	Introduction .....	125
7.2	Experimental .....	127
7.2.1	Materials .....	127
7.2.2	Membrane preparation .....	128
7.2.3	FIA manifold .....	129
7.3	Results and discussion .....	129
7.3.1	pH dependence of creatinine/creatinium ion .....	129
7.3.2	Fundamental fluidic studies .....	130
7.3.3	Baseline drift, optical studies, and electrode memory .....	135
7.3.4	pH modulation studies .....	139
7.4	Conclusions .....	143
7.5	References .....	144
8	ANTICLEPSYDRA: A ‘Smart Toilet’ for autonomous monitoring of urine conductivity and volume 146	
8.1	Introduction .....	147
8.2	Experimental .....	149
8.2.1	Reagents and materials .....	149
8.2.2	Instrumentation and measurements .....	149
8.2.3	The Smart Toilet device .....	150
8.3	Results and discussion .....	151
8.3.1	Conductivity determinations .....	151
8.3.2	Volume estimations .....	153
8.4	Conclusions .....	155
8.5	References .....	156
9	IONSENS: a wearable potentiometric sensor patch for monitoring total ion content in sweat.....	158
9.1	Introduction .....	159
9.2	Experimental .....	161
9.3	Results and discussion .....	162
9.3.1	Analytical performance of solid-contact ion-sensitive electrode based on Nafion .....	162

9.3.2	Affinity amongst cations .....	166
9.3.3	Total ion activity as a proxy for conductivity in artificial sweat solutions and integration of a pseudo-reference electrode .....	167
9.3.4	Determinations in real sweat samples .....	168
9.3.5	A wearable device for on-body dynamic monitoring of sweat conductivity.....	169
9.4	Conclusions .....	171
9.5	References .....	172
10	CONCLUSIONS .....	176
10.1	A revolution in chemical sensing by design.....	177
10.2	References .....	179
	APPENDICES.....	180
	Appendix 1. Scientific contributions .....	181
	Appendix 2. Glossary.....	182
	Appendix 3. List of tables and figures .....	186
	List of figures.....	186
	List of tables .....	192
	Appendix 4. Supporting information for Chapter 4.....	193
	Appendix 5. Supporting information for Chapter 5 .....	196
	Appendix 6. Supporting information for Chapter 8.....	197
	Appendix 7. Supporting information for Chapter 9 .....	205





## SUMMARY

---

This thesis posits that distributed chemical sensing networks will be beneficial tools towards our greater health outcomes as humans, as well as in guiding us in our self-determined role as custodians over the ecological sphere. A perspective of infusing design elements and approaches into analytical tools is shared.

The work begins by presenting a vision of how chemical sensors fit within the greater contexts of biology, history, and technology. The background to the underlying scientific foundations and technological methods and principles on which this work stands is then provided as a framework in which to consider this work. By critically reviewing the academic advances towards distributed electrochemical sensors, the barriers to commercialization become evident. These can be classified as issues of technical performance, usability, and affordability. Principal among these, usability is identified as the principal bottleneck in the widespread adoption of user-centred chemical sensors.

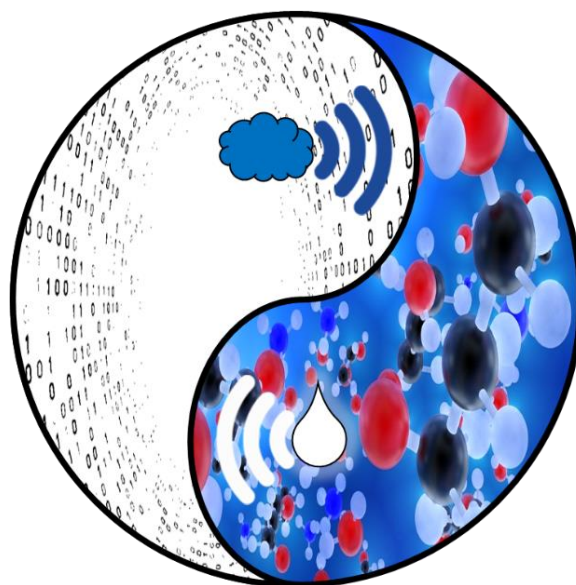
The core of the thesis offers some responses to these challenges, in the form of original experimental work. While rooted in analytical electrochemistry, the work is approached with a design methodology, with iterations of analysis and synthesis embedded in the ideation process.

- [Chapter 1](#) describes the historical and technological context in which this thesis was conceived. Distributed chemical sensors emerge from this, not as an end, but rather as a means to an end- namely, the unleashing of a new informational type.
- [Chapter 2](#) anchors the vision of Chapter 1 in a solid foundation of rigorous scientific concepts and frameworks.
- [Chapter 3](#) covers some experimental details that are common to several chapters, although most experimental information is specific to each chapter, and as such, contained therein.
- [Chapter 4](#) is a critical review entitled “Distributed electrochemical sensors: recent advances and barriers to market adoption”. This was published in *Analytical and Bioanalytical Chemistry*.
- [Chapter 5](#) introduces the concept of a *Lab-in-a-box*. That is, a device that performs tasks essential to chemical determinations with potentiometry. Several prototypes, with varying degrees of automation, were constructed and tested.
- [Chapter 6](#) explores an idea to simplify the calibration of potentiometric sensors through the use of *hydrogel capping membranes*.
- [Chapter 7](#) describes the development of a flow injection analysis system for the potentiometric determination of creatinine in biological samples.

- **Chapter 8** presents a *Smart Toilet* entitled the *Anticlepsydra*. Mounted within a toilet, this device demonstrated the capability to monitor urine conductivity and volume, as indicators of hydration status.
- **Chapter 9** elaborates a wearable potentiometric sensor patch for monitoring total ion content in sweat. This patch, named *IonSens*, was shown to track the ion levels in the perspiration of an athlete during exercise.
- **Chapter 10** reflects on the outcomes of this thesis as a small part in a burgeoning revolution of the *chemical information age*; as a minor crack in the dam holding back a flood of diagnostic chemical data with unforeseeable, yet positive and potentially revolutionary consequences.
- Several appendices are included at the end of the document to add relevant supporting information.

# 1 INTRODUCTION

---



## 1.1 Technology in context

*“May you live in interesting times”* – Purportedly an ancient Chinese curse.

We live in interesting times. The world seems to be accelerating in technological innovation, human population, and resource inequality. The invocation of the ancient Chinese curse above reflects the nature of these changes and the revolutions they entail- they present a double-edged sword. While the ironic curse is generally intended to reflect the idea that interesting times are those of turmoil- most typically war- it is conceivable that the world could be incredibly interesting *and* peaceful. Indeed, it is imperative to conceive of this in order to remain optimistic about the direction of *Homo sapiens*- the most creative and destructive species currently- and perhaps ever- on Earth. In fact, the power of our species reaches far beyond our own kind, to directly and indirectly reshape other species across the planet. Recently, the scientific community has agreed to call this time the ‘*Anthropocene*’, to denote the time in which human activity has become the dominant influence on climate and the environment. Invariably, this stems from the Godlike capabilities endowed by our powerful technologies- from the planet-wide extinction of the megafauna due to weapons and fire, to the manipulation of the natural selection of microbes due to the ‘carpet-bombing’ of antibiotics. Unfortunately, as the great historian Noah Yuval Harari explains, the goal of technology is power, and it often operates without moral compass [1].

There is however, a parallel force whose objective is to realize order- this force is myth. In this context, myth denotes concepts which create common purpose between strangers, and includes religions, political ideologies, economic theories, and scientific ideas. Often myths are so ‘close to our face’ that we mistake them for unalterable realities; a few such myths that have profound implications for the direction in which humanity launches its technologies are: that human lives have greater value than other lifeforms; that our actions are the salient cause of climatic changes, the superiority of capitalism, and the sovereignty of nation states over their citizens. ‘Trickledown inequality’ causes so much harm- for indeed the world is plentiful; bountiful planet Earth is replete with abundant food, water and all manner of resources for all her children- and as such, the root of the problem is not technological, but rather mythological. Fortunately, the question of humanity thriving is not a zero-sum game. The problems we face can therefore be addressed simultaneously at two levels: at the root, which is to reimagine the myths that guide our actions; and at the branches, by realizing powerful technologies that empower the disenfranchised.

In truth, technologies and myths do not evolve independently. Rather, they are intertwined in development and just as ideas can shape our tools, so too, our tools can adjust our perceptions. A gross example of this is the atomic bomb. As well as revealing the awesome power within a single atom, atomic bombs reshaped the conception of warfare, from direct combat to strategies of *détente*, currency wars, propaganda and the fight to

## INTRODUCTION

---

maintain exclusivity over this most destructive technology. From money to writing, from maps to aeroplanes; technologies continue to shape the world we imagine.

The conceptions of healthcare are no exception. While these vary somewhat geographically, some common themes can be seen in: availability corresponding to wealth, services being centralized, and knowledge being the domain of the expert few. From a certain perspective, these ideas are all outcomes of the associated technologies: many medical services demand costly medicines/instruments, these are rare and only operable by specialists, and it requires deep training to interpret results to diagnose and prescribe treatments. Could new tools help to reimagine the medical system to more widely distribute services across economic circumstances, geographic locations, and education levels?

Perhaps not yet in all aspects, however one area that is ripe for disruption through distribution, is diagnostics. Indeed this is already in the development pipeline- referring to paper-based diagnostic devices, thought leader George Whitesides has said, *“We and others have shown the technology works. A lot depends on whether we can get over the hump of commercialization”* [2]. This hints at a problem not only technical in nature- traditional diagnostic providers are unlikely to find it attractive to undercut their existing business model with devices that are orders of magnitude lower in cost, more widely accessible, and more intuitive to use- such is the nature of disruptive innovations. Thus, a revolution in diagnostic tools would demand strength in all three aspects of performance, affordability, and simplicity. These are considered in depth in the critical review of Chapter 4.

A similar case can be made for revolutionising the way we visualize the ‘health’ of the planet. Limitations in data about the environment can lead to either trusting in anecdotal indications or in authority figures. However, without adequate tools, how can anyone authoritatively comment on the health of the planet? By introducing tools to map the Earth’s arteries of rivers, lungs of the atmosphere, and organs of the soil, new environmental diagnoses and prognoses would become possible. Not only this, but these technological changes could herald in new and unpredictable conceptions about the planet. As is often seen with complex systems, surprising emergent narratives could result- perhaps a reimagining of the myths about what lies beneath our feet.

## 1.2 Sensors and chemical sensors

Sensors are devices that detect changes in an environment and relay that information to electronics, such as computers. This makes them excellent tools to monitor the health of the human body and the planet Earth. Sensors can broadly be divided into physical sensors and chemical sensors. For reasons that will be treated in Chapters 2 and 4, the former are already quite developed, as are some chemical sensors for the gas phase. A striking gap remains however, for chemical sensors in the liquid phase. As the ‘matrix of life’,<sup>1</sup> water is the

---

<sup>1</sup> Description by Albert Szent-Gyorgyi, Nobel prize winner in physiology or medicine.

## INTRODUCTION

---

medium through which we interface with the world, and the world interfaces with us. The aqueous media of our bodies- our saliva, tears, urine, sweat and blood- is encoded with data reflecting our well-being, as are the rivers, lakes and oceans- what has been called the “environmental nervous system” [3]. There are two obstacles to interpreting the embedded chemical data- the second of these is to decode it to arrive at meaning. Before this however, we must first address the bandwidth problem- simply that our chemical sensing tools have considerable limitations.

Chemical sensing is in fact the most ancient, primal and essential sense. According to current theories of evolution, it may date back some 3 billion years to the earliest lifeforms. Today, it is still *the* sense of unicellular organisms as they map the *extracellular world*. While it has evolved in multiple directions simultaneously, it now manifests in the forms familiar to us as mammals: smell, taste and aspects of touch. These open up our capacity to map the world beyond our skin in airborne molecules through the nose, in solid and liquid compounds through the tongue, and the sensing of heat, pain, and pressure through our skin. In fact, the majority of mammalian chemical sensing is still internal, with the majority of ‘taste’ taking place not in the mouth but in the gut, and furthermore, chemoreception taking place at the level of each individual cell. This is clearly critical in a body in which only a minority of cells are nominally human (contain human DNA). The majority- estimated at 10-100 trillion cells of thousands of species [4]- remain engaged in constant (chemical) dialogue with the human minority of ‘our’ bodies [5, 6]. It would be not just poetic but pragmatic, to say that *life is a chemical conversation*.

As a technologically-minded species, it seems our nature is to aspire to extend our senses beyond our biological gifts [7]. It is as if we are in envy of the shark, whose incredible sensitivity to electric fields extends as low as nanovolts per centimetre; the whale, whose songs can carry and be heard by others thousands of kilometres away [8]; and the bat, whose radar illuminates the darkness they live in, to map their environment in such extraordinary detail as to perceive the fluttering of their target insect’s wings. This ambitious nature of ours manifests in looking through microscopes and telescopes, from radio waves to gamma waves; in listening from the ultrasonic to the supersonic; in inventing artificial noses and chemical tongues; as well as all manner of touch, proximity and orientation sensors, such as those embedded into smartphones. In this way, we continue to extend our nervous system’s tentacle-like branches into the atom and beyond the solar-system (Figure 1.1). Quite surprisingly, it seems that the most primal biological sense- that of tracking the chemical environment we flow through and that flows through us- has the least developed tools for synthetic sensing.

## INTRODUCTION

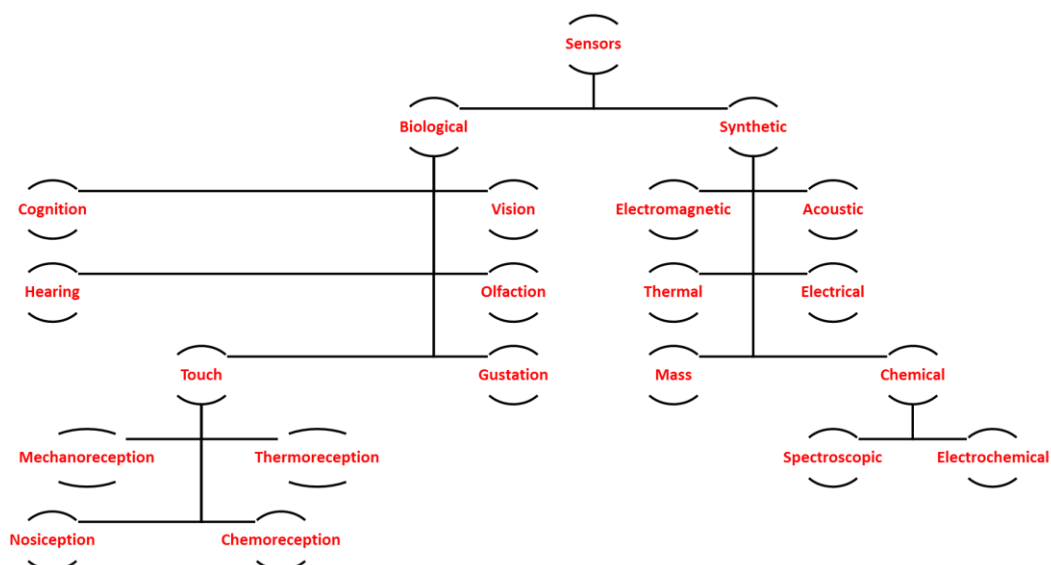


**Figure 1.1** The branching out of sensors, biological (human) and synthetic.

The mammalian sensing systems operate with chemical receptors from which an electrical signal is transduced through the nervous system. While the reality is a little more complex, this is direct electrochemical sensing and we mimic it with synthetic electrochemical sensors in our research group, and in this thesis. All techniques have their merits, but perhaps few others could be argued to be as comparable to evolved biological systems in the *'bringing forth of the world'*<sup>2</sup> as direct electrochemical sensing (Figure 1.2).

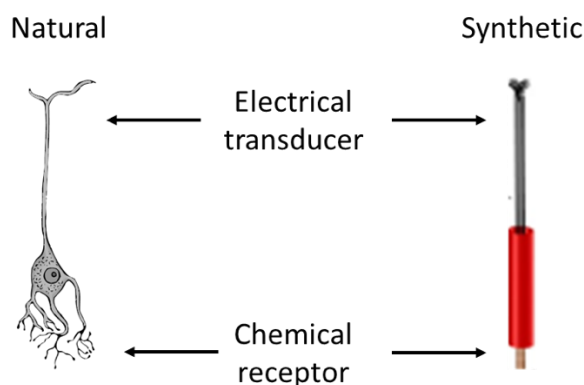


**Figure 1.2** Natural and synthetic electrochemical sensors; a nerve cell and a sodium-selective carbon fibre sensor (from [9]).

<sup>2</sup> Phrase coined by Maturano and Varela and published in *The Tree of Knowledge: Biological Roots of Human Understanding*, Shambhala, 1992.



### 1.3 Defining performance for distributed analysis in the information age

To the analyst, performance is an answer to the question, *'how good is this tool?'* The pivotal word in this question is *good*. Traditionally, analytical chemistry has answered this question in terms of parameters such as limits of detection, sensitivity, selectivity and reproducibility. By selecting these, *good* was implied to be the *exactness* of a measurement. That is, how accurate, precise and discriminating a determination could be. However, to continue to down this path once sufficient exactness has been reached, would be like continuing to sharpen a knife long after it was up to the task at hand. As Bakker has written, *'the system must be as good as required and only that good!'*[10]. It is important to understand that the question is made in a context, and that context has a critical influence on the definition of "good". Thus, the question that the analyst is faced with can be framed as, *"if I bring a sample to your lab, and give you the resources and time to perform the analysis, how good could your results be?"* Under that context, we could expect that improving the analytical tools to go beyond any limitations would be a natural path, as much as the Formula 1 cars push the limits of tolerance and speed of the engines.

So what is good? What is meaningful! And meanings are not absolute- they depend on context. Exactness is meaningful, but only to the degree that it imparts actionable information. This thesis is framed within the context of developing *distributed* chemical sensors for the information age. With this in mind, performance is redefined to mean, *the degree to which meaningful information is garnered*.

While the traditional figures of merit cannot be completely abandoned, new parameters are emerging such as *'ruggedness'*. Graham Currell has pointed out that this is a function of the method and not just the instrument, defining ruggedness as, *"a measure of the extent to which small variations in the conditions under which an analytical method is carried out may affect the reproducibility of the method"* [11]. This is very distinct from reproducibility itself.

The periods of human history tend to be named after the technologies that alter our way of life. The Stone Age, the Bronze Age, the Iron Age, and the Industrial Age. Each of these periods names a technology that we mastered until it became a *commodity*. Now we say that we are living in the information age, and indeed we see many informational types being either ultra-low cost, or indeed free. Newspapers, publishing, films, music, software, long-distance communication, international transfer of money- in multiple micro-revolutions, the digital age has freed these forms of information from the exclusive establishment and democratized them. From the *Wall Street Journal* to *WikiLeaks*, from Hollywood to *YouTube*, from *Random House* to *WordPress*, from *Universal Music* to *BitTorrent*, from exorbitant long distance charges to VoIP and *Skype*, from centralized banking services to the peer-to-peer *Bitcoin*. In each of these cases, an informational type has been

## INTRODUCTION

---

commoditized, democratized, and liberated, unleashing fresh waves of creativity- often with unexpected emergent outcomes.

Among the list of information types, chemical information is notably absent. It could of course use the same internet protocols as other information types, but would require the addition of unique nodes. Chemical nodes have been conceived of as *chemo/bio-sensor networks* [3] and (chemical) *wearables* [12] when applied to on-body measurements, and *chemical sondes* [13, 14] *autonomous field devices* [15], and *motest* in the context of environmental monitoring [3, 16, 17]. To summarize the situation in computer science terms, the network is available, but insufficient nodes are connected- this results in the current *limitation in bandwidth between the chemical and digital realms*.

THE CHEMICAL RUBBER CO.

**THE CAMERON Glass Electrode pH METER**


LOW COST - - PORTABILITY,  
RUGGED CONSTRUCTION.  
SIMPLE OPERATION by  
NON TECHNICAL MEN - -

Offers the advantages of the most versatile glass electrode pH measuring systems.

Powered by dry cells which have long life because of low current drain. Both sealed and pre-filled glass and the calomel electrodes withstand severe service and are inexpensive to replace.

With only two adjustments, a matter of seconds, the meter is calibrated and ready for the daily assignment of measurements. To determine pH, the "One-Two" switch is moved to position "One", where a simple adjustment is made, and then to position "Two", where the pH value is instantly shown directly in pH units.

Each instrument is guaranteed as to performance, workmanship, and materials for six months from date of sale.



Catalog No. E 6360

Figure 1.3 Advertisement from 1934 advertising the Cameron pH meter

Reasons for lack of nodes importing chemical information will be discussed in Chapter 2 as well as in the critical review of Chapter 4. It is striking that in the eight decades since the *Cameron pH meter* was advertised as “*low cost, portable, rugged, and simple*” (Figure 1.3), we are still striving to offer these same features- which, in large part, remain to be realized. Now, in 2018, there are diverse indicators that we are on the cusp of plugging the chemical into the digital. These include cultural indicators such as the growing popularity of self-monitoring [18] as well as the ambitious industrial outlooks for biosensors [19] and the internet-of-things [20].

It is of course possible that diverse sensing systems be connected hierarchically, as Valcárcel has termed ‘*vanguard-rearguard*’ analytical strategies [21]. In this conception, a vast number of nodes of lower performance can be utilized for screening, and only samples that merit further analysis can be relayed to sensors of higher performance. This approach is highly conducive to the rapid deployment of sensors as it mitigates the demand for their flawless performance.

## 1.4 Design, analysis, and simplicity

### 1.4.1 Design

At some level, *“Science is analytic; design is constructive”* [23].

Analysis and synthesis are complementary (Figure 1.4). Etymologically, the words derive from the classic Greek with denotations of ‘to loosen up’ and ‘to put together’ respectively [24]. From a polemic perspective, scientists problem solve by analysis, while designers problem solve by synthesis. Implicit in this, is that scientists tend to address the problem, while designers address the solution. *“Analysis is the ordering and structuring of the problem. Synthesis on the other hand is characterised by an attempt to move forward and create a response to the problem - the generation of solutions”* [25].

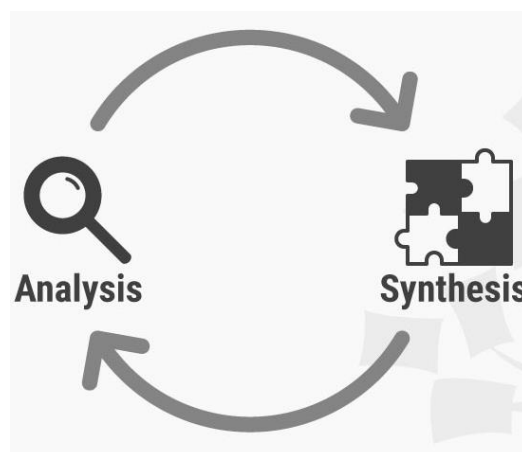


Figure 1.4 The cycle of the design process, through iterations of analysis and synthesis (from [22])

One unfortunate outcome of a narrow scientific point of view would be to regard aesthetic, economic, and socio-political considerations as secondary, to be addressed only after a ‘thing’ has been made. To a function-focussed inventor/maker, the thing is primary, and how a user experiences the thing is- at best- an afterthought. This perspective would be unfortunately short-sighted. In truth, there is no objective ‘thing’ outside the subjective experience of the user. This is not philosophy, but rather pragmatism; it is not necessary to cite the works of ancient Buddhist logic nor modern neurophysiology- one may merely glance at the billions of dollars poured into shaping the human experience, as for example in the spheres of politics and marketing.

“Designing often necessitates considering the aesthetic, functional, economic, and socio-political dimensions of both the design object and design process” [26]. While a rigid scientific viewpoint sees the world as

## INTRODUCTION

---

objective, and a postmodern artistic view sees a subjective experience of the world, “design is a targeted experience”,<sup>3</sup> a middle ground that consciously aims to shape the user’s reality.

### 1.4.2 Analysis

Analysis is the “*resolution of anything complex into simple elements*”<sup>4</sup>. This reductionist approach has traditionally proven successful in understanding chemical systems. Within this thesis, an analytical mentality is applied to resolve the complexity of distributed chemical sensors into the elements of usability, affordability, and performance. While it is useful to consider these separately at times, these elements are in fact never discrete from each other in application. Accordingly, the synthetic quality must be reincorporated. The process of invention necessarily involves iterations of analysis and synthesis (Figure 1.4), which can be seen as spiralling towards an optimal design. The geometry of this process contrasts starkly with the linearity of purely logical, reductionist reasoning.

*Modular systems thinking* is one approach to integrating analytic and synthetic methodologies. Ascribed as essential to the engineering mind-set, it includes the functional blending of *deconstructionism* and *reconstructionism* with the understanding that the sum of complex systems is greater than its parts, and cannot be understood simply by analysis of constituent components [27]. *Stepwise refinement*, or iterative prototyping is related design concept within engineering.

Guru Madhavan has outlined three properties essential to the engineering mind-set: to *see structure* even when non-obvious; to *design under constraints*, and to *make trade-offs* where compromise is demanded [27]. If these are the steps in the dance between reduction and synthesis, surely the underlying guiding principle is simplicity.

### 1.4.3 Simplicity

Simplicity is a concept closely related to user- design and technology. In his monograph entitled, “*The laws of simplicity*”, John Maeda elucidates several laws that closely align with the application of the design ethos to analytical systems [28]. His focussed first law states that, “*The simplest way to achieve simplicity is through thoughtful reduction.*” This indicates that the reductionist approach of analysis inherently tends towards simplification. However, in order to realize meaningful works, a degree of sophistication is generally required. This is accounted for in his fifth law, which states that “*Simplicity and complexity need each other.*”

In an age of ever-increasing specialisation, it is easy to fall into the trap of solving the problems that fall within the microcosm of our particular niche, while relegating the inconvenient loose ends of other specialities to the realm of externalities. In the context of this thesis, this statement is especially applicable to the temptation for chemists to be myopic in their consideration of the scope of the distributed chemical sensor problem. However,

---

<sup>3</sup> Statement by Pär Blanking

<sup>4</sup> [www.etymonline.com/word/analysis](http://www.etymonline.com/word/analysis)

## INTRODUCTION

---

as Maeda's sixth law states, "*What lies in the periphery of simplicity is definitely not peripheral*", and the periphery of chemical sensors crosses over into disciplines such as industrial user experience design, electronic and chemical engineering, and computer science. The critical review of Chapter 4 acknowledges this problem and identifies its solution as taking a multidisciplinary approach.

### 1.5 The *Maker* movement

There is longstanding debate within philosophy as to whether scientific understanding advances at a steady pace or rather in alternating waves of quiescence and insight. Certainly, the rate of publication is accelerating, although this does not necessarily reflect the advancement of understanding. At a technological level nonetheless, certain waves of innovation are apparent. Certainly, there seems to be a tendency in recent decades for widely accessible technologies to advance rapidly, and in unexpected ways. Indeed, the origins of modern chemistry are an example of this. Disregarded by the learned of universities, the nature of physical matter was initially the pursuit of European gentlemen of leisure and curiosity- although by no means the everyman, nor were they academic specialists.

Today, many technologies remain privy to the few- worked on almost exclusively by specialists, academics and powerful corporations. This exclusivity can be the natural outcome of practical considerations such as hazardous materials or high costs of equipment, or due to the protections of trade secrets or legal contracts. Whatever the reasons, history continues to show that discovery explodes when technologies are democratized or in modern parlance, made *open source*. This includes the advent of self-publishing across a multitude of internet platforms, the peer-to-peer exchange of value through decentralized money of *Bitcoin*, the uncensorable publication surface of *WikiLeaks*, the explosive adoption of the open source operating system *Linux*, the crowd-sourced encyclopaedia of *Wikipedia*- soon to re-manifest as *Everipedia*, and the growing popularity of free Massive Open Online Courses (MOOCs) that open top university training to anyone with curiosity and an internet connection.

The 2000's has seen the emergence of a new open source movement at the intersection of the *Hacker* and *DIY* cultures- namely, the *Maker* movement. Utilizing the tools *du jour*: 3D printers, microcomputers, open-source software, and of course the grand resource of internet connectivity, the *Makers* have swept the world with innovative fusions of low cost components and high creativity.

This thesis leverages a couple of *Maker* tools. One of these is the *Arduino* platform, an easily-programmable microcontroller that integrates with sensors and actuators and has libraries of open source projects shared freely amongst an enthusiastic community (Figure 1.5, left). It's Integrated Development Environment (IDE) auto-compiles human-readable code of the programming language *C++* to machine code, simplifying programming for the non-specialist. A second tool used, was a 3D printer for rapid prototyping (Figure 1.5, right).

## INTRODUCTION

---

Finally, most of the sensors used in this thesis were either screen-printed upon plastic laminate, were hand-painted upon paper, or were constructed upon household alumina foil. In this way, the research of our group is sympathetic to the *Maker* ethos while simultaneously taking advantage of sophisticated instrumentation and fine chemicals when needed. Perhaps the essence is simply to use what is functional and not make things any more complicated than necessary.



Figure 1.5 Tools of the Maker. Left: An *Arduino Uno* microcontroller. Right: A 3D printer by *Makerbot*.

## 1.6 A revolution in chemical sensing?

This thesis explores the concept of chemical sensors reaching widespread distribution. Furthermore, it is suggested that this could have revolutionary implications. Perhaps this sounds grandiose- after all, the experimental content uses basic laboratory compounds and simple electrochemical techniques. They are simply recombined in novel permutations.

However, truly disruptive technologies rarely (if ever) flourish instantaneously, instead drawing on decades of incremental progress and culminating in what may retrospectively appear as a momentous change. The Internet itself required some 40 years of cross-disciplinary innovations [29] before Tim Berners-Lee could invent the World Wide Web in what he has described as “*a gradual process of accretion*”, denying any Eureka moment [28].

The new direction taken in this work is to apply a design thinking process to the challenges of distributed chemical sensing systems. As *innovation cannot be systematize*,<sup>5</sup> the process is iterated, allowing for possibly unexpected outcomes to emerge.

---

<sup>5</sup> This statement is attributed to Steve Jobs

## INTRODUCTION

---

Recognizing that many tools to improve the *health of humanity* remain unavailable to the majority, and that the *health of the natural planet* is deteriorating without checks on those responsible and without a detailed understanding of how severe this ‘illness’ is, chemical sensors stand out as one technology with the power to redirect our course for the better. This thesis aims to contribute to the development of the field, with the vision that chemical sensors may not only have a technological impact, but may in fact conceptually shift the ideation of what we are and what we are embedded into.

## 1.7 References

- 1 Y. N. Harari, *Sapiens: a brief history of humankind*, HarperCollins, 2014.
- 2 P. Patel, Paper diagnostics that cost pennies, *Sci. Am.*, 2016, **315**, 40.
- 3 R. Byrne and D. Diamond, Chemo/bio-sensor networks, *Nat. Mater.*, 2006, **5**, 421–424.
- 4 L. M. Proctor, The Human Microbiome Project in 2011 and Beyond, *Cell Host Microbe*, 2011, **10**, 287–291.
- 5 D. A. Relman, The human microbiome: Ecosystem resilience and health, *Nutr. Rev.*, 2012, **70**, S2–S9.
- 6 A. J. Montiel-Castro, R. M. González-Cervantes, G. Bravo-Ruiseco and G. Pacheco-López, The microbiota-gut-brain axis: neurobehavioral correlates, health and sociality, *Front. Integr. Neurosci.*, 2013, **7**, 70.
- 7 K. Warwick, Homo Technologicus: Threat or Opportunity?, *Philosophies*, 2016, **1**, 199–208.
- 8 L. Zhang, T. Miyazawa, Y. Kitazumi and T. Kakiuchi, Ionic liquid salt bridge with low solubility of water and stable liquid junction potential based on a mixture of a potential-determining salt and a highly hydrophobic ionic liquid, *Anal. Chem.*, 2012, **84**, 3461–3464.
- 9 M. Parrilla, J. Ferré, T. Guinovart and F. J. Andrade, Wearable Potentiometric Sensors Based on Commercial Carbon Fibres for Monitoring Sodium in Sweat, *Electroanalysis*, 2016, **28**, 1267–1275.
- 10 E. Bakker, Can Calibration-Free Sensors Be Realized?, *ACS Sensors*, 2016, **1**, 838–841.
- 11 G. Currell, *Analytical instrumentation : performance characteristics and quality*, Wiley, 2000.
- 12 A. J. Bandoekar, I. Jeerapan and J. Wang, Wearable Chemical Sensors: Present Challenges and Future Prospects, *ACS Sensors*, 2016, **1**, 464–482.
- 13 P. Smith, R. Freshwater, R. Jones and N. Harris, in *International Meeting on New Sensing Technologies and Modelling for Air-Pollution Monitoring*, Aveiro, 2015, pp. 14–15.
- 14 W. S. Hering and H. U. Dutsch, Comparison of chemiluminescent and electrochemical ozonesonde observations, *J. Geophys. Res.*, 1965, **70**, 5483–5490.
- 15 D. Diamond, Internet-scale sensing., *Anal. Chem.*, 2004, **76**, 278A–286A.
- 16 D. Diamond, S. Coyle, S. Scarmagnani and J. Hayes, Wireless sensor networks and chemo-/biosensing, *Chem. Rev.*, 2008, **108**, 652–679.
- 17 C. Paddock, How self-monitoring is transforming health, <https://www.medicalnewstoday.com/articles/264784.php>, (accessed 22 April 2018).
- 18 Goldstein Research, *Global Biosensors Market 2024: Outlook, Insights, Forecast, Trends, Demand Analysis, Market Forecast, 2016-2024*, 2017.
- 19 Ericsson, *Mobility Report - Internet of Things outlook*, <https://www.ericsson.com/en/mobility-report/internet-of-things-outlook>, (accessed 22 April 2018).
- 20 M. Valcárcel and S. Cárdenas, Vanguard-rearguard analytical strategies, *TrAC - Trends Anal. Chem.*, 2005, **24**, 67–74.
- 21 S. Gregory, *The design method*, Springer, 1966.



## INTRODUCTION

---

- 22 T. Ritchey, *Analysis and Synthesis On Scientific Method - Based on a Study by Bernhard Riemann*, *Syst. Res.*, 1991, **8**, 21–41.
- 23 B. Lawson, *How designers think : the design process demystified*, Elsevier/Architectural Press, 2005.
- 24 Stage 2 in the Design Thinking Process – Define the Problem by Synthesising Information | Interaction Design Foundation, <https://www.interaction-design.org/literature/article/stage-2-in-the-design-thinking-process-define-the-problem-by-synthesising-information>, (accessed 12 April 2018).
- 25 [wikipedia.org/design](https://en.wikipedia.org/wiki/Design), <https://en.wikipedia.org/wiki/Design>, (accessed 17 April 2018).
- 26 G. Madhavan, *Applied minds: How engineers think*, W. W. Norton Company, New York & London, 1st edn., 2015.
- 27 J. Maeda, *The Laws of Simplicity*, MIT Press, 2006.
- 28 S. Berkun, *The myths of innovation*, O'Reilly, 1st edn., 2007.

## 2 SCIENTIFIC FOUNDATIONS

---



## 2.1 Fundamentals of electricity

The fundamental magnitudes of electricity are voltage (V), current ( $i$ ), and resistance (R). The relationships between these are summarised in Ohm's Law:

$$\Delta V = i R \quad (\text{Equation 2.1})$$

This thesis utilizes two electrochemical techniques, which interrogate terms found within this equation. The techniques are potentiometry and conductimetry (Table 2.1).

Potentiometry measures the voltage or electromotive force (EMF), while controlling the current ( $i$ ) to a near-zero level. The EMF is defined as the electric potential difference of the cell at zero current [1].

Conductimetry measures the inverse of resistance- the conductivity ( $\kappa$ ), per unit of length ( $l$ ) through a solution, while controlling the voltage.

**Table 2.1** Summary of electrochemical techniques used in the thesis and the associated electrical parameters

Method	Quantity measured	Variable controlled
Potentiometry	EMF (V)	$i = 0$
Conductimetry	$\kappa / l$ (S/m)	V

The fundamentals of conductimetry and potentiometry are described in this chapter. Guided by an underlying principle of simplicity in design, these are some of the most straightforward techniques in application, although appreciable complexity remains 'beneath the hood'.

## 2.2 Electrochemical techniques

### 2.2.1 Conductimetry

Conductimetry is conceptually the simplest electroanalytical technique [2]. It measures the electrical conductance per unit distance in an electrolytic solution with the units of the *Système international* being siemens per metre (S/m). As such, it responds to the total concentration of ions in a solution, without specificity as to which species they are. This gives conductimetry its analytical significance.

The technique has its roots in the nineteenth century when Friedrich Kohlrausch applied an alternating current across a solution. The related analytical tool of conductometry was established by Kolthoff in 1923 and was at that time popularly utilized as a titration technique for solutions where visual indicators were not well-suited [2]. It has since however, been displaced by more selective methods. A conductivity meter is now a standard instrument on analytical laboratory benchtops, alongside the pH meter.

## SCIENTIFIC FOUNDATIONS

---

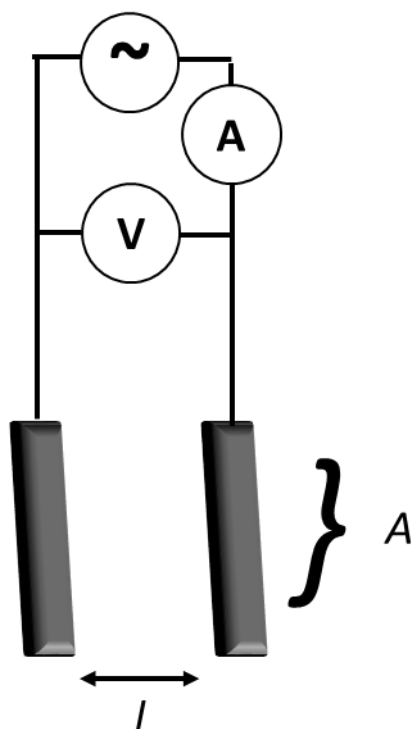


**Figure 2.1** General set-up of a two-electrode conductimetric cell. An alternating voltage is applied across two platinum electrodes of area,  $A$ , separated by distance,  $l$ . By reading the voltage and current, the resistance can be determined.

The basis of conductimetry is to apply an alternating voltage through a solution and read the current that passes through the solution (Figure 2.1). From this, the resistance can be calculated using Ohm's law. It is critical that the voltage be alternated in order to avoid polarising the solution, driving Faradaic processes upon the electrodes and building up further resistance. The frequency of cycle should be selected such that polarization becomes negligible compared to the solution's resistance. The waveform used can either be alternating current (AC) or a pulsed direct current. Both of these- operated at appropriate frequency - will avoid electrode polarization.

However, as well as reflecting the composition of the solution, the resistance is also related to the nature of the cell; it is a function of the electrode material, the electrode area, as well as the distance between electrodes  $l$ . Accordingly, any readings of resistance will be modulated by these multiple factors (Equation 2).

$$R = \frac{\rho \cdot l}{\text{Area}} \quad (\text{Equation 2.2})$$

In fact, the significant measurement to make is the *specific resistance*, or *resistivity*,  $\rho$ . This is representative of the solution, independent of the instrument. In practice, each conductimetric cell is unique in its geometry and material composition and accordingly can be ascribed a unique cell constant  $K$  that reflects this. By

## SCIENTIFIC FOUNDATIONS

---

calibrating a cell with solutions of known specific resistance, the cell constant  $K$ , can be known, and the cell calibrated. By convention however, the inverse term of resistance is usually discussed, namely *the specific conductance* or *conductivity*,  $\kappa$  (Equation 3).

$$\kappa = \frac{1}{\rho} = \frac{K}{R} \quad (\text{Equation 2.3})$$

Platinum is typically selected as the electrode material due to its high electrical conductivity, mechanical strength and resistance to electrolyte and chemical attack. As measurements are highly temperature dependant, adjustments must also be made for this. It should be noted that the second method for conductivity measurements- the inductive method- has not been discussed here.

As mentioned, the conductivity of a solution is proportional to the concentration of ions. In the simple case of a solution containing a single electrolyte the relationship can be expressed as:

$$C = \frac{\kappa}{\Lambda_m} \quad (\text{Equation 2.4})$$

where  $C$  is concentration,  $\kappa$  is the specific conductance, and  $\Lambda_m$  is the molar conductivity.

A Wheatstone bridge is the electrical circuit used for the measurement (Figure 2.2). This balances two legs of a bridge circuit and adjusts a variable resistor,  $R_2$ , in order to maintain zero current. At this balance point, the unknown value of  $R_x$  (in this case the conductivity) can be calculated from:

$$\frac{R_2}{R_1} = \frac{R_x}{R_3} \quad (\text{Equation 2.5})$$

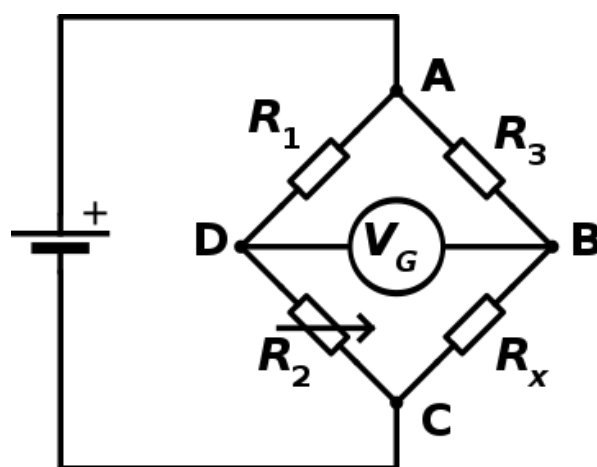


Figure 2.2 A Wheatstone bridge (from [3])

## SCIENTIFIC FOUNDATIONS

---

Chapter 8 of this thesis describes a conductimeter embedded into a toilet that takes readings of urine conductivity during flow. The information generated, offers a global snapshot of an individual's well-being, which is reported to indicate hydration levels [4]. A complementary snapshot is also provided by a wearable patch that monitors the total ion activity in sweat, also elaborated within this thesis. While the underlying technique of the patch is potentiometry, the information generated is shown to be equivalent to that garnered by a conductimetric reading.

### 2.2.2 Potentiometry

Matter is inherently electrical. As a passive analytical technique, the elegance of potentiometry is to leverage this by reading the electrification of matter as it is, naturally. Potentiometry reads the electromotive force between two electrodes. In practice, a high-impedance voltmeter (or potentiometer) reads the difference in voltage while limiting the current to near-zero levels (for example, typical impedances used for conventional ion-selective electrodes are in the order of  $10^{15} \Omega$ ).

A potentiometric cell is essentially a galvanic cell, which in lieu of allowing the current to flow between two electrodes measures the open circuit potential between them (Figure 2.3). In most cases, the arrangement consists of a reference electrode and an indicator electrode. A reference electrode is defined by its ability to maintain a fixed potential. Ideally, this remains stable irrespective of changes in the electrode's environment, the sample matrix, or the activity of the target analyte. An indicator electrode (or working electrode) on the other hand, has a potential that is dependent on the activity of the target analyte. An ideal indicator electrode would be uniquely responsive to the target and insensitive to other species. The potential of the indicator electrode is observed (or controlled) *with respect to* the reference electrode [5]. Ultimately, potentiometry measures the *cell potential*. That is, the electrochemical potential across the electrochemical cell.

## SCIENTIFIC FOUNDATIONS

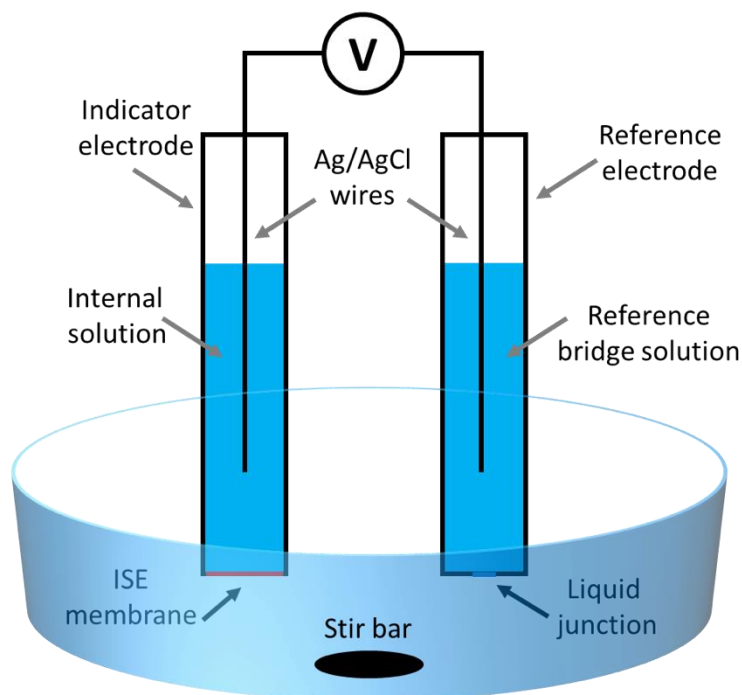


**Figure 2.3** A potentiometric cell

Potentiometry is analytically useful because changes in the potential difference between the two electrodes are proportional to the logarithm of chemical species' activity. These species may be ions or redox active molecules and their activity can be calculated using the *Nernst equation*.

$$E = E^0 + \frac{RT}{nF} \ln \frac{(Ox)}{(Red)} \quad (\text{Equation 2.6})$$

where  $E$  is the electrical potential of the cell (or EMF),  $E^0$  is the standard potential of the cell,  $R$  is the universal gas constant ( $8.314 \text{ J K}^{-1} \text{ mol}^{-1}$ ),  $T$  is the absolute temperature,  $F$  is the Faraday constant ( $96485 \text{ C mol}^{-1}$ ),  $n$  is the number of electrons or the charge of the ion involved in the reaction and  $(Ox)$  and  $(Red)$  represent the activities of the electroactive participants in the electrode process:



## 2.3 Electrochemical potential

The electrochemical potential is a thermodynamic quantity that results from the combination of the electrical and chemical potential energies. The International Union of Pure and Applied Chemistry (IUPAC) define it as the partial molar Gibbs energy of a substance in a specified phase at the specified electric potential.

All compounds have a potential. For those with associated redox processes (such as metals) a *standard electrode potential* is defined relative to the standard hydrogen electrode. This measures the energy (in Volts)

## SCIENTIFIC FOUNDATIONS

---

required to reduce the given species under standard conditions (1 atm of pressure, 298 K, and unity of activity (e.g. an effective concentration of 1 mol/L for species in water)). The symbol  $E^0$ , as for example appears in the Nernst equation, is used to represent the standard electrode potential. In practice however, as conditions are seldom standard, the *formal potential*,  $E^{0'}$ , can often prove more practical.

In this section, the electrochemical potentials of the phase-boundary potential, the Donnan potential, and the redox potential are elaborated.

### 2.3.1 Phase-boundary potential

The electromotive force (EMF) between a reference electrode and ion-selective electrode is the sum of all the electrical potentials across the path that closes the electrical circuit. They include the membrane potential ( $E_M$ ), the liquid-junction potential between the reference electrode and the solution ( $E_{D, Ref}$ ), and a constant potential due to internal interfaces of the membrane-to-conductor ( $E_{const}$ ) (Figure 2.4). As the  $E_D$  and  $E_{const}$  should remain constant in a well-controlled potentiometric cell, only the  $E_M$  term affects changes to the EMF.

$$EMF = E_M + E_D + E_{const} \quad (\text{Equation 2.8})$$



## SCIENTIFIC FOUNDATIONS

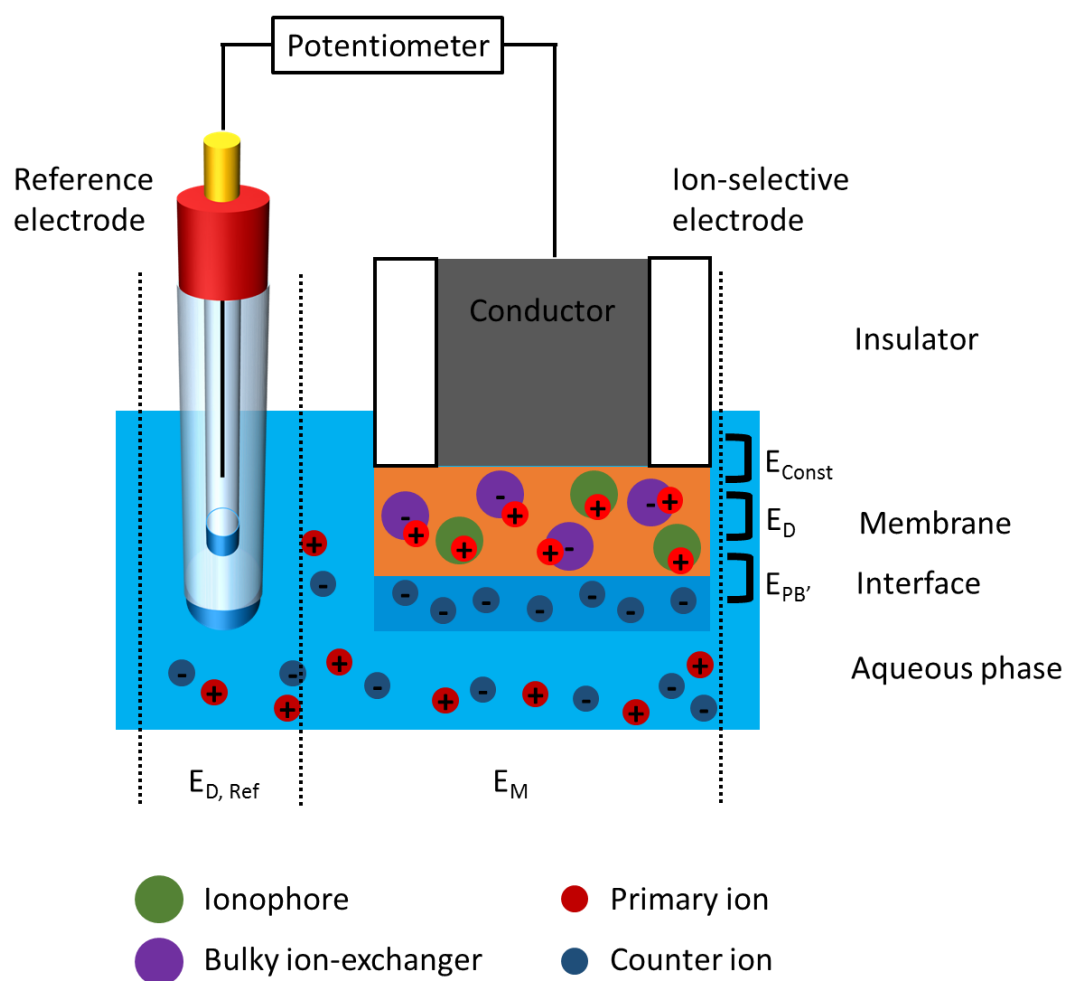


**Figure 2.4** The potentials appearing between a reference electrode and a solid-state ion-selective electrode. In this example, the primary ion is positively charged. The phase-boundary potential is generated by the partitioning of this into the membrane, while the counter ion is excluded.

To describe the  $E_M$ , the *phase-boundary potential model* is the prevailing understanding of the detection mechanism for ion-selective electrodes [6]. This relies on the fundamental understanding that the electrochemical potentials of an ion  $J$ , in two contacting phases must be equal.

The model makes two assumptions:

Firstly, that the phase-boundary potential at the aqueous/organic interface governs the membrane response. The diffusion potential, which is related to kinetic parameters of the species involved, is therefore neglected. Secondly, that the organic phase-boundary contacting the sample is in chemical equilibrium with the aqueous sample solution.

The phase-boundary model separates the  $E_M$  term into the  $E_{PB}$ ,  $E_D$ , and  $E_{PB'}$ .

$$E_M = E_{PB} + E_D + E_{PB'} \quad (\text{Equation 2.9})$$

## SCIENTIFIC FOUNDATIONS

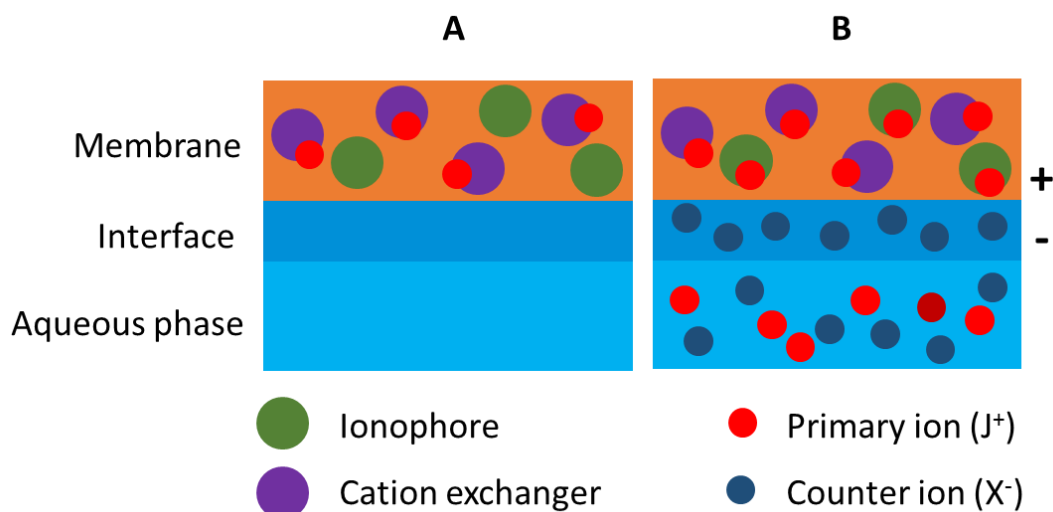


**Figure 2.5** A: an ion-selective membrane without ions in solution. B: the ion-selective electrode membrane in contact with an aqueous solution containing a primary cation ( $J^+$ ) and counter anion ( $X^-$ ).

The phase-boundary potential can be written as:

$$E_{PB} = \frac{RT}{z_J F} \ln k_J + \frac{RT}{z_J F} \ln \frac{a_{J(aq)}}{a_{J(org)}} \quad (\text{Equation 2.10})$$

Where  $a_{J(aq)}$  and  $a_{J(org)}$  are the activities of the uncomplexed primary ion with charge ( $z_J$ ) in the aqueous sample and the contacting organic phase boundary, respectively, and  $k_J$  is a function of the relative free energies of solvation in both the sample and membrane phases. The first term on the right-hand side is the standard potential, which is constant for a given ion. The second term on the right-hand side can be simplified by approximating the activity of  $J$  in the organic phase to be constant (a fair assumption for membranes with ionophores and ion-exchangers). This leads to the simplified equation:

$$E_{PB} = E_{PB}^0 + \frac{RT}{z_J F} \ln a_J \quad (\text{Equation 2.11})$$

The physical basis of the change in phase-boundary potential in response to the ions in solution, is a charge separation at this boundary (Figure 2.5). A partitioning of cations and anions between the aqueous and organic phases occurs due to their different solvation energies in these two phases. By inclusion of a cation or anion ion-exchanger, the charge separation can be controlled. By inclusion of an ionophore, the selectivity of response can be increased.

### 2.3.2 Donnan potential

When a semi-permeable membrane separates two solutions, this can limit the free diffusion of certain ions (often bulky species). The lack of mobility of this subset of ions is compensated for by the redistribution of other species and established what is called an electrochemical osmotic equilibrium or a *Donnan equilibrium*

## SCIENTIFIC FOUNDATIONS

[7]. While both solutions must remain electrically neutral, they may not necessarily contain equal activities of each species.

The gradient of concentrations across the membrane generates an electrical potential called a *Donnan potential* or *membrane potential*. This is depicted in Figure 2.6, where the large (orange coloured) anions are unable to pass through a semipermeable membrane. This drives the mobile ions to distribute in a way that while producing concentration gradients, maintains electrical neutrality.

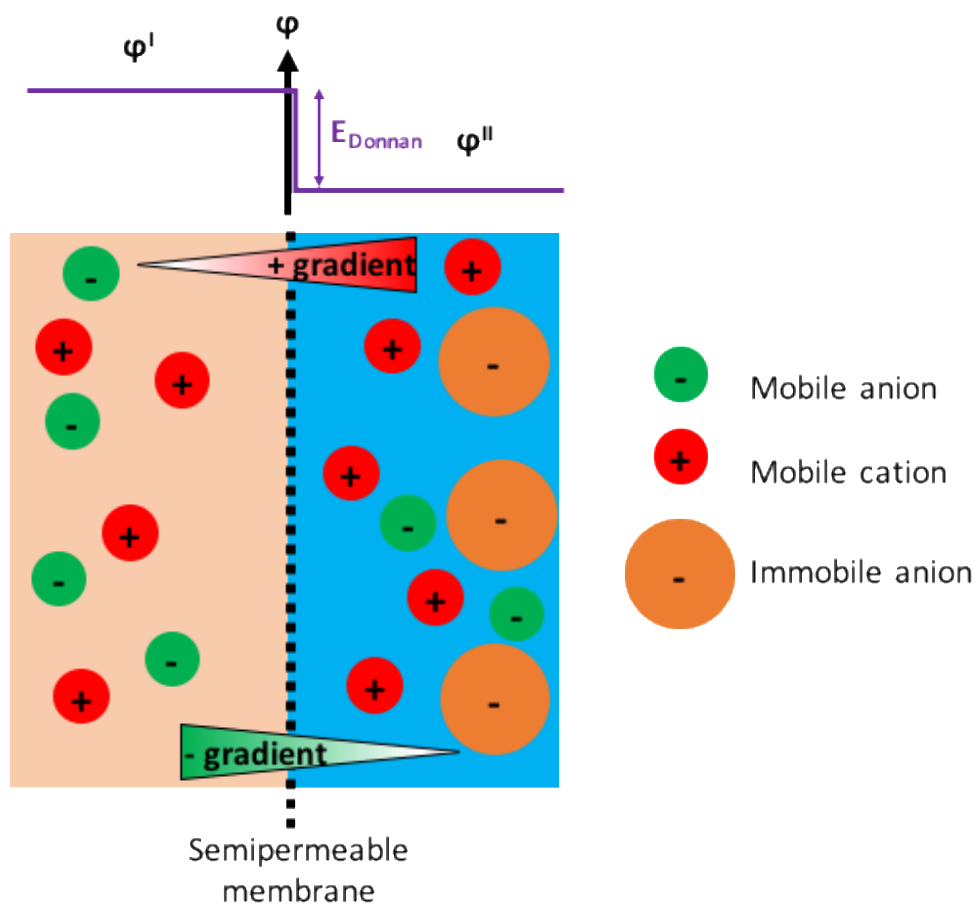


**Figure 2.6** Representation of the Donnan equilibrium and the resulting Donnan potential generated across a semipermeable membrane. The red and green arrows represent the concentration gradients of the mobile cations and anions respectively.

### 2.3.3 Redox potential

A reduction/oxidation reaction involves the transfer of electrons from one species to another. All species have different tendencies to accept or donate electrons; this is represented by their redox potential (or ORP or reduction potential). The more positive a species' redox potential, the greater its tendency to accept an electron and be reduced. In the 'free electron' model, the conduction electrons of the valence band of metals is not limited to individual atoms, but spread like an electron gas (Figure 2.7). The Fermi level- defined as the highest energy level occupied by electrons in the metal- is assumed to be independent of temperature. All energy states

## SCIENTIFIC FOUNDATIONS

---

below the Fermi level all occupied. Thus, the redox potential of a given substance can be associated to the relative differences in the Fermi levels of the atoms, since redox reactions (electron accepting or donating) are related- among other things- with these energies.

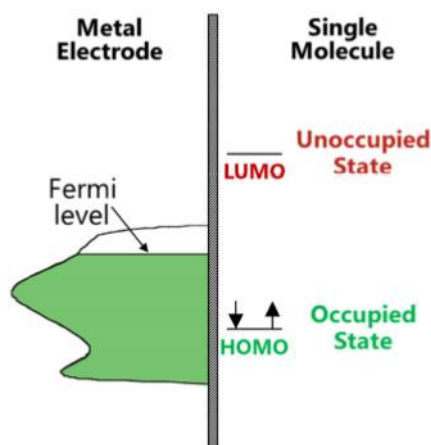


**Figure 2.7** The relationship between the Fermi level of a metal electrode and a single molecule in close proximity. For electron transfer to take place, the energy levels of an unoccupied molecular orbital (LUMO) would need to match the Fermi level of the metal electrode. Reproduced from [8].

A half-cell of a general reduction process can be represented as:



Where Ox is the oxidized species, and Red is the correspondent reduced species. The redox potential for this process can be calculated from the Nernst equation, in the form:

$$E = E^0 + \frac{RT}{z_1F} \ln \frac{(\text{Ox})}{(\text{Red})} \quad (\text{Equation 2.13})$$

As potentiometry permits near-zero flow of current, redox potential measurements only determine the *tendency* of a species to acquire or donate an electron, without the actual electron transfer taking place

The redox potential of a solution is usually measured using an inert electrode that is neither susceptible to reduction or oxidation. Because of this, platinum is typically selected as the electrode of choice.

## 2.4 Potentiometric electrodes

### 2.4.1 Indicator electrodes

Indicator electrodes are designed to vary in electrochemical potential in response to the chemistry of a solution. Here, the types of redox indicator electrode and ion-selective electrode are described.

## SCIENTIFIC FOUNDATIONS

---

### 2.4.1.1 Redox electrodes

A metal electrode in equilibrium with a solution of its ions constitutes an *electrode of the first kind* (or class) [2, 9]. An example of this would be a copper electrode in a solution of copper sulphate. If however the metal is electrochemically inert, its potential will respond to the redox potential of the solution in which it is immersed. This is exemplified by platinum.

A simple wire of a noble metal such as platinum, will respond to a solution's capacity to act as an oxidising or reducing agent. That is, the amount of work that would be required to add or remove an electron from the solution. This is known as oxidation-reduction potential (ORP) electrode. Strictly speaking, platinum is a typical mixed potential electrode, where the steady-state that produces the stable electrode potential is due to the presence of oxygen. Platinum can therefore be considered as an indicator of the presence of oxygen and oxidizing agents. For this reason, as well as its chemical inertness,<sup>6</sup> it has been adopted as an ORP probe.

### 2.4.1.2 Ion-selective electrodes

Another class of indicator electrodes are the ion-selective electrodes. The most well-known of these is the glass pH electrode. First reported in 1906, it remains a standard instrument in analytical laboratories today [10]. Its selective response is attributed to exchange between sodium groups within the glass and protons in solution [11]. By carefully controlling the composition of the glass, selective electrodes have been developed for a range of univalent cations including sodium, ammonium, and potassium [12].

Membranes selective to a wider range of analytes including multivalent and anionic species have been developed using *liquid membrane electrodes*. These entrap water-immiscible liquids within a polymer [11]. While the first generation of these included an inner-solution, recent decades have seen what has been termed a *silent revolution* in ion-selective electrodes, primarily ignited by a shift to solid-contact electrodes [13, 14]. These replaced the inner solution with a solid, conductive substrate such as glassy carbon or a metallic wire. An important step in the success of this kind of electrode, was to avoid the formation of a water layer between the membrane and the underlying conductor through inclusion of hydrophobic ion-to-electron transducing materials. These three generations of ion-selective electrodes are depicted in Figure 2.8.

One outcome of the move to solid-state electrodes has been to transform the fabrication techniques to high-throughput and low-cost methods such as screen-printing and ink-jet printing of electrode surfaces. It has also opened up the scope of what can constitute an electrode substrate, with novel proposals- from textiles to jewellery- being reported regularly.

---

<sup>6</sup> Bagotsky has pointed out that use of the term *inert* for such electrodes is somewhat unfortunate however, as the electrode in fact has a strong catalytic effect on reactions at its surface [9].

## SCIENTIFIC FOUNDATIONS

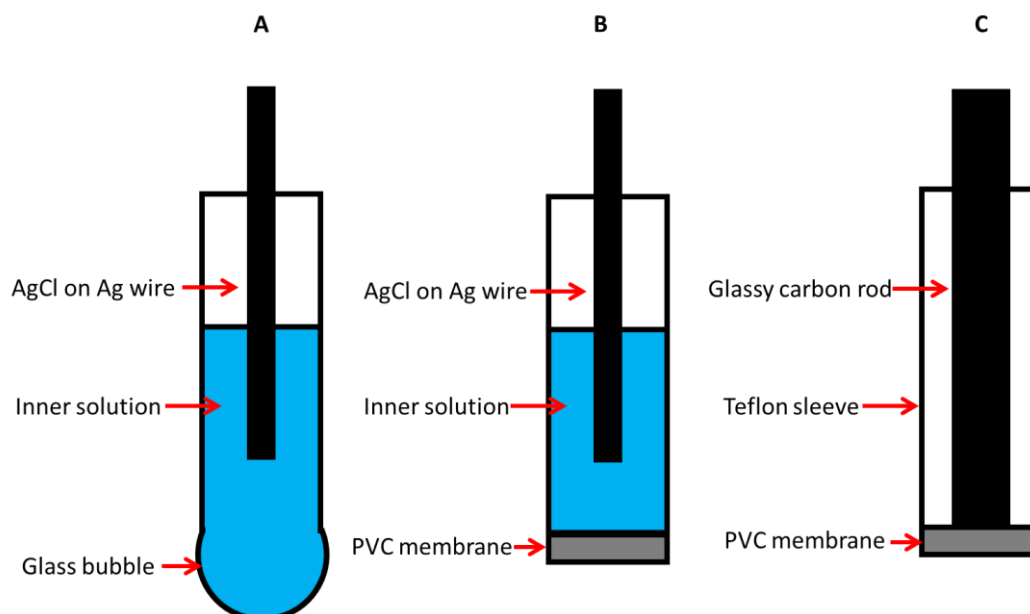


**Figure 2.8** Three generations of ion-selective electrodes. **A:** a glass membrane electrode; **B:** a liquid membrane ISE with inner solution; **C:** a solid-state ISE.

### 2.4.1.3 The potassium-selective membrane

Potassium-selective membrane electrodes based on the ionophore valinomycin are well-established. In a typical formulation, the various components of the membrane will be dissolved in tetrahydrofuran. The subsequent evaporation of the solvent will deposit a homogenous membrane. The pertinent membrane components are: the polymer (PVC), the ionophore (valinomycin) (Figure 2.9), the plasticizer bis-(2-ethylhexyl) sebacate (DOS), and the ion-exchanger (potassium tetrakis (4-chlorophenyl) borate (KTCIPB)). Each component plays an important role. The polymer provides mechanical stability and the underlying structural framework for the other components to operate. The plasticizer softens the polymeric matrix, increasing its resilience and lowering its glass transition temperature. The ionophore is a receptor macromolecule that acts as host to the target ion guest. The ionophore is the element for imparting selectivity to the membrane, which is achieved through the formation of complementary non-covalent interactions between ion and ionophore. The final element of the membrane matrix is the ion-exchanger. This is generally a bulky lipophilic anion (in this case the large borate), countered by a small counter cation (in this case the potassium ion). Its role is to ensure that the membrane exclusively exchanges positively charged ions, as the anions are immobilized.

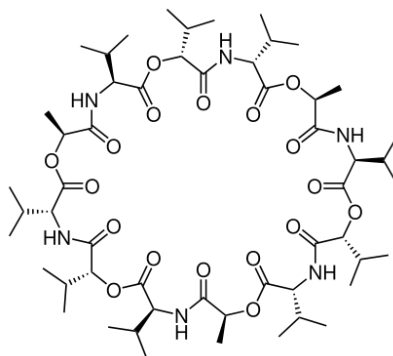


**Figure 2.9** Valinomycin, the ionophore of the potassium ion. The cavity of electronegative groups optimally accommodates the potassium ion in terms of charge and ionic radius.

### 2.4.2 Reference electrodes

As the calculation of the absolute potential of a single electrode is an impractical value, a reference value to evaluate potentials of other electrodes is needed. This is provided by a *reference electrode*, which is characterized by maintaining a constant electrochemical potential, unaffected by changes in matrix composition or environmental conditions.

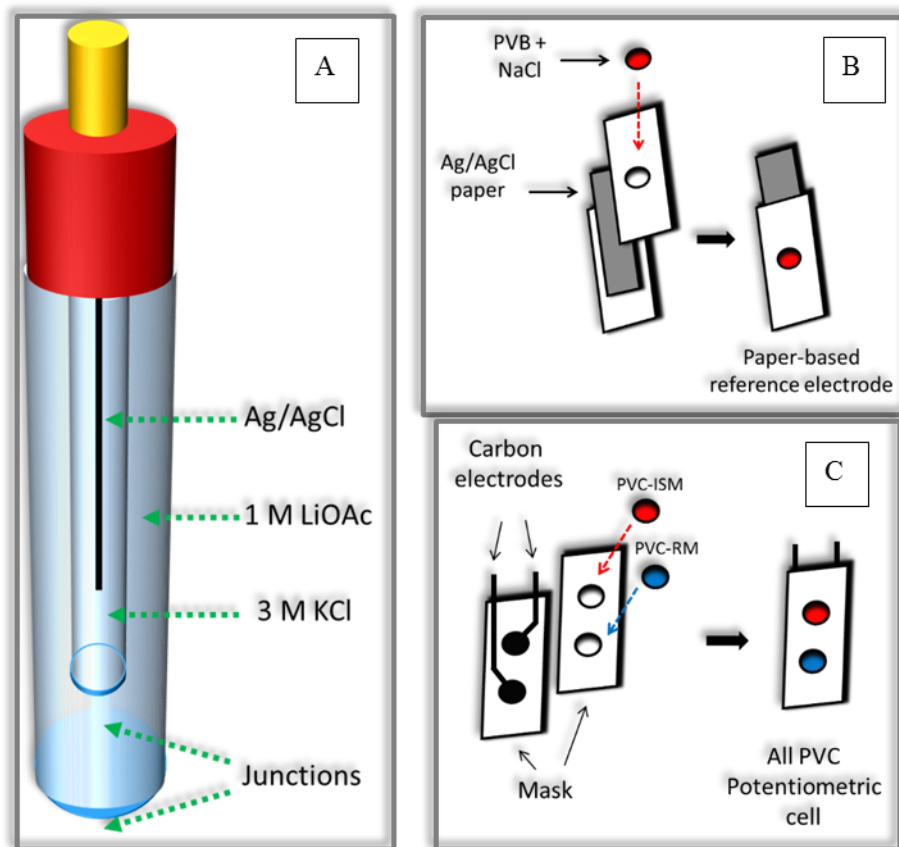
While by convention, the universal reference electrode,  $H^+/H_2$  has its potential defined as 0 V at all temperatures [15], this electrode can be challenging in practical use. Similarly, while the saturated calomel electrode ( $Hg/Hg_2Cl_2$ ) has historically proved popular, the toxicity of mercury has seen a decline of its use in recent decades.

In this thesis, the silver/silver chloride reference electrode- the most widely used configuration- is employed. The  $Ag/AgCl$  reference electrode maintains a stable potential between a silver wire and a coating of silver chloride when immersed in a solution saturated with free chloride ions. This is due to the facile reversibility of the  $Ag/AgCl$  redox couple over a wide pH range. The fast electrode kinetics of the  $Ag^+ + Cl^- \rightarrow AgCl_{(s)}$  reaction, allows for rapid and efficient dissolution of  $Ag^+$  and deposition of metallic silver. Another attractive feature of the  $Ag/AgCl$  reference electrode is its low temperature coefficient of 0.09 mV/K [16]. This reference electrode combines simple construction, stable and reproducible potential, and affordability. Its greatest weakness is a susceptibility to contamination, a problem which can be minimised by using the electrode in within the double-junction configuration.

The  $Ag/AgCl$  reference electrode exemplifies an *electrode of the second class*. That is, one in which a metal is in equilibrium with a sparingly soluble salt of itself [2, 9]. In contrast to electrodes of the first kind whose potential is defined at a biphasic (solid-liquid) interface, these electrodes have their potential defined between two materials in the solid phase.

## SCIENTIFIC FOUNDATIONS

Contact between the chloride saturated solution (typically KCl) and the sample solution is provided through a glass frit junction. Even greater stability is maintained when a second junction is included to place another buffering potential junction between the solution and the silver wire. This case is called a *double-junction*



reference electrode (

Figure 2.10 A).

In recent years, our group has developed a solid-state analogue of the single-junction reference electrode using the porous polymer poly(vinyl butyral) (PVB) in lieu of an inner solution [17, 18]. By saturating a PVB



## SCIENTIFIC FOUNDATIONS

membrane with sodium chloride upon an Ag/AgCl surface, a pseudo-reference electrode<sup>7</sup> is constructed (

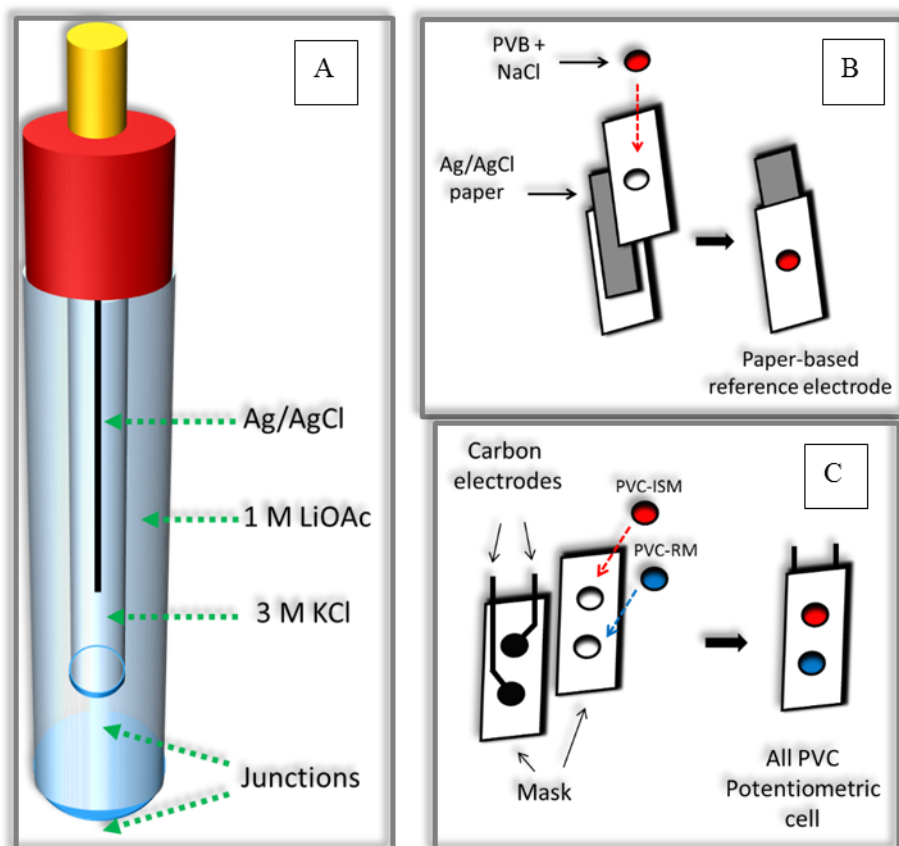


Figure 2.10 B). It has proved to provide a reasonably stable potential provided the ionic strength is maintained, and has successfully been applied to paper platforms [18, 19]. This was used in the wearable sweat patch described in Chapter 9.

More recently, a different approach to build reference electrodes has been explored using ionic liquids (ILs) [20, 21]. Comprised of an ionic liquid entrapped within a polymer such as PVC, with or without addition of a plasticizer, the hydrophobicity of these liquids ensures the membrane does not deteriorate rapidly and defines these reference electrodes as liquid-junction free. The mechanism responsible for maintaining the stable potential has been attributed to a limited degree of partitioning of the partially-soluble IL ions into the sample [20]. This then sets the aquo-membrane interfacial potential [21]. Chapters 5 and 6 make use of a solid-contact

<sup>7</sup> A pseudo-reference electrode, or quasi-reference electrode is distinct from a true reference electrode in that it lacks a thermodynamic equilibrium [31].

## SCIENTIFIC FOUNDATIONS

reference electrode based on inclusion of an ionic liquid within a PVC membrane (

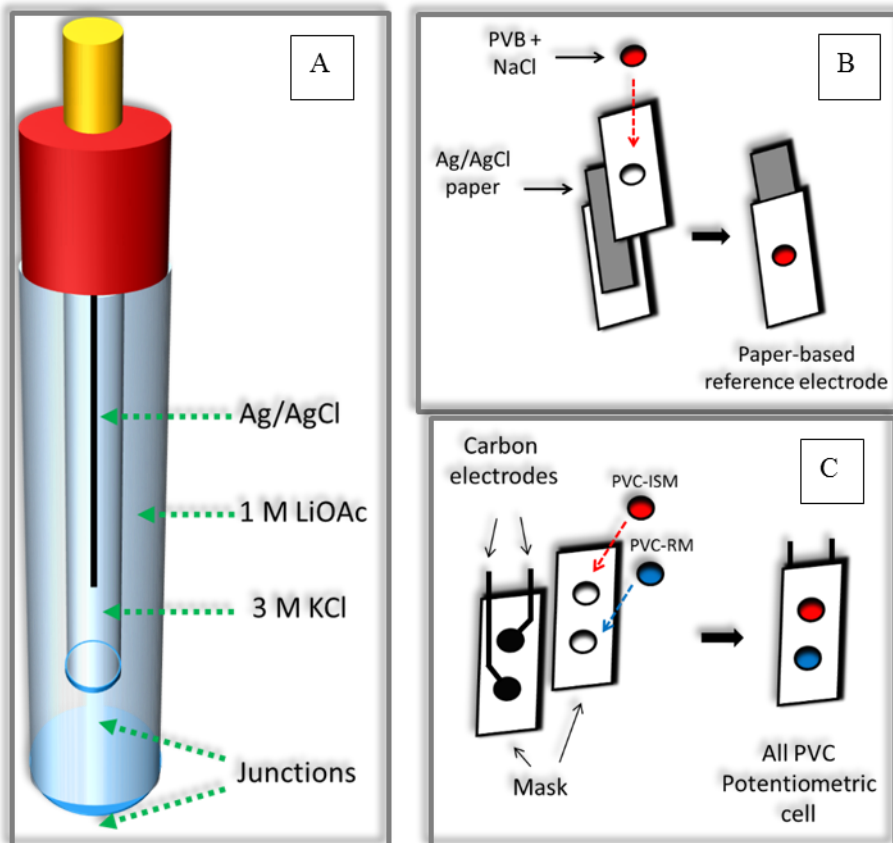
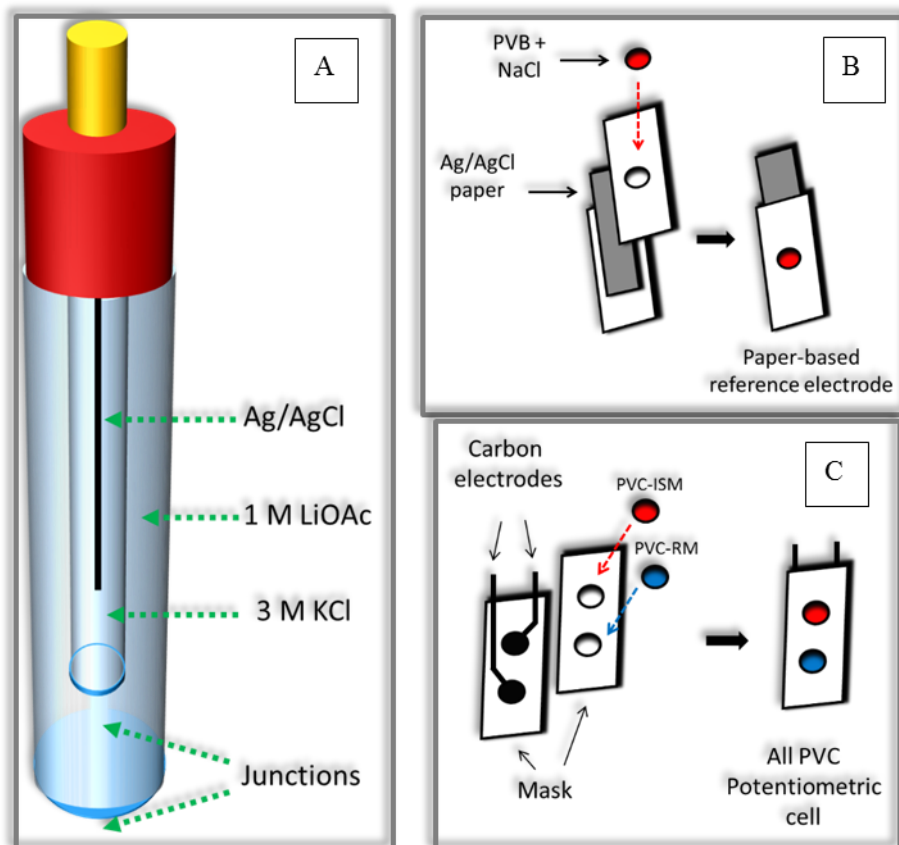


Figure 2.10, C). This is advantageous for its flexibility of form factor, miniaturisation and compatibility with mass manufacturing techniques, as well as the mechanical strength inherent to PVC.

## SCIENTIFIC FOUNDATIONS



**Figure 2.10** Reference electrodes. A: a double-junction Ag/AgCl type; B: a PBV-based Ag/AgCl type on paper; C: a PVC-based ionic liquid reference electrode on screen-printed substrate.

## 2.5 Flow injection analysis

Both conductimetry and potentiometry are traditionally measured under steady-state conditions. In practice, a conductimetric or potentiometric probe is immersed into a sample and the analyst waits some seconds to minutes for chemical equilibrium to be attained, at which time the measurement is recorded. Until recently, this was assumed the best way for all manner of analytical methods, not just electrochemical ones [22, 23]. This was logical, as it eliminated the variable of time, resulting in greater reproducibility. This same approach was therefore taken to continuous-flow analysis, in which homogeneously mixed sample packets are passed by a detector, with air bubbles separating discrete samples. While this method introduced an assembly-line style of efficiency that increased sample throughput, it was still limited by the need for equilibrium conditions to be reached in all steps such as mixing, reacting, and diluting.

In 1975 however, Ruzicka and Hansen reported a radical alternative [23]. Their flow-injection analysis (FIA) system made measurements of sample packets traveling within a carrier solution. Assuming the packets were comparatively small in volume, the detected signal would not reach the same intensity expected from the sample under static conditions, however they did prove highly reproducible in signal arrival time, peak height

## SCIENTIFIC FOUNDATIONS

---

etc. The system proved to be flexible to online dynamic dilution, reaction and mixing, and was demonstrated to facilitate spectroscopic as well as electrochemical detection methods.

A basic set up for a FIA system is depicted in Figure 2.11. A carrier solution is pumped through a fluidic system comprising a valve, a mixing coil, and a detector (D). By porting of the valve, a sample solution can be 'injected' into the fluidic system, without interrupting the flow.

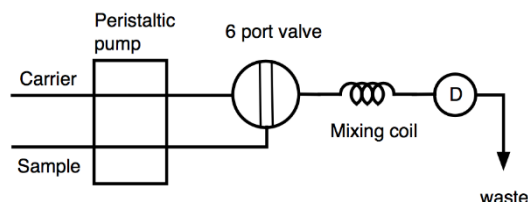


**Figure 2.11** General setup of a flow injection analysis system. The letter D represents the detector.

The response of detector can be analysed in terms of the maximum peak height ( $h$ ), the time for a signal to be detected following injection of a sample, or arrival time ( $t_A$ ), and the duration of a peak signal before returning to baseline levels, or residence time ( $t_R$ ). These parameters are depicted in Figure 2.12.

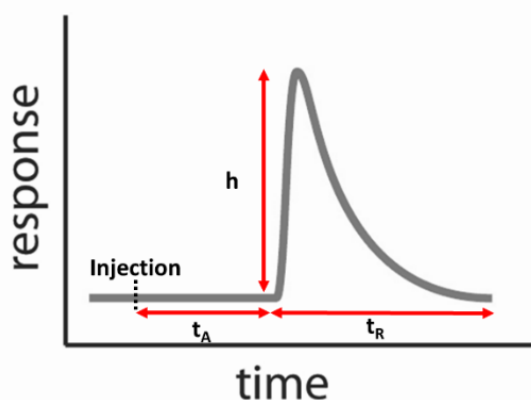


**Figure 2.12** Typical signal from flow injection analysis;  $h$  indicates peak height,  $t_A$  indicates arrival time,  $t_R$  indicates residence time.

One key parameter in the design of FIA systems is the dispersion coefficient,  $D$ . Defined as the ratio of analyte concentrations before and after dispersion has taken place in the carrier solution, it is calculated as:

$$D = C^0 / C^{\max} \quad (\text{Equation 2.14})$$

where  $C^0$  is the signal of the sample *without* dispersion, and  $C^{\max}$  is the maximum peak height of the (dispersed) sample in the FIA system. It follows from this that dispersion coefficient can have a value of 1 or greater, where a value of 1 indicates no dispersion of the sample.

Within this thesis, Chapter 7 describes the design of a FIA system for the potentiometric determination of creatinine.

## 2.6 Calibration of potentiometric sensors

### 2.6.1 *The challenge of calibration*

Building upon a rich literature of work in the development of chemical sensors, this thesis contributes little in the way of new sensors, instead seeking to address challenges associated with using chemical sensors outside of a laboratory. It focusses on strategies to overcome these. Perhaps the greatest such challenge for potentiometric sensors is the calibration question, which this work identifies as a major bottleneck to the wider implementation of chemical sensing networks.

Calibration rests on the idea of reproducing significance across time and space. Money is one of example of this, as it transports value across time and space. Early objects used as money such as shells and gems stones were not precisely fungible- that is, interchangeable- until a calibration technology was invented. While precious metals inherently had some desirable qualities of money- namely durability and scarcity- they were not fungible until minting was invented in the first millennium BCE, allowing for coins of identical size and mass to be truly interchangeable. This was the calibration of money.



**Figure 2.13** Gold. Left: pieces of irregular size and mass. Right: the Egyptian gold Stater, perhaps the first fungible form of money.

Thus, calibration gives meaning to measurements by placing the measurement of the unknown in relation to the known. In the context of sensors, this involves testing the response of the sensor to inputs of known quantities, so that unknown inputs can be evaluated relationally.

The challenge of calibration is the one of the greatest limitations to the distribution of chemical sensors. This is due to what has been called the ‘*chemical sensor paradox*’: chemical sensors must have an ‘active’ surface that is sensitive to very subtle interactions. As Byrne and Diamond wrote, “*even slight changes in the surface or bulk characteristics, through processes like leaching, fouling or decomposition, can have a significant effect on the output signal, and the overall performance of the device*” [24]. This is distinct from physical sensing components such as photodiodes or thermistors that are shielded from their environment, interacting only with light and electrons. As such, these physical components maintain the same performance characteristics from fabrication to the end of their lifetime.

How can this be emulated by chemical sensors?

## SCIENTIFIC FOUNDATIONS

---

One answer to this question is to mimic the physical analogues and protect the active surface. This is the approach taken by amperometric enzymatic biosensors in determination of uncharged small biomolecules such as glucose, in which the sensing surface is covered by a diffusion limiting membrane to protect it from fouling by ionic and bulky compounds naturally found in biological liquids such as blood and urine. While this approach has had some success, a significant weakness and a serious limitation remain. The weakness is the amperometric approach itself. As Bakker neatly summarized, “*amperometry is an inherently kinetic technique and the signal remains very sensitive to fluctuations in temperature and other processes that influence the kinetics of the rate limiting step*” [25]. Despite the glucometer being a medical success story, the field of enzymatic sensors has not fundamentally evolved in the 40 decades since it was introduced. While sensors for some other enzymatically-accessible analytes have been developed, these not reached widespread adoption for reasons discussed in the critical review of Chapter 4. Perhaps weaknesses of the technique itself may be in part responsible. In any case, a serious limitation also remains in that charged molecules cannot permeate the protective membrane, so the list of possible analytes omits many critical species.

Practically, a calibration typically necessitates the immersion of a sensor in one or more solutions of known analyte activity. While straightforward for a scientist in a laboratory, when translated outside of the lab for non-expert users, the handling of liquids presents a complicated, error-prone, and- most significantly- off-putting proposition.

### 2.6.2 Approaches to meeting the challenge

Several research groups have sought to make potentiometric sensors suitable for use outside of a laboratory by non-specialist personnel. In doing so, they have sought to mitigate the calibration challenge by preparing highly reproducible electrodes.

The variables to be made reproducible are the sensitivity and the standard potential. A well-constructed ion-selective electrode will have reproducibly have a Nernstian response to the ion to which it is selective. Drawing on this basis, Rius-Ruiz and coworkers were able to demonstrate that a single-point calibration prior to analysis of a sample was sufficient for the determination of the ion activity, as the standard potential could be extrapolated from this [26].

Other research groups have sought to obviate the need for such a calibration point by employing various strategies to make electrodes with highly reproducible standard potentials. One such approach by Vanamo *et al.* was to ‘short-circuit’ multiple indicator electrodes to a conventional reference electrode with a high redox buffering capacity [27]. By allowing these to equilibrate in a concentrated solution containing the primary ion for 3 days, the indicator electrodes were found to have highly reproducible standard potentials. Of course, the standard potential of the reference electrode must also be highly reproducible for this strategy to be viable. So far, it appears that the short-circuit method is not effective for reference electrodes [28].

A different approach has been to include a redox couple within the polymeric membrane matrix. This has been demonstrated to be effective in making uniform the standard potentials of both indicator and reference electrodes. The group of Buhlmann has shown this with use of a lipophilic Co(II)/Co(III) redox buffer salt to obtain standard deviations of  $E^0$  below 1 mV for ISEs [29] and 2.1 mV for reference electrodes [30].

### 2.6.3 Approaches in this thesis

In addressing the limitations of distributed chemical sensors, the calibration question cannot be overlooked. This thesis therefore explores two diametric approaches towards providing answers- these are in a sense, evolutionary and revolutionary.

The more gradual approach, is to use existing tools to automate calibration. That is, to reproduce the steps taken by a technician- sensor calibration, washing, and sample introduction- within an autonomous unit: a *Lab-in-a-box*. While in theory this is straightforward, the devil is in the details, and Chapter 5 describes some of the challenges encountered. While it is somewhat surprising that this approach has not been previously described as it is not non-obvious, it is not trivial in application.

In a different approach, a capping membrane was applied to connect a reference electrode and an ion-selective electrode. The membrane was designed to allow a dry calibration to be made before immersion in to a sample solution, at which time the membrane did not interfere. The rationale behind this is that the best time and place to make a calibration is immediately before contact with a sample, as conditions are identical and the requisite instrumentation is necessarily at hand. This approach is described in Chapter 6.

## 2.7 References

- 1 IUPAC, in *IUPAC Compendium of Chemical Terminology*, eds. A. D. McNaught and A. Wilkinson, Blackwell Scientific Publications, Oxford, 2nd edn., 1997.
- 2 B. H. Vassos and G. W. Ewing, *Electroanalytical chemistry*, John Wiley & Sons, Inc., United States of America, 1983.
- 3 Wheatstone bridge - Wikipedia, [https://en.wikipedia.org/wiki/Wheatstone\\_bridge](https://en.wikipedia.org/wiki/Wheatstone_bridge), (accessed 20 April 2018).
- 4 L. E. Armstrong, Assessing Hydration Status: The Elusive Gold Standard, *J. Am. Coll. Nutr.*, 2007, **26**, 575S–584S.
- 5 A. J. Bard and L. R. Faulkner, *Electrochemical methods, Fundamentals and Applications*, John Wiley & Sons, Inc., 1980.
- 6 E. Bakker, P. Bühlmann and E. Pretsch, The phase-boundary potential model, *Talanta*, 2004, **63**, 3–20.
- 7 C. H. Hamann, A. Hamnett and W. Vielstich, *Electrochemistry*, Wiley-VCH, 2007.
- 8 D. W. Kumsa, N. Bhadra, E. M. Hudak, S. C. Kelley, D. F. Untereker and J. T. Mortimer, Electron transfer processes occurring on platinum neural stimulating electrodes : a tutorial on the  $i$  (Ve) profile, *J. Neural Eng.*, 2016, **13**, 52001.
- 9 V. S. Bagotsky, *Fundamentals of electrochemistry*, John Wiley & Sons, Inc., New Jersey, 2nd edn., 2006.
- 10 M. Cremer, Über die Ursache der elektromotorischen Eigenschaften der Gewebe, zugleich ein Beitrag zur Lehre von den polyphasischen Elektrolytketten, *Z Biol*, 1906, **47**, 562.
- 11 J. Wang, *Analytical Electrochemistry*, Wiley, 3rd edn., 2006.
- 12 G. Eisenman, *Glass electrodes for hydrogen and other cations: Principles and practice*, Marcel Dekker, New York, 1967.
- 13 E. E. Pretsch, The New Wave of Ion-Selective Electrodes, *Anal. Chem.*, 2002, **74**, 1–11.
- 14 E. Bakker and E. Pretsch, Modern potentiometry., *Angew. Chem. Int. Ed. Engl.*, 2007, **46**, 5660–8.
- 15 International Union of Pure and Applied Chemistry Commission on Electrochemistry, The Absolute Electrode Potential: An explanatory note, *Pure Appl. Chem.*, 1986, **58**, 955–966.
- 16 A. Evans, *Potentiometry and ion selective electrodes*, Published on behalf of ACOL, Thames Polytechnic, London, by Wiley, 1987.
- 17 T. Guinovart, G. A. Crespo, F. X. Rius and F. J. Andrade, A reference electrode based on polyvinyl butyral (PVB) polymer for decentralized chemical measurements., *Anal. Chim. Acta*, 2014, **821**, 72–80.
- 18 M. Novell, T. Guinovart, P. Blondeau, F. X. Rius and F. J. Andrade, A paper-based potentiometric cell for decentralized monitoring of Li levels in whole blood., *Lab Chip*, 2014, **14**, 1308–14.
- 19 R. Cánovas, M. Parrilla, P. Blondeau and F. J. Andrade, A novel wireless paper-based potentiometric platform for monitoring glucose in blood, *Lab Chip*, 2017, **17**, 2500–2507.



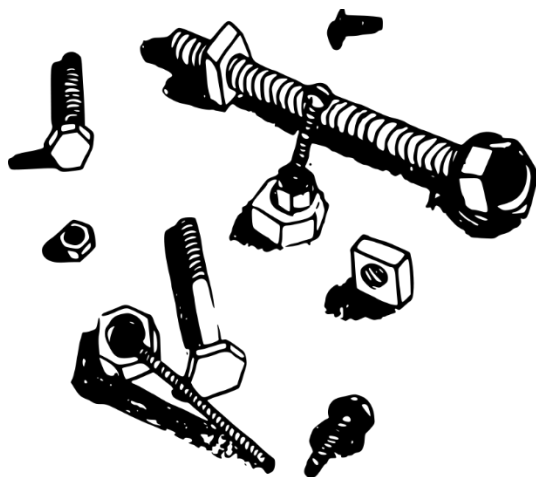
## SCIENTIFIC FOUNDATIONS

---

- 20 D. Cicmil, S. Anastasova, A. Kavanagh, D. Diamond, U. Mattinen, J. Bobacka, A. Lewenstam and A. Radu, Ionic Liquid-Based, Liquid-Junction-Free Reference Electrode, *Electroanalysis*, 2011, **23**, 1881–1890.
- 21 L. Zhang, T. Miyazawa, Y. Kitazumi and T. Kakiuchi, Ionic liquid salt bridge with low solubility of water and stable liquid junction potential based on a mixture of a potential-determining salt and a highly hydrophobic ionic liquid, *Anal. Chem.*, 2012, **84**, 3461–3464.
- 22 R. Kellner, J.-M. Mermet, M. Otto and H. M. Widmer, Eds., *Analytical chemistry*, Wiley-VCH, Weinheim, Germany, 1998.
- 23 J. Ruzicka and E. H. Hansen, Flow Injection Analysis. Part I. A New Concept of Fast Continuous Flow Analysis, 1975, vol. 78.
- 24 R. Byrne and D. Diamond, Chemo/bio sensor networks, *Nat. Mater.*, 2006, **5**, 421–424.
- 25 E. Bakker, Can Calibration-Free Sensors Be Realized?, *ACS Sensors*, 2016, **1**, 838–841.
- 26 F. X. Rius-ruiz, A. Crespo, D. Bejarano-nosas, P. Blondeau, J. Riu and F. X. Rius, Potentiometric Strip Cell Based on Carbon Nanotubes as Transducer, *Anal. Chem.*, 2011, **83**, 8810–8815.
- 27 U. Vanamo and J. Bobacka, Instrument-free control of the standard potential of potentiometric solid-contact ion-selective electrodes by short-circuiting with a conventional reference electrode, *Anal. Chem.*, 2014, **86**, 10540–10545.
- 28 M. Parrilla, J. Ferré, T. Guinovart and F. J. Andrade, Wearable Potentiometric Sensors Based on Commercial Carbon Fibres for Monitoring Sodium in Sweat, *Electroanalysis*, 2016, **28**, 1267–1275.
- 29 J. Hu, X. U. Zou, A. Stein and P. Bühlmann, Ion-Selective Electrodes with Colloid-Imprinted Mesoporous Carbon as Solid Contact, *Anal. Chem.*, 2014, **86**, 7111–7118.
- 30 X. U. Zou, L. D. Chen, C. Z. Lai and P. Bühlmann, Ionic Liquid Reference Electrodes With a Well-Controlled Co(II)/Co(III) Redox Buffer as Solid Contact, *Electroanalysis*, 2015, **27**, 602–608.
- 31 G. Inzelt, in *Handbook of Reference Electrodes*, eds. G. Inzelt, A. Lewenstam and F. Scholz, Springer, 2013, pp. 331–332.

## 3 EXPERIMENTAL INFORMATION

---



## EXPERIMENTAL INFORMATION

---

Included here are reagents, instruments and procedures that were common to several chapters.

### 3.1 Reagents

Multi-walled carbon nanotubes of 95 % purity (30–50 nm outer diameter, ~15  $\mu\text{m}$  length) were purchased from Chengdu Organic Chemicals Co. (Chengdu, Sichuan, China).

The calix[4]pyrrole phosphonate used as the ionophore for creatininium was prepared by the group of Professor Pablo Ballester at the Institute of Chemical Research of Catalonia, The Barcelona Institute of Technology, Spain.

[1-hexyl-3-methylimidazolium]<sup>+</sup>[tris(pentafluoroethyl)trifluorophosphate]<sup>-</sup> ([HMIM][FAP]) was obtained from VWR (Dublin, Ireland).

Polyvinyl butyral (PVB) B-98 was purchased from Químidroga S.A. (Barcelona, Spain).

All solutions were prepared with doubly distilled water (18.2 M $\Omega$  cm) from a Milli-Q water system (Millipore Corporation, Bedford, MA).

Urea (> 99.5 %) was obtained from GE Healthcare Bio-sciences AB (Uppsala, Sweden).

All further fine chemicals were obtained from Sigma-Aldrich (Spain or Ireland). These include: potassium tetrakis-3,5-bis(trifluoromethyl)phenylborate (KTFPB), poly(vinyl chloride) (PVC) of high molecular weight, 2-nitrophenyl-octyl ether (o-NPOE) of > 99 % purity, valinomycin (potassium ionophore I), potassium tetrakis(4-chlorophenyl)borate, bis(2-ethylhexyl)sebacate (DOS) of > 97 % purity, 4-tert-butylcalix[4]arene-tetraacetic acid tetraethyl ester(sodium ionophore X), potassium tetrakis(4-chlorophenyl)borate, and bis(2-ethylhexyl)sebacate, Nafion® 117 solution in a ~5% mixture of lower aliphatic alcohols and water, NaCl (analytical grade (AG)), KCl (AG), LiCl (AG), MgCl<sub>2</sub>·6H<sub>2</sub>O (AG), magnesium acetate tetrahydrate (99 %), creatinine (anhydrous > 98 %), acetic acid (96 %), and sodium lactate (99 %), methanol (anhydrous), tetrahydrofuran (anhydrous, 99.9 %) and poly(vinyl alcohol) (> 99 % hydrolysed, MW 89,000- 98,000) and HCl (fuming,  $\geq$  37 %).

Standard solutions of 1.413 and 12.88 mS/cm (25 °C) KCl from Mettler-Toledo GmbH (Greifensee, Switzerland) were used for calibration of the conductivity meter. Mettler-Toledo's measuring instruments were calibrated using the reference materials of the National Institute of Standards and Technology (NIST), Gaithersburg, USA.

### 3.2 Materials

*Circuitworks* conductive epoxy glue was purchased from Chemtronics (GA, USA).

## EXPERIMENTAL INFORMATION

---

Polished glassy carbon electrodes were (Sigradur®G, length 50 mm, diameter 3 mm) were inserted into Teflon® bodies to expose flat circular surfaces.

A 3D printing polylactic resin (PLA XXL True White filament) was bought from MakerBot Industries LLC (Brooklyn, NY, USA).

Polycarbonate membranes (reference: PC 100 47 TL, Albet) were purchased from Instrumentación Científica Técnica, S.L. (Spain).

### 3.2.1 Paper-based electrodes

Paper-based carbon electrodes were made by painting Number 5 Whatman™ filter papers (GE Healthcare Life Sciences) with screen-printable electrically conductive ink (122-49, Creative Materials, Inc., MA, USA). The paper-based Ag/AgCl pseudo-reference electrodes were also made with Number 5 filter papers that were painted with Ag/AgCl ink (113 – 09, Creative Materials, Inc., MA, USA). Platinum and gold papers were made by sputtering Number 5 filter papers with a 100 nm layer of the respective metal.

Paper-based electrodes were encased within a mask of polyester (ARCare 8259, Adhesives Research, Inc., PA, USA) with circular apertures exposed for deposition of working and reference electrodes respectively. This orifice exposed the electrochemically active surface of the electrode.

## 3.3 Instrumentation

Electromotive force (EMF) was measured with a high input impedance ( $10^{15} \Omega$ ) EMF16 data acquisition device from Lawson Laboratories, Inc. (Malvern, USA) unless otherwise stated. Impedance experiments were performed with a CHI660C Electrochemical Workstation from CHI Instruments, Inc. (USA). The impedance spectra were recorded in a frequency range from 100 kHz to 0.01 Hz using an excitation amplitude of 10 mV (Chapter 9), or 200 mV (Chapter 6), in a 0.1 M solution of the NaCl.

Measurements of pH were made with a GLP 21 pH meter using a Hamilton Polylyte lab probe (reference 238403). A conductivity meter (GLP 32, Crison Instruments S.A., Spain) was used to calibrate and validate conductivity measurements.

Double-junction 3 M Ag/AgCl/KCl (type 6.0726.100) reference electrodes from Metrohm AG containing 1 M LiOAc as ionic salt bridges were used for potentiometric measurements, except in Chapter 6, in which a double-junction Ag/AgCl reference electrode from Sigma-Aldrich, Dublin, was used. The single-junction reference electrode used in the *Lab-in-a-box* was the inner electrode of the aforementioned double-junction reference electrode with the outer junction removed.

The *EZO conductivity circuit* used in Chapter 8 and the *EZO pH circuit* used in Chapter 5 were produced by ATLAS Scientific LLC (NY, USA) and used in conjunction with an Arduino Nano V 3.1.

## EXPERIMENTAL INFORMATION

---

3D printing was performed with a MakerBot Replicator 2 (MakerBot Industries, LLC, Brooklyn, USA).

Atomic emission spectroscopy was performed with a Unicam 969 AA Spectrometer with an air-acetylene flame. The bandpass was 0.2 nm and the fuel flow was approximately 1L/minute. Sodium was determined by tracking emission at 589.0 nm, after diluting sample to within the linear range of 0 and 1 ppm. Potassium was determined by tracking emission at 766.5 nm after diluting sample to within the linear range of 0 and 2 ppm.

Platinum sputtering was performed with an ATC Orion 8-HV from AJA International Inc. (MA, USA) at 150 W, 3 mTorr, 20 sccm Argon as RF magnetron source in the case of platinum. Gold was applied with a sputtercoater (K575XD, Emitech, France) at 30 mA for 12.5 minutes in the case of gold.

### 3.4 Software

Calculations were carried out using *Microsoft Excel 2013* and *Matlab 2017*. Arduino sketches were written and compiled within the *Arduino 1.8.2 integrated development environment*. Data was collected and visually displayed upon a mobile phone running the Android version of the *Vernier Graphical Analysis* app, version 3.1.1 (build 8526) (Vernier Software & Technology).

Optical experiments were made with a DH-2000-BAL UV-Vis NIR using both deuterium and halogen sources, and monitored by a Maya 2000PRO spectrometer, both purchased from Ocean Optics, Inc.

### 3.5 Ion-selective membrane preparation

Potassium-selective membranes cocktails comprised: 2 wt % (18 mmol/kg) of valinomycin, 0.5 wt % (10 mmol/kg) of potassium tetrakis (4-chlorophenyl) borate (KTFPB), 32.8 wt % of poly(vinyl chloride) (PVC), and 64.7 wt % of bis(2-ethylhexyl) sebacate (DOS).

Creatinine-selective membrane cocktails were prepared by combining 3.2 mg of calix[4]pyrrole phosphonate ionophore (Figure 3.1), 1.0 mg of KTFPB, 31.9 mg of PVC and 63.9 of o-NPOE and sonicating in 1 mL of THF as described previously [1].

In all cases, these membranes were applied by drop-casting.

## EXPERIMENTAL INFORMATION

---

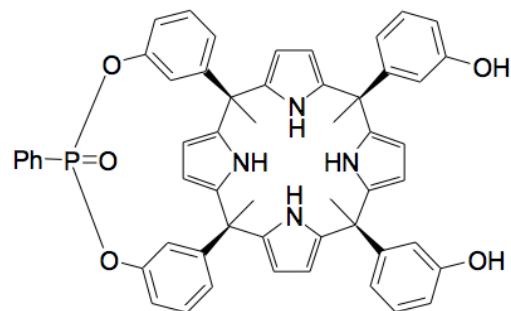


**Figure 3.1** The calix[4]pyrrole phosphonate used as ionophore for creatininium.

## EXPERIMENTAL INFORMATION

---

### 3.6 References

- 1 T. Guinovart, D. Hernández-Alonso, L. Adriaenssens, P. Blondeau, F. X. Rius, P. Ballester and F. J. Andrade, Characterization of a new ionophore-based ion-selective electrode for the potentiometric determination of creatinine in urine, *Biosens. Bioelectron.*, 2017, **87**, 587–592.

## 4 CRITICAL REVIEW:

### *Distributed electrochemical sensors: recent advances and barriers to market adoption*

---





## 4.1 Introduction

### 4.1.1 Scope

With the convergence of cloud computing, mobile devices and global connectivity, information can be now transmitted, stored, shared and accessed at any time, in any point of the planet, at near-zero cost. Combined with artificial intelligence, this technological revolution represents one of the most promising opportunities to solve some urgent global problems in healthcare, security, and environment worldwide (Figure 4.1).

Indeed, building networked sensing devices that allow faster, simpler and cheaper decision-making processes has become the new paradigm for the human development in the 21<sup>st</sup> century. However, leveraging the power of the global network to reshape social systems requires that methods to generate information move from centralized models to decentralized (distributed) approaches. Scientific instruments, traditionally conceived to be produced at small scale, confined to laboratories and operated by experts, must be now be redesigned for wide deployment across distributed networks and use by non-experts. The challenge to build new tools that must simultaneously combine robust information, low cost, unsupervised operation, i.e. no user intervention, as well as resilience to changes in the surroundings, may- in many cases- require a compromise, as described by Valcárcel and Cárdenas with the notion of “vanguard” analytical tools [1].



**Figure 4.1** Major fields of application for distributed electrochemical sensors (DECSS) and the value they contribute to the field

One important aspect to be considered in the development of decentralized system is the impact of their applications and the directions that the development of social systems may take upon their adoption. Although this topic exceeds the limits of this review, as it requires a multifaceted analysis, two major ideas need to be stressed. First, that today’s social systems –such as healthcare- cannot cope with current and future demands under an inclusive model of social development. It is not simply a matter of scale and investment. They were conceived to address the needs of a social structure that does not exist anymore. Second, the use of decentralized sensors is a way to unleash the power of the current developments in communications, cloud computing and artificial intelligence to provide one possible solution to this problem. Evidently, the

## CRITICAL REVIEW

---

development of these type of sensors is simply one more aspect of a social and technological trend towards decentralization, which will create new technological, economical and even moral dilemmas. Now more than ever, responsible research and innovation initiatives that help to analyse and understand the impact of the adoption of these technologies are needed. From the scientific domain we explore the space of possibilities to develop solutions, and we contribute to the analysis of the impact by generating robust scientific evidence, in the hope that these type of information triggers relevant discussions.

Interestingly, the development of tools for decentralized monitoring has moved at an uneven pace. Physical parameters such as heart rate, blood pressure, body temperature, position and speed, etc. can be now monitored using a plethora of portable and wearable systems available in the market. Sensing chemical properties, on the other hand, has moved at a much slower pace. The pioneering work by Diamond *et al.* on chemical sensing networks and body sensing networks provided the first steps on this field and a good overview on the problems to face, such as the  $1/f$  noise, the changes in sensitivity and the cost of the devices [2–4]. More than a decade later, and despite significant efforts in this area, many of these problems still persist, turning chemical sensing into the Achilles' heel of telemonitoring. For example, despite the clear interest in the remote monitoring of patients (telemedicine), the lack of suitable tools to generate (bio)chemical information outside the lab delays the progress of healthcare. Point-of-Care (POC) devices are a move on this direction since they provide information near the patient, but these instruments are expensive and require trained operators. It should be stressed that the adoption of mass-production criteria in the design of scientific instruments requires a shift in perspective, from the traditional instrument-centred to a user-focused approach. This is one of the main characteristics –and above all the main challenges– of this emerging field of decentralized instruments: the progress does not only depend on the development of outstanding technology (something that as chemists we know well how to do), but also (and critically) on the successful adaptation of this technology to the users' real needs and contexts (a task that requires truly multidisciplinary approaches) [3].

Gas sensors are the notable exception due to –at least in part– crucial differences in chemical activities in the gas phase. This critical review will not address these, instead focusing exclusively on chemical sensing within aqueous matrices. While it will be seen that analyses within liquids have many inherent challenges, it is pivotal to overcome these in order to access the wealth of chemical information within fluids such as blood, sweat, saliva, urine, and tears, as well as environmental and municipal waters. Furthermore, we will restrict discussion to sensors employing electrochemical techniques. Although there are many excellent sensors being reported based on optical and other techniques– even including a “wearable” mass spectrometer [5]– it is testament to the growth of the field that there is ample material for review even within the limited scope defined. While each analytical technique has both strengths and limitations, electrochemical methods have an inherent advantage particularly relevant to the wide distribution of sensors in the 21<sup>st</sup> century. Namely, they can connect the electrical to the chemical, to directly transduce chemical information into the digitally connected world.

Although there have been significant efforts in recent years to advance distributed electrochemical sensors (DECSs), with few exceptions, these have remained constrained to academic research and have not yet been proven commercially viable. Developments in this field usually follow different lines. First, the search for alternative detection approaches (since the advantages of lab-based techniques do not necessarily translate into

## CRITICAL REVIEW

---

benefits for decentralized settings) and the development of miniaturized autonomous devices. Second, the development of new materials that provide flexibility, adaptability and low cost, and their integration into daily-use objects (wearable devices, embedded sensors, etc.). Finally, the search for applications in different areas. This critical review will discuss both the advances in DECSs and the barriers to their real-world application with a particular focus on the last 5 years.

### 4.1.2 *Fields of need*

#### 4.1.2.1 Health and well-being

Telemonitoring of patients (telemedicine), i.e. the ability to generate clinically relevant information at home or at a patient's bedside, is part of the paradigm-shifting transformation of healthcare. DECSs have been recognized as potent tools in this area [6]. Telemedicine offers increased patient comfort and peace of mind as well as lowering costs for multiple medical processes: transport, prevention, hospitalization etc. Further to this, it can also facilitate a higher frequency of analyses- from irregular hospital visit testing, to regular monitoring as required- daily, for example. Without a doubt, home-based monitoring of glucose with a handheld glucometer is the archetype of DECSs, having improved the health outcomes and the quality of life for millions of people suffering from diabetes [7–9]. The glucometer offers a good point to reflect on the reasons of its success, what remains to be solved and the existing barriers for further developments (see Appendix 4).

As a rule, the value of the information generated is directly connected to the decision that it will enable. The glucometer is then a singular case, since glucose levels require frequent monitoring during the day, the number of people suffering diabetes is large and it has been steadily increasing (and is expected to continue growing). This has created a substantial market that has driven decades of research and investment in this area. Thus, analogies with other clinically relevant analytes should be made with caution, since sampling frequencies and decisions associated to abnormal levels might be significantly different. Similar handheld devices *have* in fact been developed for other enzymatically-detected analytes, including creatinine, lactate, ketone, cholesterol, uric acid, and haemoglobin (Table 4.1). However, unlike the case of glucose, the need to monitor these is often not strong enough to overcome a poor user experience and high cost (see Appendix 4). Even within well-established glucose sensing, much room regarding these aspects remains for improvement [10, 11].

Sampling is another significant barrier to the adoption of these tools, particularly when it involves invasive approaches such as the lancing of blood from a finger [12]. Consequently, and as the current medical paradigm primarily references blood, numerous studies are investigating the relationship of analyte levels in blood to other bodily fluids [10]. In the case of glucose, these include interstitial fluid [10], ocular fluid [13], sweat [14, 15], saliva [16], and urine [17]. Moving to detection in other fluids may lower the discomfort of adoption, facilitate incorporation of non-invasive sensors into wearable or otherwise embedded sensors, and possibly extend the sensor's life time without calibration beyond the maximum recorded time of approximately two weeks (in the case of glucose) [10]. However, significant work still needs to be performed in this area in order to find meaningful correlations with existing parameters.

## CRITICAL REVIEW

**Table 4.1** Commercialized devices for medically relevant analytes and their retail prices (Sources of prices listed are included in Appendix 4).

Analyte	Device name	Device price	Price per test strip
Glucose	Contour Next	\$14.75	\$0.69
Lactic acid	Lactate scout	\$350	\$2.42
Glucose, Cholesterol, Uric Acid, Haemoglobin	EasyTouch GCHb	\$53.50	\$0.16 glucose
	Multi Function Monitoring System		\$2.15 cholesterol \$0.64 uric acid \$0.58 haemoglobin
Glucose beta ketone	Bruno Pharma Innovations MD6	\$97.99	\$3.00 ketone \$0.60 glucose
Creatinine	Statsensor Analyzer XPress	\$756.04	\$5.70

### 4.1.2.2 Environmental monitoring

Natural water systems are rich in data critical to the environment as well as human health. Indeed, regulations such as the European Water Framework Directive require the restoring of water bodies to a ‘good status’ [18]. Along with this, the environmental metrology market is expected to increase over the coming years. Despite these environmental and economical imperatives, a recent review of the area by Namour *et al.* concluded that “None of analysed publications present a micro-sensor totally validated in laboratory, ready for tests under real conditions in the field” [18]. They concluded that the major factor limiting real-use applications was the ruggedness of the receptor towards environmental conditions. Blaen *et al.* have noted that the traditional strategy of “send a technician, take an isolated sample, send it to the laboratory and analyse it” will no longer satisfy the need for information to be resolved temporally as well as spatially as studies continue to indicate that nutrient concentrations can exhibit highly dynamic and non-linear behaviour in both time and space [19]. A further consideration is that the integrity of water is vulnerable to contamination when being sampled and transported for *ex situ* analysis [20]. These needs would be best satisfied by the deployment of autonomous chemical sensing units at a scale that would necessitate them having relatively low-cost.

Ions- including heavy metals- are targets of environmental analysis and ion-selective electrodes (ISEs) are the classical analytical tool for this. A recent review by Crespo summarized the key advantage of using ion-selective electrodes (ISEs) for water analysis as “direct information on so-called free or un-complexed ion activities, even within complex environmental and biomedical matrices” [20]. While the performance requirements for many cations are already being met, anions- such as nitrate, nitrite, and phosphate- are also important targets for environmental studies, however, ISEs for these are currently inadequate in selectivity, sensitivity, and detection limits.

## CRITICAL REVIEW

---

Amperometric detection using screen-printed electrodes have been reported for nitrate [21, 22], nitrite [22], and phosphate detection [23, 24]. An excellent review of screen-printed electrodes in this context was written by Hayt and Marty, and references multiple electrochemical detection techniques for heavy metals as well as organic contaminants [23].

A further limiting factor impeding deployment is the sensing receptor's ruggedness towards the environment which currently requires frequent replacement or calibration. Given these considerations, it is clear why the group of Diamond have chosen to use optical methods for their autonomous sensing units of anions in natural waters, compromising on measuring the *direct ion activity* in order to achieve sufficient analytical performance and avoid deterioration of the receptor [25, 26].

### 4.1.2.3 Homeland security

In a time of increasing concern for preventing terrorist attacks, there is a growing need for tools that can detect threats early. Where traditional tools have been expensive, bulky and few in number- primarily located at borders such as airports, a modern approach would involve tools that are inexpensive, miniaturized and widely distributed. Electrochemical sensors are well suited to this, and as such are beginning to be explored for homeland security applications.

The 'Solid-state forensic finger', or 'Lab on a finger' reported by the group of Wang is illustrative of this [27]. Their glove-based sensor used a voltammetric method to detect gunshot residue and nitroaromatic explosive compounds upon surfaces. While these measurements were not strictly made in an aqueous solution- instead analysing microparticles in contact with a solid-state electrolyte- they highlighted how electrochemical techniques can bring low-footprint sensors to the frontlines of early threat detection.

## 4.2 Challenges and advances in the field of distributed sensors

### 4.2.1 Challenges and advances in the analytical performance of distributed sensors

#### 4.2.1.1 Redefining performance: How good is good enough?

The "traditional" analytical parameters, especially the race for the limits of detection, has been the established way to compare techniques. However, when dealing with decentralized systems, sensors need to be as good as required by the intended application, and *only* that good [28]. In this context, *goodness* demands that the sensor can perform determinations in untreated real samples (such as whole blood), that the measurements are *robust*, and that the factors affecting the cost and simplicity are also considered. While soft from a technical point of view, *robustness* is a very useful concept, used to indicate determinations performed in real samples are impervious to environmental conditions. In this way, the *goodness* results from the combination of several traditional figures of merit (such as sensitivity, selectivity, limit of detection etc.) *as appropriate to target, matrix and conditions*. Here we divide the question of analytical performance into: what library of targets can we measure; and how robust our measurements are.

#### 4.2.1.2 What targets should be in our sensing library?

What type of information is needed from decentralized devices? This is a medical, environmental, and security question, rather than an analytical problem, and it is critical for the adoption of these new tools that it be approached as such. Unfortunately, it is not always properly answered. Scientific curiosity may find the search for new biomarkers at ultralow levels more attractive than the determination of potassium or sodium in blood (something that could be considered a “solved problem”). However, it is clear that at this stage, instead of the detection of cancer or a rare disease, telemedicine is focused on the remote monitoring of chronic conditions or the early detection of acute conditions requiring a fast response (e.g., a heart attack). Thus, while scope remains for expansion of the library of detectable substrates, home-use diagnostic kits for cancer or diagnostics of rare diseases seem still ill-conceived.

Limits of detection remain a very important parameter when dealing with detection of threats or environmental issues. However, many of the species that require monitoring in chronic conditions, such as potassium, creatinine, uric acid, etc., are at relatively high levels of concentration in blood (in the mM to sub mM range). These substances can be determined with high accuracy and precision within the laboratory, but they are extremely challenging to measure in a decentralized context. Monitoring potassium in blood, for example, is important to follow some chronic kidney conditions, hyper or hypokalemic paralysis disorders, etc. In the laboratory, potassium can be determined with ISEs (not to mention atomic spectroscopy), but it is still challenging to find simple, robust and affordable tools to do this determination at home. Interestingly, when using a lancet capillary blood is sampled, while clinical labs normally vein blood is collected. This and other issues –such as the contamination with intracellular potassium due to haemolysis of red cells while passing through the small puncture created by the lancet- may have significant impact in the results, and have to be accounted for when developing a solution for telemedicine. For other analytes, such as nitrate in environmental waters, the limitation is selectivity due to its low concentrations relative to other more lipophilic anions. All in all, beyond the development of a suitable detection scheme, the challenge is of analytical nature—from sampling to reporting of results-.

In general, there are many species for which electrochemical methods already meet the required action standards. Cations such as  $\text{Ca}^{2+}$ ,  $\text{Na}^+$ ,  $\text{K}^+$ , and  $\text{H}^+$  can be meaningfully monitored in freshwater and seawater samples [20]. Unfortunately, the case is more challenging for anions, as was exemplified by nitrate. In addition, a variety of clinically relevant small neutral molecules can be determined in blood using enzymatic sensors. Several examples are included within Table 4.1. Beyond ions determined by ISEs and small molecules accessible through enzymatic detection, technologies to track protein levels are being developed, with applications such as cancer diagnostics [29], but, as it was mentioned above, the relevance of these tools in a distributed context remains unclear.

The reliability of sensors that are already available also requires close scrutiny when medical decisions are in question. While decision-makers across a spectrum of industries remain divided as to wearables could replace routine healthcare services, 55 % of healthcare decision makers from regulatory bodies say these devices are not yet sufficiently accurate or reliable for diagnosis [30]. In this light, the *vanguard-rearguard* analytical

## CRITICAL REVIEW

---

strategy proposed by Válcárcel and Cárdenas seems conservative [1] as it proposes that samples flagged as critical in preliminary screening analysis be followed up with more reliable analysis before decision making. In many cases electrochemical sensors have already demonstrated adequate analytical performance to satisfy the action standards of use cases in the health, environmental, and security spheres. Of course, as with all research, room remains for improvement- however, as will be argued here- it is the questions of usability and affordability that in most cases present the bottlenecks to commercialization and adoption. For this to occur, all three aspects must act in concert, for like a wheel, its utility is ultimately limited by the weakest of its spokes. The key for distribution of chemical sensors is therefore to maintain the analytical performance of laboratory instruments- *at least to the degree that is meaningful within the given context*- while improving the usability and affordability. Additional considerations must be given to the mechanical and chemical wherewithal of the sensors to operate *ex laboratorium*.

### 4.2.1.3 How robust are our determinations?

The selection of sensing materials must take several criteria into account in order to align with the needs of distributed sensors. This is especially the case for wearable sensors, whose contact with skin necessitates that materials be non-toxic as well as flexible to conform to the curvature of the body [31]. Furthermore, they must be both resilient in structure and in response to the demands of the stretching and bending associated with bodily motion. Substrates such as plastics and textiles have been established as meeting these requirements, however, only recently did the group of Wang demonstrate the steady performance of sensors undergoing stretching of the sensing material itself, both with inks incorporating elastomeric binders [32] and with carbon nanotube-based sensors [33]. Similarly, their work with temporary tattoo-based sensors has shown the viability of this platform [34]. Comparably robust performance has also been demonstrated by paper-based sensors [35]. Because much of this work relies upon using carbon nanotubes, attention must be given to preventing contact with skin or finding alternative materials. The same applies to other materials that perform well but have associated toxicity issues. Sometimes, miniaturization and encapsulation of a device in a more rigid structure is used in order to avoid deformations and isolate the sensor. A sensing watch to monitor sweat composition has been proposed by Diamond *et al.* (Figure 4.2A) [36], and miniaturized devices that can be incorporated into garments have been also developed. In these situations, microfluidics systems must be incorporated to bring the sample to the detection zone. In an interesting twist, Wang *et al.* have recently proposed a wearable potentiostat incorporated into a ring to perform monitoring of chemical compounds in air (Figure 4.2B) [37].

## CRITICAL REVIEW

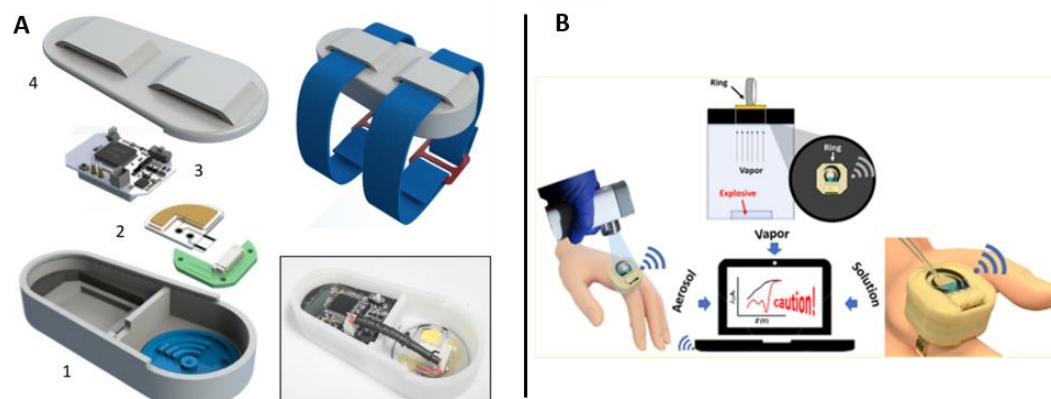


**Figure 4.2** A: ‘Sweatch’ platform for sodium monitoring in sweat (from [36]) with horizontal arrangement of electronic and fluidic components consisting of 1: sweat harvesting device in 3d-printed platform base; 2: fluidic sensing chip, 3: electronic data logger and battery, and 4: 3D-printed upper casing. B: Ring-based potentiostat for threat detection (from [37]).

As well as the mechanical considerations addressed above, an ideal sensor would also be *chemically robust*, meaning that it would maintain performance without deterioration due to its environment due to “*changes in the chemistry of the sensing surface that inevitably occur through exposure to the real world*”, as Diamond *et al.* put it [3]. This is perhaps the greatest challenge of all in moving from sensors of laboratory scale and expense, to those tailored to distributed applications. Real uses cases typically involve determinations in complex matrices such as whole blood, or water monitoring by un-serviced devices where electrode surface changes limit sensors to a single measurement before contamination becomes prohibitive. One significant advancement in this regard for enzymatic electrodes has been the addition of a diffusion limiting membrane to improve the chemical robustness by protecting the electrode from direct contact with the sample, thereby avoiding fouling (among other functions) [28].

The recent review by Crespo referred to drift values, pointed out that even the best (monovalent) ISE under controlled laboratory conditions experiences voltage drifts correspondent to a 1 % loss in precision per day [20]. It is therefore clear that extended exposure to natural freshwater- let alone seawater- would render such a sensor inviable within a day without recalibration. Constant monitoring would therefore seem impractical. There are two general approaches to mitigating this dilemma: single-use disposable sensors- as in the case of glucose test strips; or frequent calibration through fluid management- as in the case of ISEs in laboratory autoanalyzers. As far as we are aware, the frequent calibration approach has yet to be demonstrated in a decentralized setting, although it may prove the most practical solution for autonomous remote environmental monitoring.

The use of disposable sensors is a way to avoid problems of modification of the surface due to continuous interactions with the sample. Economic factors are in this case paramount. The choice of commodity materials and mass manufacturing process to build the sensors has become an increasingly important topic, as it will be discussed below.



## CRITICAL REVIEW

### 4.2.2 Challenges and advances in the usability of decentralized sensors

#### 4.2.2.1 Miniaturization

Since it was declared in 1965 [38], the field of electronics has followed Moore's Law, doubling the density of transistors in integrated circuits every two years until today, where it finds itself hitting the limits of pitch resolution- we shall see if tomorrow these limits can be stretched. Although the field of electrochemical sensors does not have such a law to follow, it does indeed seem to be following a similar trajectory of miniaturization with concomitant reductions in cost (Figure 4.3).

The advent of solid-contact electrodes [39], new substrates and modern fabrication techniques, has allowed the miniaturization of electrochemical sensors. Works such as smart bandages [40, 41], paper-based sensors [34, 42–46], temporary tattoo-based sensors [47, 48], and wearable sensor arrays with integrated flexible electronics [15, 49, 50], exemplify the creativity and accomplishment within the realm of miniaturization. While in theory, amperometric methods lose detectability when miniaturized (where potentiometric methods do not), this has not proven prohibitive to real-use cases, making the question of technique moot to miniaturisation. Indeed, examples of electrochemical sensors using both techniques have been successfully miniaturized, indicating that this is not a bottleneck to the advancement and commercialization of DECSs.

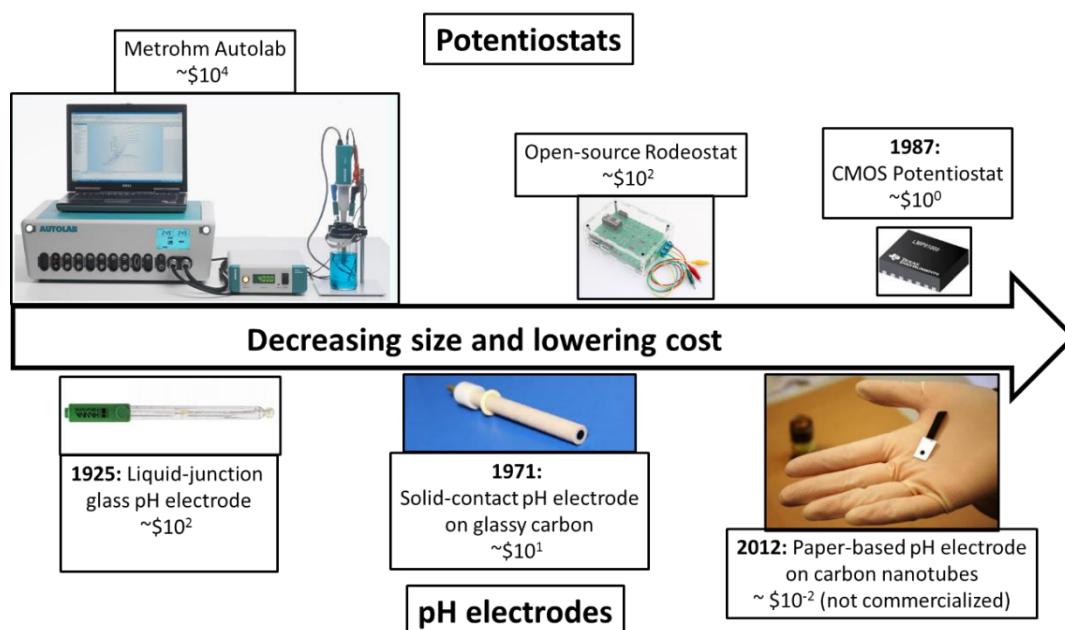


Figure 4.3 Decreasing size and cost of potentiostats (above) and pH electrodes (below)

#### 4.2.2.2 The calibration problem and sensor reproducibility

Electrochemical sensors- whether voltammetric, potentiometric, or amperometric- all rely on measuring a current or a voltage. This value can only be translated into meaningful information- such as the concentration or activity of an analyte- in relation to other known values, i.e. the sensor must be calibrated. While physical sensors- such as the ten or more found in today's smartphones [51, 52] can be manufactured with excellent

## CRITICAL REVIEW

---

reproducibility, chemical sensors exhibit far less stability in time and show considerable inter-sensor variability. The origins of this instability are in fact the same environmental processes responsible for signal generation [53], and can therefore likely never be eliminated entirely but rather, minimized below problematic levels. In this regard, the ideal chemical sensor would be highly reproducible and as such, be ready for a direct measurement by the user, without extraneous calibration steps.

In the case of the test strips used for glucose, each batch of sensors is calibrated in the factory and remains stable for a shelf-life of approximately one year. A code particular to each batch of sensors must be entered into the glucometer to calibrate the measurement. This effort is viewed as worthwhile by patients whose health outcomes depend on regular glucose readings. While some studies still raise serious questions as to their accuracy [11], overall the glucometer is considered a success in terms of analytical performance. This performance has, to a degree, been extended to other analytes such as creatinine, uric acid, cholesterol, lactate, and ketones, using the same analytical principle. However, as it was previously discussed, the lack of the complex combination of factors required to build a compelling business case for monitoring these analytes- in contrast to glucose- have made the combination of calibration hassle and significant cost, un-worthwhile to many potential users.

Potentiometric sensors- despite their many merits- have been even more disappointing in their reproducibility and long-term stability. While work towards improving inter-sensor reproducibility has advanced- the current state-of-the-art being the ISEs upon colloid-imprinted mesoporous carbon with inclusion of a redox couple [54]- long-term stability remains an issue that may make this class of sensors unamenable to factory calibration. As a user-friendly solution to the '*calibration problem*' of potentiometric sensors remains to be found they have yet to find applications without the handling of trained personnel (e.g. the pH meter). Bobacka *et al.* have proposed an interesting experimental approach to minimize these problems [55] that has been preliminarily tested by Parrilla *et al.* in the development of wearable sensors using commercial carbon fibres as a substrate [56].

### 4.2.2.3 Compatible electronic instrumentation

While the electronics industry is well advanced, the DECSs market is both very new and very small, and as such, there remains a challenge in bridging existing electronics with emerging sensors. There have been two approaches in response to this: the first is the ad-hoc use of *Maker* electronics platforms such as *Arduino*, *Yoctopuce* and *Raspberry Pi* (to name just a few) and the second is the use of purpose-built electronics such as the flexible electronics of Gao and co-workers [15, 49, 50], the custom-designed *Shimmer* board incorporated into the *SwEatch* platform reported by the group of Diamond [36], the miniaturized instrumentation reported by the Wang group [37, 47] or the wireless electrochemical system with radiofrequency reading developed by *GoSense* [40, 57] There is no doubt that electronics of greater suitability and lower cost will continue to be made available as the chemical sensor sector matures and thereby provides the necessary economic pull.

## CRITICAL REVIEW

---

### 4.2.2.4 Connectivity and data security

For widespread distribution of electrochemical sensors to be realized, developers will need to address the interdependent questions of connectivity and data security. This has been highlighted by the recent hacking of devices (or *things*) which typically have significantly lower security than personal computers [58–60]. Fortuitously, there is currently a convergence of technologies that provide an optimal environment for the emergence of DECSs: the highly advanced electronics industry complete with flexible and printed electronics, the burgeoning infrastructure stack of IOT, as well as new cryptographic protocols. Major companies such as IBM and Accenture, as well as the government of Estonia are pursuing cryptographically protected blockchains for medical record keeping [61]. Such blockchains are replacing centralized databases to allow health data to be managed in a decentralized way, have an immutable audit trail, establish data provenance, while being robust and available (without a central point of failure), with improved security and privacy [62]. Second-generation technologies such as *The Tangle*, first exemplified by *Iota* [63], are also posturing for platform of choice of the IOT, which we foresee as including the Internet Of *Chemical* Things. If we add to this mix the emergence of artificial intelligence, it would appear that a fertile ecosystem awaits suitable electrochemical sensors. Significantly, today's average user has a sophisticated computer in their pocket with multiple connectivity protocols and a native familiarity with data intensive applications- the customer is savvy and ready.

Proof of concepts in connectivity are illustrated by Smart bandages with NFC readings [40] as well as the Bluetooth-enabled *Shimmer board* used in a sodium sensing wearable [36]. In summary, excellent developments are taking place in connectivity and data security and chemical sensors have the challenge of catching up to the mature technologies around them.

### 4.2.2.5 Powering the revolution

Unlike the questions of electronics, connectivity and data security, there remain significant issues when it comes to powering distributed sensors. Researchers are addressing the power question both through *evolutionary* and *revolutionary* angles. The evolutionary approach is simply to use established battery technologies. Unfortunately, these can be bulky in wearable uses and more significantly have lifetimes that leave much to be desired. Indeed, although half of consumers consider that wearables can improve healthcare management, they also express concern about their wearable health patches running out of battery [30]. In the case of remote autonomous sensors for environmental applications, battery lifetimes must be on the order of months, if not years, to be viable.

On the revolutionary side, there is a 'demand pull' for elimination of batteries altogether. As noted in a recent market research report, "...*Wireless Sensor Networks ... Internet of Things... and embedded sensors cannot achieve 90% of their potential if batteries need to be accessed for charging or replacement. Hundreds of billions deployed is the dream with many inaccessible, e.g. in concrete, underwater and on billions of trees*" [64]. Fortunately, work is underway in energy harvesting and self-powered systems [65–68] as well as paper-based batteries (Figure 4.4A) [69] and paper-based fuel cells [70], and it is foreseen that these may converge with electrochemical sensors to form self-powered DECSs. A particularly interesting approach has been

## CRITICAL REVIEW

proposed by Wang *et al.*, in using the electrical power generated by an enzymatic reaction of naturally occurring lactate in sweat, coupled to an electrochemical sensor (Figure 4.4B) [71]. While the approach has not been yet exploited, it depicts the broad range of possibilities to be yet explored in this field.

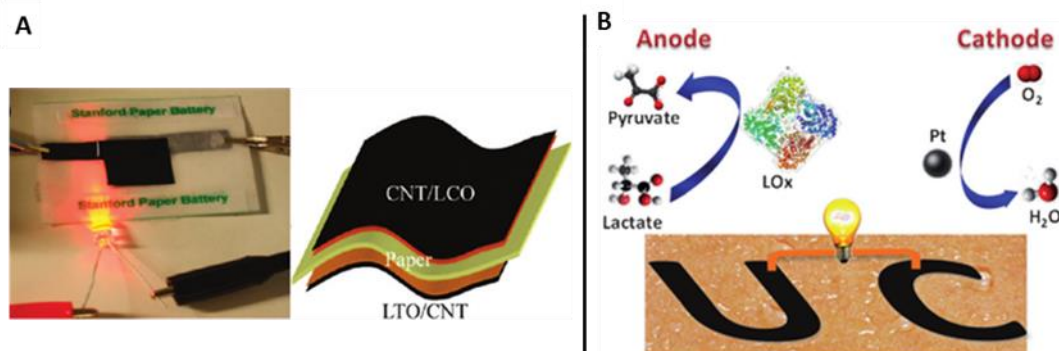


**Figure 4.4** A: Paper-based Li-ion battery (adapted from [69]). B: Epidermal biofuel cell for energy-harvesting from sweat (from [71]).

### 4.2.3 Challenges and advances in the affordability of decentralized sensors

The question of cost is critical to the widespread adoption of DECSs. Even in the oft-touted success story of the glucometer, the sensing strips remain prohibitively expensive for the majority of the world's diabetics. Considering that this technology has more than 40 years of optimization behind it and an annual market in excess of \$10 Billion [72], lowering the cost of sensing systems for other analytes is an even greater challenge. Considerations of cost must be holistic, taking into account all previously mentioned aspects: the materials used and manufacturing process, the electronics incorporated, the power consumed, and- if calibration is required- all liquids and fluid management components associated. This can be summarized as the electrochemical technique and associated instrumentation, and the material and manufacturing of the sensor. Electrochemical techniques themselves each have different requirements in instrumentation and power consumption. Generally, potentiometric methods use simpler instrumentation than amperometric methods. That said, complete potentiostats integrated into circuits are now available (Figure 4.5), making the instrumentation argument a non-sequitur. However, the passive technique of potentiometry generally consumes less power, and this may be advantageous in designing miniaturised low-cost sensing systems. In any case, it is also true that the target substances and range of applications of these techniques are different, so they must be seen as complementing rather than competing with each other.

Some materials lend themselves to lower-cost fabrication methods. Paper is notable for this, as it lends itself to ink-jet printing. Also, many plastics are amenable to screen printing. Sensors using ultra low-cost electrode substrates have already been showcased. These include paper [28, 29, 35–39, 65–70] textiles [41, 31], rubber [79], cotton yarns [80], and commercial carbon fibres [56]. Alternatives to expensive noble metals such as gold, platinum, and silver are being found in carbon-based materials [81], metal oxides [82–85], conductive polymers and ionic liquids [86]. Films of noble metals on the order or micron thickness have also been used recently by sputtering upon paper [46, 78], or by loading cellulosic material with metal salts before burning off the supporting material [87]. Both of these approaches maintained, or indeed enhanced, the properties of

## CRITICAL REVIEW

the precious metal while minimising the cost through miniaturisation. A pioneering work into affordable and utilitarian substrates by Wang and coworkers embedded voltammetric and chronoamperometric measurements into underwear by screen-printing carbon inks directly onto the elastic waistbands [31].

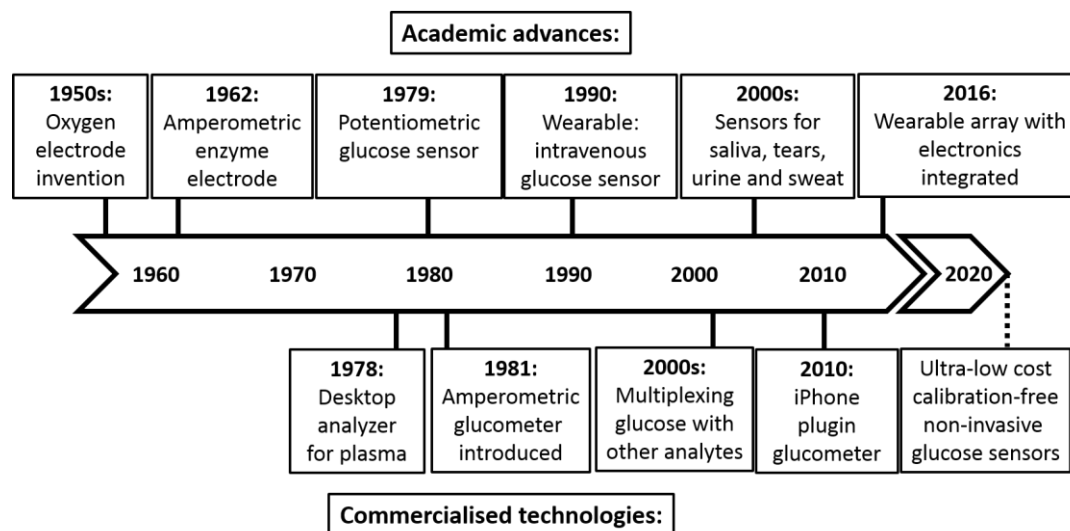


**Figure 4.5** Timeline of major academic and commercial advances in electrochemical glucose sensors (References are included in Appendix 4).

## 4.3 Summary and outlook

### 4.3.1.1 State-of-the-bottleneck

It is evident that any approach to bringing electrochemical sensors out of the laboratory and into distributed adoption must be holistic, taking into account the materials, the calibration question, power supply, connectivity and instrumentation involved. All aspects of performance, usability and affordability must be addressed in a balanced manner. Nonetheless, a quick survey of the field suggests that current investigations are leaning heavily on the side of advancing analytical performance. As usability seems to be the facet most in need of attention, this review has placed emphasis here. Were usability to be sufficiently addressed, we consider that costs could be subsequently lowered to affordable levels; trying to sell low-cost sensors that are not user-friendly would be putting the cart before the horse.

Putting all of this together and surveying all of the requirements for the deployment of user-friendly electrochemical sensors, the calibration question arises as the major hurdle. Bakker has written an excellent discussion of whether calibration-free sensors can in fact be realized [28]. The alternative- calibration *in situ* appears unattractive due the complications of fluids and fluid management, but remains to be tested extensively.

A further limitation that is perhaps not discussed frequently in the scientific community is the disparity in funding for the sector as compared with IT. While a VC can expect to be reunited with their money within 2-3 years when investing in IT start-ups, a biotech company's product may need closer to 10 years of

## CRITICAL REVIEW

development before being approved [88] or indeed ultimately failing, as in the high-profile case of *Theranos* [89]. As the regulatory question must always be answered, the investment barrier only adds to the argument for ultra-low cost and simple approaches.

### 4.3.1.2 The future is interdisciplinary

The group of Citterio has recently demonstrated the inkjet printing of potentiometric ion-sensing devices upon paper without subsequent conditioning steps (Figure 4.6) [90]. Their sensors demonstrated reproducible Nernstian sensitivities and more impressively, reproducible standard potentials of  $\pm 5.1$  mV for the  $\text{Na}^+$  sensor and  $\pm 2.8$  mV for the  $\text{K}^+$  sensor. These features make this the most advanced work in the field of calibration-free single-use potentiometric sensors. While works such as this are excellent from an academic perspective, like most sensor studies, the bubble of specialization limits their realization in practical use. While one group focusses on ultra-low cost chemical sensors, another advances their reproducibility, while yet another optimizes flexible electronics. For DECSs to be truly realized, interdisciplinary collaborations are needed from the initial conception of sensing systems- not merely the fitting together of disparate components after the fact. A survey of 900 cross-industry decision makers in healthcare, insurance, regulatory bodies, app developers, telcos and medical-technology companies considered internet companies, telecom operators and app developers as the top three preferred partners for healthcare [30]. Perhaps the efforts of chemists to incrementally advance analytical performance would be better directed towards forming interdisciplinary collaborations to solve usability issues. This could include for example, collaborations with engineers to automate calibration and industrial designers to integrate chemical sensors with power and instrumentation solutions from conception.

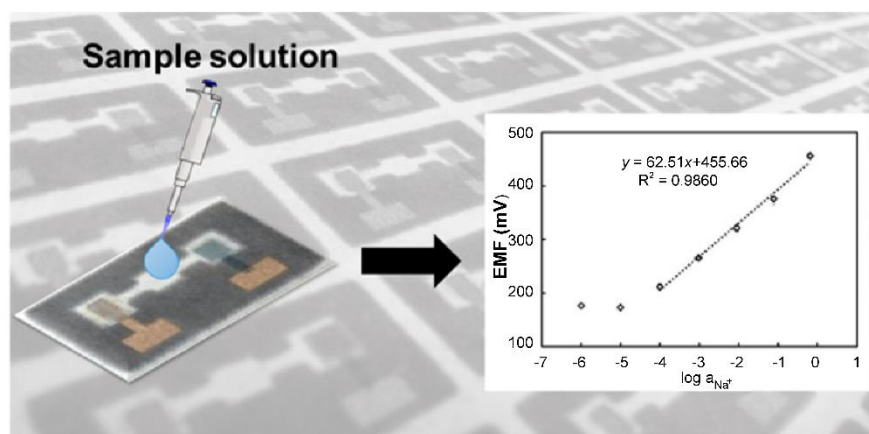


**Figure 4.6** Fully inkjet-printed paper-based potentiometric sensing device for sodium and potassium (from [90]).

This is perhaps one of the key issues to face in the future of this field. Research -and particularly development- in electronics can be ubiquitously distributed in places that promote the collaborative activity. Even more, during the last decades a real explosion of low-cost electronic tools to build sensing platforms at the mass market level has encouraged and inspired people from all disciplines to explore and expand the field of decentralized sensors. Chemical sensors have not reached the same dynamics. Chemical laboratories are

## CRITICAL REVIEW

---

centralized and for many reasons not particularly open to everyone. To build appealing sensing platforms, whether it is a ring, a watch or a patch, a deep understanding of the end-user needs and routines is required. A pioneer work in this field, the *Glucowatch* [91], is an example of how important it is to include industrial designers at an early stage in order to avoid serious market problems [92]. Finding ways to include- from the outset- doctors, nurses, patients and designers for building appealing decentralized chemical sensors is a key priority.

This paper has presented the perspective that while excellent progress is being made towards distributed electrochemical sensors, the major bottleneck limiting their successful deployment is in the usability. Fundamentally new approaches may need to be explored to overcome this barrier, and user-centred thinking is essential to this process. The future is bright for the distribution of electrochemical sensors. To realize this future, as scientists we need to look outside the lab to the brilliant opportunities that are emerging in complementary fields.

## 4.4 References

- 1 M. Valcárcel and S. Cárdenas, Vanguard-rearguard analytical strategies, *TrAC - Trends Anal. Chem.*, 2005, **24**, 67–74.
- 2 D. Diamond, R. Byrne and D. Diamond, Chemo/bio sensor networks, *Nat. Mater.*, 2006, **5**, 421–424.
- 3 D. Diamond, S. Coyle, S. Scarmagnani and J. Hayes, Wireless sensor networks and chemo-/biosensing, *Chem. Rev.*, 2008, **108**, 652–679.
- 4 D. Diamond, Internet-scale sensing., *Anal. Chem.*, 2004, **76**, 278A–286A.
- 5 P. I. Hendricks, J. K. Dalgleish, J. T. Shelley, M. A. Kirleis, M. T. McNicholas, L. Li, T.-C. Chen, C.-H. Chen, J. S. Duncan, F. Boudreau, R. J. Noll, J. P. Denton, T. A. Roach, Z. Ouyang and R. G. Cooks, Autonomous in Situ Analysis and Real-Time Chemical Detection Using a Backpack Miniature Mass Spectrometer: Concept, Instrumentation Development, and Performance, *Anal. Chem.*, 2014, **86**, 2900–2908.
- 6 M. Labib, E. H. Sargent and S. O. Kelley, Electrochemical Methods for the Analysis of Clinically Relevant Biomolecules, *Chem. Rev.*, 2016, **116**, 9001–9090.
- 7 J. Wang, Electrochemical glucose biosensors., *Chem. Rev.*, 2008, **108**, 814–25.
- 8 E. Witkowska Nery, M. Kundys, P. S. Jeleń and M. Jönsson-Niedziółka, Electrochemical glucose sensing – is there still room for improvement?, *Anal. Chem.*, 2016, **88**, 11271–11282.
- 9 K. Tonyushkina and J. H. Nichols, Glucose meters: a review of technical challenges to obtaining accurate results., *J. Diabetes Sci. Technol.*, 2009, **3**, 971–80.
- 10 D. Bruen, C. Delaney, L. Florea and D. Diamond, Glucose sensing for diabetes monitoring: Recent developments, *Sensors*, 2017, **17**, 1–21.
- 11 R. Hellman, Glycemic Variability in the Use of Point-of-Care Glucose Meters, *Diabetes Spectr.*, 2012, **25**, 135–140.
- 12 C. Zuliani and D. Diamond, Opportunities and challenges of using ion-selective electrodes in environmental monitoring and wearable sensors, *Electrochim. Acta*, 2012, **84**, 29–34.
- 13 M. Chu, T. Shirai, D. Takahashi, T. Arakawa, H. Kudo, K. Sano, S. Sawada, K. Yano, Y. Iwasaki, K. Akiyoshi, M. Mochizuki and K. Mitsubayashi, Biomedical soft contact-lens sensor for in situ ocular biomonitoring of tear contents, *Biomed. Microdevices*, 2011, **13**, 603–611.
- 14 H. Lee, C. Song, Y. S. Hong, M. S. Kim, H. R. Cho, T. Kang, K. Shin, S. H. Choi, T. Hyeon and D.-H. Kim, Wearable/disposable sweat-based glucose monitoring device with multistage transdermal drug delivery module, *Sci. Adv.*, 2017, **3**, e1601314.
- 15 W. Gao, S. Emaminejad, H. Y. Y. Nyein, S. Challa, K. Chen, A. Peck, H. M. Fahad, H. Ota, H. Shiraki, D. Kiriya, D.-H. Lien, G. A. Brooks, R. W. Davis and A. Javey, Fully integrated wearable sensor arrays for multiplexed in situ perspiration analysis, *Nature*, 2016, **529**, 509–514.
- 16 P. Abikshyeet, V. Ramesh and N. Oza, Glucose estimation in the salivary secretion of diabetes mellitus patients., *Diabetes. Metab. Syndr. Obes.*, 2012, **5**, 149–54.
- 17 H. Dong Park, K. Joung Lee, H. Ro Yoon and H. Hyun Nam, Design of a portable urine glucose monitoring system for health care, *Comput. Biol. Med.*, 2005, **35**, 275–286.



## CRITICAL REVIEW

---

- 18 P. Namour, M. Lepot and N. Jaffrezic-Renault, Recent trends in monitoring of European water framework directive priority substances using micro-sensors: A 2007-2009 review, *Sensors*, 2010, **10**, 7947–7978.
- 19 P. J. Blaen, K. Khamis, C. E. M. Lloyd, C. Bradley, D. Hannah and S. Krause, Real-time monitoring of nutrients and dissolved organic matter in rivers: Capturing event dynamics, technological opportunities and future directions, *Sci. Total Environ.*, 2016, **569–570**, 647–660.
- 20 G. A. Crespo, Recent Advances in Ion-selective membrane electrodes for in situ environmental water analysis, *Electrochim. Acta*, 2017, **245**, 1023–1034.
- 21 N. Plumeré, J. Henig and W. H. Campbell, Enzyme-Catalyzed O(2) Removal System for Electrochemical Analysis under Ambient Air: Application in an Amperometric Nitrate Biosensor., *Anal. Chem.*, 2012, **49945**, 1–13.
- 22 S. I. R. Malha, J. Mandli, A. Ourari and A. Amine, Carbon black-modified electrodes as sensitive tools for the electrochemical detection of nitrite and nitrate, *Electroanalysis*, 2013, **25**, 2289–2297.
- 23 A. Hayat and J. L. Marty, Disposable screen printed electrochemical sensors: Tools for environmental monitoring, *Sensors*, 2014, **14**, 10432–10453.
- 24 L. Gilbert, A. T. A. Jenkins, S. Browning and J. P. Hart, Development of an amperometric, screen-printed, single-enzyme phosphate ion biosensor and its application to the analysis of biomedical and environmental samples, *Sensors Actuators, B Chem.*, 2011, **160**, 1322–1327.
- 25 D. Cogan, C. Fay, D. Boyle, C. Osborne, N. Kent, J. Cleary and D. Diamond, Development of a low cost microfluidic sensor for the direct determination of nitrate using chromotropic acid in natural waters, *Anal. Methods*, 2015, **7**, 5396–5405.
- 26 I. M. Perez De Vargas Sansalvador, C. D. Fay, J. Cleary, A. M. Nightingale, M. C. Mowlem and D. Diamond, Autonomous reagent-based microfluidic pH sensor platform, *Sensors Actuators, B Chem.*, 2016, **225**, 369–376.
- 27 A. J. Bandonkar, A. M. O’Mahony, J. Ramírez, I. A. Samek, S. M. Anderson, J. R. Windmiller and J. Wang, Solid-state Forensic Finger sensor for integrated sampling and detection of gunshot residue and explosives: towards ‘Lab-on-a-finger’, *Analyst*, 2013, **138**, 5288.
- 28 E. Bakker, Can Calibration-Free Sensors Be Realized?, *ACS Sensors*, 2016, **1**, 838–841.
- 29 C. K. Dixit, K. Kadimisetty, B. A. Otieno, C. Tang, S. Malla, C. E. Krause and J. F. Rusling, Electrochemistry-based approaches to low cost, high sensitivity, automated, multiplexed protein immunoassays for cancer diagnostics, *Analyst*, 2016, **141**, 536–547.
- 30 Ericsson.com/consumerlab, *From healthcare to homecare*, 2017.
- 31 B. S. Shim, W. Chen, C. Doty, C. Xu and N. A. Kotov, Smart electronic yarns and wearable fabrics for human biomonitoring made by carbon nanotube coating with polyelectrolytes, *Nano Lett.*, 2008, **8**, 4151–4157.
- 32 A. J. Bandonkar, R. Nuñez-Flores, W. Jia and J. Wang, All-Printed Stretchable Electrochemical Devices, *Adv. Mater.*, 2015, **27**, 3060–3065.

## CRITICAL REVIEW

---

- 33 A. J. Bandodkar, I. Jeerapan, J.-M. You, R. Nuñez-Flores and J. Wang, Highly Stretchable Fully-Printed CNT-Based Electrochemical Sensors and Biofuel Cells: Combining Intrinsic and Design-Induced Stretchability, *Nano Lett.*, 2016, **16**, 721–727.
- 34 D. Nilsson, T. Kugler, P.-O. Svensson and M. Berggren, An all-organic sensor–transistor based on a novel electrochemical transducer concept printed electrochemical sensors on paper, *Sensors Actuators B*, 2002, **86**, 193–197.
- 35 C. W. Foster, J. P. Metters and C. E. Banks, Ultra flexible paper based electrochemical sensors: Effect of mechanical contortion upon electrochemical performance, *Electroanalysis*, 2013, **25**, 2275–2282.
- 36 T. Glennon, C. O’Quigley, M. McCaul, G. Matzeu, S. Beirne, G. G. Wallace, F. Stroiescu, N. O’Mahoney, P. White and D. Diamond, ‘SWEATCH’: A Wearable Platform for Harvesting and Analysing Sweat Sodium Content, *Electroanalysis*, 2016, **28**, 1283–1289.
- 37 J. R. Sempionatto, R. K. Mishra, A. Martín, G. Tang, T. Nakagawa, X. Lu, A. S. Campbell, K. M. Lyu and J. Wang, Wearable Ring-Based Sensing Platform for Detecting Chemical Threats, *ACS Sensors*, 2017, **2**, 1531–1538.
- 38 G. E. Moore, Cramming more components onto integrated circuits, *Proc. IEEE*, 1998, **86**, 82–85.
- 39 R. W. Cattrall, H. Freiser and R. W. Cattrall, Coated Wire Ion Selective Electrodes, *Anal. Chem.*, 1971, **43**, 1905–1906.
- 40 P. Kassal, J. Kim, R. Kumar, W. R. De Araujo, I. M. Steinberg, M. D. Steinberg and J. Wang, Smart bandage with wireless connectivity for uric acid biosensing as an indicator of wound status, *Electrochem. commun.*, 2015, **56**, 6–10.
- 41 T. Guinovart, G. Valdés-Ramírez, J. R. Windmiller, F. J. Andrade and J. Wang, Bandage-Based Wearable Potentiometric Sensor for Monitoring Wound pH, *Electroanalysis*, 2014, **26**, 1345–1353.
- 42 M. Novell, M. Parrilla, G. A. Crespo, F. X. Rius and F. J. Andrade, Paper-based ion-selective potentiometric sensors., *Anal. Chem.*, 2012, **84**, 4695–702.
- 43 M. Novell, T. Guinovart, P. Blondeau, F. X. Rius and F. J. Andrade, A paper-based potentiometric cell for decentralized monitoring of Li levels in whole blood., *Lab Chip*, 2014, **14**, 1308–14.
- 44 Z. Nie, C. A. Nijhuia, J. Gona, X. Chea, A. Kumacheb, A. W. Martine, M. Narovlyanska and G. M. Whitesides, Electrochemical sensing in paper-based microfluidic devices, *Lab Chip*, 2010, **10**, 477–483.
- 45 J. Yang, Y. G. Nam, S. K. Lee, C. S. Kim, Y. M. Koo, W. J. Chang and S. Gunasekaran, Paper-fluidic electrochemical biosensing platform with enzyme paper and enzymeless electrodes, *Sensors Actuators, B Chem.*, 2014, **203**, 44–53.
- 46 M. Parrilla, R. Cánovas and F. J. Andrade, Paper-based enzymatic electrode with enhanced potentiometric response for monitoring glucose in biological fluids., *Biosens. Bioelectron.*, 2017, **90**, 110–116.
- 47 J. Kim, I. Jeerapan, S. Imani, T. N. Cho, A. Bandodkar, S. Cinti, P. P. Mercier and J. Wang, Noninvasive Alcohol Monitoring Using a Wearable Tattoo-Based Iontophoretic-Biosensing System, *ACS Sensors*, 2016, **1**, 1011–1019.

## CRITICAL REVIEW

---

- 48 J. Ray Windmiller, A. Jairaj Bandodkar, G. Valdés-Ramírez, S. Parkhomovsky, A. Gabrielle Martinez and J. Wang, Electrochemical Sensing Based on Printable Temporary Transfer Tattoos, *Chem Commun*, 2012, **48**, 6794–6796.
- 49 H. Y. Y. Nyein, W. Gao, Z. Shahpar, S. Emaminejad, S. Challa, K. Chen, H. M. Fahad, L. C. Tai, H. Ota, R. W. Davis and A. Javey, A Wearable Electrochemical Platform for Noninvasive Simultaneous Monitoring of Ca<sup>2+</sup> and pH, *ACS Nano*, 2016, **10**, 7216–7224.
- 50 W. Gao, H. Y. Y. Nyein, Z. Shahpar, H. M. Fahad, K. Chen, S. Emaminejad, Y. Gao, L. C. Tai, H. Ota, E. Wu, J. Bullock, Y. Zeng, D. H. Lien and A. Javey, Wearable Microsensor Array for Multiplexed Heavy Metal Monitoring of Body Fluids, *ACS Sensors*, 2016, **1**, 866–874.
- 51 Sensors Overview Android Developers, [https://developer.android.com/guide/topics/sensors/sensors\\_overview.html](https://developer.android.com/guide/topics/sensors/sensors_overview.html), (accessed 15 December 2017).
- 52 D. Nield, All the Sensors in Your Smartphone, and How They Work, <http://fieldguide.gizmodo.com/all-the-sensors-in-your-smartphone-and-how-they-work-1797121002>, (accessed 15 December 2017).
- 53 A. Radu, S. Anastasova, C. Fay, D. Diamond, J. Bobacka and A. Lewenstam, Low cost, calibration-free sensors for in situ determination of natural water pollution, *Proc. IEEE Sensors*, 2010, 1487–1490.
- 54 J. Hu, X. U. Zou, A. Stein and P. Bühlmann, Ion-Selective Electrodes with Colloid-Imprinted Mesoporous Carbon as Solid Contact, *Anal. Chem.*, 2014, **86**, 7111–7118.
- 55 U. Vanamo and J. Bobacka, Instrument-free control of the standard potential of potentiometric solid-contact ion-selective electrodes by short-circuiting with a conventional reference electrode, *Anal. Chem.*, 2014, **86**, 10540–10545.
- 56 M. Parrilla, J. Ferré, T. Guinovart and F. J. Andrade, Wearable Potentiometric Sensors Based on Commercial Carbon Fibres for Monitoring Sodium in Sweat, *Electroanalysis*, 2016, **28**, 1267–1275.
- 57 M. Novell, Universitat Rovira i Virgili, 2015.
- 58 This Teen Hacked 150,000 Printers to Show How the Internet of Things Is Shit - Motherboard, [https://motherboard.vice.com/en\\_us/article/nzqayz/this-teen-hacked-150000-printers-to-show-how-the-internet-of-things-is-shit](https://motherboard.vice.com/en_us/article/nzqayz/this-teen-hacked-150000-printers-to-show-how-the-internet-of-things-is-shit), (accessed 9 December 2017).
- 59 Veerendra G G, Hacking Internet of Things (IoT) A Case Study on DTH Vulnerabilities, .
- 60 The 5 Worst Examples of IoT Hacking and Vulnerabilities in Recorded History | IoT For All, <https://www.iotforall.com/5-worst-iot-hacking-vulnerabilities/>, (accessed 9 December 2017).
- 61 25+ blockchain companies in healthcare to know | 2017, <https://www.beckershospitalreview.com/lists/25-blockchain-companies-in-healthcare-to-know-2017.html>, (accessed 8 December 2017).
- 62 T.-T. Kuo, H.-E. Kim and L. Ohno-Machado, Blockchain distributed ledger technologies for biomedical and health care applications, *J. Am. Med. Informatics Assoc.*, 2017, **24**, 1211–1220.
- 63 [iota.org](https://iota.org/), <https://iota.org/>, (accessed 15 December 2017).
- 64 P. Harrop, Battery Elimination in Electronics and Electrical Engineering 2018-2028: IDTechEx, 2017.
-

## CRITICAL REVIEW

---

- 65 C.-C. Wu, W.-Y. Chuang, C.-D. Wu, Y.-C. Su, Y.-Y. Huang, Y.-J. Huang, S.-Y. Peng, S.-A. Yu, C.-T. Lin and S.-S. Lu, A Self-Sustained Wireless Multi-Sensor Platform Integrated with Printable Organic Sensors for Indoor Environmental Monitoring, *Sensors*, 2017, **17**, 715.
- 66 M. Israr-Qadir, S. Jamil-Rana, O. Nur and M. Willander, Zinc Oxide-Based Self-Powered Potentiometric Chemical Sensors for Biomolecules and Metal Ions, *Sensors*, 2017, **17**, 1645.
- 67 S. Lin and J. Xu, Effect of the Matching Circuit on the Electromechanical Characteristics of Sandwiched Piezoelectric Transducers, *Sensors*, 2017, **17**, 329.
- 68 Z. G. Wan, Y. K. Tan and C. Yuen, Review on energy harvesting and energy management for sustainable wireless sensor networks, *2011 IEEE 13th Int. Conf. Commun. Technol.*, 2011, 362–367.
- 69 L. Hu, H. Wu, F. La Mantia, Y. Yang and Y. Cui, Thin, flexible secondary Li-ion paper batteries., *ACS Nano*, 2010, **4**, 5843–8.
- 70 J. P. Esquivel, J. R. Buser, C. W. Lim, C. Domínguez, S. Rojas, P. Yager and N. Sabaté, Single-use paper-based hydrogen fuel cells for point-of-care diagnostic applications, *J. Power Sources*, 2017, **342**, 442–451.
- 71 W. Jia, G. Valdés-Ramírez, A. J. Bandodkar, J. R. Windmiller and J. Wang, Epidermal Biofuel Cells: Energy Harvesting from Human Perspiration, *Angew. Chemie Int. Ed.*, 2013, **52**, 7233–7236.
- 72 IDTechEx, Biosensors for Point of Care Testing: Technologies Applications Forecasts Sample Pages, 2017.
- 73 C. Diekmann, C. Dumschat, K. Cammann and M. Knoll, Disposable reference electrode, *Sensors Actuators B. Chem.*, 1995, **24**, 276–278.
- 74 W. Dungchai, O. Chailapakul and C. S. Henry, Electrochemical detection for paper-based microfluidics., *Anal. Chem.*, 2009, **81**, 5821–6.
- 75 E. J. Maxwell, A. D. Mazzeo and G. M. Whitesides, Paper-based electroanalytical devices for accessible diagnostic testing, *MRS Bull.*, 2013, **38**, 309–314.
- 76 J. A. Adkins, E. Noviana and C. S. Henry, Development of a Quasi-Steady Flow Electrochemical Paper-Based Analytical Device, *Anal. Chem.*, 2016, **88**, 10639–10647.
- 77 W. J. Lan, X. U. Zou, M. M. Hamed, J. Hu, C. Parolo, E. J. Maxwell, P. Bühlmann and G. M. Whitesides, Paper-based potentiometric ion sensing, *Anal. Chem.*, 2014, **86**, 9548–9553.
- 78 R. Cánovas, M. Parrilla, P. Blondeau and F. J. Andrade, A novel wireless paper-based potentiometric platform for monitoring glucose in blood, *Lab Chip*, 2017, **17**, 2500–2507.
- 79 M. Cuartero, J. S. del Río, P. Blondeau, J. A. Ortuño, F. X. Rius and F. J. Andrade, Rubber-based substrates modified with carbon nanotubes inks to build flexible electrochemical sensors., *Anal. Chim. Acta*, 2014, **827**, 95–102.
- 80 T. Guinovart, M. Parrilla, G. A. Crespo, F. X. Rius and F. J. Andrade, Potentiometric sensors using cotton yarns, carbon nanotubes and polymeric membranes, *Analyst*, 2013, **138**, 5159–5504.
- 81 G. A. Crespo, S. Macho and F. X. Rius, Ion-Selective Electrodes Using Carbon Nanotubes as Ion-to-Electron Transducers, *Anal. Chem.*, 2008, **80**, 1316–1322.

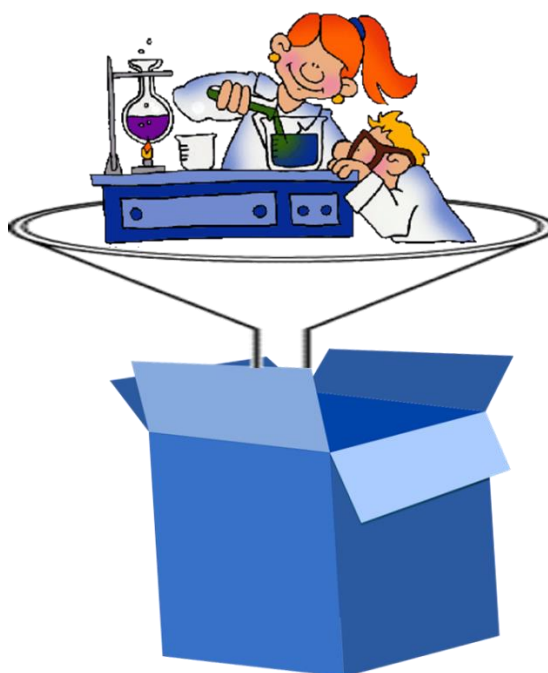
## CRITICAL REVIEW

---

- 82 Q. Li, V. Kumar, Y. Li, H. Zhang, T. J. Marks and R. P. H. Chang, Fabrication of ZnO Nanorods and Nanotubes in Aqueous Solutions, *Chem. Mater.*, 2005, **17**, 1001–1006.
- 83 A. Chrissanthopoulos, S. Baskoutas, N. Bouropoulos, V. Dracopoulos, D. Tasis and S. N. Yannopoulos, Novel ZnO nanostructures grown on carbon nanotubes by thermal evaporation, *Thin Solid Films*, 2007, **515**, 8524–8528.
- 84 M. Zhao, Z. Li, Z. Han, K. Wang, Y. Zhou, J. Huang and Z. Ye, Synthesis of mesoporous multiwall ZnO nanotubes by replicating silk and application for enzymatic biosensor., *Biosens. Bioelectron.*, 2013, **49**, 318–22.
- 85 Z. H. Ibusoto, N. Jamal, K. Khun and M. Willander, Sensors and Actuators B : Chemical Development of a disposable potentiometric antibody immobilized ZnO nanotubes based sensor for the detection of C-reactive protein, *Sensors Actuators B. Chem.*, 2012, **166–167**, 809–814.
- 86 S. Anastasova-Ivanova, U. Mattinen, A. Radu, J. Bobacka, A. Lewenstam, J. Migdalski, M. Danielewski and D. Diamond, Development of miniature all-solid-state potentiometric sensing system, *Sensors Actuators, B Chem.*, 2010, **146**, 199–205.
- 87 D. C. Christodouleas, F. C. Simeone, A. Tayi, S. Targ, J. C. Weaver, K. Jayaram, M. T. Fernández-Abedul and G. M. Whitesides, Fabrication of Paper-Templated Structures of Noble Metals, *Adv. Mater. Technol.*, 2017, **2**, 1600229.
- 88 R. E. Herzlinger, Why Innovation in Health Care is so Hard, *Harv. Bus. Rev.*, 2006, **84**, 58–66.
- 89 I. Lapowsky, Theranos' Scandal Exposes the Problem With Tech's Hype Cycle | WIRED, <https://www.wired.com/2015/10/theranos-scandal-exposes-the-problem-with-techs-hype-cycle/>, (accessed 13 December 2017).
- 90 N. Ruecha, O. Chailapakul, K. Suzuki and D. Citterio, Fully Inkjet-Printed Paper-Based Potentiometric Ion-Sensing Devices, *Anal. Chem.*, 2017, **89**, 10608–10616.
- 91 S. K. Garg, R. O. Potts, N. R. Ackerman, S. J. Fermi, J. A. Tamada and H. P. Chase, Correlation of fingerstick blood glucose measurements with GlucoWatch biographer glucose results in young subjects with type 1 diabetes., *Diabetes Care*, 1999, **22**, 1708–14.
- 92 L. Isaacs, What Happened to the GlucoWatch Biographer?, <http://www.diabetesmonitor.com/glucose-meters/what-happened-to-the-gluowatch.htm>, (accessed 16 January 2018).

## 5 LAB-IN-A-BOX: A device for user-friendly potentiometric analysis

---



## 5.1 Introduction

### 5.1.1 *The realities of externalities*

Recent years have seen a growing trend in analytical chemical research towards creating new platforms for decentralized analysis. Accordingly, there has been a boom in publications describing new sensors for everything from ions to proteins. Amongst these, many efforts have been directed towards decentralization and miniaturization and the use of new low-cost platforms such as the “hot topic” of paper-based sensors. In addition to being touted as “low-cost”, these are often trumpeted as “simple”. Limiting the scope of this discussion to electrochemical methods- and potentiometric methods in particular- there is a fundamental weakness in many of these approaches; they answer just one piece of the analytical problem, without addressing the complete mandala of the analytical process. Indeed, the past decade has seen exciting implementations of paper being used for: microfluidics [1], energy harvesting [2], energy storage [3–5], fuel cells [6], dosing valves [7], printed circuitry [8], pumps [9], as well as the printing of electrochemical instruments and displays upon plastics [10]. In general however, the majority of these have reported the advancement of one aspect, yet stopped short of incorporating all of the components required for a usable decentralized analytical device.

In this, a parallel can be drawn to the ever-promising, yet little-realized field of microfluidics. For decades, microfluidics has been *the next big thing* that is just around the corner, promising to herald in a new age of devices miniaturising complex processes that previously required sophisticated instrumentation and trained personnel through the magic of the *Lab-on-a-chip*. Indeed, the eponymously named journal frequently features images of futuristic chips with microfluidic tubes leading outside the scope of the image (Figure 5.1, left). The absurdity of the situation is that these tubes typically connect the tiny microfluidic chips with large tangles of fluidic connections to voluminous reagent bottles and large pumps with considerable power requirements (Figure 5.1, right) [11, 12]. These critical elements are disregarded as cumbersome externalities to the sexy microfluidic chips. Recently however, a second wave of microfluidics has replaced the tubing and pumps with the inherent wicking properties of paper- simultaneously eliminating the power requirement [11, 13, 14]. This has proven to be an elegant solution, even if it does lack the high sophistication (read, complexity) of lithographically fabricated *Lab-on-a-chip* devices.

## LAB-IN-A-BOX

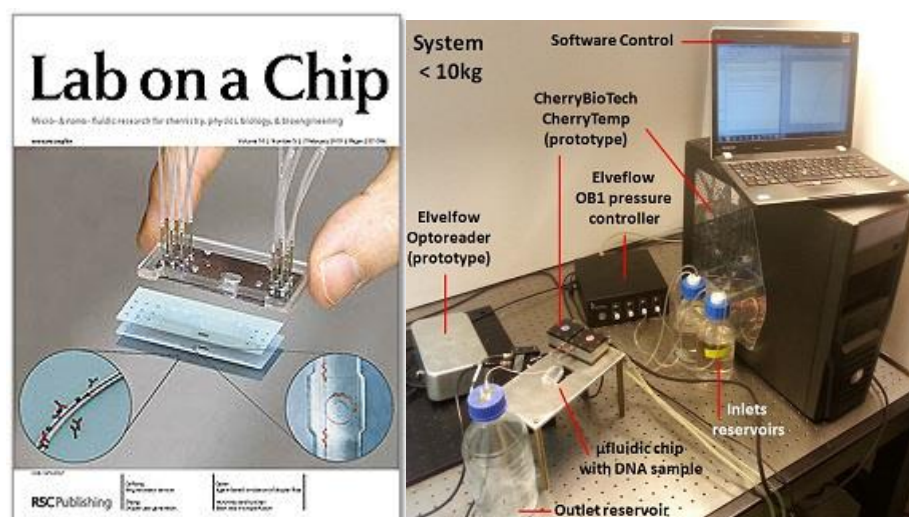


**Figure 5.1** Left: Cover of *Lab on a Chip* and; Right: the reality of a Lab on a Chip.

A parallel can be drawn between traditional pumped microfluidics and potentiometric sensors for decentralised applications- both rely on awkward externalities. In the case of microfluidics, these comprise the aforementioned pumps and the associated power requirement. In the case of ‘decentralized’ potentiometric sensors, these externalities include power, electronic instrumentation, data transmission, treatment and display, as well as the grand challenge of calibration with the associated fluid management and expertise required. The inconvenient truth is that a potentiometric sensor (and to be fair, almost all kinds of chemical sensors) is useless on its own without the aforementioned components. In fact, many reported ‘sensors’ could more accurately be described as ‘electrodes’- that is, a subsystem of a theoretically-realizable sensor.

The problem of externalities in distributed potentiometric sensor systems can be conceptually divided up and thought of as consisting of a *dry*, electronic aspect, and a *wet*, fluidic aspect. If electrochemical sensors are indeed to emerge from the laboratory and find use by non-expert users, these complexities must not be treated as externalities, but must rather be addressed holistically. This thesis- and this chapter in particular, treats these not as externalities, but rather, as the essence of the problem itself.

### 5.1.2 *The dry problem*

In a fundamental sense, the dry aspect has already been solved through advances in electronics. Nevertheless, the user-oriented integration of this aspect still remains to be well established, with few implementations realized to date; the lack of an economic driving force may be all that is required for this to advance rapidly. One example of the progress of the *dry*, instrumental aspect has been provided by the group of Whitesides’, who made a good step in this direction by fabricating an open source handheld electrochemical analysis device, comparable to a glucometer but flexible in scope to be used not only for the determination of various analytes, but also to facilitate multiple electrochemical techniques [15]. While this was an excellent contribution, it has not reached widespread adoption in the four years since its divulgation; one explanation for this could be that



there is no economic incentive to manufacture sensors for a low-cost device made by a third party with an open-source philosophy- instead, companies generally prefer to create their own isolated technological ecosystems. Additionally, the specialized nature of this non-standardised technology does not yet lend itself to interoperability of components such as sensors and instrumentation. Although the *Universal mobile electrochemical detector* of Whitesides' is capable of performing potentiometric measurements, it still remains far from user-friendly as it does not address the *wet*, calibration problem.

### 5.1.3 The wet problem

The *wet* aspect on the other hand, remains elusive and fundamentally limiting. Depending on the particular application, it may consist of calibration steps, sample conditioning, filtration and dilution. The sample, as well as any standard solutions need to be introduced to the sensor, necessitating fluid management; if the sensor is to be reused, it will most likely require washing to preclude fouling.

The *wet* problem of calibration has been discussed in some detail in Chapters 2 and 4. The group of Diamond has in fact reported the construction of an automated fluid management systems to calibrate sensors and make determinations of phosphate [16] and pH [17], incorporated both the *dry* and *wet* aspects. These however, used colorimetric detection methods. As this same research group publishes at the cutting edge of potentiometric sensors with a view towards establishing distributed sensing networks, it is notable that they have not yet presented an automated calibration system for a potentiometric sensor. As this would surely be useful, and would seem not to be non-obvious, the question arises as to whether it is tenable, or if some intractable problems prohibit its realization.

### 5.1.4 The value proposition of the Lab-in-box

One model for evaluating the value proposition of innovations is the *cost-benefit analysis model*. With diagnostic sensors in mind, the consideration of variability in complexity/cost and in the variability of performance generates four possible combinations (Figure 5.2). Amongst these, the quadrant of high complexity and low performance (in red) is of course, to be avoided. The (blue) area where high complexity is tolerated in order to achieve high performance, or the (yellow) area where low performance is tolerated as the complexity also remains low, each offer attractive propositions and have meritorious applications, as exemplified by quantitative ELISA analysis and qualitative lateral flow assays (such as the well-known pregnancy test), respectively. The green quadrant where high performance is achieved with low complexity and cost associated is naturally, the holy grail of the analyst. Were it to be brought to fruition, the *Lab-in-a-box* concept may qualify for this category, as it would be a push-button device yielding quantitative diagnostic information.

## LAB-IN-A-BOX

---

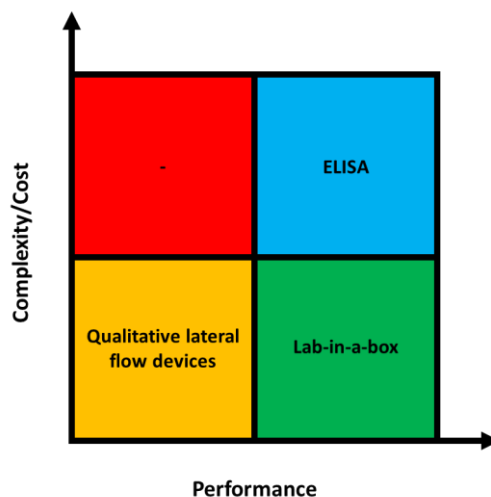


**Figure 5.2** Cost-benefit analysis diagram for diagnostic sensors

### 5.1.5 *Lab-in-a-box* prototypes

This chapter describes the development of ideas and prototypes which seek to realize an automated device for analyses using ion-selective electrodes. With the working name of *Lab-in-a-box*, the goal of the project was to combine fluid management for calibration, sample introduction and washing of potentiometric sensors, with the electronics required for signal detection. The scope was open to be as automated and miniaturised as possible. The focus was not on a particular analyte so much as a versatile system which could be tailored towards a given analyte by exchanging the working electrode and the calibration solutions.

The *Lab-in-a-box* was developed in stages of prototypes and the results are presented here following this progression. There were three major iterations in its evolution. The *Mark I* prototype was centred around a box, but externalised the pump, the flow cell, the solutions and the potentiometer- in truth, only the microcontroller and valves were housed within the box. Attempts to advance this to a *Mark II* prototype were focussed on incorporating each of these elements within a single unit, to truly put the *Lab* into the box. The third prototype presented came at the problem from a different direction by replacing the microcontroller, valves, and pump, with a little manual effort by the user- this was the *Mark III: Low-Tech Lab-in-a-box*.

## 5.2 *Lab-in-a-box*: Mark I

### 5.2.1 *Mark I: experimental*

The first prototype was conceived to manage four different solutions: two standard solutions, dilute  $\text{MgCl}_2$  solution (0.1 mM) for washing of the electrodes, and the sample. These solutions were pulled with negative pressure by a peristaltic pump (Minipuls3 from Gilson, Villiers, France) located after the flow cell. In this way, a single pump could draw from any of the four solutions, depending on how three valves were actuated (Figure 5.3). The valves in question were solenoid-driven isolation valves (075T3MP12-32 from Bio-Chem Fluidics Inc., NJ, USA). As these required 12 V to operate, the (5 V) *Arduino Uno* microcontroller could not operate them natively, and accordingly, an external power supply of 12 V was required, the switching of which was

## LAB-IN-A-BOX

made possible by incorporation of three transistors, one corresponding to each valve. The transistors were D13009K N-type procured from Premier Farnell Ltd. (Madrid, Spain). Power to the valves was supplied by a 12 V, 2A power adapter connected to the electrical mains.

Several flow cells were tested (See Figure 5.4). In each case, these were custom-made to house either a *KZT-5 low-leakage reference electrode* (Innovative Instruments, Inc., Florida, USA) or a single-junction Ag/AgCl reference electrode, and a solid-contact ion-selective membrane upon a glassy-carbon electrode, each of which were screwed into the threaded flow cell.

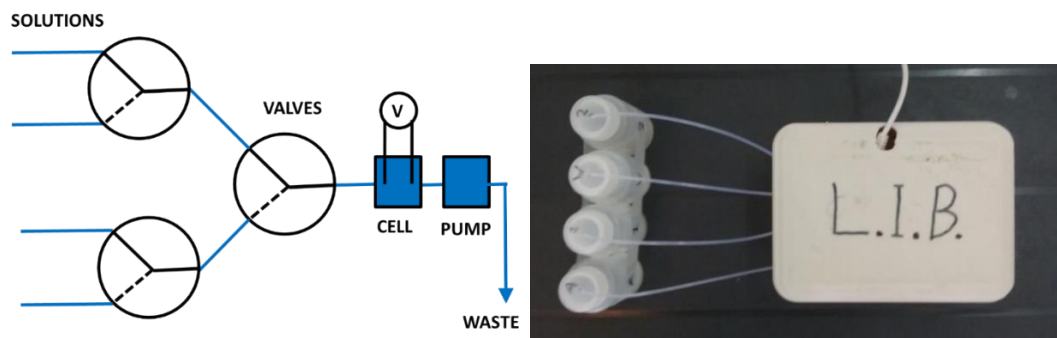


**Figure 5.3** Left: A schematic representation of the *Lab-in-a-box*. Right: an image of the *Lab-in-a-box* (L.I.B.) with the lid in place.

The fluidic system ran through PTFE tubing of 0.8 mm inner diameter (008T16-080-20) provided by Omnifit Labware (Cambridge, UK). Connections were made with ferrules (CFL-2A) from Vivi AG International (Schenkon, Switzerland) and PVC tubing of 1.295 mm inner diameter from Spetec GmbH (Erding, Germany). Components- initially just the valves and microcontroller- were housed within a custom built box produced by a 3D printer (100 mm x 132 mm with a height of 80 mm).

A potassium-selective membrane cocktail was prepared as described in Chapter 3 and drop-cast upon a glassy carbon electrode of 3 mm diameter; to account for the screwing in of the electrode however, the volume of membrane cocktail was limited to 15  $\mu\text{L}$  and the electrode surface itself was retracted within its housing by approximately 2 millimetres to ensure that the membrane did not become detached during insertion into the flow cell.

The peristaltic pump was used and set to flow at 1.25 mL/minute. The footprint of this pump was very considerable, at 15 x 17.5 x 18 cm, with a weight of 4 kg. The pattern of flow between the four solutions was directed by the isolation valves which were in turn controlled by an *Arduino Uno* with custom-written sketches. In general, the pattern was to calibrate with the two standard solutions in order of progressive concentration, and select the sample (with intermediate concentration) between these. Following this, the electrodes were washed with the dilute  $\text{MgCl}_2$  solution. The duration for which each sample was selected was varied from 30 seconds to 5 minutes, ensuring that a steady-state signal was reached for each solution.

## LAB-IN-A-BOX

---



**Figure 5.4** An exemplary range of the flow cells fabricated for and tested with glassy carbon and paper electrodes.

### 5.2.2 Mark I: Results

#### 5.2.2.1 Determinations of potassium in standard solutions

Potassium was selected as a model analyte, and the relevant ISE was incorporated within the *Lab-in-a-box*. On each of four consecutive days, the same protocol was run. In practice, this simply entailed pressing the reset button on the microcontroller to restart the programmed procedure, or *sketch*. The protocol was to calibrate the electrode with solutions of  $10^{-4}$  and  $10^{-2}$  M KCl, make an intermediate determination of a sample, and wash the electrodes. In the first case, the “sample” was a standard solution known to contain  $10^{-3}$  M KCl. Each solution was selected for a duration of 60 seconds. The procedure was repeated 5 times on each day, for a total of 20 minutes of operation per day. The instrumental response recorded during the five calibrations made on one day is shown in Figure 5.5.

## LAB-IN-A-BOX

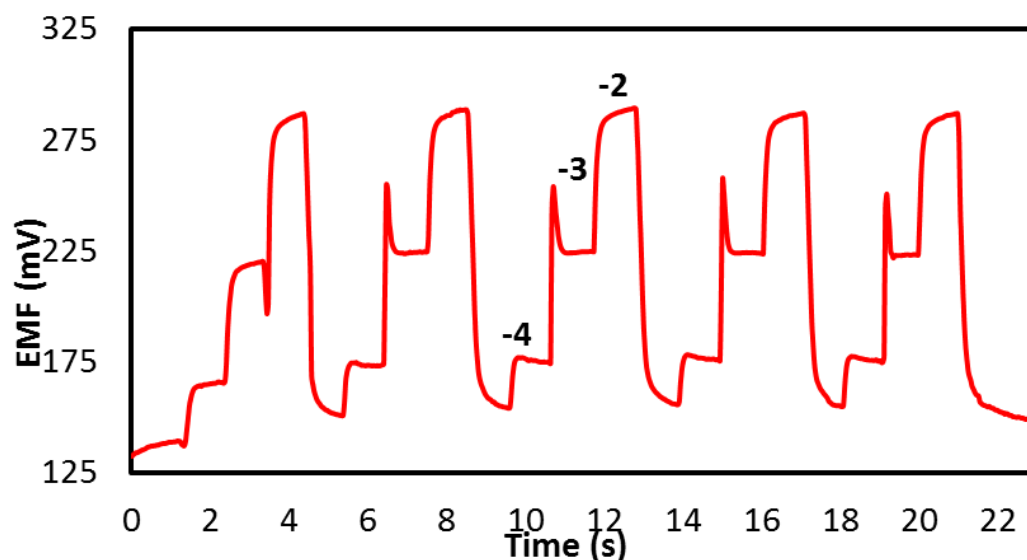


**Figure 5.5** Instrumental response of the potassium-selective electrode in the *Mark I Lab-in-a-box* recorded during five consecutive determinations. The numbers indicate the logarithm of the three KCl concentrations.

Table 5.1 summarises the results of the four day trial. Although not highly accurate, with errors of recovery that do not exceed 10 %, the *Lab-in-a-box* qualifies as a suitable tool for *Vanguard*<sup>8</sup> analysis. Notably, the sensitivity did not appreciably diminish during the four days of testing. This is likely to be- at least in part- attributable to the washing of the electrodes immediately following each determination.

**Table 5.1** Sensitivities of the sensor and recoveries of a potassium solution determined on each of four consecutive days

Day	1	2	3	4	Mean
Sensitivity (mV/dec. <sub>[K<sup>+</sup>]</sub> )	57.5 ± 0.3	56.9 ± 0.3	56.4 ± 0.5	56.5 ± 2.1	56.8 ± 0.5
Recovery (%)	91.5	94.0	103.2	101.1	97.4 ± 5.6

<sup>8</sup> This phrase and concept was described by Valcárcel and Cárdenas and indicates a rapid preliminary phase of screening, with the possibility of subsequent *Rearguard* analysis [35].

## LAB-IN-A-BOX

### 5.3 Lab-in-a-box: Mark II

Based on the encouraging results of the *Mark I* prototype, modifications were made to the system in several ways which can be summarized as trying to get the full lab *inside* the box. This consisted of working towards:

- Exchanging the bulky and expensive benchtop potentiometer for a miniature breakout board
- Exchanging the glassy carbon working electrode substrate and the liquid-junction glass reference electrode for paper-based electrodes.
- Automating the calculations with a *Matlab* function
- Exchanging the bulky benchtop pump for a miniature pump
- Exploring a relationship between baseline potential and standard potential to reduce frequency of calibration and consumption of reagents

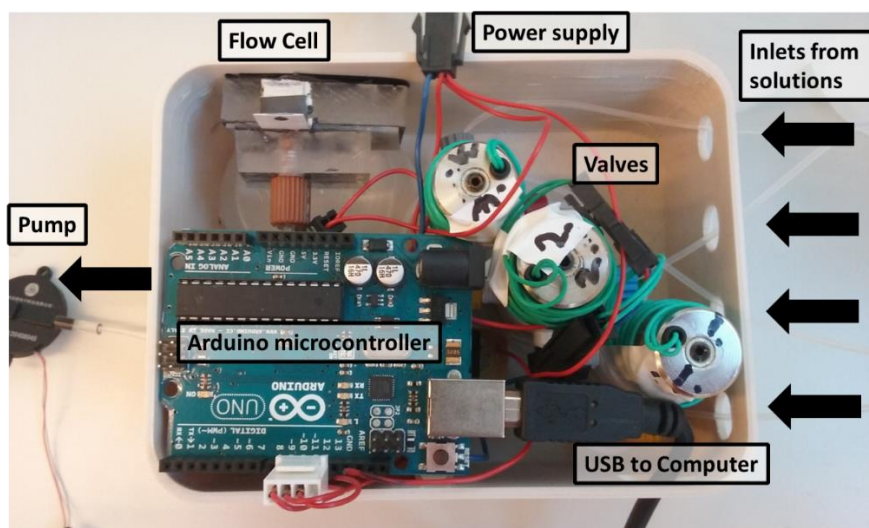


**Figure 5.6** The inside of the *Lab-in-a-box*. In this photograph, a miniature piezoelectric pump is being tested. Also, a paper-based working electrode is housed in a flow cell; the reference electrode is not shown in the image. Electronics are not visible as they are located underneath the microcontroller.

#### 5.3.1 Mark II: Integration of a miniature potentiometer

A substitution for the large and expensive benchtop potentiometer was desirable in order that this critical component was no longer an externality, but rather an integrated part of the *Lab-in-a-box*. As ion-selective electrodes are typically high in impedance, a high-input impedance voltmeter was required. In essence, potentiometry is as simple as reading the voltage between two electrodes. From an electronics perspective this is very simple- and a feature of the *Arduino* microcontroller itself- except for this demand that near-zero current can be drawn. After considerable experimentation in constructing circuits based around an instrumentational amplifier, it was found to be simple only in practice. On the advice of an electronic engineer, a compromise was sought between the large and expensive benchtop potentiometer, and constructing an instrument from first principles.

## LAB-IN-A-BOX

---

### 5.3.1.1 Experimental

A small breakout board designed for pH measurements was procured. This was the *EZO pH circuit* (Figure 5.7). Measuring just 1 cm<sup>2</sup>, it was connected as an intermediary between the electrode inputs and the microcontroller. Its internal analogue-to-digital (ADC) converter sent digital signals to the microcontroller once per second as specified by its firmware. As this signal was internally converted into a pH value, an Arduino sketch was written to revert this back to a voltage value that could equate to the activity of the ion being measured. In other words, the pH breakout board was hacked to perform as a multipurpose potentiometer. The sketch was automated to average data values correspondent to each solution and make calculations based on these to print the sample's ion activity directly to the serial monitor.



**Figure 5.7** The pH breakout circuit board

### 5.3.1.2 Results

The *Mark II* prototype with the integrated miniature potentiometer initially appeared to function ideally; the analysis procedure was autonomous without issue. However, the resulting determinations were highly variable. When examining the raw voltage readings as measured each second, noise in the order of 100 mV was discovered. It was found that this issue arose due to the appearance of grounding loops within the circuitry, because two distinct ground levels were defined. These were the ground of the USB ported to the computer, and the ground of the electrical mains in to which the power adaptor for the valves was plugged.

While these grounding loops would also have been present in the *Mark I* prototype, they were not an issue and were not detected because the reading of the EMF was electrically isolated, being read from an external potentiometer. Although this problem is theoretically simple to solve, in practice it proved challenging. On the one hand, because the USB connection would not provide sufficient power to drive the solenoid valves, it could not act as the common ground. On the other hand, using the electrical mains as the common ground would demand removing the USB connection to the computer. In this case, the question would arise as to how the data output could be communicated. While there are Arduino-style microcontrollers with WiFi or Bluetooth connectivity- these however, would have provided new challenges, primarily in an extra level of coding.

Because of this obstacle, as well as the limitations imposed by the firmware of the breakout board, this direction was not pursued further. Rather, efforts were directed towards the electrodes- specifically, using disposable paper electrodes.

### 5.3.2 *Mark II: Integration of paper-based electrodes and automation of calculations*

#### 5.3.2.1 Experimental

As a step towards the miniaturisation and integration of components within the box, paper-based working and reference electrodes were used. The procedure for their fabrication upon filter papers painted with carbon ink and Ag/AgCl ink is described in the Chapter 3. New flow cells were fabricated to house the new form-factor of these electrodes. As previously, a carrier solution of 0.1 mM MgCl<sub>2</sub> and calibration solutions of 10<sup>-5</sup> M and 10<sup>-2</sup> M KCl were used. The *Lab-in-a-box* was programmed to automatically make a two-point calibration with an intermediate measurement being made of a urine sample that had previously been diluted 100x in the carrier solution. Again operating at a flow rate of 1.25 mL/minute, and this time selecting each of the four solutions for a period of 30 s, the *sketch* was written to make five consecutive determinations. A *Matlab* function was written to automatically select values at each of the steady state levels based on the time since initiation of operation, and to calculate the corresponding sensitivities and standard potentials for each calibration, in order to finally calculate the value of potassium in the sample. At each point, the *Matlab* function averaged the data to produce a mean recovery with an associated standard deviation of confidence. This *Matlab* protocol was seen as a step in the direction of automating the determination and calculation- replacing the need for an analyst to interpret the data by instead offering the direct display of the potassium value.

#### 5.3.2.2 Results

The raw time trace of the determinations is shown in Figure 5.8, and includes the initial 90 s during which the fluidics were primed with the each solution (indicated in the figure as “Prime”)- the data for which was automatically disregarded by the calculation function.



## LAB-IN-A-BOX

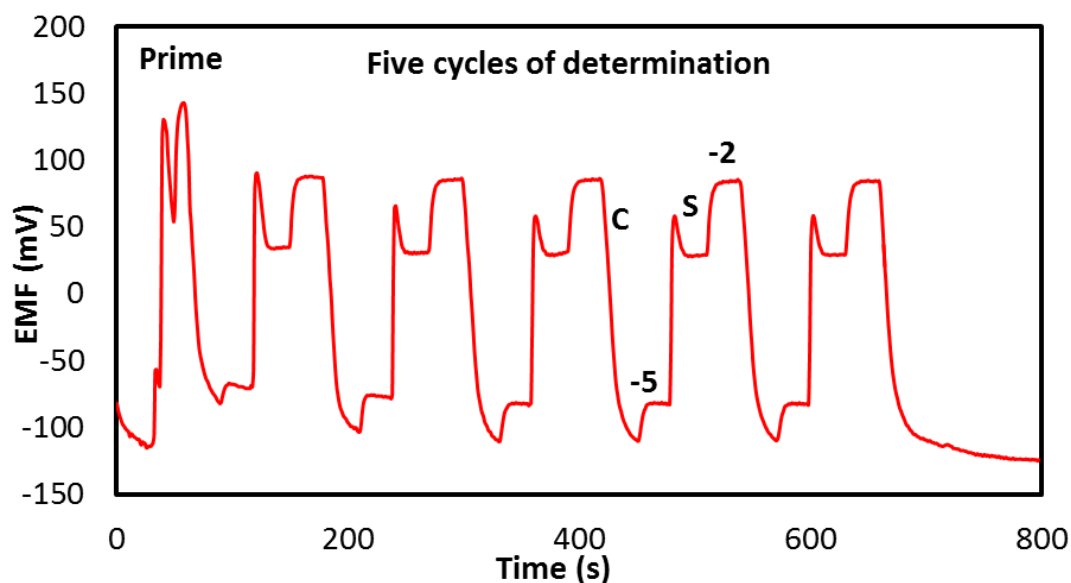


**Figure 5.8** Time trace of five consecutive determinations of potassium. Following an initial priming period of 90 s, the protocol selected the standard of low concentration, followed by the sample, before the standard of high concentration. Between determinations, the electrodes were washed with the blank carrier solution. Within the figure, C indicates the (blank) carrier solution, -5 indicates a standard of  $10^{-5}$  KCl, -2 indicates a standard of  $10^{-2}$  KCl, and S indicates the sample.

By atomic emission spectroscopy, the potassium concentration in the diluted urine sample was determined to be 1.01 mM. Using this as the reference value, the results of the five determinations are summarized in Table 5.2. The average recovery of  $98.4 \pm 2.1$  % validated that paper-based electrodes were compatible within the *Lab-in-a-box* system and that they maintained operation across at least five calibrations. Furthermore, it validated the *Matlab* calculation function written. The recoveries remained remarkably consistent despite variations in sensitivity and standard potential; this is attributed to the recalibration made in each determination. In summary, the paper-based electrodes were successfully integrated within the *Lab-in-a-box*.

## LAB-IN-A-BOX

---

**Table 5.2** Figures of merit during five determinations of potassium in a urine sample (diluted 100x)

Calibration	1	2	3	4	5	Mean
Sensitivity (mV/dec. <sub>[K<sup>+</sup>]</sub> )	52.26	54.07	55.79	55.48	55.53	54.63
Standard potential (mV)	191.70	193.46	196.83	195.21	195.22	194.48
[K <sup>+</sup> ] found (mM)	0.97	0.97	1.01	1.00	1.02	0.99
Recovery (%)	96.36	96.20	99.58	98.76	100.99	98.4 ± 2.1

### 5.3.3 Mark II: Incorporation of a miniature pump

The *Mark I Lab-in-a-box* used an external peristaltic pump weighing some 4 kg. Naturally, it was desirable to minimise the footprint of this element and incorporate it within the box. Furthermore, in lieu of manually switching on and off the pump, and having it run continuously, actuating this with the Arduino allowed for consecutive experiments to be run, between which the pump could be at rest. The miniature peristaltic pump (RP-Q1-S-P45A-DC3V) from *Takasago Electric, Inc.* (Nagoya, Japan) was found to be well-suited to this purpose. It measured just 30 × 12 × 14 mm and so it fit within the box (Figure 5.9). Consuming just 0.12 W, it could be driven directly from a digital pin of the Arduino to pump at 0.4 mL/minute.

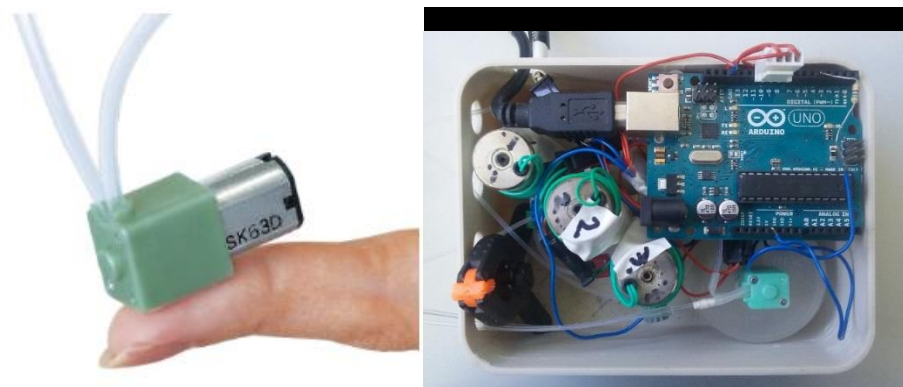


**Figure 5.9** The miniature peristaltic pump seen alone (left), and within the *Lab-in-a-box* (right).

### 5.3.4 Mark II: The relationship between baseline potential and standard potential

‘Drift’ is the term commonly used to describe the gradual shifting of an electrode’s standard potential. It is a form of pink, or 1/f noise. To the analyst working with ion-selective electrodes, drift is generally interpreted as a source of error- accordingly recent years have seen numerous efforts dedicated to this. For example, the

## LAB-IN-A-BOX

---

inclusion of a hydrophobic layer such as that provided by carbon nanotubes has been shown to greatly reduce drift by preventing the formation of a ‘water layer’ between the membrane and conductor of a solid-contact ISE [18].

Ion-selective electrodes contain two junctions at which potentials are variable. Namely, the junction between the aqueous sample and the organic membrane (or phase-boundary potential), and the junction between the membrane and the conductor, indicated as  $E_{PB}$  and  $E_J$  respectively in Figure 5.10. It is proposed that drift predominantly arises from changes at the membrane-electrode junction [19]. This is why minimising the formation of a water layer at this interface through inclusion of hydrophobic components results in greater long-term stability of ISEs.

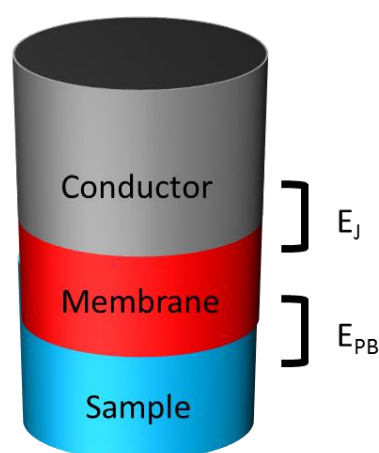


**Figure 5.10** Junction potentials in a solid-contact ion-selective electrode

What is the problem with drift though? With drift values around  $10 \mu\text{Vh}^{-1}$  being reported (under controlled laboratory conditions) [20], any determination lasting less than an hour would not encounter any appreciable changes, and drift would seem to be a non-consideration for disposable ISEs. Indeed, batches of ion-selective electrodes fabricated in a highly reproducible fashion through screen printing have been reported [21]. Although less reports of solid-state reference electrodes have appeared- it is not clear whether is due to lower interest, or greater challenge- these are now also being reported. Both electrodes are of course critical, as the error in the final determination will be a product of variations in the response of both.

Recently, paper-based potentiometric cells fabricated by ink-jet printing were reported with notable inter-sensor reproducibility [22]. Such devices nevertheless remain constrained to single-use applications, such as point-of-care diagnostics. This is because their standard potential is likely to fluctuate following contact with samples, due to drift and perhaps to fouling. Alternative solutions are needed for those sensors intended for long-term ongoing use- such as in remote environmental monitoring. For these, drift remains an issue, and alternatives to using fresh electrodes for each determination are still required. As Crespo wrote in a recent review of ion-selective electrodes for environmental water analysis, “*Unfortunately, while this concept (of*

## LAB-IN-A-BOX

---

*reproducibly manufactured disposable ISEs) seems to work well for new emergent point-of-care platforms that minimize contamination between different patients, it is not yet appropriate for in situ analysis as the change of electrode with every single measurement is not physically possible” [23].*

The *Lab-in-a-box* is a tool suited to- but not limited to- remote environmental analysis, as frequent recalibrations can be made *in situ* and in this way, the same electrodes may be reused for multiple determinations. This renders drift a non-consideration. It does however, consume both power and reagents every time a calibration is made. This section seeks not to minimise drift, but rather to study it. In doing so, a relationship between the baseline potential- that is the potential in an unspecific carrier solution, and the standard potential was discovered and exploited.

### 5.3.4.1 Experimental

Standard solutions of 0.1, 1, and 10 mM creatinine were prepared in a buffer of 50 mM acetic acid/Mg(acetate)<sub>2</sub> at pH 3.7. These, as well as the blank buffer solution, comprised the four solutions managed by the *Lab-in-a-box*.

A creatinine-selective electrode was prepared by drop casting 25  $\mu\text{L}$  of membrane cocktail containing an ionophore selective to creatinine upon a glassy carbon electrode, as described in Chapter 3. This was allowed to dry overnight before conditioning for 5 hours in a 10 mM buffered solution of creatinine as reported [24]. This electrode was housed in a flow cell along with a single-junction reference electrode.

The miniature peristaltic pump from *Takasago* was incorporated within the box and driven directly from the Arduino to provide a flow rate of 0.4 mL/minute.

The Arduino sketch defined a pattern in which the solutions were actively pumped in a sequence lasting 22 minutes. Following this, the pump was stopped for 38 minutes. This cycle of 60 minutes was repeated for 10 consecutive hours. After a break of some four hours, it was then continued for a further 5 hours. In this way, 15 three-point calibrations were collected across a period of 19 hours. The pattern of the cycle is depicted in Figure 5.11.

## LAB-IN-A-BOX

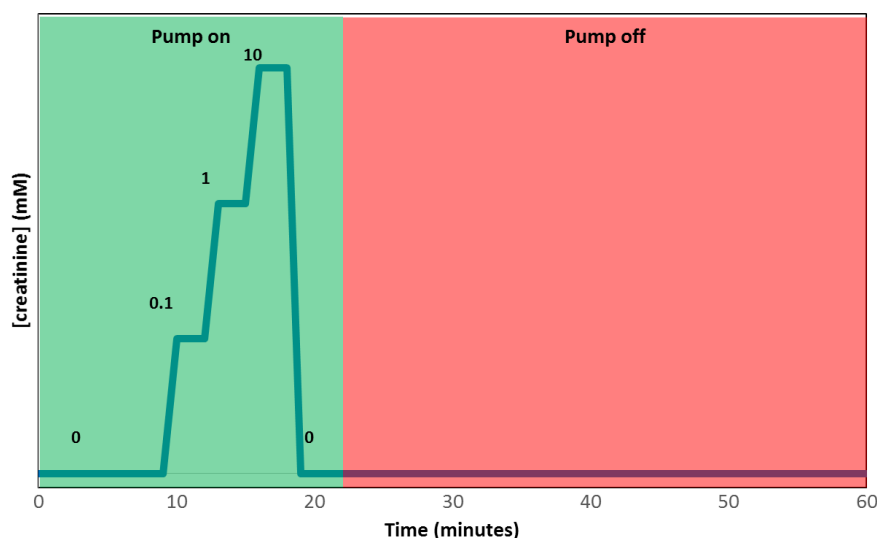


**Figure 5.11** The 60 minute calibration cycle repeated each hour. Times in which the pump was on are indicated by green, times in which the pump was off are indicated by red.

### 5.3.4.2 Results

Ten consecutive calibrations of the creatinine sensor were carried out during 10 consecutive hours in a fully automated procedure. The effect of flow rate was not tested as the miniature peristaltic pump was limited to operating at a flow rate of 0.4 mL/minute. Nevertheless, signals at this flow rate were found to be clean, with no appreciable noise. This is likely to be due in part to the high ionic strength- and hence conductivity- of the carrier solution.

The time trace in Figure 5.12 depict the results of this experiment. It can be seen that following each calibration, the electrodes were washed with the blank carrier buffer, resulting in a decrease in potential. After this washing period, when the pump was stopped, a slow and spontaneous increase in potential was consistently observed. One explanation for this is a gradual diffusion occurring throughout the fluidic system, together with the dynamic characteristics of the detection. The EMF rose to a level a little less than that correspondent to 0.1 mM. In any case, the blank carrier buffer was again pumped for 10 minutes prior to the next hour's calibration.

## LAB-IN-A-BOX

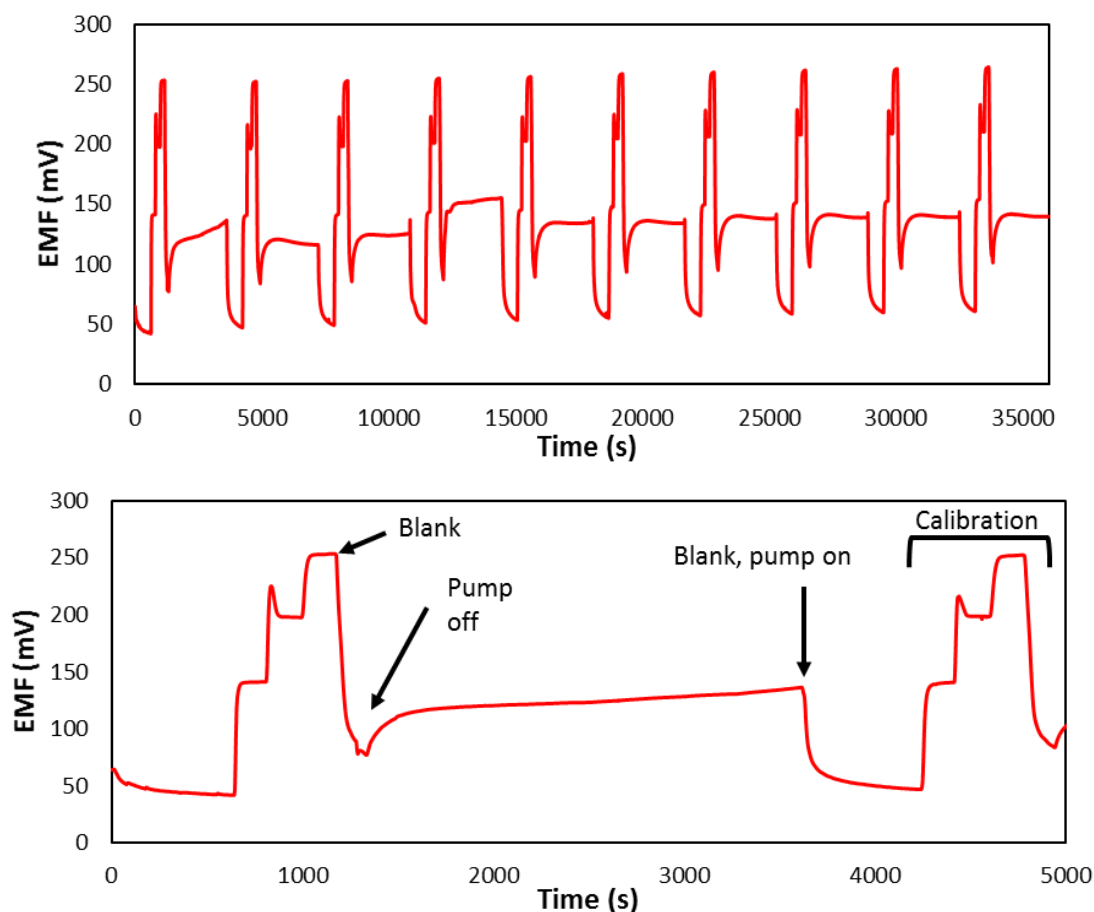


**Figure 5.12** Above: time trace recorded during 10 calibrations in 10 hours. Below: time trace of the first two calibrations.

The EMF was recorded during the latter part of this 10 minute period and termed the baseline potential, or  $E_{\text{baseline}}$ . This potential is *unspecific* to creatinine, as no appreciable concentration was at that time in contact with the electrode.

From each three-point calibration, the standard potential and sensitivity were calculated. This same process was repeated during hours 15- 19. While the sensitivity of the sensor across the 54 hours of calibrations remained reasonably steady at  $54.9 \pm 1.3$  mV/dec. with a range of 51.1 to 56.1 mV/dec., the standard potential saw more appreciable variation, or drift, averaging  $370.7 \pm 4.7$  mV and ranging from 363.8 to 381.3 mV across the same time period. This is typical of ion-selective electrodes. That is, the sensitivity is reproducibly Nernstian, while the standard potential varies considerably, both between sensors and between determinations, making determinations meaningless without recalibration. The utility of this observation was highlighted by the report of the viability of one-point calibrations by Rius-Ruiz *et al.* [25]. Their work used a single-point to predict standard potential while the sensitivity was reasonably assumed to be Nernstian.

The rate of drift was approximately 0.3 mV/h, which is high compared with values reported for ion-selective electrodes in steady-state measurements. This is however, the drift experienced by a potentiometric cell in

## LAB-IN-A-BOX

dynamic and automated use; by contrast with the static conditions typically applied to evaluate and report the stability of a single electrode.

Some of the drift may have been due to the gradual accumulation of a water layer between the membrane and the carbon contact. This could perhaps be reduced by including a hydrophobic material at this interface. One such material, is carbon nanotubes (CNTs), which have proven effective ion-to-electron transducers [26]. These, or more traditional conducting polymer or redox couple transducers could be used to reduce the level of drift. Nevertheless, the drifting of the standard potential and the baseline potential was studied and compared.

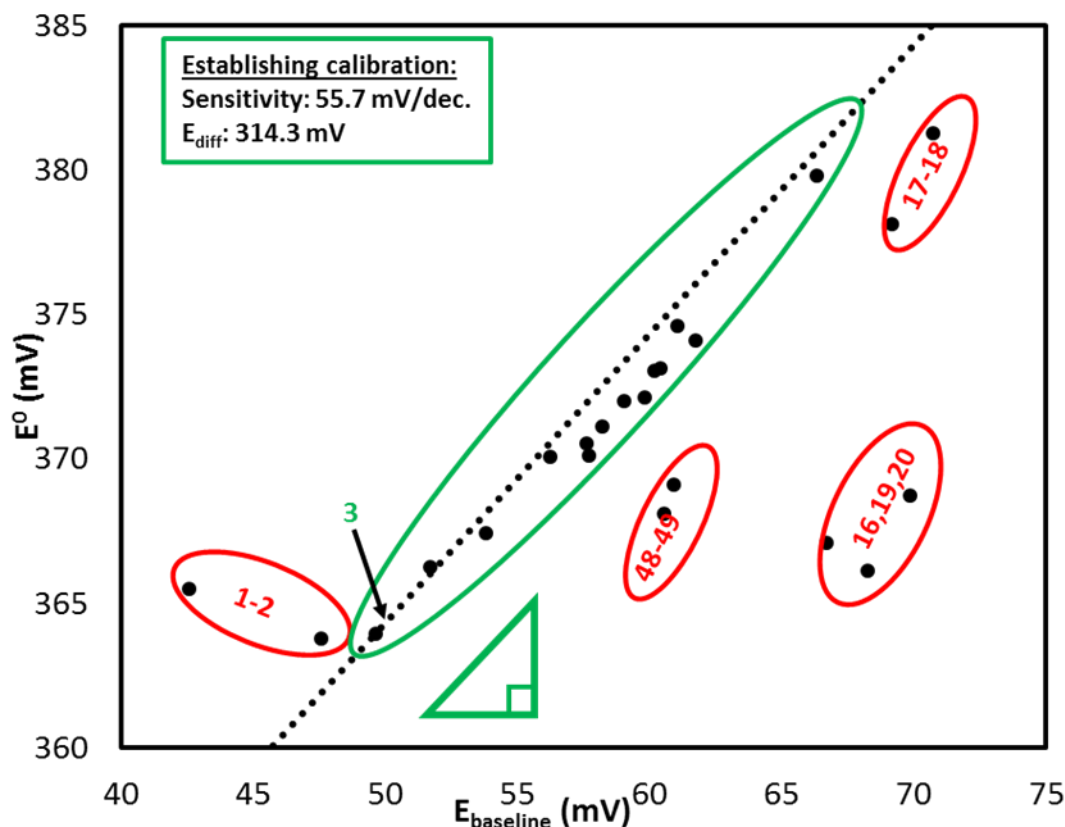


**Figure 5.13** The relationship between baseline potential to standard potential during 54 hours. The dashed line passes through the point of calibration 3 and has a slope of 1. The establishing calibration at hour 3 is indicated by the black arrow. The numbers indicate the hours of calibration that were outliers to the trend.

Within the time period of hours 3- 15, a relationship was observed between the baseline potential and the standard potential (Figure 5.13). Only appearing after the first two calibrations may suggest that the creatinine-selective electrode was not fully conditioned to the point of stability until after this time. From the third calibration on however, a pattern approaching a one-to-one relationship became evident. Accordingly, this third calibration was considered as the *establishing calibration* and was used to establish the sensitivity and the difference in potential ( $E_{diff}$ ) between the  $E_{baseline}$  and the  $E^0$ . The assumption was made that they moved linearly in a one-to-one relationship to each other.

This near one-to-one relationship held strongly until hour 16, after which it became less pronounced or indeed was not apparent. This progression is represented in Figure 5.14, which plots the  $E_{diff}$  at each hour that a

## LAB-IN-A-BOX

calibration was made. During hours 3-15 (shown in the inset), this did not deviate from the  $E_{\text{diff}}$  of the establishing calibration by more than 1.42 mV. From this, it can be said that the baseline potential was a strong predictor of the standard potential up to the 16<sup>th</sup> hour of the experiment.

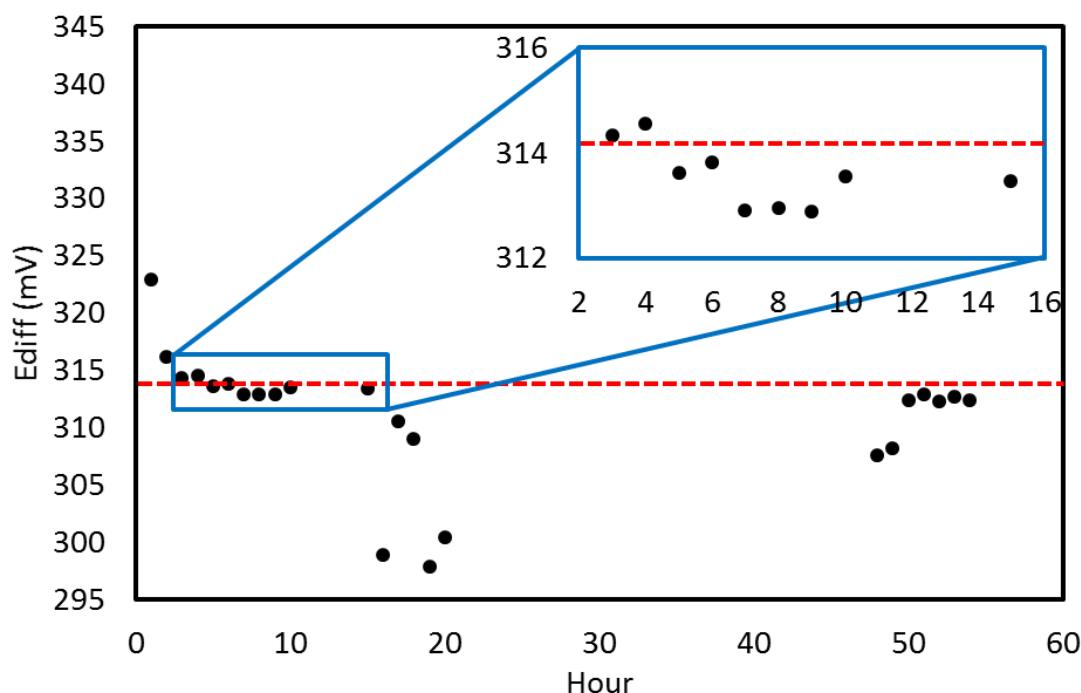


**Figure 5.14** The  $E_{\text{diff}}$  (difference between  $E^0$  and  $E_{\text{baseline}}$ ) during 54 hours of measurements. The red line indicates the  $E_{\text{diff}}$  of the third calibration (314 mV). The inset highlights the reproducibility of the  $E_{\text{diff}}$  during hours 3 and 15.

It should be noted that the line of best fit for hours 3-15 (using the least squares model) for the  $E_{\text{baseline}}$  to  $E^0$  plot in fact had a slope of 0.92 ( $R^2 = 0.991$ ). However, this could not have been known *a priori* to the experiment, and as such, the slope of 1.0 (as indicated by the dashed red line passing through the establishing calibration in Figure 5.13) was used in the following prediction algorithm.

### 5.3.4.3 Algorithm to predict standard potential

During the *establishing calibration*, the sensitivity was determined as 55.7 mV/dec., and the  $E_{\text{diff}}$  was determined as 314.3 mV. By assuming these parameters to be constant, a prediction algorithm was established, that adjusted for drift and thereby obviated the need for recalibration (Equation 5.1). The algorithm was:

$$a_{\text{crt}} = 10^{\left( E - \frac{E_{\text{baseline}} + E'_{\text{diff}}}{S'} \right)} \quad (\text{Equation 5.1})$$

which can be rearranged to a form more recognizably analogously to the Nernst equation:

$$E = (E_{\text{baseline}} + E'_{\text{diff}}) + S' \log a_{\text{CRT}} \quad (\text{Equation 5.2})$$

in which  $E'_{\text{diff}}$  and  $S'$  respectively indicate the  $E_{\text{diff}}$  and the sensitivity of the *establishing calibration*, and  $a_{\text{crt}}$  is the activity of creatinine.



## LAB-IN-A-BOX

This algorithm was used to predict the creatinine concentrations of each of the three standard solutions introduced during the subsequent 51 hours. Figure 5.15 graphically exhibits the accuracy of the predictions made in the experiment using the algorithm and compares them with the predictions made without the adjustment based on the baseline potential- that is, by assuming the sensitivity as well as the standard potential to be constant. In both cases, the accuracies of prediction made at each hour were averaged and one standard deviation of error between these is shown. The full data is also tabulated in Appendix 5.

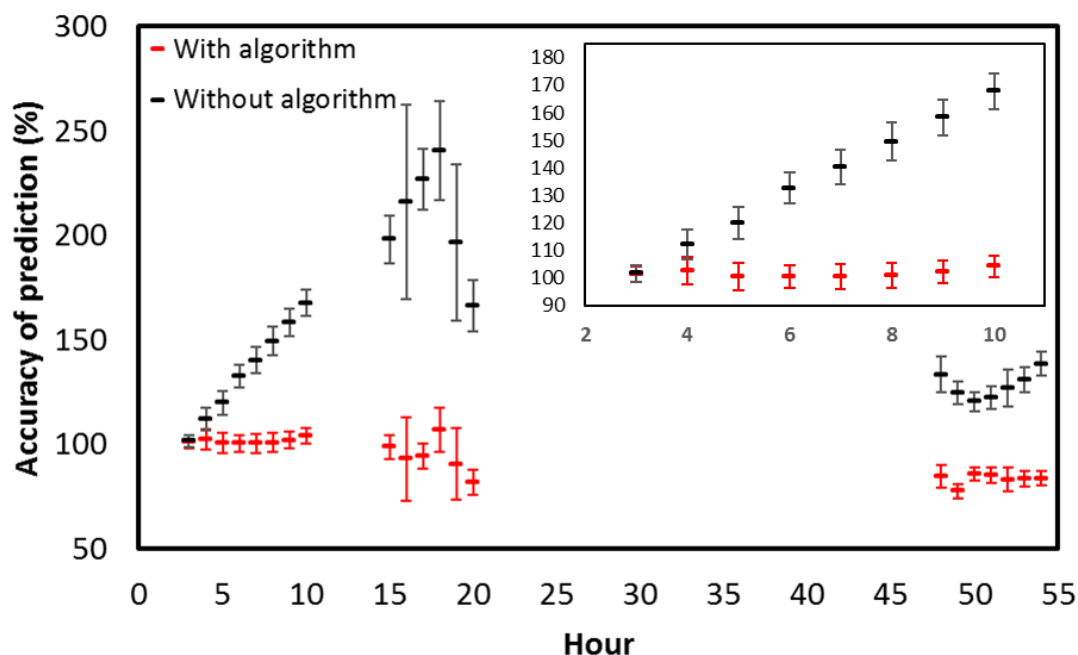


**Figure 5.15** Accuracy of predictions of creatinine concentrations made during 54 hours. At each hour, three concentrations were tested and the accuracy of these was averaged; error bars represent one standard deviation in the accuracy between these. The divergent accuracies of predictions when assuming the sensitivity and standard potential to be constant (black), or when predicted by the algorithm (red) are highlighted in the inset showing the first 10 hours.

At a crude level, the algorithm could be said to have adjusted for drift throughout the entire 54 hours. However, depending on the action standards of the intended application, the error that appeared after 15 hours may be considered unacceptable. To accommodate this in long-term studies- such as may be required for remote autonomous environmental monitoring- a new calibration could be made at set intervals, such as every 15 hours. The benefits of applying such an algorithm would be a reduced power requirement and less consumption of the calibration solutions. As Crespo has written regarding devices for environmental water analysis, “Reducing both the frequency of the calibration steps towards calibration-free sensors and the complexity of the manifolds is an urgent necessity for in situ monitoring” [23].

The one-to-one relationship between the baseline potential and the standard potential seems not to have been previously reported. It is remarkable because *the baseline potential is non-specific* to the analyte. The physical basis of this relationship is not definitively known. It is proposed however, that changes at the electrode-

## LAB-IN-A-BOX

---

membrane interface and the associated  $E_j$ , were being tracked. In contrast to changes at the membrane-solution interface (affecting the  $E_{PB}$ ) which are analyte dependant, the  $E_j$  is theoretically identical irrespective of analyte activity. Accordingly, it is understandable that its variation would equally affect the baseline potential as the standard potential.

One possible application of this, could be in simplifying the calibration of a multiplexed sensor system. Instead of calibrating each sensor individually- each with distinct standard solutions- a singular baseline potential of a solution unspecific to any of the analytes could be used. Tracking the baseline potentials of each ion-selective electrode in *the same unspecific background solution*- could facilitate the simultaneous prediction of the standard potentials for each potentiometric cell. This would significantly reduce the frequency of recalibration, as well as the volume of calibration solutions used, among other complications.

In summary, the near one-to-one relationship of the baseline potential to the standard potential, coupled with the reliably Nernstian sensitivity of an ion-selective electrode allowed for a one-point calibration to be made, time-and-again in a washing buffer absent of analyte.

## 5.4 Lab-in-a-box: Mark III

Having garnered mixed results in the pursuit of integrating the myriad components within a single, miniaturised unit, an alternative, low-tech prototype was explored. This approached the problem from a different angle, with different use cases in mind. While it compromised on the degree of automation, it also concomitantly reduced the degree of complexity, with all actuation being hand-operated, and the microcontroller focussed exclusively on sensing. This led to a prototype more suited to point-of-analysis than autonomous remote monitoring (Figure 5.16). Point-of-analysis includes point-of-care, as well as self-monitoring applications, in addition to non-medical applications such as industrial chemical testing.

The absence of moving parts and power supply, makes such a platform attractive to resource limited settings, such as primary care diagnostics in aid settings, as well as rural water testing. Wine analysis is a particular application for which the described device offers value. This is due to the wide distribution, and low budget of most vineyards within this cottage industry. With the only available option being expensive outsourcing of chemical tests to commercial laboratories, many winemakers instead proceed without such chemical tests. A simple, affordable, in-house device for tests would therefore be attractive to boutique vintners. While some oenologically important analytes require sophisticated methods such as gas chromatography or inductively coupled plasmas coupled with mass spectrometry [27], many are not so instrumentally demanding. These include two dozen enzymatically accessed analytes [28], as well as many ions for which electrochemical methods are well suited. As potassium is an ion of oenological significance [29, 30] and was also determined with the Mark I and Mark II prototypes, it was selected as the model analyte for the Mark III prototype.

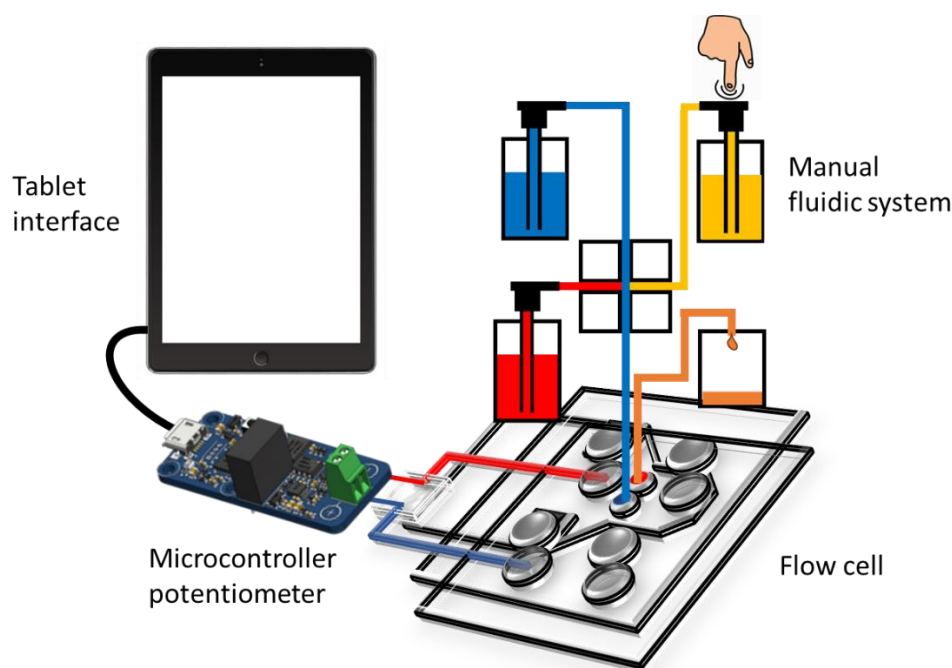


**Figure 5.16** The full setup of the Lab-in-a-box: Mark III. Fluidic system, potentiometric flow cell, microcontroller, tablet.

## LAB-IN-A-BOX

### 5.4.1 Mark III: Experimental

The *Mark III* prototype was constructed from scratch, using three bottles with manual dosing pumps connected to a bespoke four-way junction point (as depicted in Figure 5.17). In this arrangement, three inputs converged into a single output channel, and backflow was minimised by inclusion of three one-way valves. This setup removed the need for electrically actuated pumps and valves. Instead, the user was required to dose the solutions in the appropriate order by pressing them as they would a soap dispenser pump. The exact volume dosed was unimportant as measurements were made at steady-state, after pumping.

A four-way junction point was drilled into Perspex to connect the flow cell with three fluidic input channels. Three check valves (from *Prodac International, S.R.L.* (Italy) purchased from a local aquarium shop) were placed immediately before the entrance of the inputs into the 4-way junction. These connected via microfluidic tubing to three dosing valves that had been removed from soap dispensers after purchase at a local supermarket. These were screwed onto 100 mL plastic bottles. A fourth bottle was added as a waste receptacle and connected after the flow cell. Conductive Velcro pads (*Conductive Hook and Loop 100mm*, SK Pang Electronics, Ltd., Essex, UK) were glued to two of the magnets inside the flow cell. These acted as the electrical contacts to the underlying paper electrodes. Wires were similarly glued to the outside of the magnets- in both cases conductive epoxy glue (*Circuitworks*) was used.

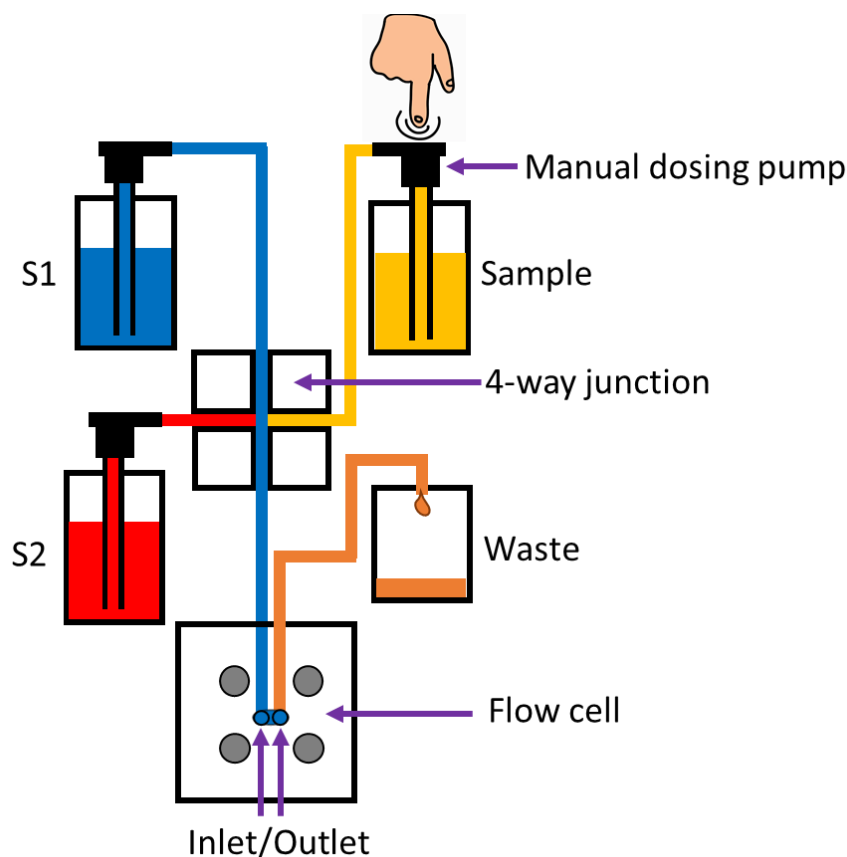


**Figure 5.17** Schematic representation of the Mark III Lab-in-a-box. S1 and S2 indicate two standard solutions. These, as well as the sample, are selectively pumped using hand-pumped dispensers through the 4-way junction point, through the flow cell, and finally collected in a waste receptacle. Check valves were located immediately before the entrance of the three input channels into the 4-way junction.

## LAB-IN-A-BOX

---

Paper electrodes were formed by painting a filter paper with carbon ink and cutting this into two rectangles of 20 mm x 5 mm (Figure 5.18). These were sealed within a plastic mask to expose circular electrode surfaces of 2.1 mm<sup>2</sup>. One of these was covered with a mask while to the other was applied 15  $\mu$ L of potassium-selective membrane cocktail in 6 equal aliquots. After drying for two hours, this membrane was conditioned in 0.1 M KCl for 2 h. At this point a calibration was made to determine the sensitivity of the electrode before removing it from solution, removing the mask from the other electrode, and applying 15  $\mu$ L of reference electrode membrane cocktail in 6 equal aliquots. This was allowed to dry for 2 h before use.

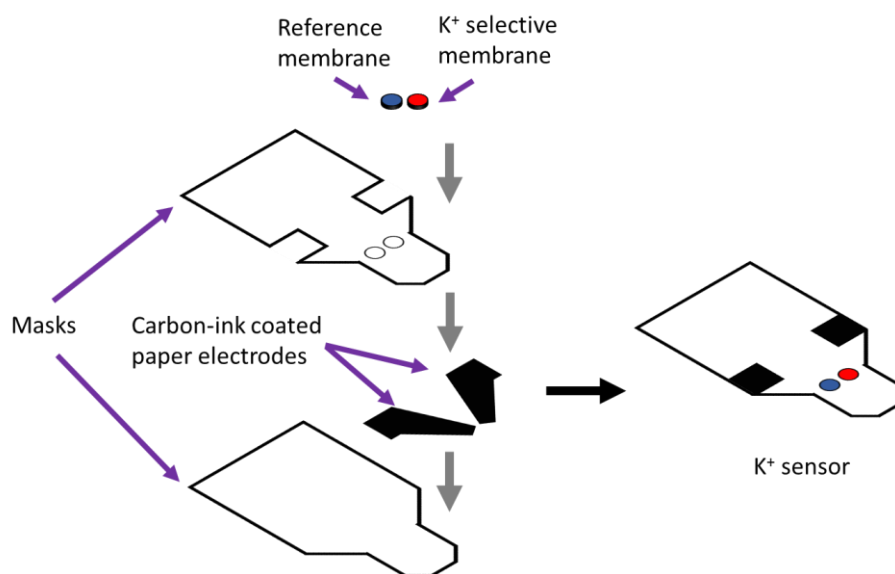


**Figure 5.18** Construction of a paper-based potassium selective potentiometric cell.

A flow cell was fabricated in-house for the paper-based electrodes (Figure 5.19). It was comprised of two Perspex plates, each measuring 6.5 x 5.5 cm, with a thickness of 0.5 cm. Eight rare earth magnets were embedded in the Perspex plates to firmly sandwich the paper potentiometric cell between them. This arrangement provided a hermetic seal that resisted the elevated pressures generated by the hand pumps. Two of the magnets also served as the electrical connections between the paper-based electrodes inside the flow cell and the external electrical circuit.

Rubber with a thickness of 1 mm (green in colour, as photographed in Figure 5.20) slightly separated the two Perspex plates. An oval section was removed from this to expose a volume of 31  $\mu$ L. As this aligned with the electrode membranes, it constituted the interior of the flow cell.

## LAB-IN-A-BOX

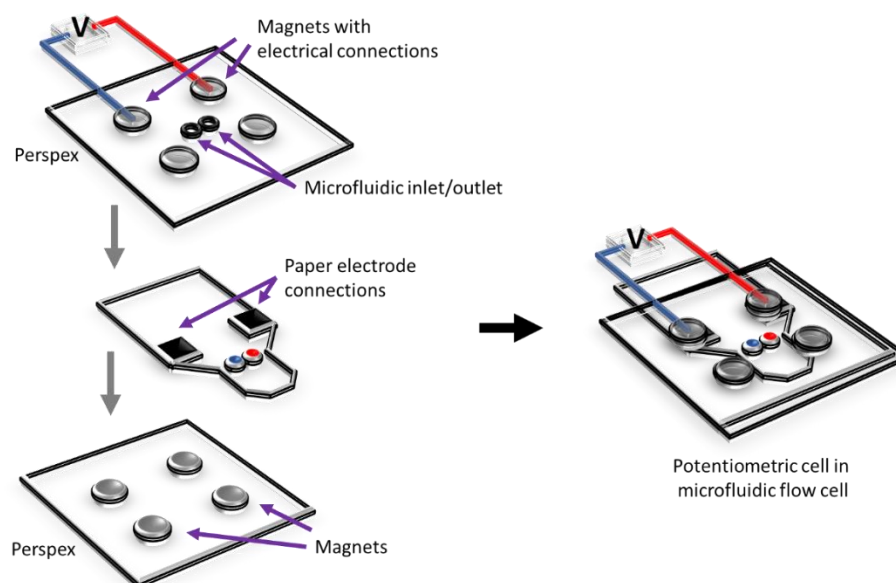


**Figure 5.19** The flow cell with four magnetic seals to sandwich a paper-based potentiometric cell between.

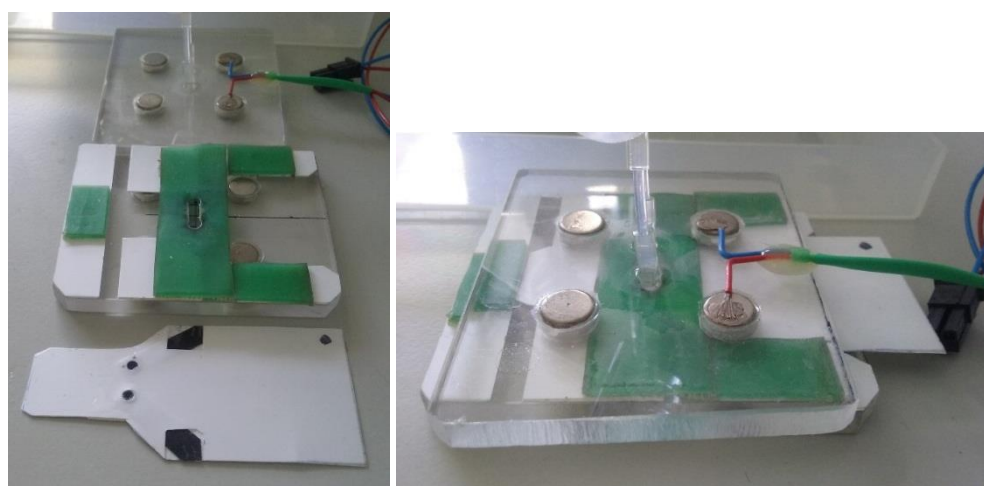


**Figure 5.20** The flow cell used in Mark III. Left: Open, with electrochemical cell removed. Right: Closed, with electrochemical cell inside.

The voltage was read with a *Yocto-milliVolt-Rx* (Yoctopuce Sarl, Cartigny, Switzerland) (Figure 5.21, Right). This high-input impedance microcontroller interfaced with a tablet computer (*Lenovo ideapad MIIX 310-10ICR*) with a custom-designed user-interface which used the two-point calibration to determine the potassium concentration of the sample (as shown in Figure 5.24, Right).

The full setup of the *Mark III Lab-in-a-box* is represented schematically in Figure 5.16, as well as photographically in Figure 5.21.

## LAB-IN-A-BOX

---

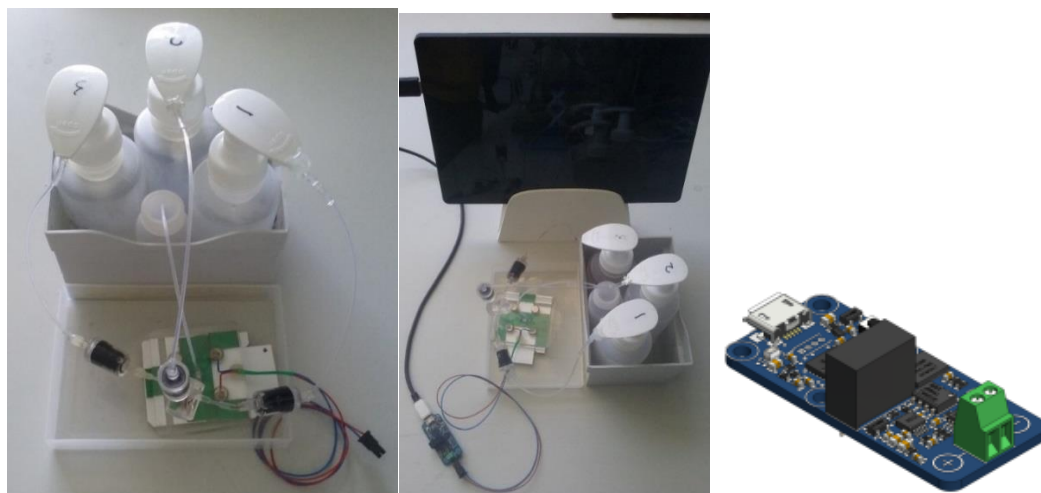


**Figure 5.21** Left and center: The Mark III Lab-in-a-Box. Right: The Yocto-milliVolt-Rx.

### 5.4.2 Mark III: Results

It was found that each depression of the pumps dosed  $169 \pm 15 \mu\text{L}$  (average of ten doses). A small degree of backflow and mixing between the four-way junction and the flow cell was inevitable within the system, so it was found that multiple doses were required to arrive at a steady-state potentiometric signal. The experiment described below used potassium as a model ion, in continuance of the earlier prototypes.

Before starting, the electrodes were calibrated in bulk against a common conventional reference electrode (Figure 5.22). Across the range of 0.1 to 100 mM, the sensitivity of the working electrode was established as Nernstian and the reference electrode was found to be reasonably stable.

## LAB-IN-A-BOX

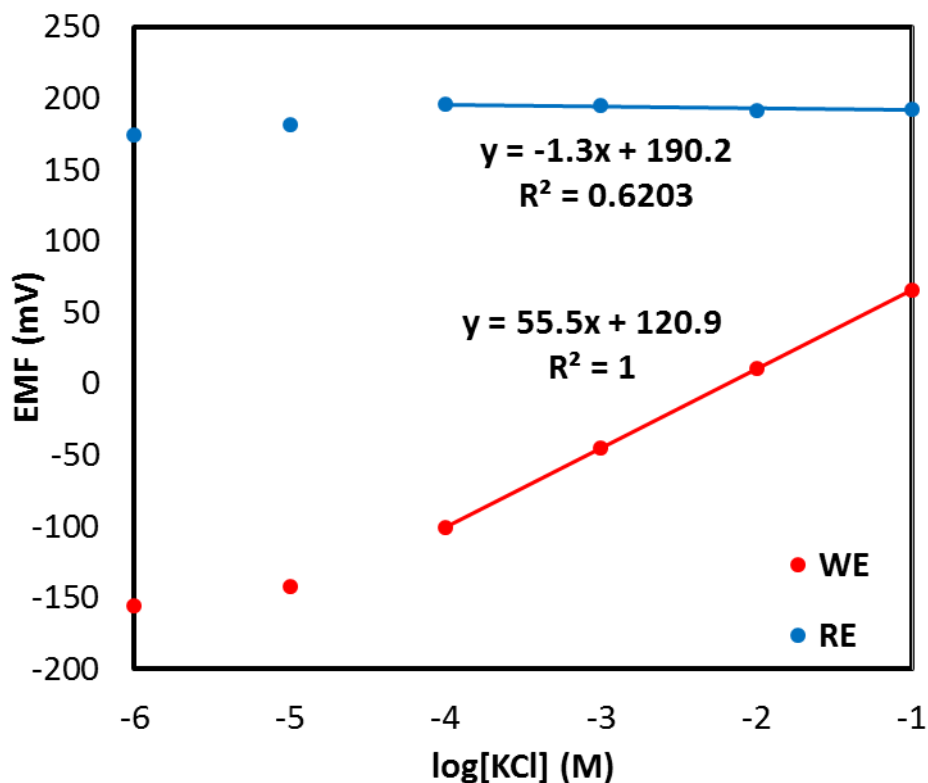


**Figure 5.22** Calibration plot of the paper-based potassium-selective electrode (WE) and ionic liquid-based reference electrode (RE) in bulk against a common conventional reference electrode.

This sensor was locked into the flow cell and the three dosing bottles were filled with: a 10 mM KCl standard solution, a 3.162 mM KCl standard solution, and a wine sample diluted ten-fold in milli-Q water. The pumps were manually depressed 20 times each during 20 s to change solutions after which the steady-state signal was allowed to stabilize for 70 s. In this way, the sensor could be calibrated and a wine sample analysed in less than 5 minutes.

Within the Lab-in-a-box, eight wine samples were then analysed following a ten-fold dilution. A two-point calibration was made prior to each wine determination; the reproducibility of these is indicated by Figure 5.23. A representative time trace during a two-point calibration and sample analysis is shown in Figure 5.24. Each of the three periods of the process can be divided into two components: an initial stage during pumping and equilibration of the sensor; and a steady-state stage from which the signal value was taken- this is indicated by the arrows in the figure.



## LAB-IN-A-BOX

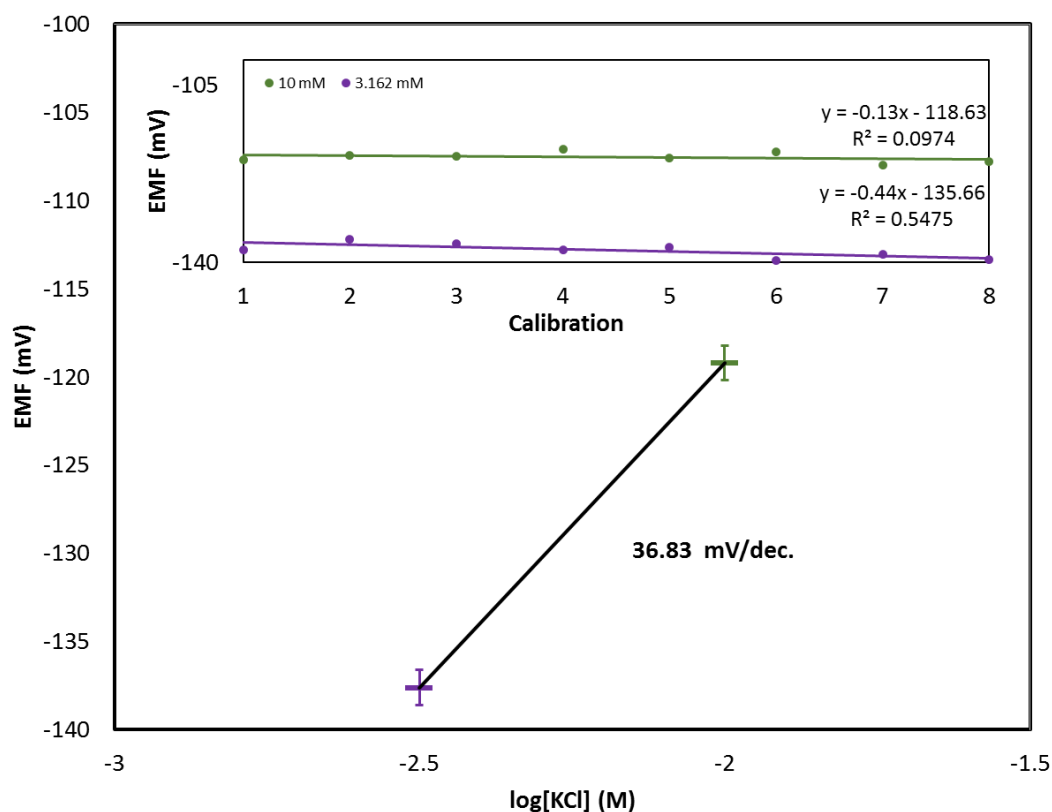


**Figure 5.23** Two-point calibration plot showing the reproducibility of the potentiometric cell within the flow cell. Error bars indicate one standard deviation of error between the 8 calibrations. Inset: the EMF recorded at each concentration during each of the 8 calibrations.

The first point that must be drawn out from the experiment is that the sensitivities were sub-Nernstian. Across the eight calibrations associated with the eight analyses of wine, the sensitivity- as determined from the two-point calibrations- averaged  $36.8 \pm 3.2$  mV/dec.<sub>[K<sup>+</sup>]</sub>, a significant drop from the 55.5 mV/dec.<sub>[K<sup>+</sup>]</sub> in bulk. This is hypothesized to be due to leaching of ionic liquid from the reference membrane with consequent fouling of the working membrane.<sup>9</sup> It is conceivable that this partially blocks the active surface of the potassium-selective membrane. This was not predictable, as it has not been observed in bulk experiments (as will be presented in Chapter 6). It would therefore seem to arise from the high pressure applied to the membranes in pumping and/or the close proximity of the two membranes within the constrained volume of 31  $\mu$ L.

The ionic liquid PVC-based reference electrode membrane was selected due to its high mechanical and chemical resistance in consideration of the high-pressure flow generated by the hand pumps. Although several ionic liquid reference electrode membranes have been reported [22, 31, 32], their performance has consistently been described under steady-state conditions. While mechanically resistant, the dynamic flow of this system appears to have placed a high demand on the chemical stability of the reference electrode.

<sup>9</sup> This hypothesis is supported by an experiment in which a 0.5  $\mu$ L drop of ionic liquid was added to a 50  $\mu$ L KCl solution connecting the two electrodes. This resulted in a > 200 mV drop in potential and the cell subsequently being rendered insensitive to KCl.

## LAB-IN-A-BOX

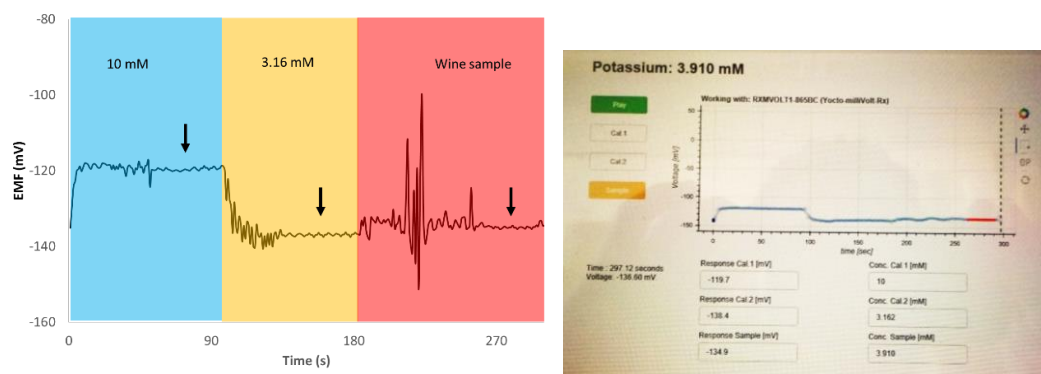


**Figure 5.24** Left: Time trace during the calibration of the sensor and determination of potassium in a wine sample. The three colours indicate the three stages of the analysis while the arrows indicate the time after pumping at which steady-state values were considered. Right: Screen shot of the user-interface of the potassium sensing system during the analysis.

Nonetheless, the potassium levels in wine were determined for each of the eight samples based on the two-point calibrations and the predictions were found to average  $117.7 \pm 22.6\%$  of the potassium values determined by atomic emission spectroscopy, as summarized in Table 5.3. In regard to the positive bias of determinations, one factor contributing to this could be that potassium is known to complex with tartrate within wine [29]. Naturally, this decreases the activity of the free uncomplexed potassium available for detection by an ion-selective electrode. By atomizing all components, atomic emission on the other hand does not distinguish between free or complexed ions, and would accordingly measure the total concentration of potassium present.

**Table 5.3** Key values in evaluating the recovery of potassium values in wine.

Wine	Sensitivity (mV/dec. <sub>[K<sup>+</sup>]</sub> )	[K <sup>+</sup> ]- AES (mM)	[K <sup>+</sup> ]- LIB (mM)	Recovery (%)
1	35.6	58.2	38.4	151.5
2	33.2	48.1	39.1	123.1
3	34.3	48.3	39.9	121.1
4	39.9	44.8	39.7	113.1
5	35.0	46.4	35.7	129.9
6	42.6	44.4	42.3	105.1
7	35.2	17.6	24.2	72.8
8	38.8	37.0	29.5	125.3

There was a possibility that a fluidic issue such as dead volume, back flow, and mixing may have been responsible for the diminished sensitivity observed within the flow cell. To test this, one bottle was filled with distilled water and another was filled with a blue dye with peak absorbance at 609 nm. The flow cell was replaced with a microfluidic cuvette and placed in the path of a broad spectrum light source. The absorbance at 609 nm was monitored between each depression of the pumps in a cycle of the two solutions, with five depressions of each (Figure 5.25).

## LAB-IN-A-BOX

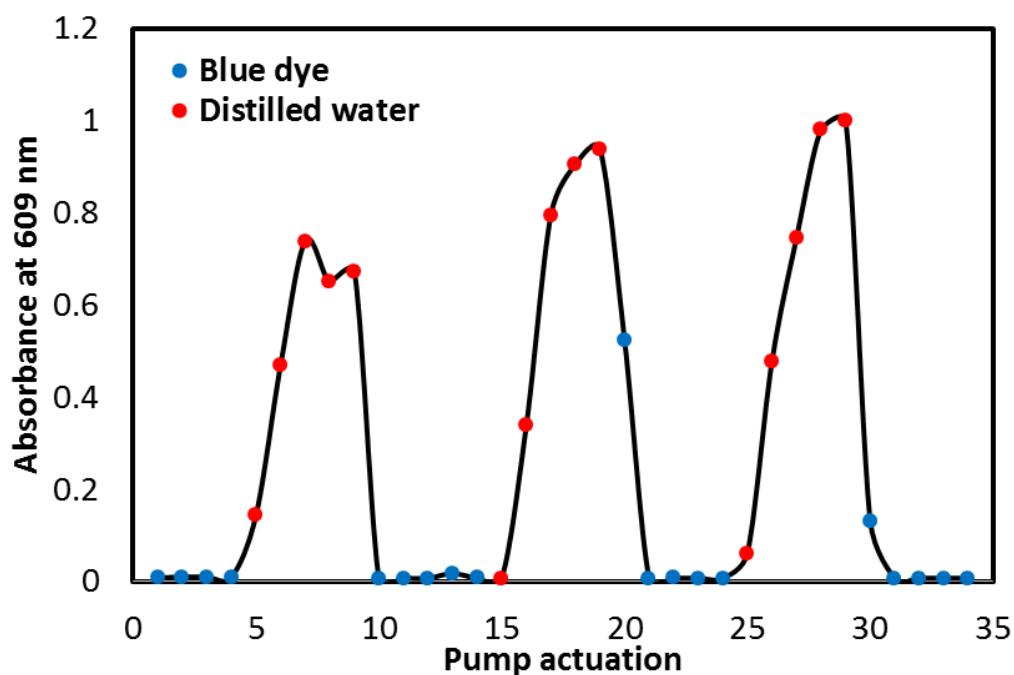


**Figure 5.25** Absorbance of light at 609 nm following the manual pumping of a blue dye (shown by blue markers), and distilled water (shown by red markers).

In the case of pumping the blue dye, a sharp change in the absorbance was evident within two actuations of the pump. When pumping in the distilled water, it took up to five depressions of the pump to saturate the absorbance to a reasonably stable level. This is understandable because distilled water will reveal any traces of dye remaining in the light path. This optical test indicates that five pump actuations are required for the appreciable replacement of one solution for another. The twenty pump actuations made during the determinations in wine are thereby considered more than accurate, and the fluidics of the system are not considered to be responsible for the diminished sensitivity observed.

All in all, this result is simultaneously disappointing and encouraging. While the recoveries initially appeared inaccurate, in consideration of the expected positive bias, it is not conclusive whether the accuracy was indeed biased. Furthermore, the low sensitivity is indicative of issues with the reference electrode, and it would be advisable to test alternative reference electrode membranes. The overall result- consistent recoveries, even in the face of diminished sensitivity- suggests that there is merit to the concept of the system, however. It could be that the use of an alternative reference electrode, the system may be highly attractive.

One feature of the device design that merits mention is the use of magnets as electrical connections.<sup>10</sup> In the context of generating solutions for user-friendly electrical analyses, a small but not trivial consideration is how electrodes- especially disposable electrodes- are to be connected and exchanged. Within the laboratory, a

<sup>10</sup> This idea was conceived by Francisco J. Andrade

## LAB-IN-A-BOX

---

common method of connecting planar electrodes such those made with paper, is to attach an alligator clip. Needless to say, this is cumbersome and alternative designs are needed for decentralized applications. The now-ubiquitous USB devices offer a successful example of a user-friendly electrical connection; perhaps future solutions may draw inspiration from it. In this case, an elegant solution was found with the magnetic connections (Figure 5.19). While four of these magnets were used to provide a tight hydraulic seal around the flow cell, two of them had the additional function of providing electrical connection between the paper electrodes and the potentiometer.

In summary, the *Mark III* prototype offered a meaningful and alternative direction to the Lab-in-a-box exploration. In testing wine samples the device was user-friendly and extremely low-cost. The total retail price of the three dosing pumps and three check valves was approximately 12 Euros, although the wholesale price would be significantly lower. Calculating in the remaining components of Perspex and magnets, the total cost remained under 15 Euros, with considerable margin for savings at wholesale prices. The *Yoctopuce* potentiometer was the only significant cost, at 45 Euros and the tablet can safely be considered an externality in this cost analysis, as any tablet or computer could be used and these are already in wide employ. Thus, the total retail price was less than 60 Euros- a price expected to be affordable to most vintners.

As vineyards tend to be widely distributed and with limited access to resources for chemical analysis, this would seem to be a useful application. Professional winemakers should have no problems in making a precise ten-fold dilution prior to analysis. Finally, as the major cation in wine, potassium plays a key role in grapevine physiology and impacts wine quality [30]. Accordingly, it merits monitoring, as do many other ions and enzymatically assayed species in wine. A device like the *Mark III Lab-in-a-box* could open the way to offering vintners insight into a wealth of previously inaccessible chemical information.

## 5.5 Conclusions

Three *Lab-in-a-box* prototypes have been described. Each had its strengths: *Mark I* demonstrated the best analytical performance; the *Mark II* prototypes pursued increasing degrees of automation and miniaturisation; while *Mark III* showed the greatest simplicity and the lowest cost. In this way, these three evolutions of the concept pursued the three aspects of performance, usability and affordability, described in Chapter 4 as essential to the propagation of distributed sensors.

Among practical considerations, the flow cells used in the first two prototypes were delicate to handle in that threaded glassy carbon electrodes needed to be tightened just so, with silicon tape and sometimes tapped vigorously to remove air bubbles. Exchanging electrodes was always a delicate affair. For these reasons, this type of flow cell could not be described as robust. The third prototype was a major improvement over this, made possible with planar electrodes and a tight magnetic seal. Nevertheless, it had other challenges associated. Finding a solid-state reference electrode that was suitably robust, both chemically and mechanically, primary among these.

Simplicity of instrumentation is often touted as a strong point of the technique of potentiometry. Theoretically, this is true. However, in working towards the integration of all components of the *Mark II Lab-in-a-box*, efforts were made to build a high-input impedance voltmeter from first principles. It was found to be problematic in practice, and in retrospect appears a project for an electronic engineer. The non-intuitive user-interface of the *Arduino* integrated development environment utilized for the first two prototypes highlighted the need for the skills of a computer programmer, electronics engineer, and perhaps a UI/UX expert. This was greatly improved in the third evolution of the project, with a user-interface programmed by a colleague within our lab.

The accurate analytical results obtained with the *Mark I* prototype demonstrated the promise of an automated device to make potentiometric measurements. Integrating all the functions and components required to miniaturise the device in a user-friendly way proved to be highly demanding on multiple fronts, necessitating skills from diverse areas of specialization.

As reported, while disposable ISEs are well-suited to point-of-care applications due to their high sensor-to-sensor reproducibility, this does not translate well to applications requiring reuse of the sensor [23]. This is not only due to the loss of the reproducibility feature, but also due to the damage caused to the sensing surface by extended exposure to many sample matrices. The *Lab-in-a-box* addressed this issue in a subtle yet potent manner through the subsampling protocol, common to all prototypes.

That is, all prototypes introduced some microliters of a sample to the sensor surface for a strictly limited time, before washing the surface with a buffer solution in a procedure that prolonged the lifetime of the active sensing surface by minimising leaching, fouling and decomposition. These, as well as biofilm development, are common issues with reuse of sensor membranes, and stymie the continuous immersion of potentiometric

## LAB-IN-A-BOX

---

probes for environmental monitoring. In this way, the subsampling protocol mitigated *'the chemical sensor paradox'* [33], of needing a surface simultaneously exquisite in sensitivity to chemical changes, yet protected from degradation.

In the end, it seems that a simple idea needs to have a high degree of complexity behind, in order to appear simple on the surface. Congruent with Maeda's fifth law of simplicity,<sup>11</sup> trying to arrive at a simple solution demanded extensive complexity. It has been said that *"some things can never be made simple"*.<sup>12</sup> Although no breakthrough success was arrived at in the pursuit of the *Lab-in-a-box*, it was not a failure. All meaningful innovations require iterations of reduction and synthesis to subtract the superfluous, and keep the essential.<sup>13</sup> This is *test-driven development*, the bread-and-butter of engineers, as opposed to theorists.

As has been mentioned, the concept of automating user-operated electrochemical sensing with microfluidic management is not non-obvious. It even seems easy, in contrast with many complex problems and perhaps has even been tried before, successfully or otherwise. It is however, of little interest to the scientific community, which relishes in fundamental novelties, rather than meaningful syntheses of established technologies. As the work described in this chapter has demonstrated- perhaps despite appearances, this project is not easy. The synthesis of multidisciplinary elements is inherently challenging and leaves no room for relegating inconvenient details to the realm of externalities. For *"what lies in the periphery of simplicity is definitely not peripheral"*,<sup>14</sup> but rather an essential facet of the problem itself. The pursuit of such a problem requires *modular systems thinking* with the understanding that *"the relationships among the modules of a system give rise to a whole that cannot be understood by analysing its constituent parts"* [34]. In an age of increasing specialisation, the assembly of unrelated components is the purview of non-experts, such as the *Makers*.

The *Lab-in-a-box* explored solutions to the challenges of making distributed potentiometric measurements intuitively user-friendly and affordable while offering meaningful performance outcomes. In the iterations realized, compromise was required on at least one of these fronts in order to advance on another. The next chapters reduce the complexity significantly by focussing more explicitly on one aspect at a time, beginning with usability.

---

<sup>11</sup> John Maeda's fifth law of simplicity, "Simplicity and complexity need each other." From [36].

<sup>12</sup> John Maeda's ninth law of simplicity. From [36].

<sup>13</sup> To paraphrase John Maeda's tenth law of simplicity, "Simplicity is about subtracting the obvious, and adding the meaningful." From [36].

<sup>14</sup> John Maeda's sixth law of simplicity. From [36].

## 5.6 References

- 1 A. W. Martinez, S. T. Phillips and G. M. Whitesides, Three-dimensional microfluidic devices fabricated in layered paper and tape, *Proc. Natl. Acad. Sci.*, 2008, **105**, 19606–19611.
- 2 H.-K. Chang, E. Choi and J. Park, Paper-based energy harvesting from salinity gradients, *Lab Chip*, 2016, **16**, 700–708.
- 3 M. Hilder, B. Winther-Jensen and N. B. Clark, Paper-based, printed zinc–air battery, *J. Power Sources*, 2009, **194**, 1135–1141.
- 4 L. Hu, H. Wu and Y. Cui, Printed energy storage devices by integration of electrodes and separators into single sheets of paper, , DOI:10.1063/1.3425767.
- 5 G. Nystrom, A. Razaq, M. Strømme, L. Nyholm and A. Mihranyan, Ultrafast all-polymer paper-based batteries, *Nano Lett.* 9, 2009, 3635–3639.
- 6 J. P. Esquivel, J. R. Buser, C. W. Lim, C. Domínguez, S. Rojas, P. Yager and N. Sabaté, Single-use paper-based hydrogen fuel cells for point-of-care diagnostic applications, *J. Power Sources*, 2017, **342**, 442–451.
- 7 N. R. Gabriel Lenk, Sören Sandkvist, Anton Pohanka, Göran Stemme, Olof Beck, G. Lenk, S. Sandkvist, A. Pohanka, G. Stemme, O. Beck and N. Roxhed, A disposable sampling device to collect volume-measured DBS directly from a fingerprick onto DBS paper, *Bioanalysis*, 2015, **7**, 2085–2094.
- 8 W. J. Hyun, O. O. Park and B. D. Chin, Foldable graphene electronic circuits based on paper substrates., *Adv. Mater.*, 2013, **25**, 4729–34.
- 9 J. A. Adkins, E. Noviana and C. S. Henry, Development of a Quasi-Steady Flow Electrochemical Paper-Based Analytical Device, *Anal. Chem.*, 2016, **88**, 10639–10647.
- 10 T. Ahmadraji, L. Gonzalez-Macia, T. Ritvonen, A. Willert, S. Ylimaula, D. Donaghy, S. Tuurala, M. Suhonen, D. Smart, A. Morrin, V. Efremov, R. R. Baumann, M. Raja, A. Kemppainen and A. J. Killard, Biomedical Diagnostics Enabled by Integrated Organic and Printed Electronics, *Anal. Chem.*, 2017, **89**, 7447–7454.
- 11 A. W. Martinez, S. T. Phillips, M. J. Butte and G. M. Whitesides, Patterned paper as a platform for inexpensive, low-volume, portable bioassays, *Angew. Chemie - Int. Ed.*, 2007, **46**, 1318–1320.
- 12 L. R. Volpatti and A. K. Yetisen, *Trends Biotechnol.*, 2014, 32, 347–350.
- 13 Z. Nie, C. A. Nijhuia, J. Gona, X. Chea, A. Kumacheb, A. W. Martine, M. Narovlyanska and G. M. Whitesides, Electrochemical sensing in paper-based microfluidic devices, *Lab Chip*, 2010, **10**, 477–483.
- 14 A. Nemiroski, D. C. Christodouleas, J. W. Hennek, A. A. Kumar, E. J. Maxwell, M. T. Fernandez-Abedul and G. M. Whitesides, Universal mobile electrochemical detector designed for use in resource-limited applications, *Proc. Natl. Acad. Sci.*, 2014, **111**, 11984–11989.
- 15 C. M. McGraw, S. E. Stitzel, J. Cleary, C. Slater and D. Diamond, Autonomous microfluidic system for phosphate detection, *Talanta*, 2007, **71**, 1180–1185.

## LAB-IN-A-BOX

---

- 16 I. M. Perez De Vargas Sansalvador, C. D. Fay, J. Cleary, A. M. Nightingale, M. C. Mowlem and D. Diamond, Autonomous reagent-based microfluidic pH sensor platform, *Sensors Actuators, B Chem.*, 2016, **225**, 369–376.
- 17 Gastón A. Crespo, A. Santiago Macho and F. X. Rius\*, Ion-Selective Electrodes Using Carbon Nanotubes as Ion-to-Electron Transducers, , DOI:10.1021/AC071156L.
- 18 M. Fibbioli, W. E. Morf, M. Badertscher, N. F. de Rooij and E. Pretsch, Potential Drifts of Solid-Contacted Ion-Selective Electrodes Due to Zero-Current Ion Fluxes Through the Sensor Membrane, *Electroanalysis*, 2000, **12**, 1286–1292.
- 19 J. Hu, A. Stein and P. Bühlmann, Rational design of all-solid-state ion-selective electrodes and reference electrodes, , DOI:10.1016/j.trac.2015.11.004.
- 20 A. Radu, S. Anastasova, C. Fay, D. Diamond, J. Bobacka and A. Lewenstam, Low cost, calibration-free sensors for in situ determination of natural water pollution, *Proc. IEEE Sensors*, 2010, 1487–1490.
- 21 N. Ruecha, O. Chailapakul, K. Suzuki and D. Citterio, Fully Inkjet-Printed Paper-Based Potentiometric Ion-Sensing Devices, *Anal. Chem.*, 2017, **89**, 10608–10616.
- 22 G. A. Crespo, Recent Advances in Ion-selective membrane electrodes for in situ environmental water analysis, *Electrochim. Acta*, 2017, **245**, 1023–1034.
- 23 T. Guinovart, D. Hernández-Alonso, L. Adriaenssens, P. Blondeau, M. Martínez-Belmonte, F. X. Rius, F. J. Andrade, P. Ballester, M. Martínez-Belmonte, F. X. Rius, F. J. Andrade and P. Ballester, Recognition and Sensing of Creatinine, *Angew. Chemie*, 2016, **55**, 2435–40.
- 24 F. X. Rius-ruiz, A. Crespo, D. Bejarano-nosas, P. Blondeau, J. Riu and F. X. Rius, Potentiometric Strip Cell Based on Carbon Nanotubes as Transducer, *Anal. Chem.*, 2011, **83**, 8810–8815.
- 25 G. A. G. A. Crespo, S. Macho, F. X. Rius, Gastón A. Crespo, A. Santiago Macho and F. X. Rius, Ion-Selective Electrodes Using Carbon Nanotubes as Ion-to-Electron Transducers, *Anal. Chem.*, 2008, **80**, 1316–1322.
- 26 ThermoFisherScientific, An analytical testing digest of the wine manufacturing process.
- 27 S. J. Charnock and B. V. McCleary, Grape and Wine Analysis Oenologists to exploit advanced test kits, 2005, 117.
- 28 R. S. Jackson, *Wine Science: Principles and Applications*, Elsevier, 3rd edn., 2014.
- 29 C. Conde, P. Silva, N. Fontes, A. C. P. Dias, R. M. Tavares, M. J. Sousa, A. Agasse, S. Delrot and H. Gerós, Biochemical changes throughout grape berry development and fruit and wine quality, *Food*, 2007, **1**, 1–22.
- 30 D. Cicmil, S. Anastasova, A. Kavanagh, D. Diamond, U. Mattinen, J. Bobacka, A. Lewenstam and A. Radu, Ionic Liquid-Based, Liquid-Junction-Free Reference Electrode, *Electroanalysis*, 2011, **23**, 1881–1890.
- 31 M. Novell, T. Guinovart, P. Blondeau, F. X. Rius and F. J. Andrade, A paper-based potentiometric cell for decentralized monitoring of Li levels in whole blood., *Lab Chip*, 2014, **14**, 1308–14.
- 32 D. Diamond, R. Byrne and D. Diamond, Chemo/bio sensor networks, *Nat. Mater.*, 2006, **5**, 421–424.
- 33 G. Madhavan, *Applied minds: How engineers think*, W. W. Norton Company, New York & London, 1st edn., 2015.



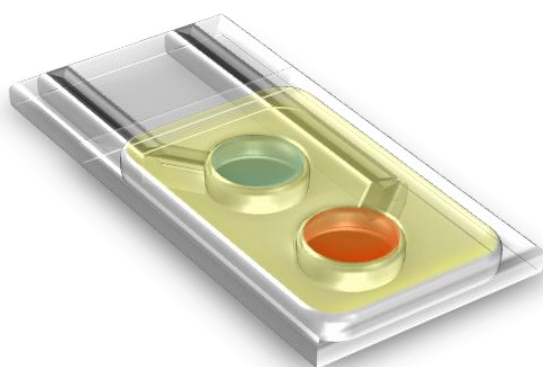
## LAB-IN-A-BOX

---

- 34 M. Valcárcel and S. Cárdenas, Vanguard-rearguard analytical strategies, *TrAC - Trends Anal. Chem.*, 2005, **24**, 67–74.
- 35 J. Maeda, *The Laws of Simplicity*, MIT Press, 2006.

## 6 HYDROGEL CAPPING MEMBRANES: A strategy for the dry *in situ* calibration of potentiometric sensors

---



## 6.1 Introduction

This thesis argues that suitable usability, affordability, and performance constitute the three-point checklist for the maturation of distributed chemical sensing systems. While the previous chapter aimed at addressing the triad of elements simultaneously, this chapter narrows the focus to usability. This aspect is the weakest link in the trinity, and forms the bottleneck that suppresses these sensors from wider adoption.

Within the scope of usability of potentiometric sensors, one of the most restrictive challenges lies in their calibration. Extensive research continues to pursue the manufacturing of highly reproducible electrodes [1–3]. In this, a disproportionate degree of focus has been placed on fabricating indicator electrodes in a reproducible fashion, with less advancement being made on the equally important reference electrodes. There is certainly merit to this pursuit of reproducibility- and indeed progress- although the real applications of such strategies remains to be demonstrated. As such, alternative strategies also warrant exploration.

It is important to recognize that the instrumentation for taking calibration readings is necessarily present at the site of analysis, therefore the only complication involves user handling steps, particularly in relation to liquids. If calibration could be carried out *without* liquids therefore, it may present a user-friendly solution. To frame this in the terms introduced in the previous chapter, the *dry* aspect required for calibration is inherently in place, the only remaining challenge therefore lies in the *wet* aspect.

One-point calibrations have already been demonstrated to show suitable performance when simplicity of operation is of greater interest than high precision [4]. Furthermore, the *Lab-in-a-box* presented in Chapter 5 made a preliminary demonstration of one-point calibrations in a solution *absent* of the analyte. This chapter explores extends this idea to test one-point ‘*dry calibrations*’ through ‘*capping membranes*’ that cover and connect the working and reference electrodes. In this, the unspecific calibration solution used by the *Lab-in-a-box* is replaced by an unspecific dry capping membrane.

The model system was a sodium-selective potentiometric cell made with screen-printed carbon/graphite electrodes designed for the ‘*SWEATCH*’ wearable platform (Figure 6.3) [5]. This was first demonstrated to respond appropriately to the sodium ion before calibration strategies were tested. These strategies were approached in two stages: first, the principle of using a non-specific baseline potential reading (i.e. one that is not based on sodium) was examined in solution; secondly, the non-specific baseline potential was read through a solid membrane that *capped* the two electrodes.

The original inspiration for this study was an article by Lenk and coworkers, that used poly(vinyl alcohol) (PVA) for ‘*dissolvable film valving*’ in order to create a precise dosing mechanism of sample volume within an analytical device [6]. Drawing on this inspiration, this work tested PVA, as well as other hydrogels for a different purpose.

## HYDROGEL CAPPING MEMBRANES

---

A hydrogel is a material with appreciable absorption and retention of water. This property is due to hydrophilic groups such as  $-\text{OH}$ ,  $-\text{COOH}$ , and  $-\text{SO}_3\text{H}$ . Hydrogels can be neutral or ionic in nature [7].

Poly(vinyl alcohol) has the characteristics of being partially water-soluble, swellable, biocompatible, and non-conductive (Figure 6.1). Being water-soluble was desirable in order that the capping membrane could be deposited upon the underlying PVC membranes without dissolving them. It is further advantageous that PVA is only *partially* water-soluble, as the dissolution of the capping membrane may interfere with the measurement taking place at the same surface, for example by lowering the water activity and thereby increasing the activity of species dissolved in an aqueous sample. In this way, the swelling of the PVA is an attractive feature- the aqueous samples may permeate the capping membrane without dissolving it. Finally, it is crucial that the capping membrane is non-conductive. Were it to be so, the system would be short-circuited, and measurements would not be possible.

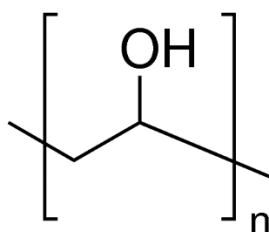


**Figure 6.1** Chemical structure of poly(vinyl alcohol) (PVA). The particular PVA used in this work had an average of:  $2023 < n < 2227$ .

Another consideration is that sensing membranes are known to be affected by their environment, and as such, their sensing surfaces can be altered prior to use. A capping membrane may therefore have the additional benefit of protecting the sensing surfaces from the environment during transport and storage right up to the moment of analysis. Figure 6.2 illustrates the concept of a capping membrane.

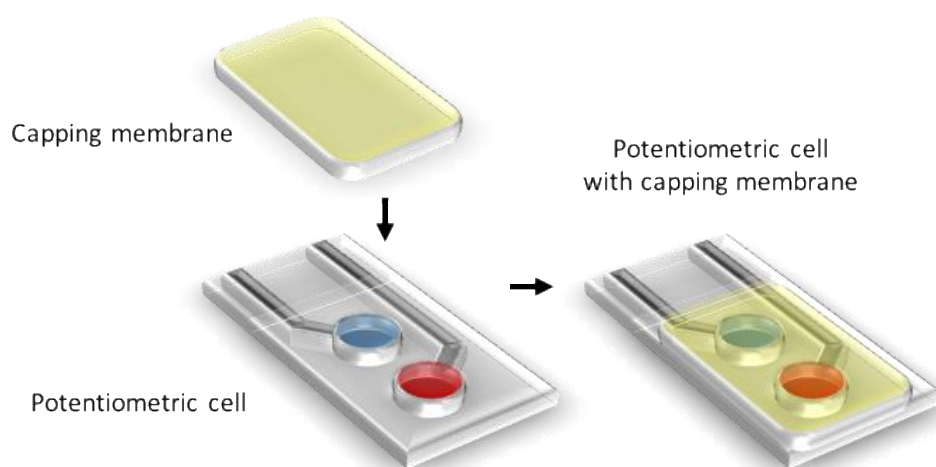


**Figure 6.2** Graphical representation of the capping membrane concept. The electrodes of a solid-state potentiometric cell are covered and connected by overlaid membrane.

## HYDROGEL CAPPING MEMBRANES

---

The electrodes were built upon a commercial carbon/graphite ink, without the addition of a specialized ion-to-electron transducing layer. Traditionally ISEs include such a layer, for example a conducting polymer like the poly-3,4-ethylenedioxythiophene (PEDOT) as previously reported within the SWEATCH platform [5]. The inclusion of such a layer tends to require complex and time consuming steps such as electrodeposition, as well as expensive reagents such as ionic liquids. Buhlman and coworkers list some 20 different materials reported as ion-to-electron transducers [8], several of which are carbonaceous. The carbon/graphite paste used herein had the combined functions of hydrophobic ion-to-electron transducer and electron-conducting substrate. Other works have similarly found suitable ion-to-electron transduction functionality in carbon black [9], carbon nanotubes [10], three-dimensionally ordered macroporous carbon [11], graphene [12], and graphite [12]. While sensors intended for long-term deployment may benefit from optimization of the ion-to-electron transduction manifold, for disposable sensors, a carbonaceous material would seem simple and sufficient.



**Figure 6.3** Left: The ‘Sweatch’ platform for sodium monitoring in sweat (from [5]) with horizontal arrangement of electronic and fluidic components consisting of 1: sweat harvesting device in 3d-printed platform base; 2: fluidic sensing chip, 3: electronic data logger and battery, and 4: 3D-printed upper casing. Right: one of the screen-printed disposable potentiometric cells used in the *Sweatch* platform.

## 6.2 Experimental

### 6.2.1 Materials

Carbon and dielectric inks used in the preparation of the screen-printed electrodes were obtained from Gwent Inc. Pontypool, UK (product codes C2030519P4 and D50706D2, respectively). PET sheets (175 mm thick, from HiFi, Dublin, Ireland) were used as the electrode substrate, and PMMA (0.5 mm thick) was obtained from GoodFellow, UK.

## HYDROGEL CAPPING MEMBRANES

---

### 6.2.2 Instrumentation

Potential was measured against a conventional reference electrode, except in tests made with a single-drop of solution upon the cell, in which case it was recorded directly against the PVC solid-state reference electrode. Photopolymerisation was carried out with a CL-1000 ultraviolet cross-linker UVP source produced by UVP, LLC (Upland, CA, USA).

### 6.2.3 Membrane preparation

The sodium selective cocktail was prepared by dissolving: 4.4 mg of sodium ionophore X, 1.1 mg of potassium tetrakis(4-chlorophenyl)borate, 101.4 mg PVC, 402.2 mg of bis(2-ethylhexyl) sebacate, in 3.556 g (4 mL) of THF.

The reference cocktail was prepared by dissolving 29.34 mg PVC, 58.67 mg of bis(2-ethylhexyl) sebacate and 37.99 mg of [1-hexyl-3-methylimidazolium]<sup>+</sup> [tris(pentafluoroethyl)trifluorophosphate]<sup>-</sup> ([HMIM][FAP]) in 1 mL of tetrahydrofuran (THF).

The membrane cocktails were agitated for 1 h before drop-casting in two additions of 5  $\mu$ L (total volume of 10  $\mu$ L per membrane). The membranes were allowed to dry for at least 3 h before conditioning for 1 h in 10 mM NaCl with 0.1 mM MgCl<sub>2</sub> as background electrolyte.

### 6.2.4 Preparation of capping membranes

#### 6.2.4.1 Poly(vinyl acetate)

A 0.1 M solution of poly(vinyl acetate) was prepared in a 1:1 mixture of water and ethanol. This cloudy solution was cast in 4 equal aliquots of 50  $\mu$ L upon a prepared potentiometric cell, allowing for partial evaporation of solvent between each addition.

#### 6.2.4.2 Poly(acrylamide)

The monomer acrylamide (200 mg, 100 mol %), the photopolymerisation initiator 2-hydroxy-2-methylpropiophenone (HMPP) (46.2 mg, 1 mol %), and the cross-linker (N,N'-methylenebisacrylamide) (MBIS) (12.4 mg, 0.5 mol %) were dissolved in 0.5 mL of ethanol and vortexed for 1 h to dissolve. A plastic frame (with inner dimensions of 4.5 x 6.7 mm and a depth of 0.13 mm) was placed around the border of the potentiometric cell, within which 30  $\mu$ L of this cocktail was pipetted and photopolymerised under a UV lamp for 20 minutes.

#### 6.2.4.3 Poly(ionic liquid)

Phosphonium sulfopropylacrylate (PSPA) was prepared in-house as reported [13]. PSPA (193.5 mg, 100 mol %), HMPP (0.6568 mg, 1 mol %), and poly(propylene glycol) (MW 800, PPG800) (16 mg, 5 mol %) were dissolved in a 1:1 mixture of ethanol:water and vortexed for 1 h to dissolve.

## HYDROGEL CAPPING MEMBRANES

---

A plastic frame (with inner dimensions of 4.5 x 6.7 mm and a depth of 0.13 mm) was placed around the border of the potentiometric cell, within which 30  $\mu\text{L}$  of this cocktail was pipetted and photopolymerised under a UV lamp for 20 minutes.

### 6.2.4.4 Poly(vinyl alcohol)

A 2 % (wt./vol.) PVA (average molecular weight 89,000-98,000, >99 % hydrolysed) solution was prepared in 0.1 mM  $\text{MgCl}_2$ . A 100  $\mu\text{L}$  drop of this was cast over the surface of the sensor to connect and cover the two electrodes (photographed in Figure 6.4 (left) and illustrated in Figure 6.5).

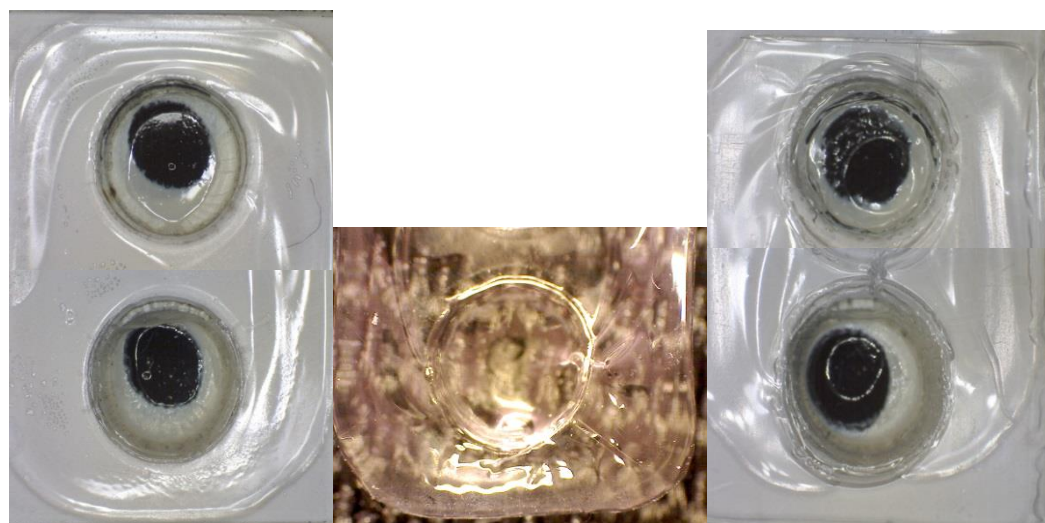


**Figure 6.4** Micrographs of the capping membrane. Left: over the electrodes. Center: after separation from the sensor. Right: capping membranes cast in water *without*  $\text{MgCl}_2$ .

### 6.2.5 Sensor preparation

The solid-state electrodes were prepared on a conducting carbon/graphite ink (C2030519P4) insulated by a dielectric layer (D50706D2) both procured from Gwent Electronic Materials Ltd. (Pontypool, UK). These layers were screen printed using a DEK 248 printer on 175  $\mu\text{m}$  thick PET sheets using the protocol reported by Zuliani *et al.* [14]. Two separate 3.0 mm diameter reservoirs were laser cut in 0.5 mm PMMA that was placed over the carbon electrodes in to which the sodium-selective and reference membrane cocktails were drop cast. This process is depicted in Figure 6.5.

## HYDROGEL CAPPING MEMBRANES

---

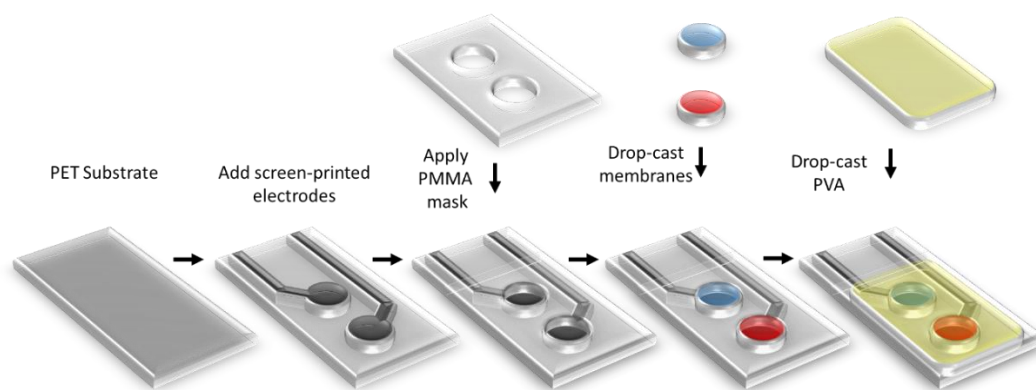


**Figure 6.5** Construction of the potentiometric cell. The substrate was prepared with screen-printed electrodes, working and reference membranes were drop-cast, finally, a PVA capping membrane was applied.

## 6.3 Results and discussion

### 6.3.1 Sodium sensing

As a basis for testing the *dry calibration* strategy, the electrodes were first demonstrated to respond appropriately to the sodium ion (Figure 6.6). The Na<sup>+</sup>-ISE responded in a Nernstian fashion and the solid-state pseudo-reference electrode remained stable across three orders of magnitude of NaCl concentrations, from 0.1 to 100 mM in a triplicate test.

While this is typical behaviour for ISEs, it is worth pointing out that no ion-to-electron transduction layer was included- the PVC membranes were in direct contact with the carbon/graphite layer. While enhanced stability may be an attractive feature for certain applications, this functionality is not relevant to single-use sensors, and so it would be extraneous to include. In general, this thesis argues for functional, usable and affordable sensors- if sensors are geared towards long-term use however, the ‘affordable’ price may be orders of magnitude higher than that of single-use devices.



## HYDROGEL CAPPING MEMBRANES

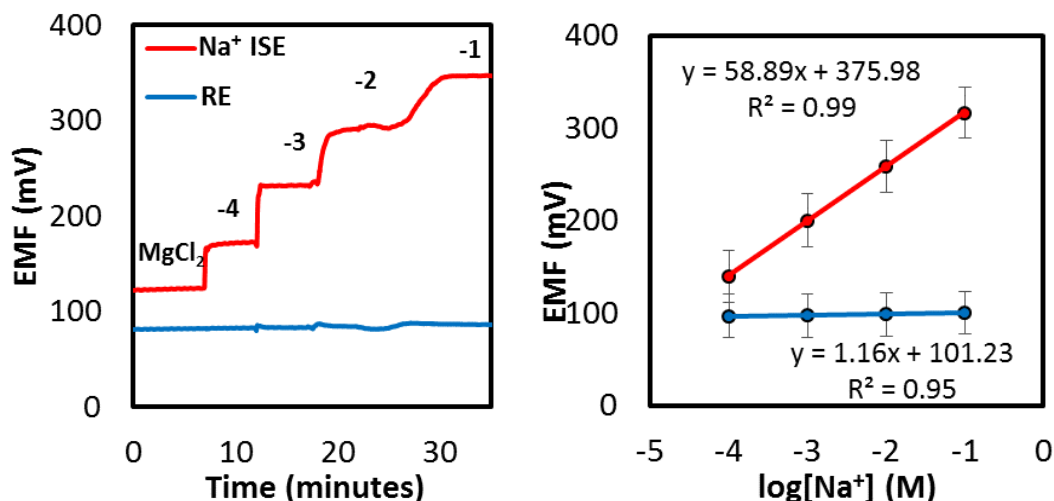


Figure 6.6 Left: time trace of a solid-state Na<sup>+</sup>-ISE and a solid-state RE's response to NaCl in a background electrolyte of 0.1 mM MgCl<sub>2</sub>. Numbers indicate logarithms of concentration. Right: the corresponding calibration plot; error bars represent one standard deviation of error between three of each electrode type.

### 6.3.2 The relationship of baseline potential to standard potential

The first five minutes of the time trace in Figure 6.6 shows that the EMF was stable in the background electrolyte solution of 0.1 mM MgCl<sub>2</sub>. While traditionally, calibrations are made exclusively with solutions of the primary analyte, here the question was whether a meaningful point of calibration could be taken in a background solution that did not contain the sodium ion. The idea was that the solution of MgCl<sub>2</sub> could act as a model for a similar system, only using a solid membrane in place of the solution. In this way, it may be hypothesized that a calibration could be made without the use of liquids.

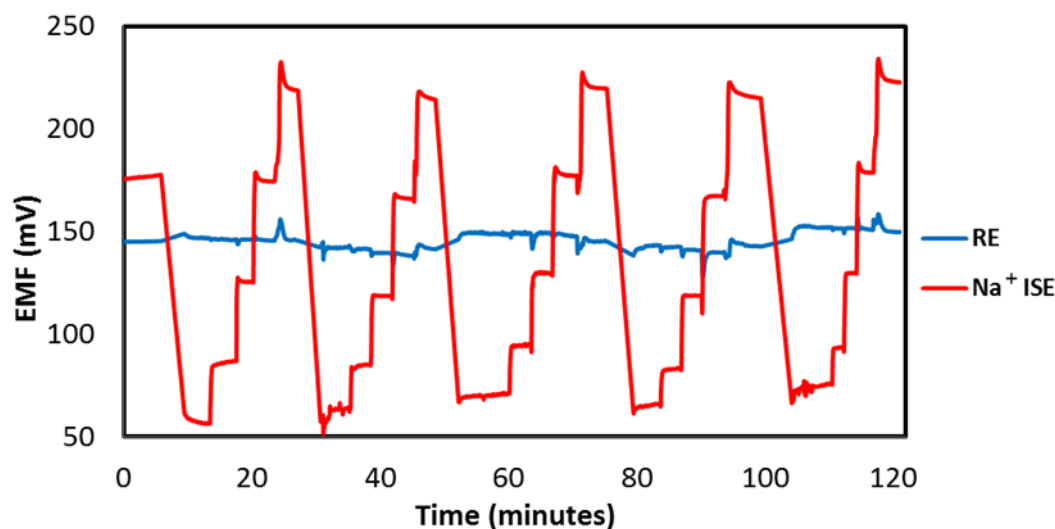


Figure 6.7 Time trace during five calibrations with NaCl from 0.1 to 100 mM NaCl. A point of 0.1 mM MgCl<sub>2</sub> is recorded between each calibration.

Towards this, three sensors were prepared as described. Five successive calibrations of each were made with 0.1 mM MgCl<sub>2</sub> acting as the background electrolyte (Figure 6.7). The baseline potential in MgCl<sub>2</sub> ( $E_{\text{baseline}}$ ) was

## HYDROGEL CAPPING MEMBRANES

recorded prior to each calibration and subsequently compared with the standard potential of the given calibration. A pattern was discerned across the three sensors and five calibrations. The relationship of baseline potential to standard potential is illustrated in Figure 6.8 and can be summarized in an equation to estimate the standard potential:

$$E^0 = (0.66 \pm 0.05) E_{\text{baseline}} + (170.82 \pm 6.85) \text{ mV} \quad (\text{Equation 6.1})$$

There was a correlation between the two terms, although this was with a considerable amount of error. The question was whether this relationship would hold when the background electrolyte solution was replaced for a ‘solid background electrolyte’ - a polymer capping membrane, and whether the correlation would be stronger or weaker.

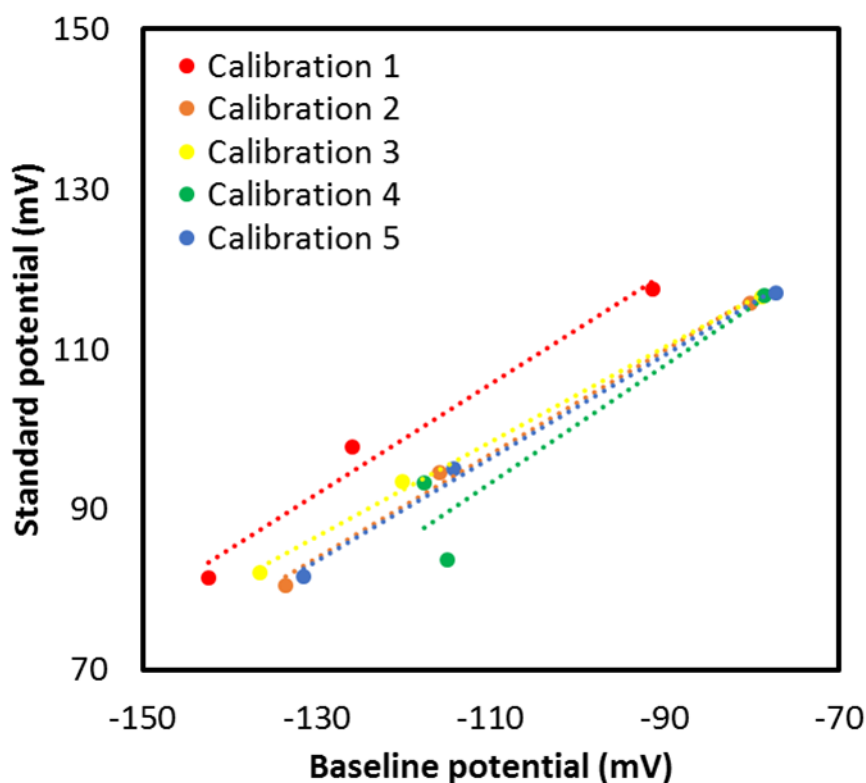


**Figure 6.8** Plot of the relationship between baseline potential and standard potential for three sensors during five calibrations.

### 6.3.3 Screening of capping membranes

A preliminary screening of four capping membrane materials was made. The four materials and their associated properties are summarized in Table 6.1. In this, membrane consistency refers to the visual appearance; whether a homogeneous, smooth coverage was obtained or otherwise. This is important both for ensuring that the capping membrane connects the circuit and for reproducibility. Poly(vinyl acetate) was eliminated as a candidate due to its poor solubility in solvents which would not dissolve the underlying PVC

## HYDROGEL CAPPING MEMBRANES

membranes. While a solution of poly(vinyl acetate) was prepared, it was so dilute that upon evaporation of solvent, no appreciable layer of polymer remained- certainly not sufficient for the function of capping the underlying electrodes.

The electrical impedance is also an important consideration. Were this to be too low, the capping membrane would effectively short-circuit the cell, whether wet or dry, and would likely result in a cell unresponsive to changes in sodium concentration. On the other hand, the electrical impedance cannot be so high that it approaches the input impedance of the potentiometer. As the instrument in question has an input impedance of  $10^{15} \Omega$ , the impedance must certainly remain at least two orders of magnitude below this. This is an instrumental limitation.

**Table 6.1** The four materials tested as capping membranes with their associated consistency and electrical impedance

Composition	Membrane consistency	Impedance, dry (M $\Omega$ )	Impedance in 0.1 M NaCl (M $\Omega$ )
<b>Poly(vinyl acetate)</b>	Non-homogenous, non-continuous, poor coverage, due to poor solubility	N / A	N / A
<b>Poly(ionic liquid) hydrogel</b>	Consistent coverage, transparent	170	100
<b>Poly(acrylamide) hydrogel</b>	Consistent coverage, white dry, transparent wet	110	70
<b>Poly(vinyl alcohol) hydrogel</b>	Smooth, homogenous, transparent	150	1

The impedance measurements also revealed a chemical limitation; the permeability of the capping membrane. While sensors with poly(ionic liquid), poly(acrylamide) and poly(vinyl alcohol) all shared a similar impedance between 110 and 170 M $\Omega$  when dry, and visibly swelled in contact with 0.1 M NaCl, their wet impedances differed significantly. The minor change in impedance of the poly(ionic liquid) and poly(acrylamide) suggests that while they swelled with water, very little of the sodium chloride was able to permeate these capping membranes and reach the sodium-selective membrane. This may be attributable to ion-polar group interactions between the NaCl and the polar groups of the poly(acrylamide) or indeed the ionic groups of the poly(ionic liquid).

The sensors capped with these hydrogels showed no appreciable response to NaCl, providing further evidence to the hypothesis that they are poorly permeated by ions.

## HYDROGEL CAPPING MEMBRANES

On the other hand, the two order of magnitude decrease in impedance of the sensor capped with poly(vinyl alcohol) indicates that indeed NaCl was able to permeate this membrane significantly. The complex impedance spectra of the PVA-capped sensor when dry and when exposed to 0.1 M NaCl are shown in Figure 6.9. The uncapped potentiometric sensor experienced 0.75 M $\Omega$  of impedance through 0.1 M NaCl. The addition of a PVA capping membrane increased this only a minor degree to 1 M $\Omega$ .

As these capped sensors also showed potentiometric response to NaCl, it was selected as the capping membrane of choice for the subsequent experiments.

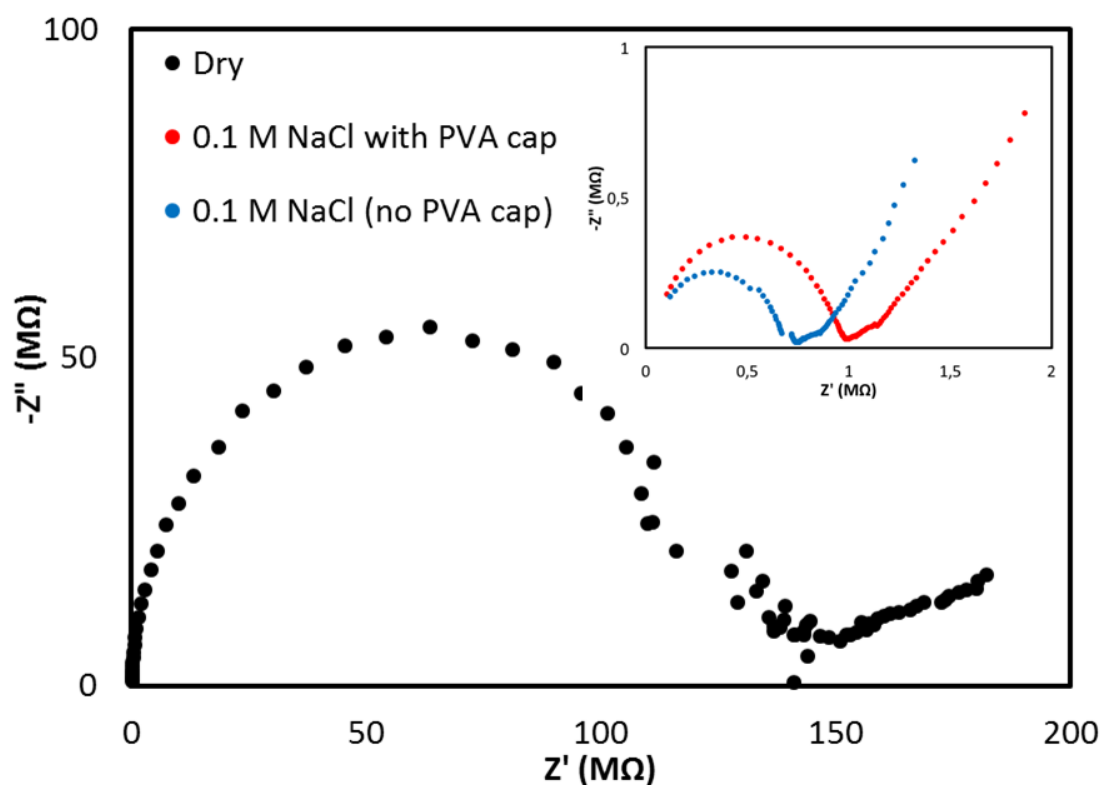


**Figure 6.9** Complex impedance plot of the potentiometric cell with PVA capping membrane when dry (black markers) and when swelled with 0.1 M NaCl (red markers) (inset).

### 6.3.4 Poly(vinyl alcohol) capping membranes

#### 6.3.4.1 Properties of PVA capping membranes

Sodium sensors were prepared and conditioned as already described and rinsed with distilled water. By careful separation of the capping membrane from the sensor, it was measured to have a thickness of  $130 \pm 20 \mu\text{m}$  ( $n = 3$ ) (Figure 6.4, centre). Being aqueous, it was not expected to, and indeed not visually observed to alter the underlying organic membranes.

## HYDROGEL CAPPING MEMBRANES

---

The capping membrane solution was optimized in two regards. Firstly, in terms of concentration, the 2 % solution was found to deposit sufficient PVA to cover the electrodes while being of a suitable viscosity for drop-casting. Secondly, the low concentration of  $\text{MgCl}_2$  was included with the intent of *slightly* increasing the conductivity of the membrane. Experimentally it was found to result in smooth capping membranes which adhered well to the underlying substrate as seen in Figure 6.4, left. By contrast, excluding this salt led to ‘jagged’, ‘edgy’ capping membranes that easily peeled away from their underlying substrates (Figure 6.4, right).

It was found that the EMF through the dry capping membrane- the  $E_{\text{dry}}$ - could be read as a stable signal, which confirmed that the PVA functioned in closing the electrical circuit. Signals were not entirely steady-state however, instead appearing sinusoidal in form, with an amplitude that was a function of the sodium chloride concentration. Figure 6.10 shows the time trace of a sensor during a calibration with sodium. After removing the sensor from solution, the EMF could still be monitored as the solution of 100 mM was soaked inside the capping membrane. Although the amplitude of the sinusoidal signal increased, the EMF corresponding to the 100 mM could still be read some 30 minutes later, at which time the capping membrane began to dry out. The EMF changed during the drying process until it returned to the same  $E_{\text{dry}}$  as previously. The inset of Figure 6.10 shows the sinusoidal signal form which had a period of around 17 seconds throughout the calibration and an amplitude that decreased from 9 mV when dry to 1 or 2 mV in solution.

The PVA capping membranes were found to swell in solution and if the solution was stirred vigorously, they would ultimately separate from the sensor. Experiments with capping membranes were therefore carried out with very gentle stirring or by placing the sensor horizontally and placing a 100  $\mu\text{L}$  drop of solution upon them.

The physical meaning of this sinusoidal signal is not well understood. It is suggested that it is not specific to the capped sensors, but rather is instrumental in origin. This could be from other instruments within the lab, or indeed from the potentiometer itself.<sup>15</sup>

---

<sup>15</sup> This last explanation may be due to the particular instrument used lacking the required 75  $\Omega$  resistors on unused input channels. When tested with another potentiometer of the same model in a different laboratory, the signal was observed to be stable, without the sinusoidal noise.

## HYDROGEL CAPPING MEMBRANES

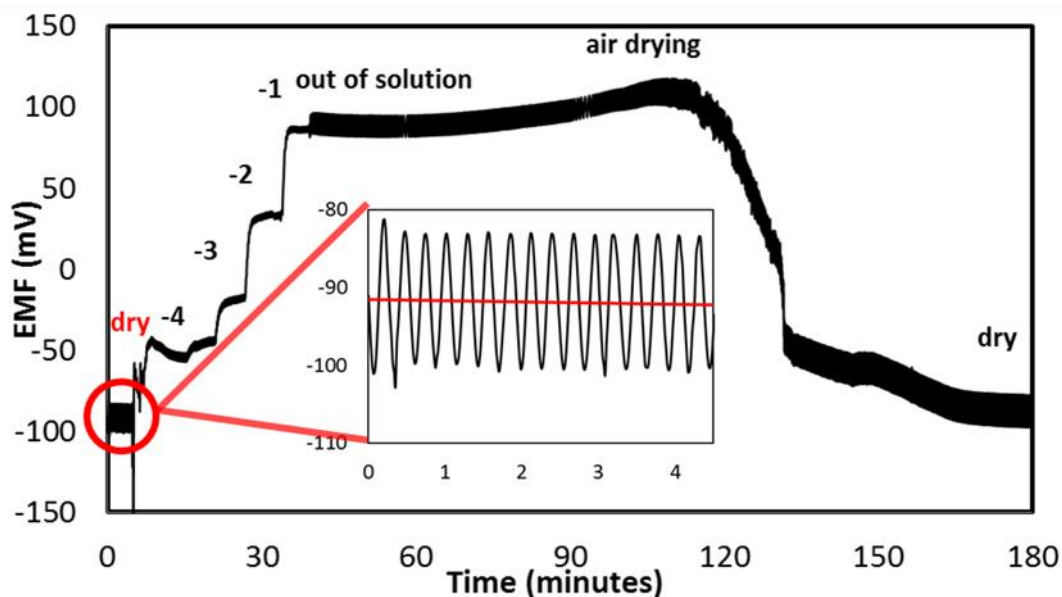


**Figure 6.10** Time trace during calibration of a capped sensor. The first 4.5 minutes while dry the sensor is dry are shown within the inset.

### 6.3.4.2 Predicting standard potentials with PVA capping membranes

To test if the EMF through capping membranes could be used to predict the standard potential of the underlying sensor, six sodium sensors were prepared as described previously. They were calibrated to obtain what we shall here call their *pre-capping standard potential* before being capped with PVA. The  $E_{dry}$  was read through the dry capping membrane, and finally a subsequent calibration was made to determine the *post-capping standard potential*.

**Table 6.2** Sensitivity and standard potentials of six sodium sensors before and after capping with PVA

	Pre-capping	Post-capping
<b>Sensitivity (mV/dec.<sub>[Na<sup>+</sup>]</sub>)</b>	53.87 ± 1.08	50.58 ± 2.18
<b>Standard potential (mV)</b>	236.90 ± 11.87	73.71 ± 55.37

The difference in sensitivity before and after capping was not statistically significant (Table 6.2). This was important to ascertain, as one-point calibrations rely on assuming the sensitivity to be Nernstian. It may be perhaps be related to the higher impedance of the sensor described when measuring through the PVA capping membrane.

The standard potential however, did change appreciably, as also shown in Table 6.2. Thus, it would seem that the underlying PVC membranes were indeed affected by the capping membrane, resulting in a minor loss in sensitivity and a considerable shift in standard potential. It is to be expected that the potential drop between an electrode and PVA will differ from that between the electrode and an aqueous solution, were this effect to be equally pronounced at each electrode, the net effect would be zero.

## HYDROGEL CAPPING MEMBRANES

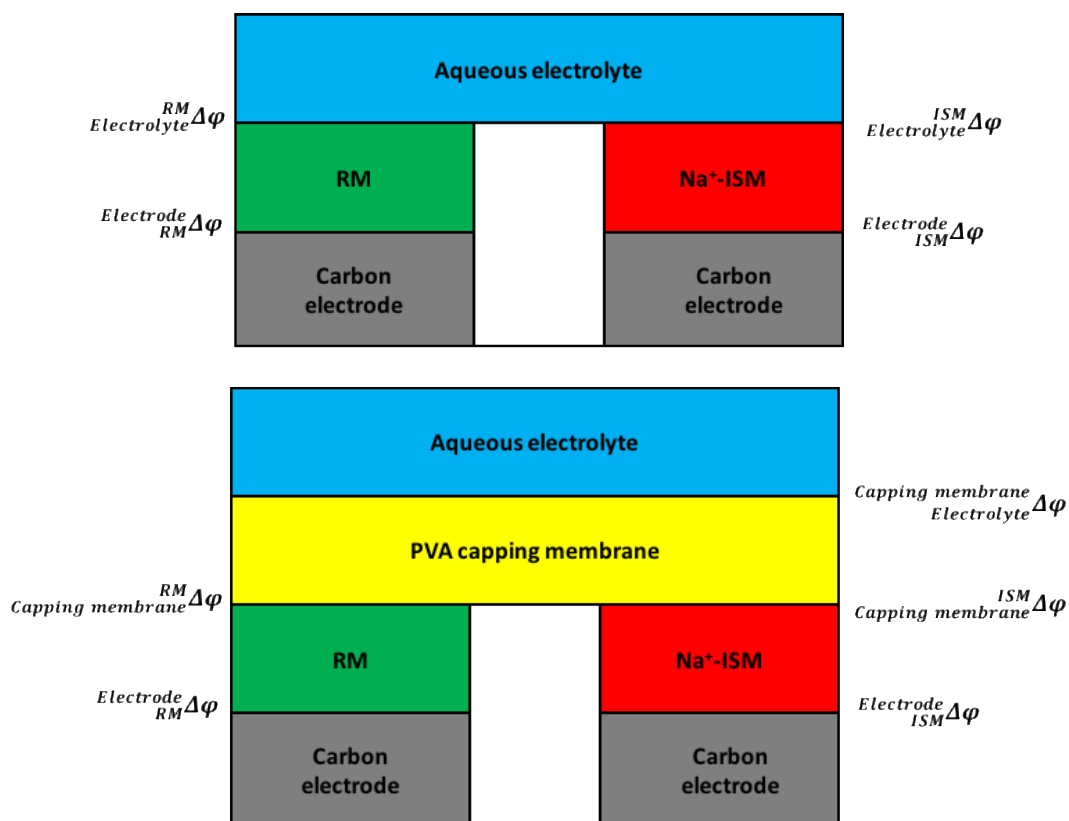


**Figure 6.11** Junction potentials appearing in the circuit of the potentiometric cell. Above: through aqueous electrolyte; Below: through PVA after a capping membrane has been applied. (RM = reference membrane; ISM = ion-selective membrane).

Figure 6.11 depicts the potentiometric cell with the junction potentials that appear at each interface. As described in Chapter 2, the diffusion potential is assumed to be zero in accordance with the phase-boundary model. Furthermore, the junction potentials between the electrodes and the PVC membranes ( $Electrode_{RM}^{RM}\Delta\phi$  and  $Electrode_{ISM}^{ISM}\Delta\phi$ ) are assumed to be almost constant- although subject to minor fluctuations commonly termed ‘drift’. The -163 mV shift in standard potential would therefore most likely be attributable to the interface between the PVC membranes and the ‘electrolyte phase’, be it water or poly(vinyl alcohol). As water and PVA are very different compounds, it is understandable that:

$$Electrolyte^{RM}\Delta\phi \neq Capping\ membrane^{RM}\Delta\phi; \text{ and } Electrolyte^{ISM}\Delta\phi \neq Capping\ membrane^{ISM}\Delta\phi$$

However, the shift in standard potential would suggest that the change at the reference membrane was not the same as at the sodium-selective membrane. That is:

$$(Electrolyte^{RM}\Delta\phi - Capping\ membrane^{RM}\Delta\phi) \neq (Electrolyte^{ISM}\Delta\phi - Capping\ membrane^{ISM}\Delta\phi)$$

While there is no experimental evidence to explain this phenomena, it is not surprising since the chemical interactions and capacitive effects- among other factors, are very different in both cases.

## HYDROGEL CAPPING MEMBRANES

In contrast to chemical and instrumental approaches to making highly reproducible standard electrodes in order to obviate calibration within the literature, this approach led to highly *irreproducible* standard potentials. That is, the novel step of applying the capping membrane led to greater inter-sensor variability in the standard potential values. Nevertheless, it will be seen whether the approach has merit.

Figure 6.12 plots the *pre-capping* and *post-capping* standard potentials against our predictive parameter, the  $E_{dry}$ . The relationship between the *pre-capping standard potential* and the  $E_{dry}$  was not strong. The *post-capping* standard potential however, did show some correlation with the  $E_{dry}$ , which is of course, more predictively useful. A one-to-one relationship between the two terms would indicate that the dry signal could be used to predict the standard potential. This relationship was indeed observed, although it was statistically poor, having a coefficient of determination of just 0.80. Nonetheless, a predictive relationship was arrived at:

$$E_{\text{post-capping}}^0 = (1.08 \pm 0.27) E_{\text{dry}} + (187.32 \pm 30.79) \text{ mV} \quad (\text{Equation 6.2})$$

In which the uncertainty represents one standard deviation of confidence between the 6 cells from an ANOVA regression.

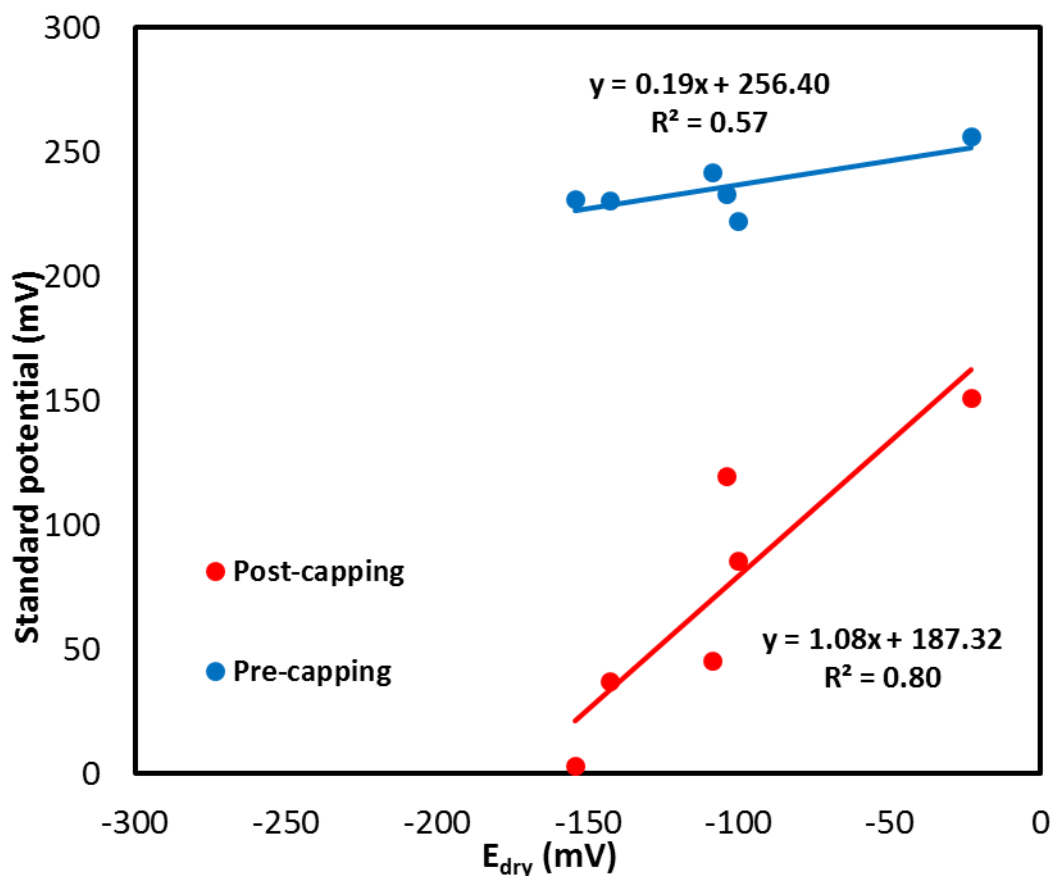


**Figure 6.12** Relationship between the dry potential and the standard potentials, before and after capping



## HYDROGEL CAPPING MEMBRANES

---

Because the offset of 187 mV between the two terms was not known prior to the experiment, prediction was not possible. Nevertheless, in principle it could have been established from testing a few sensors within a larger batch, so this is not prohibitive.

It is not suggested that the capping membrane *introduced* a relationship between  $E_{dry}$  and  $E_{post-capping}^0$ . Rather, that the capping membrane facilitated an interrogation of the  $_{Electrode}^{ISM}\Delta\varphi$  and  $_{RM}^{Electrode}\Delta\varphi$ , in a dry environment just as an unspecific electrolyte ( $MgCl_2$ ) was previously used to interrogate this interfacial potential in solution.

### 6.4 Conclusions

Within the limited scope of this exploration and the six sensors tested, a loose one-to-one correlation between the dry potential and the (post-capping) standard potential was established. From this, a predictive relationship was established, albeit with high statistical margins of error. Although the scale of the study was too small to draw strong conclusions, the preliminary patterns observed indicate there to be some merit in the idea.

The preliminary screening of candidate materials revealed some desired properties of capping membranes. These include swelling, yet having low solubility; being permeable to not just water, but also to ions; and having very low inherent conductivity. Given these specifications, a further range of candidates could be tested as capping membranes.

Beyond simply replacing the material, consideration could also be given to the geometry of the sensor and capping membrane. With the understanding that it is the potential at the electrode-PVC membrane interface that is being interrogated, a capping membrane need not completely cover the PVC membrane surface. The capping membrane could be applied in such a way that it only covered half of the underlying membrane surface. This is just one of many possible design and geometric variations that could be tested.

It may be that with optimization of the capping membrane material, design or geometric adjustments, or with the greater reproducibility afforded by mass-manufacturing, a dry calibration approach could indeed prove functional. In any case, larger scale studies would be needed to provide greater statistical confidence of the relationship tentatively indicated here. At this stage however, the weak predictability would not lend itself to real-world applications requiring accurate determinations of sodium.

## 6.5 References

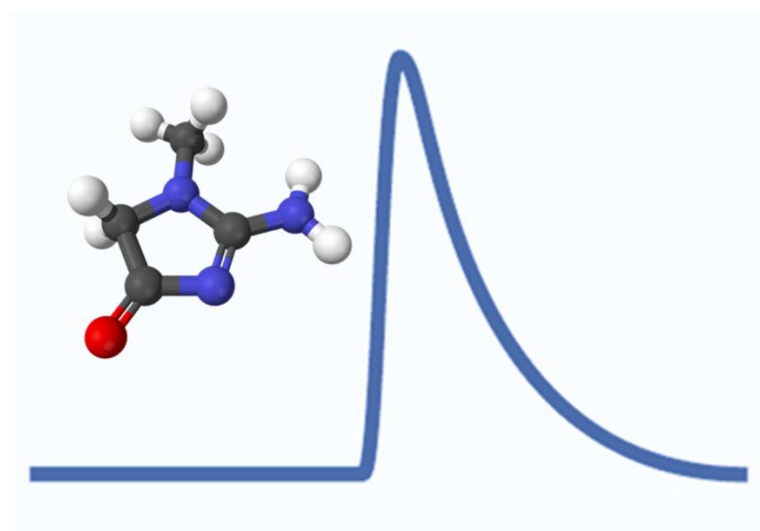
- 1 U. Vanamo and J. Bobacka, Electrochemical control of the standard potential of solid-contact ion-selective electrodes having a conducting polymer as ion-to-electron transducer, *Electrochim. Acta*, 2014, **122**, 316–321.
- 2 U. Vanamo and J. Bobacka, Instrument-free control of the standard potential of potentiometric solid-contact ion-selective electrodes by short-circuiting with a conventional reference electrode, *Anal. Chem.*, 2014, **86**, 10540–10545.
- 3 X. U. Zou, X. V. Zhen, J. H. Cheong and P. Bühlmann, Calibration-Free Ionophore-Based Ion-Selective Electrodes With a Co(II)/Co(III) Redox Couple-Based Solid Contact, *Anal. Chem.*, 2014, **86**, 8687–8692.
- 4 F. X. Rius-Ruiz, G. A. Crespo, D. Bejarano-Nosas, P. Blondeau, J. Riu and F. X. Rius, Potentiometric Strip Cell Based on Carbon Nanotubes as Transducer Layer: Toward Low-Cost Decentralized Measurements, *Anal. Chem.*, 2011, **83**, 8810–8815.
- 5 T. Glennon, C. O’Quigley, M. McCaul, G. Matzeu, S. Beirne, G. G. Wallace, F. Stroiescu, N. O’Mahoney, P. White and D. Diamond, ‘SWEATCH’: A Wearable Platform for Harvesting and Analysing Sweat Sodium Content, *Electroanalysis*, 2016, **28**, 1283–1289.
- 6 N. R. Gabriel Lenk, Sören Sandkvist, Anton Pohanka, Göran Stemme, Olof Beck, G. Lenk, S. Sandkvist, A. Pohanka, G. Stemme, O. Beck and N. Roxhed, A disposable sampling device to collect volume-measured DBS directly from a fingerprick onto DBS paper, *Bioanalysis*, 2015, **7**, 2085–2094.
- 7 N. A. Peppas and A. R. Khare, Preparation, structure and diffusional behavior of hydrogels in controlled release, *Adv. Drug Deliv. Rev.*, 1993, **11**, 1–35.
- 8 J. Hu, A. Stein and P. Bühlmann, Rational design of all-solid-state ion-selective electrodes and reference electrodes, *TrAC - Trends Anal. Chem.*, 2016, **76**, 102–114.
- 9 B. Paczosa-Bator, All-solid-state selective electrodes using carbon black, *Talanta*, 2012, **93**, 424–427.
- 10 G. A. G. A. Crespo, S. Macho, F. X. Rius, Gastón A. Crespo, A. Santiago Macho and F. X. Rius, Ion-Selective Electrodes Using Carbon Nanotubes as Ion-to-Electron Transducers, *Anal. Chem.*, 2008, **80**, 1316–1322.
- 11 C. Z. Lai, M. A. Fierke, A. Stein and P. Bühlmann, Ion-selective electrodes with three-dimensionally ordered macroporous carbon as the solid contact, *Anal. Chem.*, 2007, **79**, 4621–4626.
- 12 F. Li, J. Ye, M. Zhou, S. Gan, Q. Zhang, D. Han and L. Niu, All-solid-state potassium-selective electrode using graphene as the solid contact, *Analyst*, 2012, **137**, 618–623.
- 13 A. Tudor, J. Saez, L. Florea, F. Benito-Lopez and D. Diamond, Poly(ionic liquid) thermo-responsive hydrogel microfluidic actuators, *Sensors Actuators, B Chem.*, 2017, **247**, 749–755.
- 14 C. Zuliani, G. Matzeu and D. Diamond, A potentiometric disposable sensor strip for measuring pH in saliva, *Electrochim. Acta*, 2014, **132**, 292–296.

## HYDROGEL CAPPING MEMBRANES

---

## 7 POTENTIOMETRIC DETERMINATION OF CREATININE BY FLOW INJECTION ANALYSIS

---



## POTENTIOMETRIC DETERMINATION OF CREATININE BY FIA

---

### 7.1 Introduction

In frequency and importance of clinical analysis, creatinine (Figure 7.1) is perhaps second only to glucose. Evaluation of the creatinine clearance rate is considered the primary indicator of glomerular filtration rate [1]. Thus, creatinine is recognized as a principal indicator of renal function and its determination is therefore crucial in routine medical check-ups, and critical in the monitoring of chronic kidney disease. Its levels are of paramount significance in acute conditions and accidents, while diagnosing infections (particularly of the urinary tract), after delivery of certain drugs (e.g., while performing contrast diagnostic imaging) and any other situation in which acute kidney condition may represent a serious risk for life. Unfortunately however, the determination of creatinine is not free of problems [2, 3].

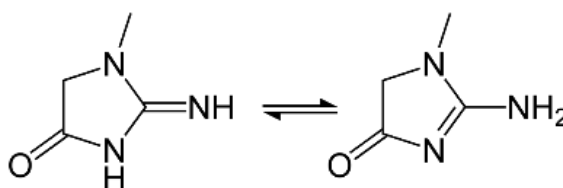


**Figure 7.1** The creatinine molecule.

Until recently, the primary methods of creatinine determination were variations on the Jaffe method [2]. This is a colorimetric approach that monitors changes in the brilliantly coloured product of picric acid and creatinine under basic conditions in a complex, tedious, and time-consuming procedure. Moreover, it suffers from interferences from several other compounds naturally present in biological samples.

Alternative assays are either based on (colorimetric) enzymatic reactions or isotope dilution gas chromatography. While the former still shows analytical challenges [2, 4], the latter is accurate yet remains unsuitable for most use cases due to the high specialisation, cost and instrumentational footprint involved [5].

Recently our research group reported a polymeric membrane with a novel synthetic receptor for the protonated form of creatinine, the creatinium ion [6]. Ion-selective electrodes prepared with this ionophore demonstrated excellent performance for the determination of creatinine in urine and blood plasma when acidified and diluted appropriately. This offers an alternative method for creatinine determination, which could be adapted for adoption by clinical laboratories, or indeed for user-centred decentralized applications, such as home-based analysis. One way to integrate with existing clinical instrumentation would be to develop a flow injection analysis (FIA) method compatible with the flow injection analysers currently used for ion determination. This would facilitate the affordable, high-throughput determination of creatinine for clinical applications.

Flow injection analysis is an automated method of fluid handling developed in the mid-1970's. It involves the injection of liquid samples into the continuous flow of a carrier stream within microfluidic tubing. Thus, it operates under laminar flow, and mixing between samples and the carrier (and in some cases reagents) is primarily dispersive as opposed to convective. One advantage of this is a low likelihood of carry-over between

## POTENTIOMETRIC DETERMINATION OF CREATININE BY FIA

successive samples [7]. Unlike its predecessor technique, segmented flow analysis (SFA), FIA does not separate samples with air bubbles- it uses unsegmented flow [7]. The different flow profiles of these methods are illustrated in Figure 7.2.

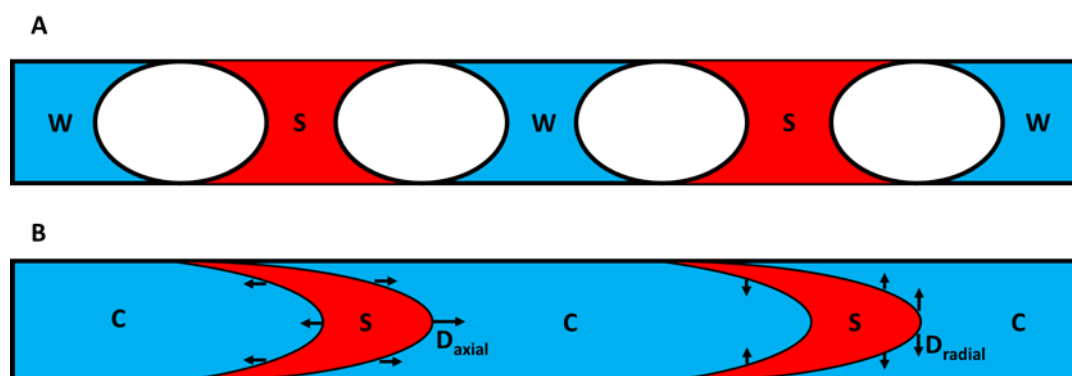


**Figure 7.2** Sample profiles during, A: Segmented flow analysis (SFA); and B: Flow injection analysis (FIA). During SFA, W indicates a washing solution between samples (S). These are separated by air bubbles. During FIA, a carrier stream (C), is punctuated by injection of samples (S) that diffuse radially ( $D_{\text{radial}}$ ) and axially ( $D_{\text{axial}}$ ).

In general, FIA has several attributes that make it an attractive analytical tool. It requires minimal sample volumes, has a low cost and complexity of instrumentation, is time efficient, and it can be easily tuned for different analytes [8]. The time efficiency stems from creating a ‘production line’ within microfluidic tubing to combine processes such as sample dilution, reagent addition, and sensor washing- all within a temporally controlled, highly reproducible system, and without necessarily arriving at equilibration of convection or reaction. In fact, this is the standout quality of FIA- they can make reproducible measurements under dynamic conditions; a feature afforded by the precise timing inherent to flow systems.

A further advantage- and one that Elo Harold Hansen, one of the fathers of FIA, has considered underexploited- is the availability of a continuum of concentration ranges [9]. When operating under a limited dispersion regime, FIA acts a well-controlled transport mechanism of (nearly undiluted) samples to the detector. In a medium dispersion regime however, mixing of reagents can play a significant role, and offer an appreciable advantage to the FIA technique. This is because it provides reproducible analysis following a chemical reaction, without the time-inefficiency of waiting for chemical equilibrium to be obtained [9]. The desired point within the spectrum of dispersion can be accessed by considering any point on a signal peak between zero and the peak maxima,  $C^{\text{max}}$ . This can also be tuned by changing the  $V_{\text{reactor}}$ , or the length of microfluidic tubing between the injection valve and the detector.

Flow injection analysis has proved highly versatile in being coupled with various analytical detection methods. While the first report demonstrated potentiometric as well as spectrophotometric detection [10], subsequent works have gone on to expand the range of optical and electrochemical methods incorporating FIA. These include, among optical methods: colorimetry, fluorimetry, chemiluminescence, atomic fluorescence, and

## POTENTIOMETRIC DETERMINATION OF CREATININE BY FIA

---

atomic absorption spectroscopy; and among electrochemical methods: conductimetry, potentiometry, voltammetry, and amperometry [11].

Potentiometry is highly favoured as a detection method in flow analysis. This is due to its extremely wide dynamic ranges, and ease of operation [7]. Operating within an ionic strength buffer, it simply requires an indicator and reference electrode along with a grounding device. The indicator acts as the detector, while the reference electrode is typically collocated or placed slightly downstream, ensuring that no appreciable resistance is incurred between the two electrodes. The grounding device is simply an electrical grounding point located as close to the detector as possible. This is important to avoid the accumulation of streaming potentials or static discharges.

In consideration of creatinine determinations within a FIA system, the sample acidification demanded by the method described by Guinovart *et al.* could in principle be performed on-line, within the flow manifold, thereby eliminating a source of error and the time costs associated with these manual handling steps [6]. As the described method required dilutions of 10 or 100 fold, for determinations in serum or urine respectively, a high dispersion procedure could eliminate the need for this manual sample preparation step. Furthermore, the brief contact time between sample and sensor within a flow system, could prevent or minimise membrane fouling, a problem commonly encountered with determinations within these complex matrices [9].

The flipside of the high tunability of FIA systems is the myriad variables involved. As such, many modifications to the system were tested- only some of which are presented here, each to illustrate a principle of the technique, and the challenges encountered in developing a flow method for creatinine determination.

## 7.2 Experimental

### 7.2.1 Materials

FIA systems were made using FEP tubing of 0.5 mm inner diameter (JR-T-6804-M10) manufactured by Vic International AG (Schenk, Switzerland). Connections between tubing were made with PVC tubing of 1.295 mm inner diameter (reference: 38-0046) made by Spetec GmbH (Erding, Germany), which was also used in the Gilson peristaltic pump. Injections were made with the manual actuation of an injection valve that had been removed from a HPLC instrument.

Two types of single-junction Ag/AgCl reference electrodes were used: a KZT-5 low-leakage reference electrode from Innovative Instruments, Inc. (Tampa, USA); and also, separately, the inner Ag/AgCl junction of a modified double-junction 3 M Ag/AgCl/KCl (type 6.0726.100) reference electrode from Metrohm AG, Switzerland.

Creatinine-selective and potassium-selective membranes were cast onto glassy carbon electrodes of 3 mm, as well as copper wires of 1 mm diameter.

## POTENTIOMETRIC DETERMINATION OF CREATININE BY FIA

Flow cells were made in-house from poly(methyl methacrylate). An inlet and outlet to connect with the microfluidic tubing were drilled into the flow cell, as were apertures with tapped screw threads to tightly accommodate electrodes (Figure 7.3, A). This screw thread sealed reference electrodes, glassy carbon electrodes (Figure 7.3, B), and copper micro electrodes (Figure 7.3, C).

A grounding device was included in the form of a carbon tube located immediately after the flow cell. All flow passed through this tube, which was electrically grounded to the potentiometer with a copper wire (shown in Figure 7.4).

A screw thread was tapped into the Teflon body housing the glassy carbon electrodes in order to make an air-tight connection within the flow cell. Glassy carbon electrodes were mirror polished before being retracted some 2 mm from the exterior of the housing. This prevented the membrane cast within the space from being damaged when the electrode was screwed into the flow cell. Microelectrodes were fabricated by drilling holes through a plug of PVC and inserting copper wires. The exposed tips of these wires were polished with alumina to form a flat surface, 1 mm in diameter.

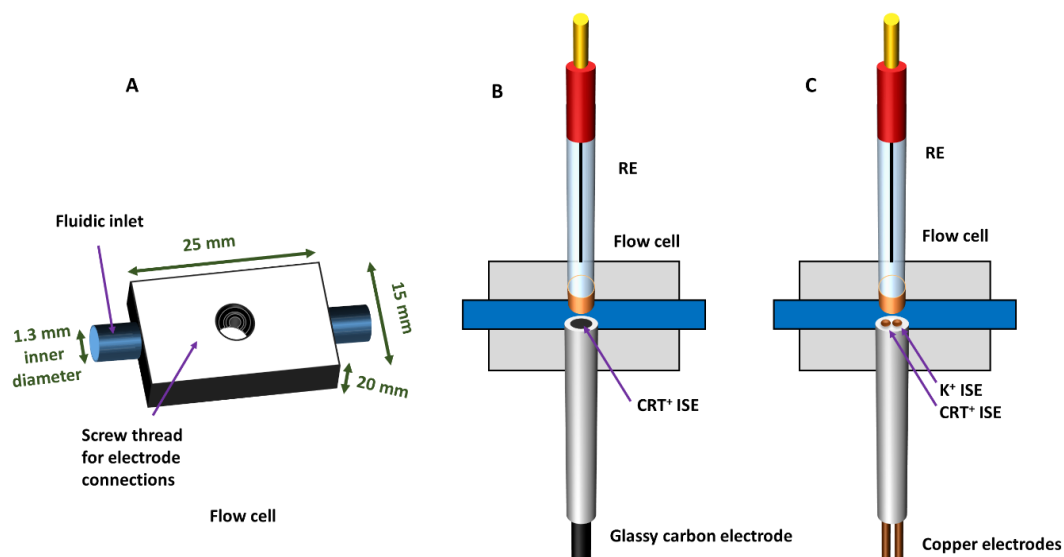


**Figure 7.3** Flow cells within the FIA system. **A:** detail of the flow cell. **B:** Flow cell with a single creatinine-selective membrane upon a glassy carbon electrode. **Right:** Flow cell with both potassium and creatinine-selective membranes upon copper wires.

### 7.2.2 Membrane preparation

Membrane cocktails were drop cast upon glassy carbon electrodes as 15  $\mu\text{L}$  in three equal aliquots, or upon copper electrodes as 1.25  $\mu\text{L}$  in 5 equal aliquots.

The preparation of the membrane cocktails is described in Chapter 3.

In the case of microelectrodes upon copper, 0.5 mg of multi-walled carbon nanotubes (MWCNTs, 95 % purity, 30–50 nm outer diameter,  $\sim 15 \mu\text{m}$  length) were included per millilitre of membrane cocktail. They were



## POTENTIOMETRIC DETERMINATION OF CREATININE BY FIA

purchased from Chengdu Organic Chemicals Co. (Chengdu, Sichuan, China). These were ground with a mortar and added to the membrane cocktail, which was then sonicated for 20 minutes prior to casting, to ensure dispersion.

### 7.2.3 FIA manifold

The basic setup used a peristaltic pump to drive a carrier solution through an injection valve and into the flow cell. A second fluidic channel upon same pump pulled samples through the injection valve (Figure 7.4). Samples were injected by turning the injection valve by hand. The microfluidic tubing initially corresponded to a sample volume of 12  $\mu\text{L}$  and a reactor volume of 27  $\mu\text{L}$ , which was used unless otherwise stated. The tubing diameter (of 0.5 mm inner diameter) was not varied.

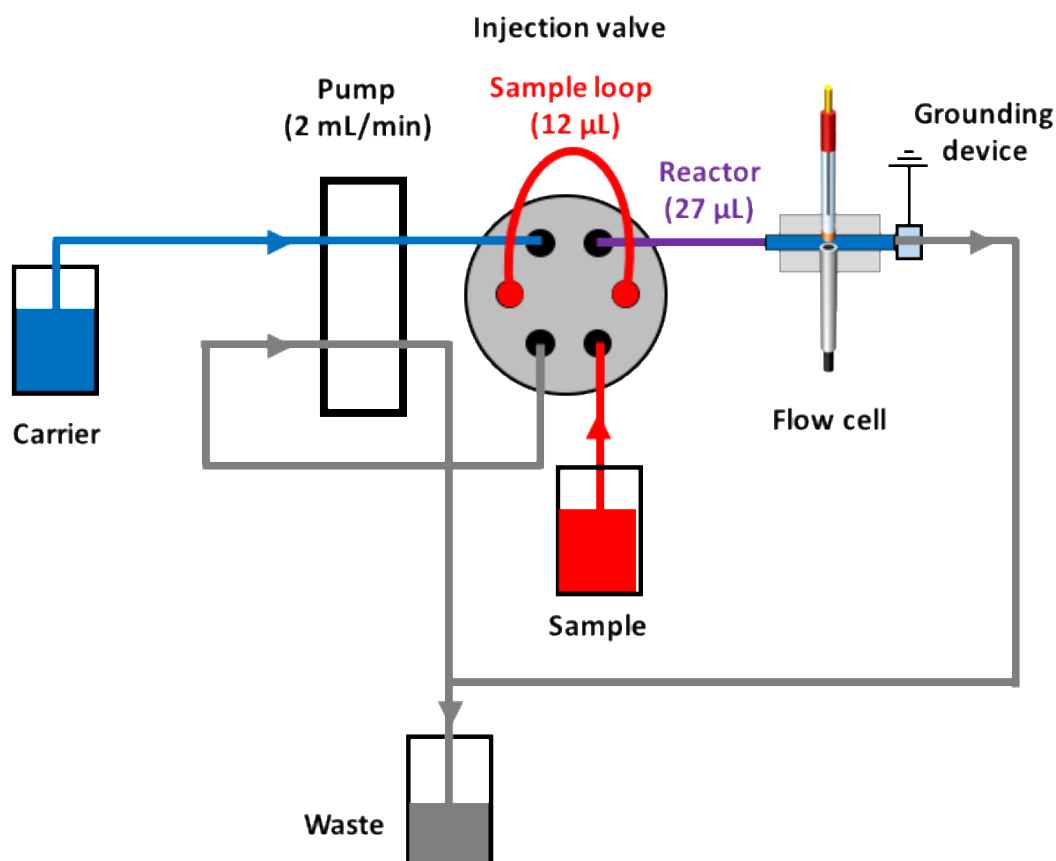


Figure 7.4 Schematic representation of the flow injection manifold.

## 7.3 Results and discussion

### 7.3.1 pH dependence of creatinine/creatininium ion

Previous work has established that it is the protonated form of creatinine- the creatininium ion that is responsible for the potentiometric signal of a creatinine-selective electrode (creatinine-ISE) [6]. This is congruent with the theory of ion-selective electrodes which requires the spatial separation of *charged* species

## POTENTIOMETRIC DETERMINATION OF CREATININE BY FIA

in order to generate an electromotive force. As a neutral molecule, creatinine does not qualify as a target for ion-selective electrodes, and it was therefore essential to convert it to a charged species.

Creatinine has a  $pK_a$  of 4.8. Accordingly, greater than 90 % of the creatinine is present in the protonated form when working at pH below 3.8. The pH-dependency of creatinine protonation predicted by the Henderson-Hasselbach equation is plotted in Figure 7.5. Following previous works in potentiometric creatinine sensing, that found the optimum working pH to be 3.7 to 3.8 [6, 12, 13], a 10 mM acetic acid/ $Mg(\text{acetate})_2$  buffer of pH 3.8 was used.

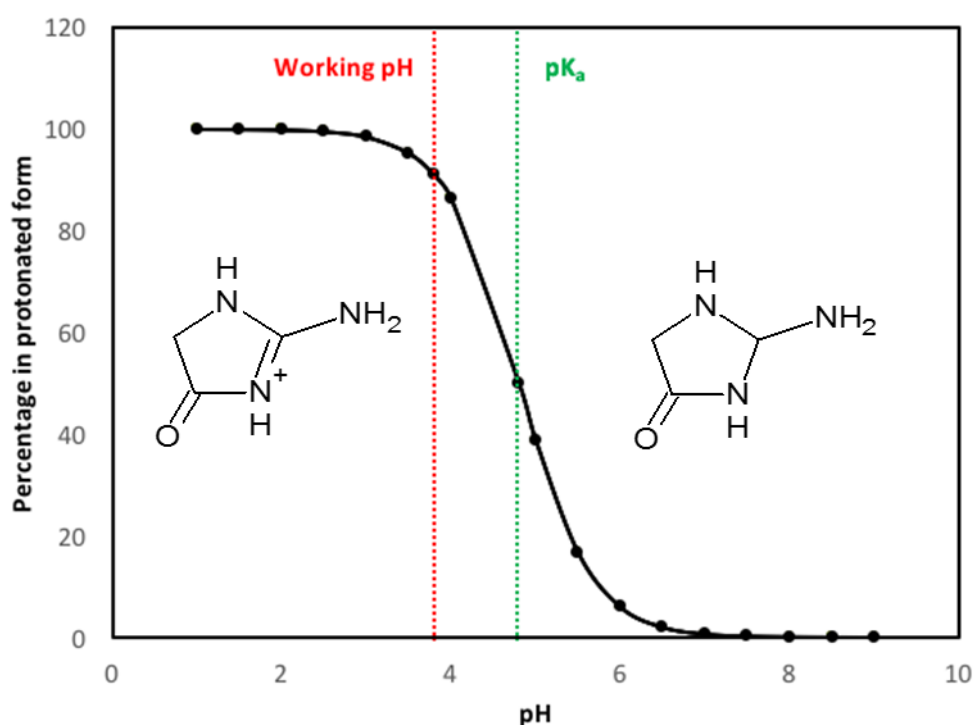


**Figure 7.5** Percentage of creatinine in the protonated form (creatininium ion) as a function of pH as predicted by the Henderson-Hasselbach equation. The dashed green line indicates the  $pK_a$  of creatinine and the dashed red line indicates the working pH of the buffer.

### 7.3.2 Fundamental fluidic studies

Preliminary studies were made to optimise the microfluidic tubing correspondent to the flow rate as well as the sample volume. Optimisation was initially made by comparing the calibration plots during flow injections, with that of steady-state signals introduced under flow. A representative plot comparing these two calibration regimes is shown in Figure 7.6.

As the steady-state plot exhibited the best limit of detection and dynamic range, it offered a suitable reference for the optimal possible performance. This implied aiming towards a low dispersion coefficient.

## POTENTIOMETRIC DETERMINATION OF CREATININE BY FIA

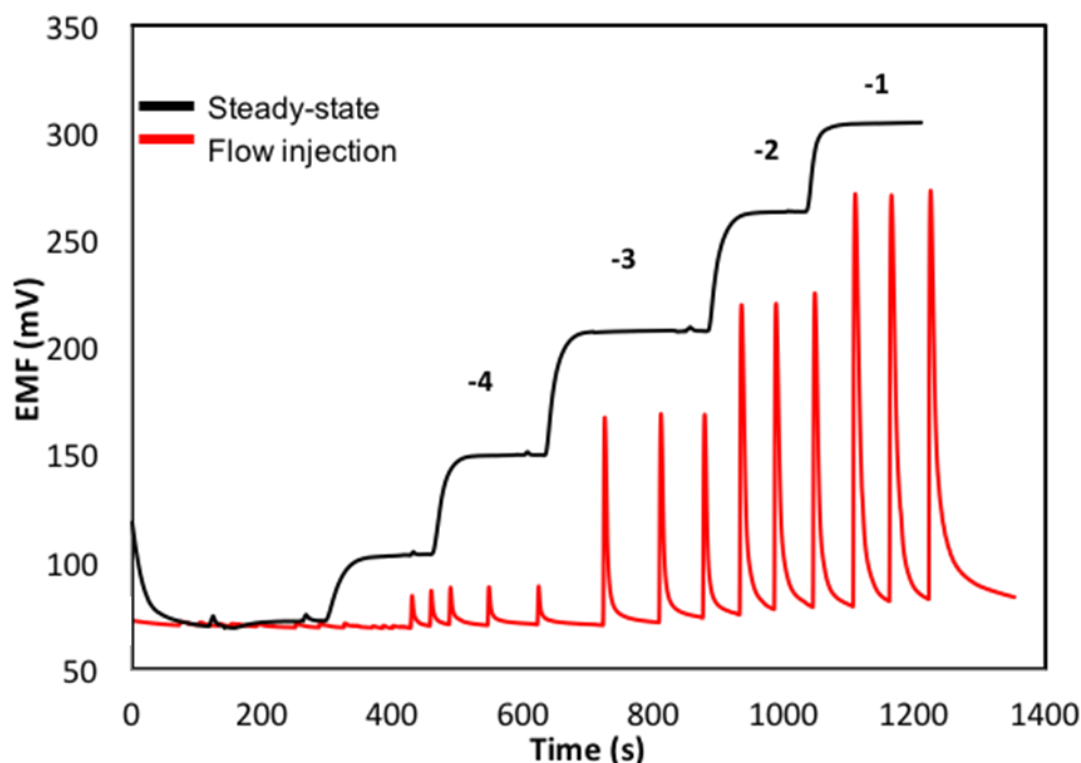


**Figure 7.6** Calibration of the creatinine-selective electrode under flow conditions. **Black:** steady-state calibration. **Red:** flow injection calibration. Numbers indicate the logarithm of concentration.

### 7.3.2.1 Flow rate and dispersion coefficient

In general, higher flow rates decrease the residence time of a sample, and thereby decrease the physical dispersion [7]. In the present case, two simultaneous processes occurred to creatinine injected into the carrier. Firstly, it was diluted- measurable as an increase in the dispersion coefficient. Secondly and simultaneously, it was protonated by the acidic buffer to the detected species, the creatinium ion- measurable as a decrease in the dispersion coefficient. In order to study and separate these effects, two calibrations were made under injection regimes and compared with the steady-state calibration plot.

The first injection calibration was made with creatinine standards within the same buffer as the carrier solution (*conditioned standards*). As these were not exposed to any change in pH, the ratio of creatinine:creatinium ion should not change and the only effect should be dilution due to dispersion.

The second calibration was made with creatinine standards in Milli-Q water (*unconditioned standards*). As these experienced a sharp gradient of pH, they should be affected by this, as well as by the dilution of dispersion.

## POTENTIOMETRIC DETERMINATION OF CREATININE BY FIA

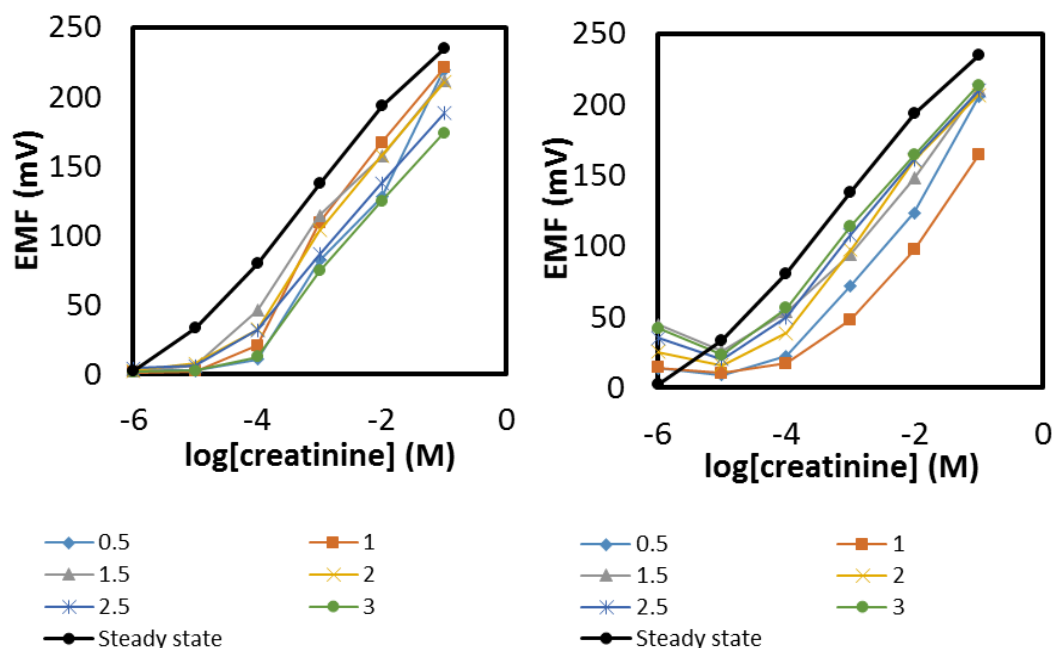


**Figure 7.7** Calibration plots during injection of creatinine. Left: with conditioned standards. Right: with unconditioned standards. The numbers in the legend refer to flow rates, as measured in mL/minute.

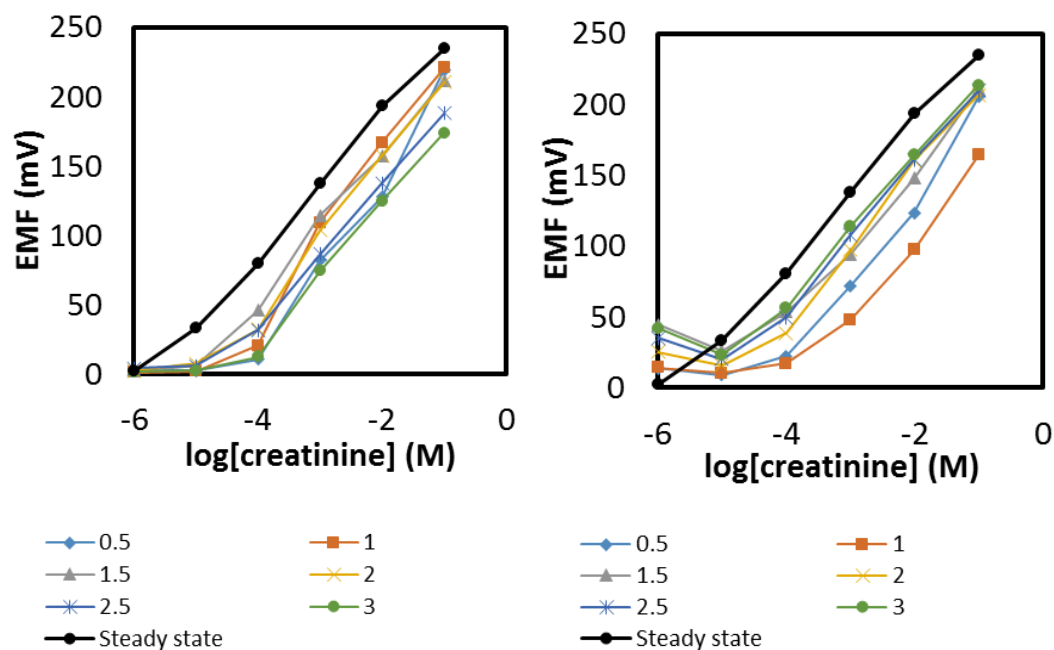


Figure 7.7 depicts the results of both experiments. In the case of *conditioned standards*, lower flow rates led to lower dispersion coefficients. Lower flow rates for *unconditioned standards* on the other hand, led to higher dispersion coefficients. Both of these phenomena can be seen within the calibration plots by the strengths of the potentiometric signals at different flow rates relative to each other.

Table 7.1 summarized these results in a different way, by highlighting the compromise between the desirable protonation (shown in green), and the necessary dilution associated with this (shown in red).

**Table 7.1** Dispersion coefficients as a function of flow rate, separated into the effects of dilution and protonation. A high degree of protonation (as indicated by the green colour) is desirable, while a high degree of dilution (as indicated by the red colour) was undesirable.

## POTENTIOMETRIC DETERMINATION OF CREATININE BY FIA

Flow rate	1.5	2	2.5	3
$D_{\text{dilution}}$	1.39	1.68	1.83	3.28
$D_{\text{protonation}}$	1.04	0.96	0.77	0.54
$D_{\text{total}}$	1.42	1.57	1.36	1.27
Scale	Protonated			Diluted

### 7.3.2.2 Sample volume

With the unexpected results of flow rate experiments still under consideration, the parameter of sample volume was examined (while operating at 3 mL/minute). In general, larger sample volumes allow for less dispersive dilution, leading to higher signal peaks and lower dispersion coefficients [7]. This is true up to a saturation point at which the central portion of a sample plug does not undergo further dilution by the carrier. The pH modulated protonation of creatinine is an additional factor of complexity within the dynamic.

Sample volumes of 12, 22, 32, and 42  $\mu\text{L}$  were tested, and the resulting calibration plots are displayed in Figure 7.8. While the response of injections of the lower volume differed significantly upon conditioning, the higher sample volumes reduced this dependency. The optimal sample was determined to be 32  $\mu\text{L}$ , as this most closely resembled the steady-state calibration curve and encompassed the widest linear range.

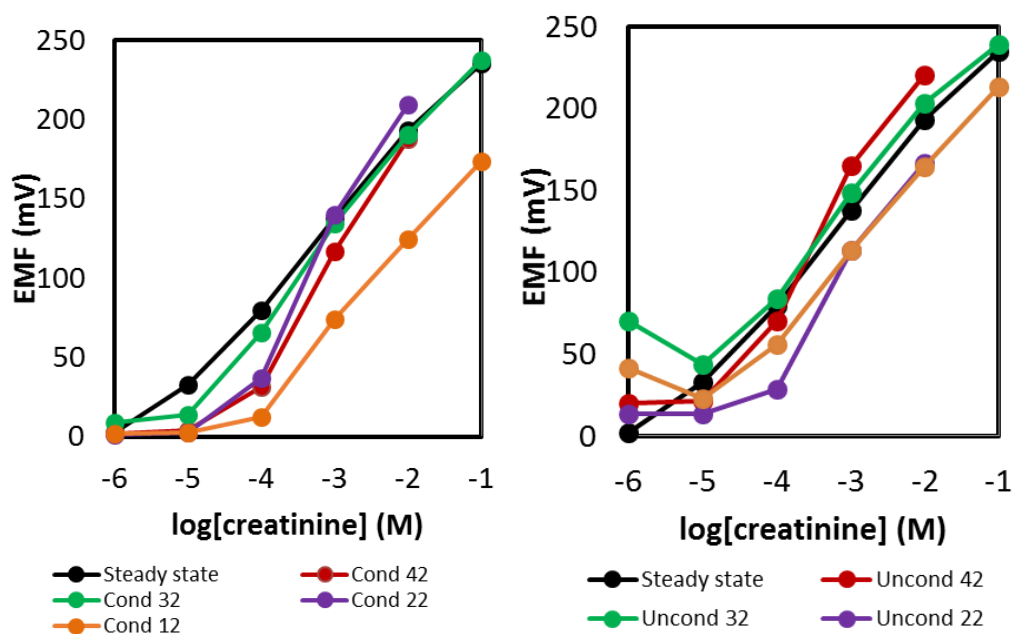


**Figure 7.8** Calibration plots comparing the signals from steady-state signals during flow, with those generated by injections of 12, 22, 32 and 42  $\mu\text{L}$ . Left: injections of conditioned samples (Cond). Right: injection of unconditioned samples (Uncond). The numbers in the legends indicate the sample volumes.

## POTENTIOMETRIC DETERMINATION OF CREATININE BY FIA

Furthermore, following the increase in sample volume, the system dependent response to flow rate was significantly reduced. This is evident in Figure 7.9, which overlays the calibration plots of both conditioned at unconditioned samples being injected into a carrier stream at various flow rates. Their superimposition highlights how their responses were barely distinguishable. Nevertheless, a flow rate of 2 mL/minute was selected going forward. This proved to have a sensitivity of 56.2 mV/dec. of creatinine across the dynamic range of 0.1 to 100 mM.

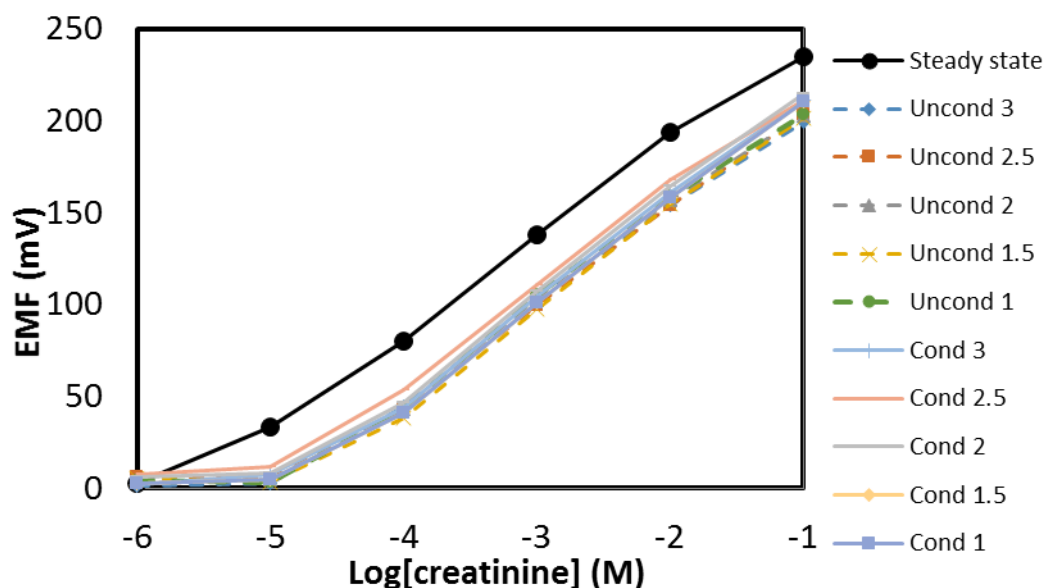


**Figure 7.9** Calibration plots of conditioned (Cond) and unconditioned (Uncond) creatinine standards injected into the flow system. The numbers in the legend indicate the flow rate (mL/minute). The steady-state calibration under flow is also shown.

The dynamic nature of flow systems requires empirical testing to optimize parameters such as flow rate, sample volume, and reactor volume. While some heuristic rules have been proposed [7], the unique nature of each system demands individual customization. In this case, a significant source of complexity within the fluidic arrangement was in establishing the appropriate degree of mixing between carrier and sample. While insufficient mixing would only protonate the outer limits of an injected sample- possibly resulting in a double peak, excessive mixing would overly dilute the sample and thereby the signal. This mixing arose from both radial and axial dispersion.

In summary, the flow rate and sample volumes were examined and optimized. While some variations of reactor volume- including the addition of a confluence point, were tested, no appreciable advantages were found from this. The system was evaluated as being fluidically sound, having demonstrated a Nernstian sensitivity across three orders of magnitude relevant to analysis within biological fluids.

## POTENTIOMETRIC DETERMINATION OF CREATININE BY FIA

### 7.3.3 Baseline drift, optical studies, and electrode memory

Using the optimised fluidic parameters, determinations of creatinine in diluted urine samples were conducted. However, a significant problem quickly became apparent- the baseline potential was unstable. That is, after injection of a sample- or indeed, simply a creatinine standard solution- the baseline potential would not return to the previous level- instead remaining elevated. An exemplary time trace of this is shown in Figure 7.10, in which the baseline potential can be seen to rise from its initial level, and not recover. There are at least two major areas that must be considered in determining the cause of this growing baseline; these are issues with the fluidics of the system, and issues with the electrode membrane.

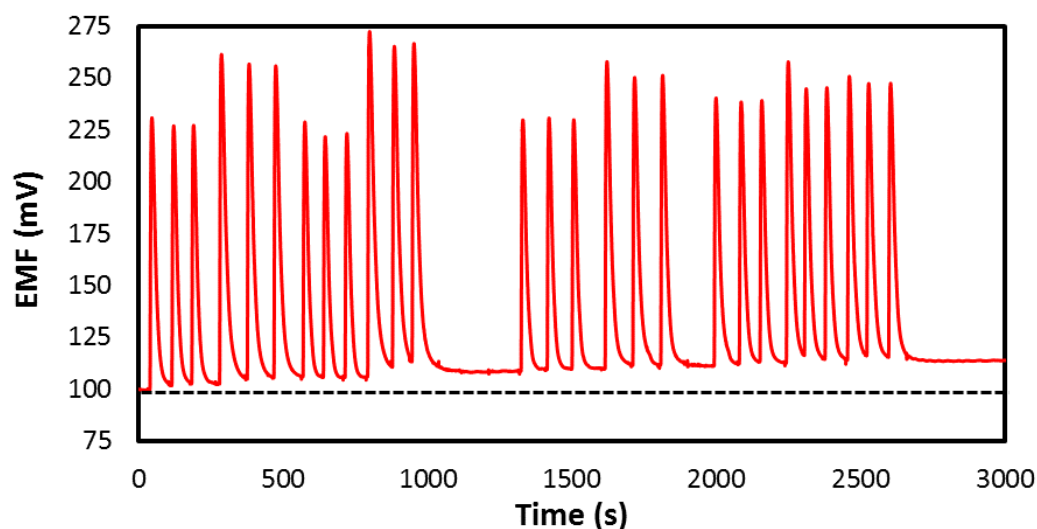


**Figure 7.10** Typical time trace during flow injection as detected by the creatinine ISE. The baseline is seen to rise above the initial level (indicated by the dashed line) and not recover.

#### 7.3.3.1 Fluidic considerations

Firstly, the problem could be due to fluidics- in which case it may simply be a question of waiting sufficient time to ensure adequate washing of the flow cell, ensuring that traces of creatinine were cleared. In fact, it would not be necessary to wait, instead injections could be continued as the peak heights would be expected to be almost identical regardless of any analyte traces remaining (so long as the new levels injected were higher than the remaining traces). This was not found to be the case however- peak heights increased as the baseline potential increased.

In order to interrogate whether this was indeed a fluidic issue, a comparison was made between the potentiometric detection method and an optical method. In this experiment, a creatinine standard (of 10 mM) was injected into the flow system with a  $K^+$ -ISE present and separately, with a creatinine-ISE present. It is important to note that the potassium ion has been identified as a significant interferent with respect to the creatinine-ISE [14]. Although the interference of the creatinium ion in the  $K^+$ -ISE is appreciably less, both electrodes nonetheless respond to both ions.

## POTENTIOMETRIC DETERMINATION OF CREATININE BY FIA

In both arrangements, the UV absorption of the creatinine molecule (abbreviated as CRT) was monitored at 227 nm. The resulting potentiometric and optical signals were then normalized, baseline corrected and compared (Figure 7.11). In comparing the resulting signal profiles, it is apparent that all four are indistinguishable in their rise, yet their decay's differ markedly. The symmetrical form of the optically generated signals suggests that the flow cell is indeed being rapidly and effectively washed of the analyte. In juxtaposition to this, the highly asymmetric potentiometric signals indicate the affinity of the sensing surfaces for the analyte. It should be stressed that the optical detector integrates in a volume of the flow cell, while the electrochemical detector responds to the surface concentration. Therefore, some variations in profiles are expected. However, the comparison between optical and ISE detection clearly shows that this effect is particularly pronounced in the system that includes the creatinine-ISE (abbreviated as CRT ISE).

These results indicate that the issue is not fluidic, but rather related to the electrode membrane, and that the effect responsible operates more powerfully in the creatinine-ISE than in a  $K^+$ -ISE.

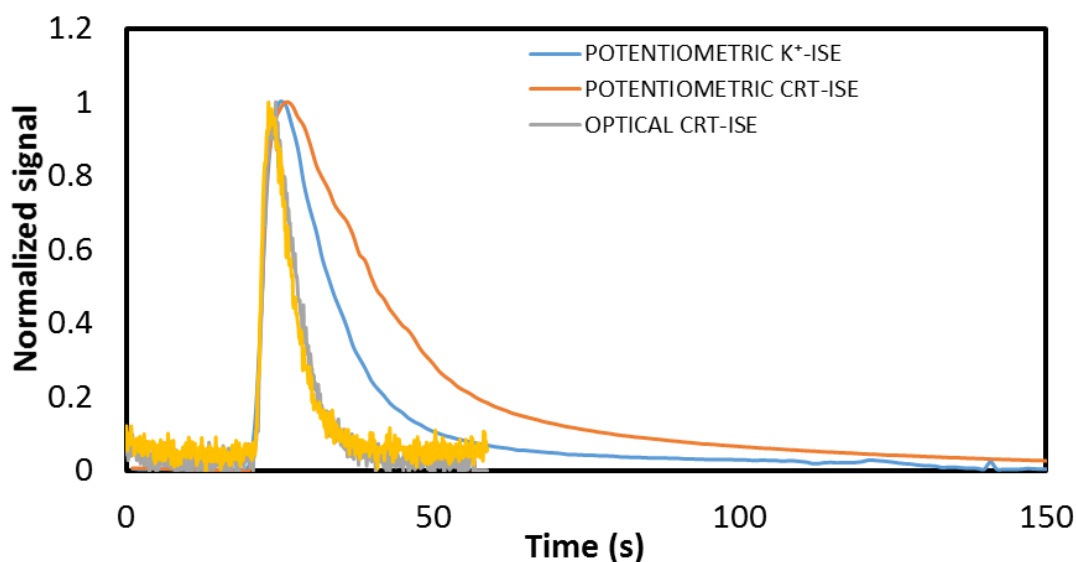


**Figure 7.11** Normalised signals from both optical and potentiometric detection of creatinine (CRT) injected into the flow system.

### 7.3.3.2 Membrane considerations

The second factor that could explain the increasing baseline potential is that the electrode is undergoing changes. That is to say, there are changes occurring on the membrane surface that induces a 'memory' in the electrode.

Polymer-based ion-selective electrodes are typically employed for determination of inorganic (ionic) species. Although organic polymer membranes such as plasticized PVC have an inherent affinity for more lipophilic ion species- as described by the Hoffmeister series, this is usually modulated by inclusion of an ionophore that imparts selectivity. The present membrane- selective towards the creatininium ion- is no exception to this.



## POTENTIOMETRIC DETERMINATION OF CREATININE BY FIA

However, by its very nature as an organic molecule, creatinine's lipophilicity is significantly greater than the inorganic targets typical of ion-selective membranes.

Indeed, EMF drifts have been reported for plasticized PVC membranes previously when working in the same acidified buffer [15]. The author's however, only encountered this issue when working with urine samples-not in simple creatinine standard solutions. In trying to identify the species responsible, they concluded that it was not attributable to a single species but rather many compounds found in urine, most significantly creatinine, potassium, and sodium.

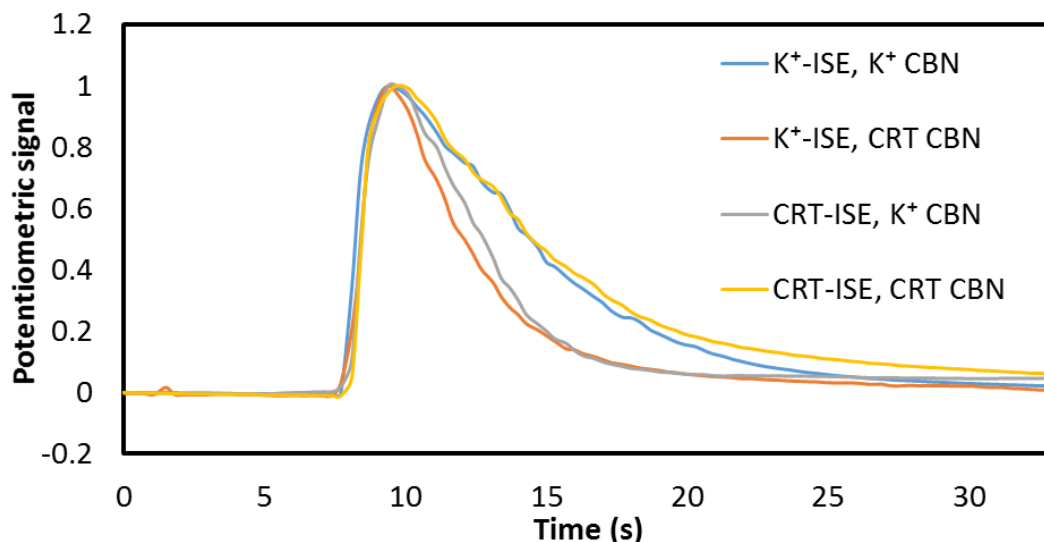


**Figure 7.12** Superimposed peak profiles tracking injection of 1 mM of potassium and creatinine, as detected by a  $K^+$ -ISE and a creatinine-ISE. Profiles were normalized and the baselines aligned. (CRT indicates creatinine: CBN indicates calibration).

To test whether changes in the electrode memory were responsible for the shifting baseline, comparisons were made between the well-understood potassium-ISE and the newly reported creatinine-ISE. The peak profiles of each of these were compared following the separate injection of creatinine and potassium. To make a fair comparison, the profiles were normalised and the baselines aligned (Figure 7.12). As expected, the signals due to injection of primary analytes lead to a greater area under the curve- that is to say, a longer time of recovery to the baseline. While at a glance the profiles of sensors responding to their primary analytes may appear similar, the difference between them can be brought out by considering the relationship of peak width to peak height, a parameter that indicates the recovery time of the sensor (Figure 7.13). This shows the return to 0.5, or 50 % of the maximum peak heights of the two systems to be nearly indistinguishable. The return to 0.05, or 5 % of the maximum peak height however was more than 13 s longer for the creatinine system as opposed to the potassium system. As flow systems behave as exponential mixing chambers in the tailing edge, the return to baseline potential is expected to be a negative exponential function. Of these functions, the recovery of the creatinine-ISE in response to injection of creatinine is the most extended in time. The conclusion of these studies is that the rising baseline potential is attributable to the creatinine molecules affinity to the electrode membrane, causing a memory effect.

## POTENTIOMETRIC DETERMINATION OF CREATININE BY FIA

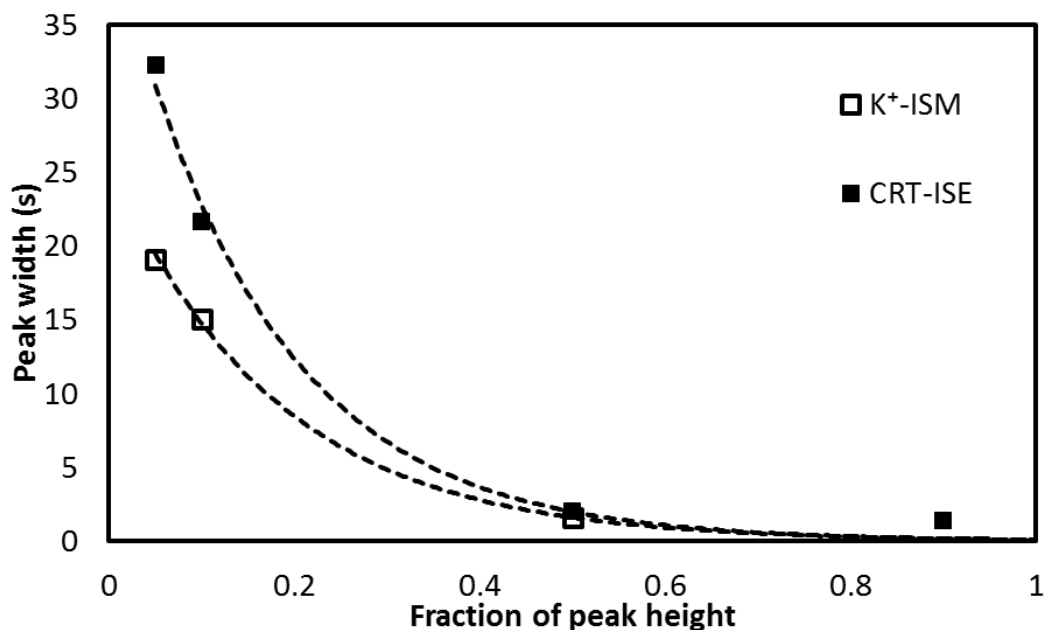


**Figure 7.13** The relationship of peak width to peak height for the creatinine and potassium selective systems in response to their primary analytes (creatinine (CRT) and potassium respectively).

But what is the source of this electrode memory? Why is it disruptive for the creatinine ISE and not for the potassium ISE (which does return to its baseline level)?

One possibility is that the electrode memory effect could be attributed to the strong affinity of creatinine/creatininium to the ionophore or perhaps to the *o*-NPOE plasticizer used in this membrane (where the K<sup>+</sup>-ISE uses a different plasticizer (DOS)). A test of a *blank* electrode- that is, an electrode that lacks the creatininium ionophore- was informative in this regard (Figure 7.14). After injecting creatinine in a calibration series up to 10 mM, the baseline did not return to the initial value at all, instead stabilizing at a new level some 17 mV higher (indicated in the figure by the dashed line). This indicates that the issue of electrode memory has its origins in the affinity of the creatinine/creatininium species to the membrane composition of PVC and plasticizer, and is not uniquely specific to the ionophore. It is likely that the plasticizing compound *o*-NPOE is plays a significant role in this issue.

There is a strong possibility that this electrode memory is pronounced by working in acidic media. Previous work has suggested that no single cation is responsible for the positive EMF drifts, and that many species can protonate at pH 3.8 [15]. One possible means of mitigating this issue therefore, may be to work at a higher pH.

## POTENTIOMETRIC DETERMINATION OF CREATININE BY FIA

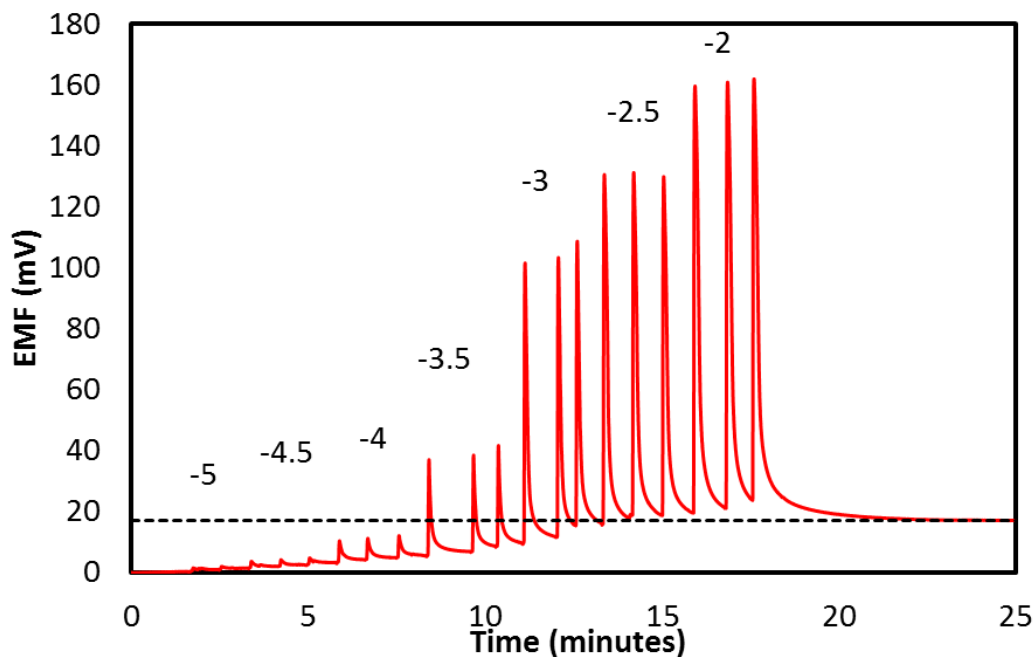


**Figure 7.14** Time trace during calibration of a *blank* electrode with creatinine. The dashed line offers a guide as to the shifting of the baseline potential.

### 7.3.4 pH modulation studies

As mentioned, working at a pH of 3.8 ensures that 91 % of creatinine is in its protonated form, at least under steady-state conditions. Intuitively, it would seem optimal to work at this acidic pH therefore. However, it must be remembered that in the work of Guinovart et al., it was deemed necessary to dilute samples in order to avoid fouling of the membrane. The dilution factor was one hundred in the case of urine samples. A similar *effective* dilution factor of the creatininium ion could be obtained simply by modulation of the pH of the carrier solution. For example, an effective dilution factor of 10 could be obtained by working in a buffer of pH 5.8 instead of 3.8, as 9 % rather than 91 %, of creatinine would be expected to appear in its protonated form at this pH.

This change in pH of course, affects all components of the sample, which in the case of urine includes urea, sodium, chloride, potassium, and various proteins as well as organic and inorganic components- the complexity of which could have unexpected consequences. Also significantly, while this pH modulation effectively dilutes the analyte- creatininium- it has no dilution effect whatsoever upon the major interferents found in urine samples, namely sodium and potassium. As such, the selectivity coefficients can be expected to be poor, in reflection of this. In order to adjust for this, the system was modified to simultaneously determine potassium, as it is acknowledged to be the principal interferent. Additionally, the sodium concentration of each sample was determined by atomic emission spectroscopy. These two ions represent the major interferents to creatinine-ISEs [6, 15].

The experimental setup used microelectrodes formed from copper wires of 1 mm diameter that had been mirror polished and covered by ion-selective membranes with inclusion of carbon nanotubes to enhance their

## POTENTIOMETRIC DETERMINATION OF CREATININE BY FIA

hydrophobicity. The addition of nanotubes was important to discourage the formation of a water layer and to prevent corrosion of the copper substrate.

Figure 7.15 depicts the time trace of a creatinine-ISE and a potassium-ISE during calibration with creatinine and potassium, as well as the injection of 20 urine samples. Both samples and standards were diluted 10x in the carrier buffer of 50 mM acetic acid/Mg(acetate)<sub>2</sub> at pH 5.8 prior to injection. The combination of prior dilution and the effective dilution due to pH should lead to an overall dilution of the creatininium ion of approximately 100x, comparable to that proven to be efficacious in the steady-state method of Guinovart *et al.*

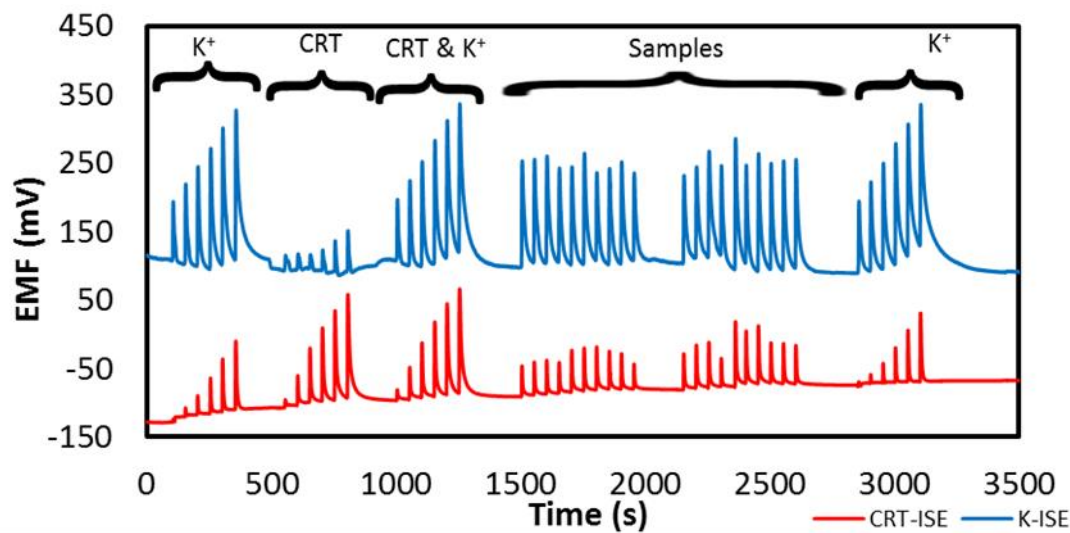


**Figure 7.15** Time trace during injection of creatinine and potassium standards, as well as 20 samples. In each calibration, the peaks sequentially increase as they represent concentrations of  $10^{-3.5}$ ,  $10^{-3}$ ,  $10^{-2.5}$ ,  $10^{-2}$ ,  $10^{-1.5}$ ,  $10^{-1}$  M.

There are several features of the data that can be extracted and unpacked when considering the calibrations. Firstly, the upward drifting of the creatinine-ISE's baseline is evident. Nonetheless, both ISEs displayed the expected Nernstian sensitivity towards their primary analyte. In the case of the creatinine-ISE, this is plotted in

Figure 7.16. However, while the K<sup>+</sup>-ISE was highly selective against creatinine, the creatinine-ISE was not so discriminatory. Indeed, by applying the separate solution method to the data generated within the experiment, the logarithm of the potentiometric selectivity coefficient was calculated as  $\log K^{\text{pot}}_{\text{CRT},\text{K}^+} = -1.00$ . This is poor compared to the -2.5 reported by Guinovart and does not meet the threshold of -1.9 calculated to be necessary for clinical use [16]. It is however, understandable, given the effective dilution of the creatininium ion relative to the interfering potassium ion, as already described. Nevertheless, as determinations of potassium were also simultaneously made for each sample, the calculations of creatinine values were adjusted accordingly by subtracting the additional signal expected to be due to the potassium in each sample. This was calculated by multiplying the potentiometric selectivity coefficient by the potassium activity determined in each sample.

## POTENTIOMETRIC DETERMINATION OF CREATININE BY FIA

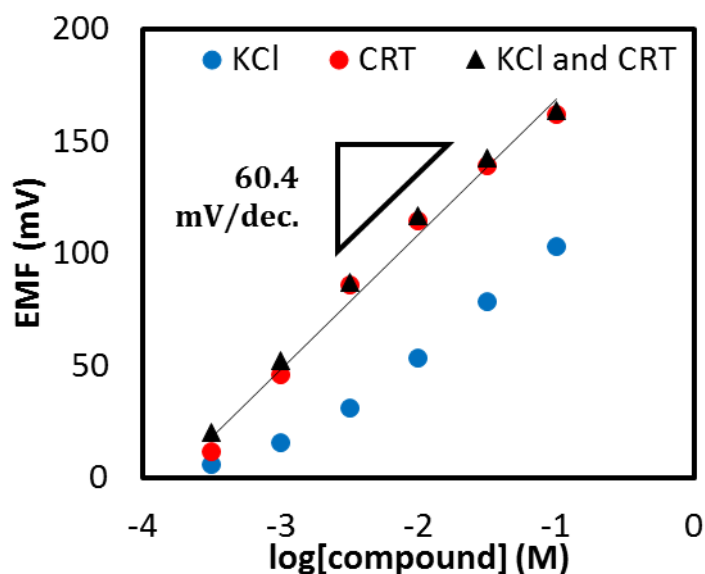


**Figure 7.16** Plot of the creatinine-ISEs response to three injected solutions: KCl, creatinine (CRT), and both KCl and CRT together.

The initially determined and the adjusted creatinine values for each sample were compared with reference values provided by the laboratory of Santa Tecla hospital that were obtained using the colorimetric Jaffe method. This adjustment for potassium generally lowered the calculated levels slightly. They were still however significantly overestimated, as seen in Figure 7.17. There appears to be a grouping of 13 values that correlate well with the reference method, as indicated by the black line (of best fit for this subset). Meanwhile, seven other values appear as outliers to this trend, by dramatically overestimating the creatinine levels.

## POTENTIOMETRIC DETERMINATION OF CREATININE BY FIA

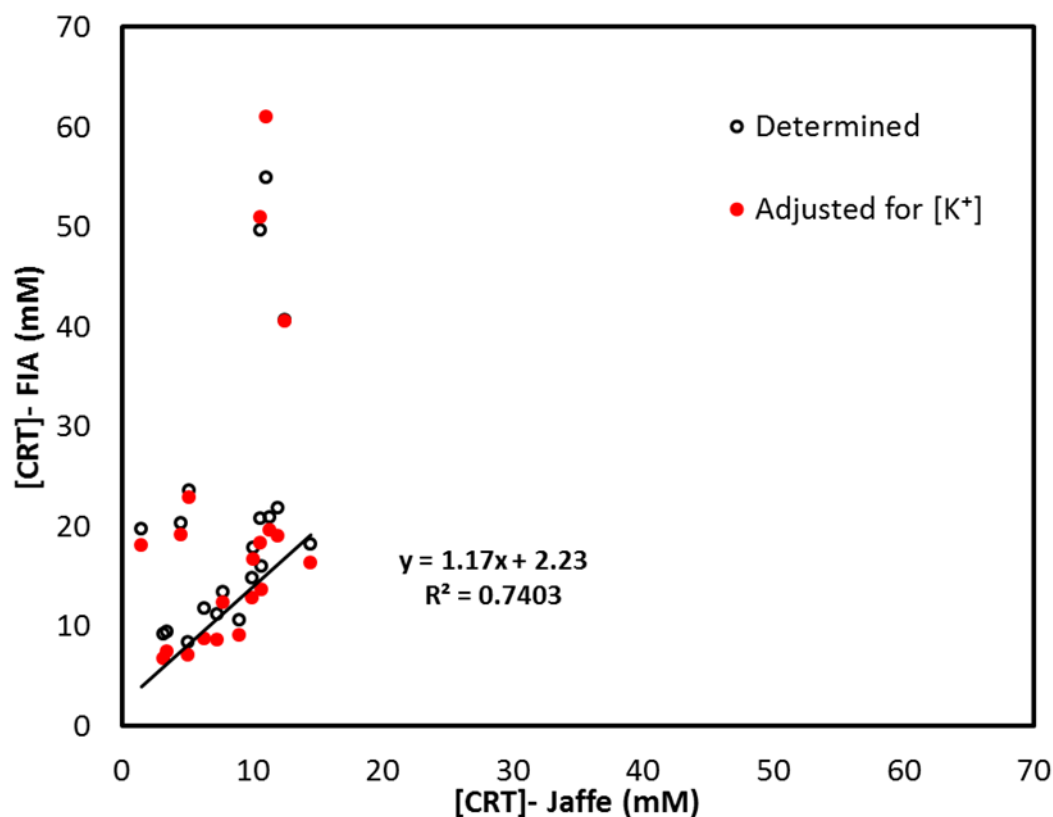


**Figure 7.17** Comparison between creatinine values in urine determined by the reference Jaffe method and those using the described FIA system. The line indicates a line of best fit for 13 of the samples (the 7 outliers were omitted in fitting this line).

The sodium levels were also considered as a possible source of the over-estimation. The creatinine, potassium, and sodium levels of each sample are compared in Figure 7.18. These constitute the three principal species thought to contribute to the potentiometric signal of the creatininium sensor. Unfortunately, no pattern was observed between these that may have explained the over-estimation of creatinine levels. That is, no correlation was seen between overestimated creatinine values and the potassium or sodium levels.

## POTENTIOMETRIC DETERMINATION OF CREATININE BY FIA

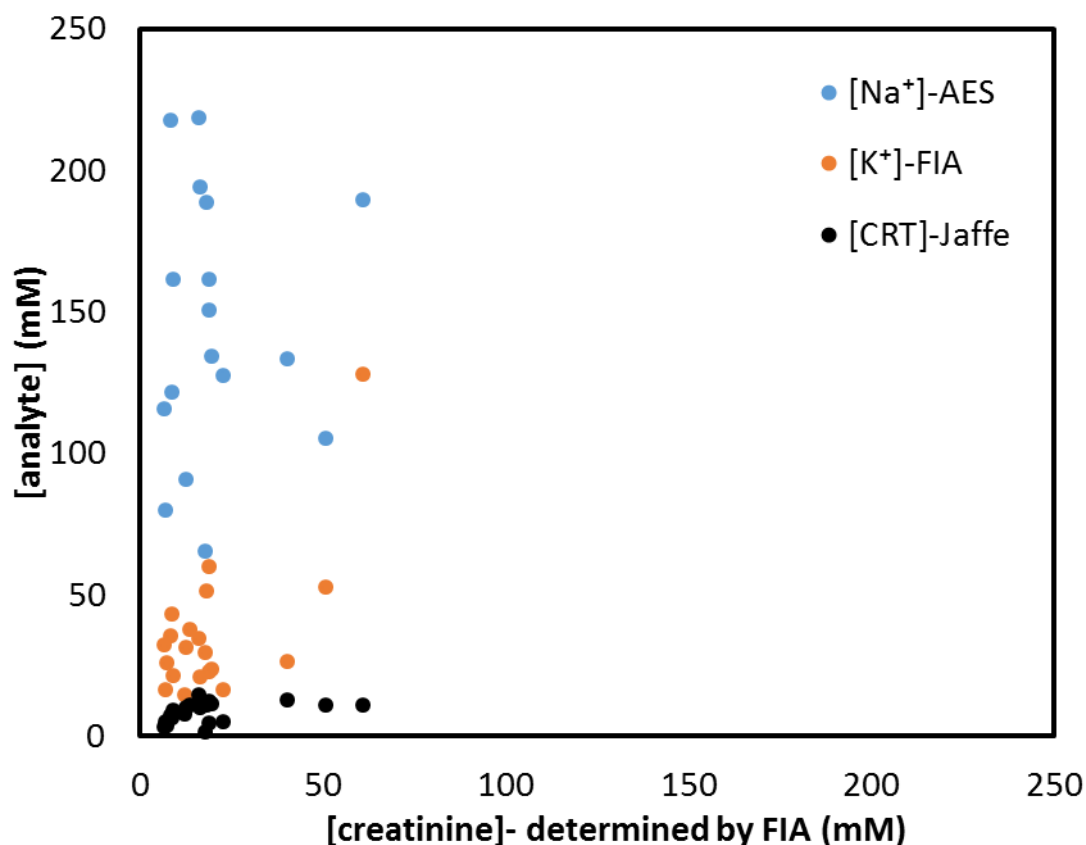


**Figure 7.18** Comparison of the creatinine levels determined by FIA with the values of creatinine from the reference method as well as potassium and sodium levels.

## 7.4 Conclusions

The potentiometric sensor reported by Guinovart *et al.* displayed excellent performance towards determinations of creatinine in biological fluids under steady-state conditions. The manual handling associated with diluting and acidifying the sample, calibrating the sensor and making the determinations, and finally washing the sensor, has left room for adaption of the system to high throughput modes for use in hospital laboratories, or towards decentralized applications by non-experts, such as in home-use. It was hoped that embedding the sensor into a flow injection system could automate much of the manual operations. This however, proved elusive due to the electrode memory demonstrated by the creatinine-selective electrode. Through optical studies it was established that this was indeed a membrane issue, and not a fluidic problem. Because a blank membrane- lacking the ionophore- also displayed significant electrode memory, the problem seems to arise from the strong interaction between the organic, plasticized membrane and the lipophilic creatinine molecule. Such a problem does not occur with inorganic ions such as potassium, which are not as lipophilic. Experiments with modulation of pH failed to mitigate the electrode memory, and indeed exacerbated the problems by reducing the effective selectivity of the sensor by increasing the concentration of interfering species relative to the target. Despite thorough studies and various approaches, the construction of a FIA system to determine creatinine has so far proved intractable. Future work involving more sophisticated flow-based methods, such as sequential injection analysis (SIA), where the sample-electrode contact could be more easily controlled, may help to overcome some of these issues [17].

## 7.5 References

- 1 J. B. Henry and G. H. Newman, Clinical Significance of Creatinine Measurements, *Postgrad. Med.*, 1971, **5481**, 236–239.
- 2 P. Delanaye, E. Cavalier and H. Pottel, Serum Creatinine: Not so Simple!, *Nephron*, 2017, **136**, 302–308.
- 3 L. Hoste, K. Deiteren, H. Pottel, N. Callewaert and F. Martens, Routine serum creatinine measurements: How well do we perform?, *BMC Nephrol.*, 2015, **16**, 1–9.
- 4 R. M. Jacobs, J. H. Lumsden, J. A. Taylor and E. Grift, Effects of interferents on the kinetic Jaffe reaction and an enzymatic colorimetric test for serum creatinine concentration determination in cats, cows, dogs and horses, *Can. J. Vet. Res.*, 1991, **55**, 150–154.
- 5 L. M. Thienpont, A. P. De Leenheer, D. Stockl and H. Reinauer, Candidate reference methods for determining target values for cholesterol, creatinine, uric acid, and glucose in external quality assessment and internal accuracy control. II. Method transfer, *Clin. Chem.*, 1993, **39**, 1001–1006.
- 6 T. Guinovart, D. Hernández-Alonso, L. Adriaenssens, P. Blondeau, M. Martínez-Belmonte, F. X. Rius, F. J. Andrade, P. Ballester, M. Martínez-Belmonte, F. X. Rius, F. J. Andrade and P. Ballester, Recognition and Sensing of Creatinine, *Angew. Chemie*, 2016, **55**, 2435–40.
- 7 V. Cerdà and C. Amalia, *An introduction to flow analysis*, Sciware, S.L., Palma de Mallorca, 2009.
- 8 R. Kellner, J.-M. Mermet, M. Otto and H. M. Widmer, Eds., *Analytical chemistry*, Wiley-VCH, Weinheim, Germany, 1998.
- 9 E. H. Hansen, in *Contemporary electroanalytical chemistry*, eds. A. Ivaska, A. Lewenstam and R. Sara, Plenum Press, New York, USA, 1990, pp. 245–254.
- 10 J. Ruzicka and E. H. Hansen, *Flow Injection Analysis. Part I. A New Concept of Fast Continuous Flow Analysis*, 1975, vol. 78.
- 11 V. Cerda, L. Ferrer, J. Avivar and A. Cerda, *Flow analysis: a practical guide*, Elsevier Science, Elsevier, 2014.
- 12 T. Guinovart, D. Hernández-Alonso, L. Adriaenssens, P. Blondeau, F. X. Rius, P. Ballester and F. J. Andrade, Characterization of a new ionophore-based ion-selective electrode for the potentiometric determination of creatinine in urine, *Biosens. Bioelectron.*, 2017, **87**, 587–592.
- 13 P. Bühlmann, M. Hayakawa, T. Ohshiro, S. Amemiya and Y. Umezawa, Influence of natural, electrically neutral lipids on the potentiometric responses of cation-selective polymeric membrane electrodes., *Anal. Chem.*, 2001, **73**, 3199–3205.
- 14 T. Guinovart, D. Hernández-Alonso, L. Adriaenssens, P. Blondeau, M. Martínez-Belmonte, F. X. Rius, F. J. Andrade and P. Ballester, Recognition and Sensing of Creatinine, *Angew. Chemie - Int. Ed.*, 2016, **55**, 2435–2440.
- 15 P. Bhlmann, M. Hayakawa, T. Ohshiro, S. Amemiya, Y. Umezawa and P. Bu, Influence of Natural , Electrically Neutral Lipids on the Potentiometric Responses of Cation-Selective Polymeric Membrane



## POTENTIOMETRIC DETERMINATION OF CREATININE BY FIA

---

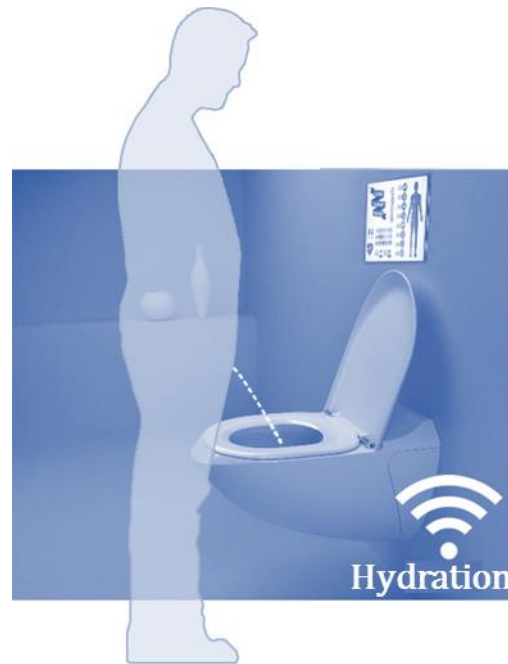
Electrodes Articles Influence of Natural , Electrically Neutral Lipids on the Potentiometric Responses of Cation-Selective Polyme, *Anal. Chem.*, 2001, **73**, 3199–3205.

16 T. de A. Guinovart Pavón, Universitat Rovira i Virgili, 2015.

17 A. Economou, Sequential-injection analysis (SIA): A useful tool for on-line sample-handling and pre-treatment, *TrAC - Trends Anal. Chem.*, 2005, **24**, 416–425.

## 8 ANTICLEPSYDRA: A ‘Smart Toilet’ for autonomous monitoring of urine conductivity and volume

---



## 8.1 Introduction

Water is the primary ingredient of life. Despite this, our means to measure its levels within the human body are limited and a gold standard method of hydration assessment remains elusive <sup>[1]</sup>. As Shirreffs has pointed out, while the dictionary definition of euhydration- or being in water balance- is easy, establishing the physiological definition is not <sup>[2]</sup>. Nevertheless, hydration is critical and as the current medical paradigm thirsts for objective measurements, there are numerous efforts underway to develop tools and quantify hydration <sup>[2-7]</sup>.

Imbalances of water and electrolyte levels are involved with numerous disorders- either as cause or result. These include hypernatremia, hyponatremia, polyuria, polydipsia, hypokalemia, hyperkalemia, sickle cell anaemia, diabetes insipidus, and chronic renal failure, and hypothyroidism <sup>[8]</sup>. The maintenance of minerals and water is regulated by the kidneys and is affected by three factors: circadian rhythms, osmoregulation, and volume regulation <sup>[7]</sup>.

Hydration assessment techniques can be divided into subjective and objective methods. Subjective observations include skin turgor, thirst and mucous membrane moisture <sup>[2,9]</sup>. Despite The American Journal of Nursing naming these as the most simple, fast and economical in 1975, they were also deemed the least reliable, so objective methods remained attractive <sup>[2,9]</sup>.

The past four decades advanced a small kit of objective hydration assessment techniques. Some of these such as isotope dilution and neutron activation analysis are highly costly and require technical expertise <sup>[1]</sup>. Others such as plasma/serum osmolarity are more portable and lower cost, are invasive methods. While no gold standard has been agreed upon, body weight is regarded as the simplest and most accurate, albeit only when frequent serial measurements are made <sup>[1,6]</sup>. This limits the technique's practical utility to most people outside of settings such as professional athletic training centres.

Uroanalytic methods offers some advantages as they are non-invasive, and tend to be low-cost with the possibility of using portable meters. The established methods for hydration assessment in urine are osmolarity, specific gravity, conductivity, colour and 24-hour volume <sup>[1-7,10,11]</sup>. These have been found to have medium to strong positive correlations with each other <sup>[3,5,7,10,11]</sup>. although one study raised doubt as to how any of these relates to real-time hydration <sup>[11]</sup>. Largely, the four measures of urine conductivity, osmolarity, colour and specific gravity are agreed to give the same estimate of hydration status <sup>[3,10]</sup>. Sherriffs' review of numerous assessment techniques concluded that "urinary measures are more sensitive than other methods, but may have a time lag over the short term" <sup>[2]</sup>. Armstrong has recommended that future research efforts be focussed on novel assessment techniques that measure fluid volume and concentration in real time with excellent precision, accuracy and reliability, while being portable, inexpensive, safe and simple, non-invasive, with results that can be interpreted in concert with other hydration indices <sup>[1]</sup>. This is indeed a tall order, but one that the present work aims to contribute towards.

## ANTICLEPSYDRA SMART TOILET

---

With a growing world population and a straining medical system that remains unaffordable to many, new paradigms in healthcare are paramount. Low-cost distributed diagnostic tools are one aspect of this. Indeed, by moving the analyses out of the laboratory, simpler and more affordable tools can be used to arrive at meaningful diagnostic information with a modest compromise in analytical performance. These tools often fall within the categories of point-of-care devices, wearables and decentralized diagnostic instruments, for which the glucometer has been the flagship product. This burgeoning field of portable, low-cost and robust decentralized chemical diagnostics is now beginning to interface with the more established field of miniaturised, wireless and flexible electronics and the marriage of these two are promising access to a wealth of new chemical information. Furthermore, where traditionally an individual's physiology was examined against an average of the population, the tools are now appearing to track an individual over the long-term, allowing for baseline levels and patterns of the individual to be established. When connected to the internet, this information can be called the Internet-of-you and opens the door to a new realm of insightful personalized analytics.

Except in acute cases, invasive or even obtrusive sampling is more than prohibitive to long-term monitoring- it is anathema to a healthy individual's participation. Non-invasive and even invisible ways of gathering information must therefore be developed. A Smart Toilet for which no behavioural change is required by the user, overcomes this adoption barrier.

As described in Chapter 1, the last decade has been a boom of interest for amateur homemade hardware/software devices, comparable to that seen for personal computers in the 1970's by what has come to be known as the Maker community<sup>[12-17]</sup>. The Arduino platform, launched in 2003, is perhaps the best known microcontroller of this class with its user-friendly integrated development environment. There are several examples of Arduino microcontrollers being integrated with chemical sensors, one case even being dubbed 'Chemduino'<sup>[18]</sup>.

One platform for embedded sensors that is beginning to emerge is the Smart Toilet- a quick web search shows multiple versions of this concept appearing from start-ups as well as from large companies. This chapter offers one more Smart Toilet concept to the idea marketplace.

Inspiration is drawn from the water clocks of the ancient world which, after sundials and candle clocks, are the oldest known means of measuring time. These devices- named Clepsydrae- date back at least to the 16<sup>th</sup> century BCE in the cultures of Babylon and Egypt, before spreading to Athens, Japan, and Rome where they displaced sundials as the official timepieces of Roman law<sup>[18]</sup>. One author dates clepsydrae back to 4000 BCE in China<sup>[18]</sup>. These devices- built by Isaac Newton as a child- have a working principle of using the flow of water through a restricted aperture to measure time (Figure 8.1)<sup>[19]</sup>. In this way, the passage of time is displayed as the height of water relative to either the upper or lower vessel. Today's digital technologies offer various methods of counting time with extraordinary accuracy. On the other hand, methods of measuring volume have only progressed incrementally since the industrialization of glass-

## ANTICLEPSYDRA SMART TOILET

---

blowing furnished graduated cylinders, to the delicate mass balances of today's modern laboratories- neither of which is automated.

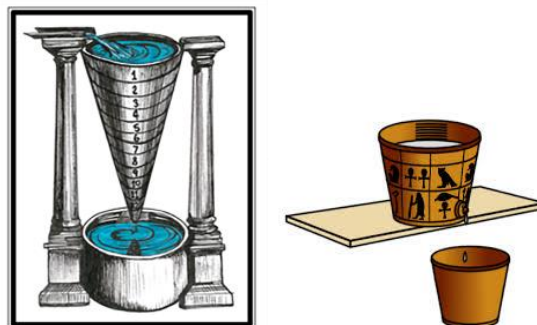


**Figure 8.1** Two styles of ancient Clepsydrae (water clocks)

The word 'Clepsydra' translates from the Greek as "stealing water" or "water thief". The Smart Toilet presented here is termed Anticlepsydra- which seems appropriate both in meaning, and because it is based on the inverse principle of the water clock. That is, it uses the time of efflux to estimate the volume of liquid passing through. To the best of our knowledge, this is a nonobvious and previously unreported technology with utility that will be demonstrated. The most similar technology is perhaps the electromagnetic flow meters used to track household water usage.

This paper brings together the Maker tools of 3D printing and Arduino microcontrollers with the Anticlepsydra principle to offer a new tool to the affordable, user-friendly diagnostic toolkit.

## 8.2 Experimental

### 8.2.1 Reagents and materials

Commercial standard solutions from Mettler-Toledo (traceable to NIST values) of 1.413 and 12.88 mS/cm (25 °C) KCl were used for calibration of the commercial conductivity meter and to determine the conductivities of solutions of 0.01 M and 0.5 M KCl solutions prepared in-house. Volume estimations were calibrated using a 100 mM NaCl solution. Aluminium foil was purchased from a supermarket.

### 8.2.2 Instrumentation and measurements

Analytical grade graduated cylinders were used to calibrate the Smart Toilet's volume estimation. An *EZO conductivity circuit* was used in conjunction with an *Arduino Nano V 3.1*. A 100 nm layer of platinum was sputtered upon aluminium foil. Reference conductivity measurements were made with a commercial conductivity meter at room temperature (approximately 19 °C). The conductivity measurements of the Smart Toilet were made in situ, and were therefore assumed to be at the body temperature of 37 °C. Both instruments were calibrated for temperature accordingly. A Teclast Ultrpad (X80 Pro W32GB DG) tablet computer from Guangzhou Shangke Information Technology Limited was used for communication with the Arduino.

## ANTICLEPSYDRA SMART TOILET

---

### 8.2.3 The Smart Toilet device

#### 8.2.3.1 Device structure

The Smart Toilet device was 3D printed. The funnel area was oval in shape with a collection capacity of 170 mL. This collected urine into the cuvette of 1 cm<sup>2</sup>, to fill its 4.3 cm height during micturition events. The outlet aperture size was optimized to be 3 mm in diameter to limit the flow rate.

The cuvette was housed inside using silicone glue to ensure a watertight seal. Inside and in the upper section of the cuvette, two square electrodes of platinum upon aluminium foil were placed, each 8 mm<sup>2</sup>. A small hole was drilled through either side of the cuvette behind the electrodes through which a copper wire was threaded and held in place with conductive epoxy glue. In this way, the electrodes were separated by 1 cm on the horizontal plane, and remained disconnected until the cuvette was filled as they were situated above the waterline of the cuvette at equilibrium.

The Smart Toilet was designed to fit a standard Western toilet. It was located at the front of the toilet to collect urine from a sitting user- male or female- while not interfering with other operations of the toilet. The front-most edge of the device was oriented so as to collect water when the toilet was flushed and in doing so, rinse the device. Schematics of the device are shown in Figure 8.2 and it is photographed within a toilet in Figure 8.4. The Arduino microcontroller and EC EZO conductivity circuit are located inside a 3D printed plastic box outside of the toilet.

#### 8.2.3.2 Device electronics

The copper wires connected to the electrodes were used as inputs into the EZO conductivity circuit. This in turn, communicated with the Arduino Nano microcontroller using two digital *pins for RX/TX communication in UART Mode*. The Arduino was connected to a tablet computer via USB port to print data to the serial monitor, and this tablet was mounted on the wall beside the toilet.

#### 8.2.3.3 Arduino code

In practice, it continuously reads the conductivity. A micturition event is defined. The full sketch of the code used in the Smart Toilet is included in Appendix 6. as conductivity exceeding 2 mS/cm (at 25 °C). This level ensures that flushing events are not recorded. The duration of each micturition event is recorded and volume is calculated based on an established relationship between time and volume specific to the fluidics of the device.

## ANTICLEPSYDRA SMART TOILET

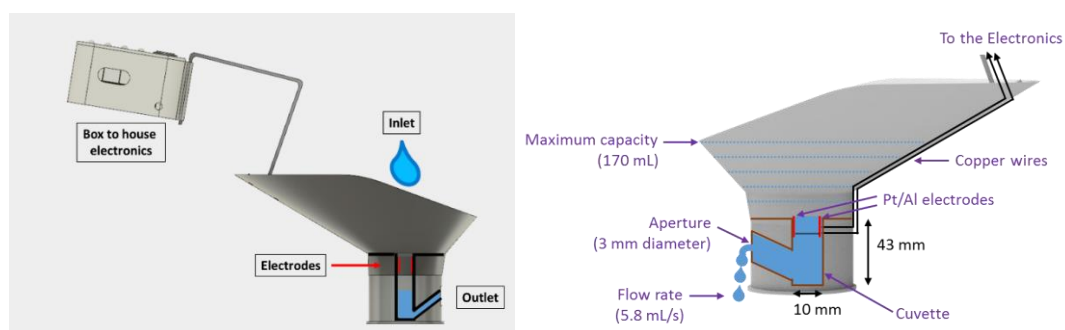


**Figure 8.2** Schematic representation of the Smart Toilet shown in section view. **Left:** full device. **Right:** detail of the funnel.

## 8.3 Results and discussion

### 8.3.1 Conductivity determinations

The EC EZO conductivity circuit is the size of a US quarter dollar and reads conductivity across the range of 0.07 – 500,000+  $\mu\text{S}/\text{cm}$  with an accuracy of  $\pm 2\%$  with temperature compensation [19]. Within the Smart Toilet, it was connected to the platinum electrodes to read conductivity of urine passing through. Prior to initial use, it was calibrated dry, followed by a two point calibration with 1.523 and 55.5  $\text{mS}/\text{cm}$  (25  $^{\circ}\text{C}$ ) solutions of KCl. This was in accordance with the instructions of the datasheet [19]. It was then set to read conductivity of solutions at 37  $^{\circ}\text{C}$ - again, using input commands specified in the datasheet.

After being connected via USB cable to a wall-mounted tablet computer, people were asked to urinate through the Smart Toilet and to also collect a small volume for subsequent validation. The conductivity and volume of each micturition event were immediately printed out on the tablet. The system was set to disregard values below 2  $\text{mS}/\text{cm}$  (at 25  $^{\circ}\text{C}$ ) to avoid false readings from flushing of the toilet. The 6 female and 13 male urine samples were analysed within this trial and the conductivity values were validated by analysing the collected portions with a commercial conductivity meter. This revealed a positive bias of 21% which can be attributed to the measurements being made in a matrix distinct from the aqueous KCl solutions used for calibration. As this bias was consistent across all samples, a simple correction factor was added to the calculations. For both instruments, temperature differences were accounted for during calibration and the agreement between both readings was excellent (Figure 8.3). The conductivity values recovered by the Smart Toilet were  $97.0 \pm 9.5\%$  of those of the commercial instrument.

## ANTICLEPSYDRA SMART TOILET

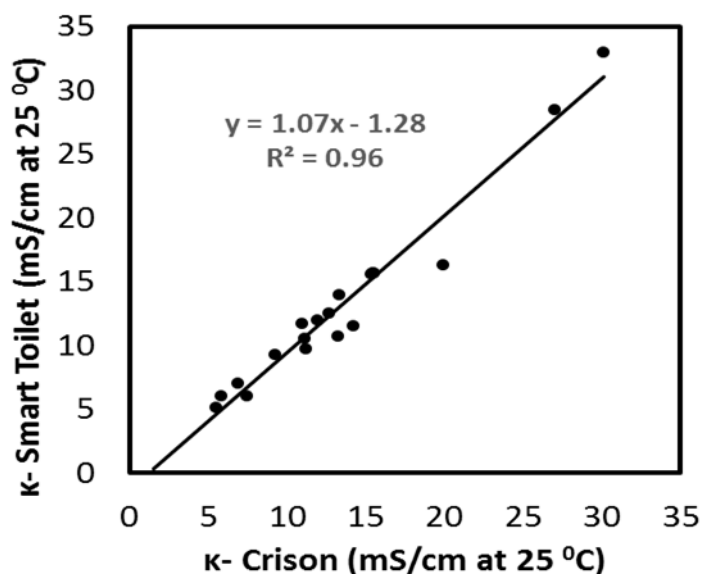


**Figure 8.3** Plot of the conductivity readings ( $\kappa$ ) of 19 urine samples validated against the readings of a commercial conductivity meter

While this degree of error would not be desirable for a high-end instrument, it is tolerable for an affordable high frequency, user-friendly, embedded sensor for non-critical applications such as hydration monitoring of athletes <sup>[20]</sup>.

The Smart Toilet's medium term stability in conductivity determinations was evaluated by assessing twenty-one micturition events during the next month and validating in the same way as previously described. No subsequent calibration was made to the device during this time. The conductivity values remained accurate yielding recoveries of  $103.5 \pm 6.8 \%$  (full data for this is provided in Appendix 6). The stability beyond one month has yet to be tested.



**Figure 8.4** The Smart Toilet installed with tablet computer connected and mounted to the wall



## ANTICLEPSYDRA SMART TOILET

---

### 8.3.2 Volume estimations

Theoretically, the speed of efflux,  $v$ , of a fluid from a hole at the lower part of a container is predicted by Torricelli's Law (Equation 8.1), which states that that  $v$  is proportional to the acceleration due to gravity ( $g$ ) and the height ( $h$ ) of the fluid.

$$v = \sqrt{2gh} \quad (\text{Equation 8.1})$$

One outcome of this equation is that as the height of the fluid column changes during flow, so too does the flow rate. From Torricelli's Law, an equation for the time required to empty a cylindrical container may be derived as follows.

For a cylinder of cross-sectional area  $A$ , and an opening of cross-sectional area  $a$ , filled with liquid to a height  $h$ , the velocity of efflux  $v$ , may be described as:

$$v = \frac{dx}{dt} = \sqrt{2gh}$$

$$dx = \frac{A dh}{a}$$

$$\frac{dx}{dt} = \frac{A dh}{a dt} = \sqrt{2gh}$$

$$\frac{A dh}{a \sqrt{2gh}} = dt$$

$$\frac{A}{a \sqrt{2g}} \int_0^h \frac{dh}{\sqrt{h}} = \int_0^t dt$$

$$t = \frac{2A}{a\sqrt{2g}} (\sqrt{h_i} - \sqrt{h_f})$$

Which integrates to:

Where  $h_i$  and  $h_f$  respectively represent the initial and final height of the liquid

The change in time during efflux,  $\Delta t$  may then be written as:

$$\Delta t = \frac{2A}{a\sqrt{2g}} \sqrt{\Delta h}$$

And because  $\Delta h = \frac{\Delta V}{h}$

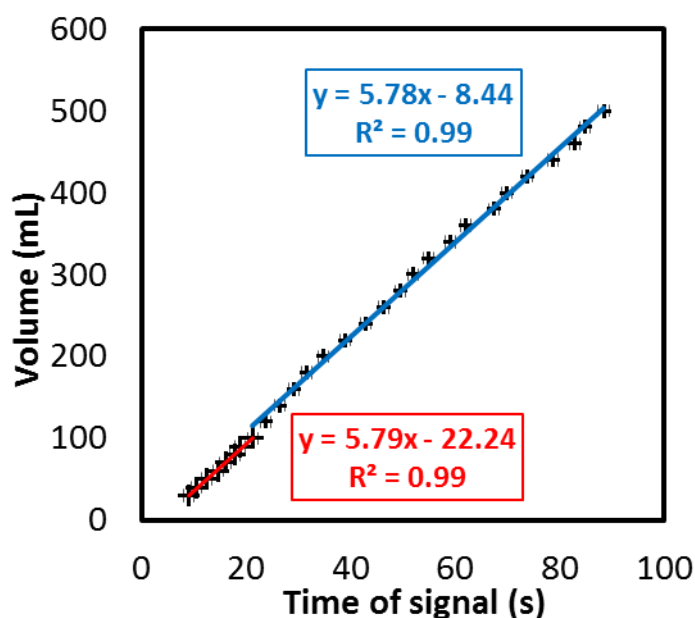
$$\Delta t = \frac{2A}{a\sqrt{2g}} \sqrt{\Delta V/A} \quad (\text{Equation 8.2})$$

In this, way a relationship between the volume of liquid and the time of efflux can be established for a cylinder. During prototyping, a cylindrical device was tested, and the power law relationship described by Equation 8.2 was indeed found to hold true. However, in order to tailor a device towards application within a toilet, a cylindrical vessel is not optimal. Rather, a more bowl-shape is preferable. Indeed, such a shape is also advantageous in calculations. This is because while its volume-to-time relationship would be far more complex to theoretically derive, in practice this relationship tends towards linearity. This is because, while within a

## ANTICLEPSYDRA SMART TOILET

cylinder, the pressure decreases dramatically as the vessel empties, a bowl-shaped device maintains a more constant pressure during efflux. In fact, a shape with a uniform rate of efflux can be mathematically described<sup>[21]</sup>.

In any case, an experimental approach is recommendable as each particular design will differ in its modulation of flow. The practical considerations involved in a Smart Toilet- specifically the need to limit the size of reservoir that must be prevented from overflowing- make rapid flow most suitable, which was achieved by optimizing the outlet area. This also tended to increase the linearity of the volume to flow time relationship, which was optimised at a flow rate of approximately 5.8 mL/s. In the case of the device presented here, this relationship slightly diverged from linearity at volumes below 100 mL (Figure 8.5). Slightly different equations were therefore used- these are shown in Figure 8.5 **Error! Reference source not found.** and termed below as Red and Blue equations. Volumes below 30 mL flowed too rapidly through the device to be detected reliably. Accordingly, volume was calculated in the following manner as written into the Arduino code: if the signal time corresponded to a volume below 30 mL, “insufficient volume” was printed; if the signal time corresponded to a volume between 30 and 100 mL, the Red equation was used; if the signal time corresponded to a volume greater than 100 mL, the Blue equation was used. The triplicate calibration in Figure 8.5 was made by pouring 100 mM NaCl through the Smart Toilet in a range of volumes. Following the protocol of calculations described above, the recovery for each volume across this range was  $99.9 \pm 2.5 \%$ . Given that mean urination rates are reported as  $13.05 \pm 6.12$  mL/s and mean maximum rates as  $22.5 \pm 9.2$  mL/s<sup>[22]</sup>, future prototypes could be improved by allowing for these faster flows .



**8.3.2.1** Figure 8.5 The relationship of volume to the time of signal. (Error bars represent 1 standard deviation; N = 3).

## 8.4 Conclusions

While strong correlations have been demonstrated between urine conductivity, osmolarity, colour and specific gravity [2–7,9–11], as well as urine creatinine levels<sup>[10]</sup>, its particular meaning in the context of an individual's hydration requires further study. Some research has also suggested that conductivity and osmolarity levels could be used to infer glucose levels<sup>[10]</sup>. This is just one example of the information that may be garnered from large data sets. In a Catch 22 situation, it is only with tools such as the Smart Toilet that such studies can be carried out to generate a large enough data set for powerful analyses to be made. The same can be said with tracking micturition volumes which- with the exception of the awkward 24-hour total volume collection- are not generally recorded as diagnostic information. By generating such new data, the common adage of needing to drink 8 glasses of water per day may one day be expressed as needing to pee 1.2 L per day. Of course, the ultimate vision is to replace all such generalisations with personalized and dynamic guidelines for individualized health monitoring. The Smart Toilet presented here offers an example of fusing Maker electronics with simple electrodes to produce an inexpensive, embedded sensing system. There remains scope for additional sensors to be embedded within the same platform to garner further data and furnish physiological insights.

## 8.5 References

- 1 L. E. Armstrong, Assessing Hydration Status: The Elusive Gold Standard, *J. Am. Coll. Nutr.*, 2007, **26**, 575S–584S.
- 2 S. M. Shirreffs, Markers of hydration status, *Eur. J. Clin. Nutr.*, 2003, **57**, S6–S9.
- 3 M. Kutlu and G. Guler, Assessment of hydration status by urinary analysis of elite junior taekwon-do athletes in preparing for competition, *J. Sports Sci.*, 2006, **24**, 869–873.
- 4 L. E. Armstrong, Hydration Assessment Techniques: the importance of hydration assessment, *Nutr. Rev.*, 2005, **63**, 40–54.
- 5 L. E. Armstrong, A. C. Pumerantz, K. A. Fiala, M. W. Roti, S. A. Kavouras, D. J. Casa and C. M. Maresh, Human hydration indices: Acute and longitudinal reference values, *Int. J. Sport Nutr. Exerc. Metab.*, 2010, **20**, 145–153.
- 6 L. E. Armstrong, J. A. Herrera Soto, F. T. Hacker, D. J. Casa, S. A. Kavouras and C. M. Maresh, Urinary indices during dehydration, exercise, and rehydration., *Int. J. Sport Nutr.*, 1998, **8**, 354–355.
- 7 L. E. Armstrong, C. M. Maresh, J. W. Castellani, M. F. Bergeron, R. W. Kenefick, K. E. LaGasse and D. Riebe, Urinary indices of hydration status., *Int. J. Sport Nutr.*, 1994, **4**, 265–79.
- 8 T. Berl and R. W. Schrier, *Renal and electrolyte disorders*, Wolters Kluwer/Lippincott Williams & Wilkins, Philadelphia, PA, 7th edn., 2010.
- 9 M. M. Grant and W. M. Kubo, Assessing a Patient’s Hydration Status, *Am. J. Nurs.*, 1975, **75**, 1306.
- 10 S. Kavukcu, M. Turkmen, A. Soylu and F. Kuralay, Could conductivity be used as a parameter in urinalysis?, *J. Pak. Med. Assoc.*, 1998, **48**, 238–240.
- 11 E. M. R. Kovacs and F. Brouns, Urine color, osmolality and specific electrical conductance are not accurate measures of hydration status during postexercise rehydration, *J. Sports Med. Phys. Fitness*, 1999, **39**, 47–53.
- 12 M. Sharples, in *Innovating Pedagogy*, The Open University, 2013.
- 13 B. Morin, What Is the Maker Movement and Why Should You Care?, [http://www.huffingtonpost.com/brit-morin/what-is-the-maker-movemen\\_b\\_3201977.html](http://www.huffingtonpost.com/brit-morin/what-is-the-maker-movemen_b_3201977.html), (accessed 11 December 2017).
- 14 M. Pasquier, Makers in the City - How 11 makerspaces around the world grow communities and hack urban issues, <http://www.innovationiseverywhere.com/makers-city-11-makerspaces-around-world-grow-communities-hack-urban-issues/>, (accessed 11 December 2017).
- 15 E. Parker, In China, Lessons of a ‘Hackerspace’, <https://www.wsj.com/articles/SB10001424052702303722604579111253495145952>, (accessed 11 December 2017).
- 16 J. Kalish, DIY ‘Hackers’ Tinker Everyday Things Into Treasure, <http://www.npr.org/2010/11/12/131268511/diy-hackers-tinker-everyday-things-into-treasure>, (accessed 11 December 2017).

## ANTICLEPSYDRA SMART TOILET

---

- 17 T. Baden, A. M. Chagas, G. J. Gage, G. Gage, T. C. Marzullo, T. Marzullo, L. L. Prieto-Godino and T. Euler, Open Labware: 3-D printing your own lab equipment., *PLoS Biol.*, 2015, **13**, e1002086.
- 18 Š. Kubínová and J. Šlégr, ChemDuino: Adapting Arduino for Low-Cost Chemical Measurements in Lecture and Laboratory, *J. Chem. Educ.*, 2015, **92**, 1751–1753.
- 19 A. A. Mills, Newton's Water Clocks and the Fluid Mechanics of Clepsydrae, *Notes Rec. R. Soc. Lond.*, 1982, **37**, 35–61.
- 20 S. M. Shirreffs and R. J. Maughan, Urine osmolality and conductivity as indices of hydration status in athletes in the heat, *Med. Sci. Sports Exerc.*, 1998, **30**, 1598–602.
- 21 Wikipedia.org, [https://en.wikipedia.org/wiki/Torricelli%27s\\_law](https://en.wikipedia.org/wiki/Torricelli%27s_law), (accessed 4 June 2018).
- 22 B. T. Haylen, D. Ashbey, J. R. Sutherst, M. I. Frazer and C. R. West, Maximum and Average Urine Flow Rates in Normal Male and Female Populations-the Liverpool Nomograms, *Br. J. Urol.*, 1989, **64**, 30–38.

## 9 IONSENS: A wearable potentiometric sensor patch for monitoring total ion content in sweat

---



## 9.1 Introduction

The development of body sensing networks [1] using wearable sensors to monitor physiological parameters in real time and in real settings is becoming possible due to the exponential progress in electronics and communication technologies. These platforms may have a significant impact in areas such as medical care [2], sports performance [2], homeland security, etc. Today, a wide range of devices that can monitor and wirelessly transmit physical parameters (heart rate, body temperature, movements, etc.) are available. Tools to generate chemical and biochemical information have not progressed at the same pace, creating an increasing gap that is fueling the interest for the development of wearable chemical and biochemical sensors. For this reason, since the pioneering works of Diamond *et al.* and Wang *et al.* this topic has been receiving a continuously increasing amount of attention in analytical chemistry [1-5]. The challenge is multifaceted, since wearable devices must work under very stringent dynamic conditions- including mechanical stresses, vibrations, temperature changes, etc.- and must adapt to the end-users needs without interfering in their routines. Given these constraints, the analytical problem must be reframed beyond the traditional performance-focused parameters, in order to include other equally relevant factors such as simplicity of operation, low power consumption, robustness, size, ergonomics and cost. The need to simultaneously meet all these requirements may offset the advantages of many well-established lab-based techniques. Therefore, the search for alternative detection approaches is an essential task in order to develop truly wearable (bio)chemical systems.

A good example of the complexity of this challenge is the analysis of sweat, a biological fluid that provides opportunities for the non-invasive monitoring of physiological information [5–7]. Electrolyte levels in sweat can be correlated with physical activity, physiological processes and some health-related issues, such as cystic fibrosis. Traditional lab-based methods require sampling sweat using absorbing pads, a step that is not free from problems (contamination, evaporation and changes on sample composition, etc.) and that stresses the advantages of using wearable devices. Total electrolyte levels are usually estimated by monitoring the sweat conductivity due to the overwhelming simplicity of this technique. However, many of these advantages vanish when dealing with wearable systems. Conductimetric measurements strongly depend on the cell geometry (electrode distance, spatial arrangement, shape and size), a factor that is easy to control in a lab, but that is harder to maintain in a wearable, flexible environment. To overcome this problem, a miniaturized, rigid wearable conductivity cell, as reported by Liu *et al.* for the real-time monitoring of athletes' sweat during exercise [6], can be employed. While this solution is effective, it requires coupling to a sweat pumping and transport system. This increases the complexity and reduces the robustness of the overall approach. Clearly, wearability favours the use of detection schemes that are more impervious to these geometrical constraints.

Colorimetric systems have been widely explored [8, 9], but electrochemical detection provides significant advantages. In particular, potentiometric sensors have shown significant benefits for the development of wearable devices, due to their simplicity of instrumentation and operation, robustness, low power consumption and ease of miniaturization. Potentiometry displays a great deal of versatility in the design of cells, thus

## IONSENS: A WEARABLE POTENTIOMETRIC SENSOR PATCH

---

allowing the construction of patches [10], yarns [11], band aids [12] and even tattoos [13] for the detection of different kind of ions. Multi-ion detection [5, 14–16] and- more recently- the successful development of flexible potentiometric sensors [17–19] emphasize the importance of this technique in the field of wearable devices.

It is worth mentioning that despite being a century-old technique, periodical waves of innovation have renewed the interest on potentiometric sensors. From the introduction of polymer-based electrodes in 1967 [20, 21], to the *silent revolution* of the solid-state technology in the 1990s [22]- invigorated later by the use of nanomaterials [23]- the past decade has seen creative advances in the use of novel substrates such as paper [24, 25], rubber [26], cotton [11], commercial carbon fibres [10], and plastics such as polyethylene terephthalate (PET) [5] to build potentiometric sensors. This wide range of substrates has increased the versatility of potentiometry across various applications.

The range of polymeric materials used in sensing membranes has also been expanding -the most widely-used being plasticized PVC [22]. While this material has proven to be highly versatile, limitations remain such as poor control over pink noise or  $1/f$  noise, high impedance, issues with water layer formation, and the high desolvation energy required for recognition of hydrophilic anions. Furthermore, these membranes are prone to fouling by biomolecules and cells, which often causes issues in analysis in biological media [27]. Because of these limitations, significant research has been devoted to find alternative polymeric substrates, such as polyurethane [18], conductive polymers such as PANI [12] and polypyrrole [28], and ion-exchange polymers such as Nafion® (from now on simply Nafion) [29–31]. Heng and Hall have also explored ‘self-plasticizing’ acrylates which obviate the addition of toxic plasticizers and avoid their leaching [32], and Poplawski *et al.* have reported the use of silicone rubber without plasticizer for Na<sup>+</sup>-ISEs [33]. More recently, Bakker *et al.* have described the use of sparingly-selective ion-exchange Donnan exclusion membranes. Their work included studies of Nafion- the sulfonated tetrafluoroethylene based fluoropolymer-copolymer- using commercially available membranes and inner-solution electrodes. Interestingly, they emphasized that selectivity should be less dependent on the ion lipophilicity (as described by the Hoffmeister series), and instead depend primarily on coulombic interactions [31]. Michalska *et al.* reported solid-contact permselective (Nafion) membranes upon conducting polymers (poly(pyrrole)) as early as 2001 [34]. The cationic responses they observed were limited to electrolyte concentrations below 1 mM, which they acknowledged as limiting its applied utility.

Nafion membranes have been extensively used in electrochemical sensors, particularly in voltammetric and amperometric detection. It has been shown that this negatively charged fluoropolymer acts as an effective permselective barrier against anions, reduces the biofouling and improves the stability of the system. More recently, the successful use of Nafion membranes in potentiometric biosensors has been also demonstrated [30]. In most of these cases, Nafion was used to improve the performance of the detection, but was not directly involved in the detection of substances. Nevertheless, in light of recent reports, this material offers a good



## **IONSENS: A WEARABLE POTENTIOMETRIC SENSOR PATCH**

---

opportunity to develop a potentiometric system that responds generically to the overall activity of the ions dissolved in solution.

This work aims to introduce, optimize and validate a wearable potentiometric sensor for monitoring the total ion activity in sweat. First, a disposable solid-contact potentiometric sensor that responds to the total electrolyte levels is presented. This sensor is built by casting a Nafion membrane on a paper substrate coated with a carbon ink. Due to the nature of Nafion as an ion-exchange membrane, this system is shown to respond in a sparingly-selective way to different types of ions, as has already been reported for similar electrodes with inner-solutions [31]. The performance of the working electrode to sodium (the predominant cation in sweat) is then expanded to other monocations, before extending the media to an artificial sweat solution of mixed electrolytes. Analytical parameters for different type of ions show a Nernstian response with very little difference between cations. To validate this result, the potentiometric response is compared to that obtained with a lab conductimeter. Thereafter, the system is integrated with a pseudo-reference electrode in the form of a wearable patch and applied to the direct monitoring of total electrolyte levels in sweat during exercise. The results show that the system can be used as an alternative approach to conductimetry, with advantages in overall simplicity and flexibility of form factor.

### **9.2 Experimental**

Artificial sweat was composed following a minor modification of European Standard number EN1811:2012 by dissolving 0.5 % w/v NaCl (85 mM), 0.1 % w/v KCl (13 mM), 0.1 % w/v urea (16 mM) and 0.1 % w/v sodium lactate (11.1 mM) into doubly distilled water, and adjusting the pH to  $5.4 \pm 0.3$  with HCl (100 mM).

A *Go Wireless* Electrode Amplifier by Vernier Software and Technology (OR, USA) was used to make wireless measurements with the wearable device for on-body measurements. Data was sent via a Bluetooth connection to a mobile phone running the Vernier Android app.

Paper-based electrodes of carbon, Ag/AgCl, platinum and gold were prepared as described in Chapter 3. In a method similar to that previously reported [35], the electrodes were encased within a 1.5 x 2 cm mask of polyester with circular apertures of 2.1 mm and 2.9 mm diameter exposed for deposition of working and reference electrodes respectively (Figure 9.1). This orifice exposed the electrochemically active surface of the electrode. The working electrode was completed by drop-casting 10  $\mu$ L of Nafion in 5 equal portions, allowing for evaporation of solvent between additions. Adapting the work previously published by our group [25, 36], the reference electrode was completed by adding some 1-3 mg of finely ground NaCl crystals to the Ag/AgCl surface before drop-casting 30  $\mu$ L of the reference cocktail (10 mg NaCl, 120 mg poly(vinyl butyral) (PVB), 1 mL MeOH), in three equal aliquots, allowing for evaporation of the bulk of the solvent between additions. These membranes were dried overnight at 4  $^{\circ}$ C.

## IONSENS: A WEARABLE POTENTIOMETRIC SENSOR PATCH

For experiments in which a conventional double-junction reference electrode was used, no conditioning of the membranes was performed. However, when the PVB pseudo-reference electrode was integrated, both electrodes were conditioned by immersion in a stirred solution of 1 M NaCl for at least 3 hours followed by rinsing with artificial sweat solution diluted 1:10 for 5 minutes.

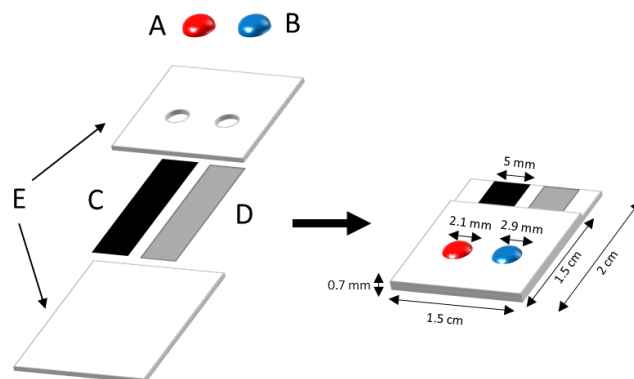


**Figure 9.1** Illustration of the elements comprising the IonSens device. A Nafion membrane (A) and reference membrane (B) were drop-cast over carbon paper (C) and Ag/AgCl paper (D) respectively. These papers were protected by a mask (E).

For on-body dynamic measurements, a polycarbonate membrane filter was applied in order to avoid direct contact between the membranes and the skin while allowing permeation of sweat. Connection to the wireless instrument was made with copper wires attached to the conductive papers with conductive epoxy. All exposed connections were insulated and waterproofed by wrapping in Teflon tape, cotton padding and electrical insulation tape. The sensor was affixed to the skin on the shoulder beneath a Hansaplast Aquaprotect XXL sterile plaster (8 x 10 cm). Data was collected and visually displayed upon a mobile phone running the Android version of the Vernier Graphical Analysis app, version 3.1.1 (build 8526) (Vernier Software & Technology).

## 9.3 Results and discussion

### 9.3.1 Analytical performance of solid-contact ion-sensitive electrode based on Nafion

The response of Nafion to different type of ions has already been described using inner-solution electrodes [31]. This approach clearly cannot be implemented in wearable systems. Therefore, the first step of this research is focused on finding a suitable strategy to build and characterize solid-contact, flexible and ideally disposable electrodes. To this end, paper was used as a substrate and different types of coating materials—namely, platinum, gold and carbon—were used for testing. The metals were sputtered on the paper, while the carbon was applied in the form of an ink, and the Nafion membranes were cast on the electrochemically active window as described above (Figure 9.1). As a first approach, considering the predominant component of sweat, the responses of these electrodes to NaCl were evaluated. The corresponding time-trace and calibration plot are displayed in Figure 9.2 and the analytical parameters summarised in Table 9.1 (as well as in Appendix 7).

## IONSENS: A WEARABLE POTENTIOMETRIC SENSOR PATCH

For clarity, the first 15 minutes are not shown in the time trace as no appreciable change in EMF took place, although they are included in Appendix 7.

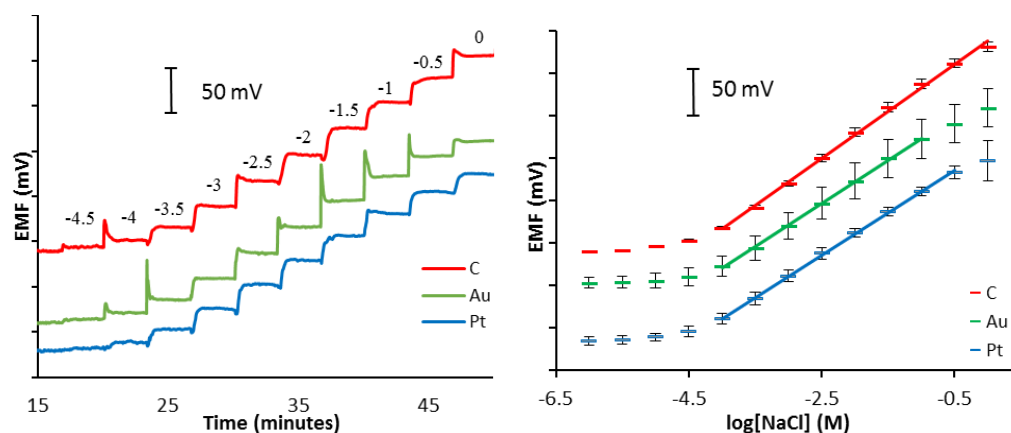


**Figure 9.2** Time trace (left) and calibration plot (right) comparing response of working electrodes based on carbon, gold and platinum papers.

Once the electrodes are initially immersed, the signal rapidly rises to reach a steady-state. At a low ionic strength such as 0.1 mM, the signal will take approximately 10 minutes to stabilize; for stronger tonicities, the signal will stabilize within a couple of minutes. As the membrane is hydrophilic, the electrode can be removed from solution and reused shortly thereafter without the need to wait for rehydration.

After this initial time, the electrodes remain remarkably stable, with a resting potential that depends on the electrode material, and that responds to the mixed potential of the system, modulated by the Nafion membrane.

The comparison of the sensitivities shows that for each one of the substrates an approximately Nernstian response to addition of sodium was observed. This is consistent with the results already reported, that attribute this trend to the change in the Donnan potential of the membrane [31]. Although electrodes upon all substrates tested showed somewhat similar performance, those upon carbon were selected to continue this study. Firstly, this was because this material displayed the greatest upper limit of linear range, which is desirable for applications in undiluted biological fluids such as sweat, whose composition easily reaches a sub-molar range. Additionally, of the three, carbon is known to be insensitive to redox active molecules, which are known to be present in biological fluids. Furthermore, it has been already shown that metal coatings on flexible substrates are more sensitive to cracking upon mechanical stress, leading to fissures that severely affect the electrical characteristics of the material. Last– but not least- carbon is a very low-cost substrate and it can be applied by direct printing, simplifying the potential mass manufacturing of the sensors. For all these reasons, carbon ink was selected as the conductive substrate of choice.

## IONSENS: A WEARABLE POTENTIOMETRIC SENSOR PATCH

**Table 9.1** Comparison of key analytical parameters between the three substrates (N = 3).

Substrate	C	Au	Pt
<b>Sensitivity (mV/dec)</b>	55.3 ± 1.0	51.1 ± 4.6	49.8 ± 0.2
<b>Standard potential (mV)</b>	588.2 ± 6.0	524.5 ± 28.3	510.2 ± 5.6
<b>Linear range (mM)</b>	0.1 – 1000	0.1 - 100	0.1 – 316
<b>Limit of detection (uM)</b>	48.3 ± 5.0	55.0 ± 4.1	40.3 ± 5.1
<b>Response time (s)</b>	17 ± 6	22 ± 14	18 ± 6

An important factor affecting the usability of a wearable device is the simplicity of its operation, which in the case of chemical sensors finds in the calibration step, a major challenge. Potentiometry offers very attractive features, since the highly reproducible Nernstian sensitivity (as shown above) reduces the problem to the stabilization of the standard potential. It has been shown that single-point calibrations can be successfully applied [37]. More recent works on the stabilization of the standard potential by chemical [38] or instrumental [39] approaches have been closing the gap towards the development of truly calibration-free potentiometric sensors. The instrumental approach proposed by Bobacka *et al.* has been recently explored by our group for the development of wearable systems [10].

The Nafion-coated carbon ink electrodes developed in this work show a decent reproducibility of the standard potential, of  $\pm 6$  mV ( $n = 5$ ) as shown in Table 9.1. This may be due in part to the mechanism of response of the electrode and the particular structure of Nafion. This polymer contains a lipophilic Teflon ( $-\text{CF}_2\text{CF}_3$ ) group, which has been reported to adhere to metallic (in this case, carbon) surfaces. On the other hand, the hydrophilic sulfonate groups ( $-\text{SO}_3^-$ ) have very strong interactions with water molecules. The structure and properties of Nafion are not yet fully understood and they continue to receive extensive investigation. It is accepted, however, that hydrophilic domains formed by the sulfonate groups create nano-channels that strongly interact with water. It is also understood that the aqueous phase partially percolates through the porous nanostructures into the membrane. The activity of water in the membrane, as well as the concentration of oxygenated species that may lead to the electrode resting potential through a mixed potential mechanism are also modulated by the Nafion membrane. All these factors may contribute to the stabilization of the response that is observed when this polymer is used. From a practical point of view, these results encourage the development of calibration-free, wearable sensors.

The mechanism of generation of the Donnan potential in this type of membranes is well known and has been extensively described in the literature [40, 41]. Briefly, taking into account the ion-exchange between monovalent cations, Figure 9.3 illustrates this process and the potential drops at each interface.

## IONSENS: A WEARABLE POTENTIOMETRIC SENSOR PATCH

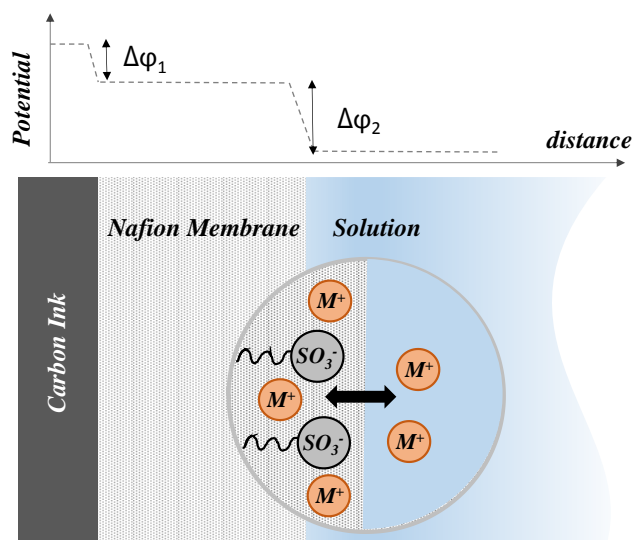


**Figure 9.3** Ion-exchange between the solution and Nafion interface between cations,  $M^+$ , with sulfonate groups immobilized within the Nafion.

Drawing on the work of Michalska [34], the two main contributions to the electrical potential are at Carbon ink-Nafion ( $\phi_1$ ) and at the Nafion-solution interface ( $\phi_2$ ). The potential generated at the electrode ( $E_{el}$ ) is then:

$$E_{el} = \phi_1 + \phi_2 \quad (\text{Equation 9.1})$$

Making the reasonable assumption that  $\phi_1$  is independent of the electrolyte concentration, this simplifies to:

$$E = \text{constant} + \phi_2 \quad (\text{Equation 9.2})$$

It has been shown that this can be rearranged in the form of the Nernst equation:

$$E = E^{0'} + \frac{RT}{F} \ln a_{\text{Cations, Solution}} \quad (\text{Equation 9.3})$$

This, treatment, however, is an approximation, since Nafion presents a very complex structure, with hydrophilic nanopores across the membrane segregated from the hydrophobic domains. Despite of this highly inhomogeneous structure, the Nernstian dependence is phenomenologically observed.

## IONSENS: A WEARABLE POTENTIOMETRIC SENSOR PATCH

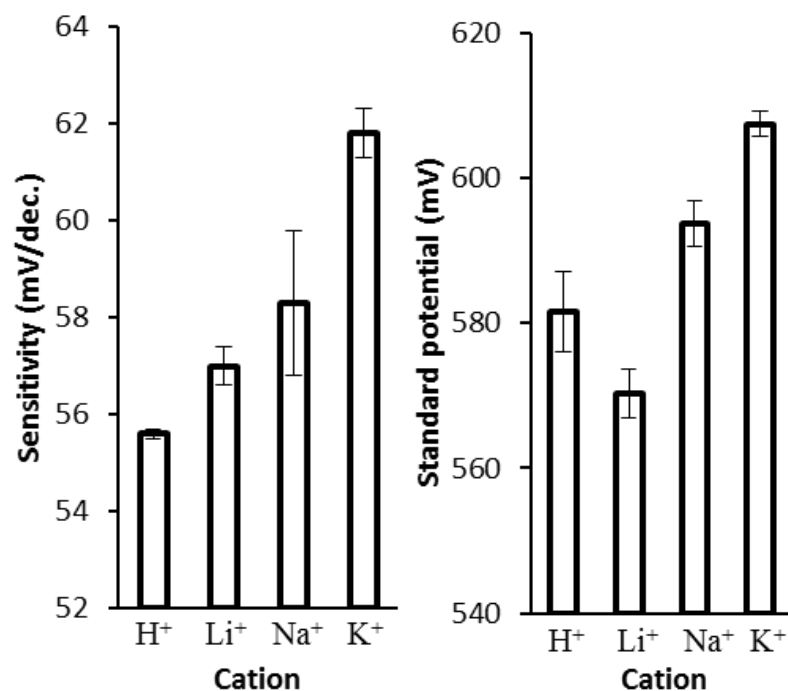


**Figure 9.4** Comparison of the working electrode's response to a series of monocations. Left: sensitivities to each cation. Right: standard potentials to each cation.

### 9.3.2 Affinity amongst cations

Not only was the reproducibility between electrodes very good, but also the successive calibrations with the same cation (such as sodium) show similar figures of merit (see Appendix 7). Therefore, experiments were conducted in order to evaluate the response of the sensor to different monovalent ions. When electrodes were tested in parallel against different monocations, it was observed that the Nafion membrane -while not highly selective- did indeed exhibit a subtle affinity amongst cations in accordance with the Hoffmeister series. This is reflected in both the sensitivities and the standard potentials (Figure 9.4). With the exception of the outlying standard potential during calibration with HCl, the observed trend shows an increment of values towards greater sensitivity and greater absolute value of response to the cations of the lower periodic rows. Although this tendency aligns with the Hoffmeister series, it is not necessarily due to differences in lipophilicity, as indicated by Bakker *et al.* [31]. Michalska *et al.* have also reported lower sensitivities for the lower primary cations, observing the lowest sensitivity with Li<sup>+</sup> [42].

It is also worth noting that reusing an electrode for the calibration of distinct monocations leads to significant changes in the standard electrode potential as one cation species is exchanged for another. However, this memory effect seems to be negligible for practical applications as an approximation of response to monocations can be made by combining the results of all calibrations with the four different salts to give an overall sensitivity of  $58.3 \pm 2.5$  mV/dec.<sub>[MCl]</sub> and a standard electrode potential of  $581.3 \pm 34.3$  mV (N = 11).

## IONSENS: A WEARABLE POTENTIOMETRIC SENSOR PATCH

---

Using these parallel calibrations with the four electrolytes mentioned, logarithms of potentiometric selectivity coefficients were calculated by treating the data as though it had resulted from the separate solution method, as electrode memory made reuse of the same electrodes unviable. Given that prior to any conditioning, Nafion contains protons as the exchangeable-ions to the immobile sulfonate groups, protons were (arbitrarily) selected as the primary analyte for these calculations (Table 9.2). All logarithms of potentiometric selectivity coefficients were between -0.6 and 0.5. While these affinities are minor, they do exceed those reported by the group of Bakker by an order of magnitude (in their study sodium was the primary ion) [31]. However, as mentioned in Section 1, the bespoke membranes used in this study were not in contact with an inner solution which may have had a role in the observed differences in affinities.

With the objective of constructing a wearable sensor which neither requires conditioning nor calibration, this working electrode is very attractive (as it requires neither). However, as will be seen, the integration of a reference electrode to complete the sensor currently still necessitates both of these steps.

**Table 9.2** Potentiometric selectivity coefficients approximated from a separate solution method treatment of parallel calibrations of each electrolyte.

Ion (A)	Ion (B)	$\log K^{\text{pot}}_{A,B}$
H <sup>+</sup>	H <sup>+</sup>	0
	Li <sup>+</sup>	-0.54 ± 0.07
	Na <sup>+</sup>	0.38 ± 0.10
	K <sup>+</sup>	0.44 ± 0.13

### 9.3.3 Total ion activity as a proxy for conductivity in artificial sweat solutions and integration of a pseudo-reference electrode

While the experimental evidence has revealed a weak affinity between monocations, the general response to all ions encourages the exploration of this electrode as a proxy for conductivity ( $\kappa$ ) measurements. Experiments where the conductivity and EMF were both read across a range of dilutions of artificial sweat to establish the relationship between the two techniques were conducted. While this could in principle be done using a sodium ion-selective electrode, the point of difference here is that we expect the relationship to also hold for mixed electrolyte solutions.

Furthermore, in order to move towards a wearable device, a paper-based pseudo-reference electrode was integrated into the platform using a modification of the method reported by our research group [25, 36]. Although this showed a sensitivity  $-6.9 \pm 1.7$  mV/dec.<sub>(Artificial Sweat)</sub> ( $N = 3$ ) across the one decade of change in ionic strength when tested against a conventional double-junction Ag/AgCl/KCl reference electrode, this response contributed to the total sensitivity of the paper-based cell. Accordingly, the sensitivity of the IonSens cell increased to approximately 60 mV per decade of conductivity. The ability of the IonSens system to approximate conductivity in mixed electrolyte solutions was tested using ten dilutions of an artificial sweat

## IONSSENS: A WEARABLE POTENTIOMETRIC SENSOR PATCH

solution. At each increment, the conductivity was also recorded with a commercial instrument and the results are shown in Figure 9.5. This confirmed that both instruments- the commercial conductivity meter and the bespoke IonSens device- had a predictable relationship to dilutions of a mixed electrolyte artificial sweat solution.

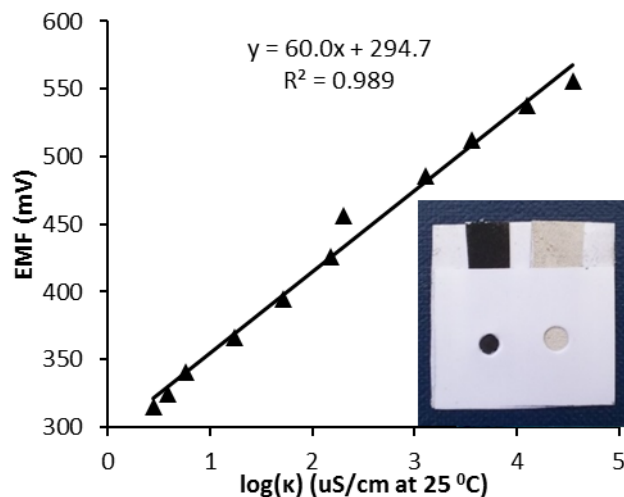


**Figure 9.5** Plot validating the relationship of EMF to the logarithm of conductivity in a series of dilutions of artificial sweat. The inset is a photograph of the Ions cell.

It is worth mentioning at this point that the system does not show any response to the neutral molecules tested, namely glucose, hydrogen peroxide and urea. As sweat is predominated by ions, the global reading of these is suggested to provide a snapshot of composition (Table 9.3).

**Table 9.3** Typical sweat constitution components on the scapula [43]

Ion	Concentration of ions
Na <sup>+</sup>	41.10 ± 24.80 mM
Cl <sup>-</sup>	38.10 ± 24.10 mM
K <sup>+</sup>	3.49 ± 1.23 mM
Lactate	7.65 ± 1.49 mM
HCO <sub>3</sub> <sup>-</sup>	1.80 ± 2.51 mM
pH	5.82 ± 0.81

### 9.3.4 Determinations in real sweat samples

Real sweat samples were collected inside a plastic vial, by sliding it across the across the skin of the upper body of 11 athletes after playing basketball. These were analysed by the benchtop conductivity meter and in triplicate with IonSens cells (on the lab bench). Prior to each determination, the IonSens cells were calibrated with 2 points of artificial sweat and rinsed with Milli-Q water. An exemplary time trace of these experiments is shown in Figure 9.6A. The protocol was: a 2-point calibration with artificial sweat was made, the sensor was dried, the sample was introduced, the sensor was dried, and a final 2-point calibration was made. It is



## IONSENS: A WEARABLE POTENTIOMETRIC SENSOR PATCH

notable that the potential was not stable, but rather decreased for several analyses- in the figure, this can be seen for sensor 1. In this, the potential through the sample could be recorded at a maxima (marked 'M') or at the subsequent steady-state value (marked 'S'). Related to this, the initial or final calibration could be considered in order to evaluate the sample. A pattern was observed from this: using the initial calibration led to appropriate recoveries relative to the maxima; whereas the steady-state potential- which followed some minutes- later gave an appropriate recovery relative to the final calibration. The reasons for this phenomena- observed with some sensors but not with others- is not yet understood.

By using the initial calibration and taking the maxima of the potential generated by the sample, all eleven raw sweat samples were analysed and validated with a conductivity meter as recovering  $95.2 \pm 6.6$  % of the conductivity. These analyses were made in triplicate and are summarized in Figure 9.6B. (The complete data is included in Appendix 7). It is worth noting that the error introduced by the logarithmic response of potentiometric method also applies to these measurements in which conductivity was estimated from a potentiometric measurement. Although the pH of sweat varies widely- typically ranging from 4.5 to 6 for eccrine sweat while thermal apocrine sweat has higher pH values [44]- this did not impact the recoveries (see Appendix 7 for sample pH values). As described in Section 3.2, the working electrode responds to free protons as it does other monovalent cations.

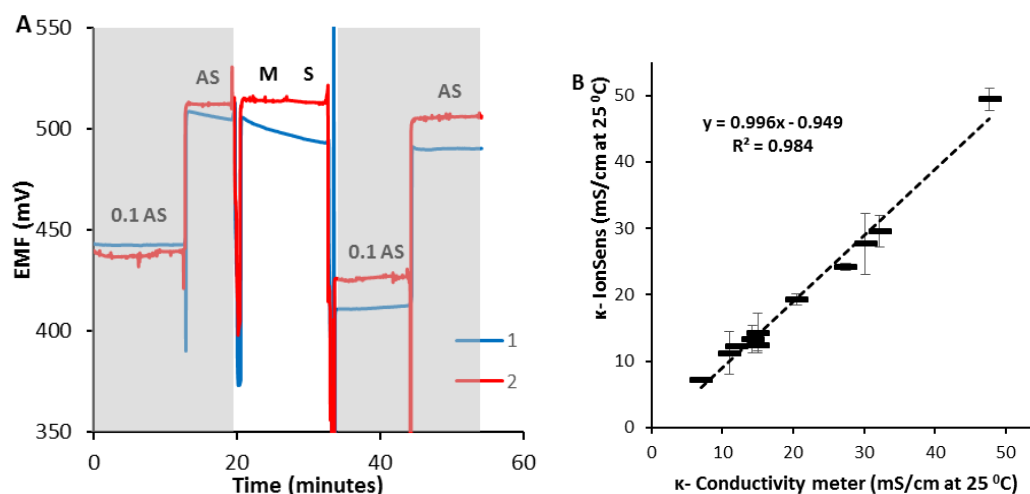


**Figure 9.6** A: time traces of two IonSens cells (labelled 1 and 2). Grey background indicates a calibration with artificial sweat, white background indicates a sweat sample. 'AS' indicates artificial sweat, '0.1 AS' indicates artificial sweat diluted 10x, 'M' indicates the signal maxima, 'S' indicates the signal at steady-state. The noise seen at times 15 minutes, 21 minutes, 35 minutes and 45 minutes are due to the sensor being momentarily dry between changes of solution. B: validation of conductivity determinations by IonSens in real sweat samples against those made by a commercial conductivity meter.

### 9.3.5 A wearable device for on-body dynamic monitoring of sweat conductivity

In moving from static steady-state detection to real-time on-body tracking of chemical information with a wearable device, several new challenges arise. Very practical issues include the electrical isolation and waterproofing of sensitive elements such as paper electrodes, as well as the need for flexibility of sensors to respond to the stretching and bending of the body during movement. If not managed appropriately, these

## IONSENS: A WEARABLE POTENTIOMETRIC SENSOR PATCH

---

elements can each introduce noise and error into measurements. Additionally, there is a challenge in fluidics- to truly represent real-time analysis, sweat must be allowed to flow freely across the sensing surface.

In this on-body trial, an IonSens device was affixed beneath a plaster to the shoulder of a cyclist riding a stationary bicycle and the sensor's dynamic response during 35 minutes of exercise was monitored. Data was transmitted via Bluetooth from a small device in the athlete's clothing to a mobile phone app (see Appendix 7 for a photo of the full device). Perspiration was evident after 10 minutes of exercise, after which time sweat samples were collected at 5 minute intervals from bulk sweat of the shoulder. These were subsequently tested 'off-body' (on the lab bench) using the same sensor in order to validate the on-body measurements.

The time trace recorded during exercise is reproduced in Figure 9.7 and the corresponding conductivities measured statically in the on-bench analyses are superimposed at the time corresponding to when the sample was collected. The (calculated) conductivity rose from the initiation of exercise until  $t = 8$  minutes, at which time the signal stabilized and sufficient sweat was present for bulk collection from the shoulder. While during these first minutes of exercise the electrode membranes were already hydrated, the athlete's skin was dry so no bulk liquid connected the circuit. It is therefore notable that the signal is not dominated by the noise associated with an open circuit. This attractive result may be attributable to the membrane impedances being 1-3 orders of magnitude lower than those typical of PVC (see Appendix 7), as well as being hydrophilic. A positive bias in the dynamic recording (of  $141 \pm 17\%$ ) as compared to the static measurements can be seen, although there is a preliminary correlation in the profiles of the two series. Variations in the sample collected manually from the shoulder as compared with the sample exposed to the sensor may have contribute to the bias. Additionally, mixing with previous sweat and evaporation may have been factors. Ultimately, these challenges are common to the validation of wearable sensors.

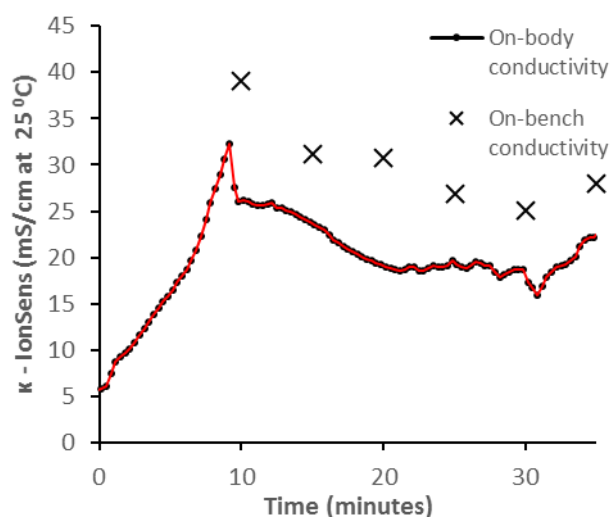


**Figure 9.7** Plot of conductivity values generated by the on-body IonSens device during 35 minutes of exercise. Subsequent on-bench measurements were made at five minute intervals and the values are superimposed at the corresponding times.

## 9.4 Conclusions

Nafion has been demonstrated to monitor total ion concentration within a solid-state electrode. This electrode-a drop-cast membrane upon carbon ink- is attractive for its simplicity, low-cost and reproducibility. Determinations in both synthetic solutions and real sweat samples have been validated by a commercial instrument to show correlation with conductivity. Furthermore, by fashioning the electrode into a wearable device with the inclusion of a pseudo-reference electrode, a low-impedance, low-consumption, paper-based conductivity sensor was realized. Through a Bluetooth connection to a mobile phone app, its utility for real-time gathering of chemical data was demonstrated by tracking the conductivity profile of an athletes' sweat during exercise. In contrast to the more accurate but bulky and expensive high-end instruments, this wearable offers a new value proposition to the user.

Sweat is a parameter rich in physiological information. It has been reported that the concentration of sodium and chloride varies significantly depending on sweat rate, while potassium and calcium concentrations remain unaffected [45]. Sweat rate and composition also varies regionally over the surface of the body while pH values can span some four orders of magnitude [43]. One approach is to multiplex sensors to monitor multiple analytes such as in the work of Gao *et al.* [5]. Another proposition is to take a single global reading that incorporates as much information as possible as in the case of conductivity readings. The IonSens device offers such a global reading. In this way, the IonSens platform *'plugs in'* to the vision of chemical sensors being embedded into a person's environment to gather meaningful information about the chemical gestalt of the individual.

## 9.5 References

- 1 D. Diamond, S. Coyle, S. Scarmagnani and J. Hayes, Wireless sensor networks and chemo-/biosensing, *Chem. Rev.*, 2008, **108**, 652–679.
- 2 R. T. Li, S. R. Kling, M. J. Salata, S. A. Cupp, J. Sheehan and J. E. Voos, Wearable Performance Devices in Sports Medicine, *Sports Health*, 2016, **8**, 74–78.
- 3 T. Glennon, C. O’Quigley, M. McCaul, G. Matzeu, S. Beirne, G. G. Wallace, F. Stroiescu, N. O’Mahoney, P. White and D. Diamond, ‘SWEATCH’: A Wearable Platform for Harvesting and Analysing Sweat Sodium Content, *Electroanalysis*, 2016, **28**, 1283–1289.
- 4 A. J. Bandodkar, I. Jeerapan and J. Wang, Wearable Chemical Sensors: Present Challenges and Future Prospects, *ACS Sensors*, 2016, **1**, 464–482.
- 5 W. Gao, S. Emaminejad, H. Y. Y. Nyein, S. Challa, K. Chen, A. Peck, H. M. Fahad, H. Ota, H. Shiraki, D. Kiriya, D.-H. Lien, G. A. Brooks, R. W. Davis and A. Javey, Fully integrated wearable sensor arrays for multiplexed in situ perspiration analysis, *Nature*, 2016, **529**, 509–514.
- 6 G. Liu, C. Ho, N. Slappey, Z. Zhou, S. E. E. Snelgrove, M. Brown, A. Grabinski, X. Guo, Y. Chen, K. Miller, J. Edwards and T. Kaya, A wearable conductivity sensor for wireless real-time sweat monitoring, *Sensors Actuators, B Chem.*, 2016, **227**, 35–42.
- 7 D. P. Rose, M. E. Ratterman, D. K. Griffin, L. Hou, N. Kelley-Loughnane, R. R. Naik, J. A. Hagen, I. Papautsky and J. C. Heikenfeld, Adhesive RFID sensor patch for monitoring of sweat electrolytes, *IEEE Trans. Biomed. Eng.*, 2015, **62**, 1457–1465.
- 8 V. F. Curto, S. Coyle, R. Byrne, N. Angelov, D. Diamond and F. Benito-Lopez, Concept and development of an autonomous wearable micro-fluidic platform for real time pH sweat analysis, *Sensors Actuators B Chem.*, 2012, **175**, 263–270.
- 9 V. F. Curto, C. Fay, S. Coyle, R. Byrne, C. O’toole, C. Barry, S. Hughes, N. Moyna, D. Diamond and F. Benito-Lopez, Real-time sweat pH monitoring based on a wearable chemical barcode micro-fluidic platform incorporating ionic liquids, *Sensors Actuators B. Chem.*, 2012, **171–172**, 1327–1334.
- 10 M. Parrilla, J. Ferré, T. Guinovart and F. J. Andrade, Wearable Potentiometric Sensors Based on Commercial Carbon Fibres for Monitoring Sodium in Sweat, *Electroanalysis*, 2016, **28**, 1267–1275.
- 11 T. Guinovart, M. Parrilla, G. A. Crespo, F. X. Rius and F. J. Andrade, Potentiometric sensors using cotton yarns, carbon nanotubes and polymeric membranes, *Analyst*, 2013, **138**, 5159–5504.
- 12 T. Guinovart, G. Valdés-Ramírez, J. R. Windmiller, F. J. Andrade and J. Wang, Bandage-Based Wearable Potentiometric Sensor for Monitoring Wound pH, *Electroanalysis*, 2014, **26**, 1345–1353.
- 13 A. J. Bandodkar, W. Jia and J. Wang, Tattoo-Based Wearable Electrochemical Devices: A Review, *Electroanalysis*, 2015, **27**, 562–572.
- 14 M. Parrilla, R. Cánovas, I. Jeerapan, F. J. Andrade and J. Wang, A Textile-Based Stretchable Multi-Ion Potentiometric Sensor, *Adv. Healthc. Mater.*, 2016, **5**, 996–1001.

## IONSENS: A WEARABLE POTENTIOMETRIC SENSOR PATCH

---

- 15 H. Y. Y. Nyein, W. Gao, Z. Shahpar, S. Emaminejad, S. Challa, K. Chen, H. M. Fahad, L. C. Tai, H. Ota, R. W. Davis and A. Javey, A Wearable Electrochemical Platform for Noninvasive Simultaneous Monitoring of Ca<sup>2+</sup> and pH, *ACS Nano*, 2016, **10**, 7216–7224.
- 16 W. Gao, H. Y. Y. Nyein, Z. Shahpar, H. M. Fahad, K. Chen, S. Emaminejad, Y. Gao, L. C. Tai, H. Ota, E. Wu, J. Bullock, Y. Zeng, D. H. Lien and A. Javey, Wearable Microsensor Array for Multiplexed Heavy Metal Monitoring of Body Fluids, *ACS Sensors*, 2016, **1**, 866–874.
- 17 A. J. Bandodkar, I. Jeerapan, J.-M. You, R. Nuñez-Flores and J. Wang, Highly Stretchable Fully-Printed CNT-Based Electrochemical Sensors and Biofuel Cells: Combining Intrinsic and Design-Induced Stretchability, *Nano Lett.*, 2016, **16**, 721–727.
- 18 R. Cánovas, M. Parrilla, P. Mercier, F. J. Andrade and J. Wang, Balloon-Embedded Sensors Withstanding Extreme Multiaxial Stretching and Global Bending Mechanical Stress: Towards Environmental and Security Monitoring, *Adv. Mater. Technol.*, 2016, **1**, 1–11.
- 19 A. J. Bandodkar, R. Nuñez-Flores, W. Jia and J. Wang, All-Printed Stretchable Electrochemical Devices, *Adv. Mater.*, 2015, **27**, 3060–3065.
- 20 R. Bloch, A. Shatkay and H. A. Saroff, Fabrication and evaluation of membranes as specific electrodes for calcium ions, *Biophys.*, 1967, **7**, 865–877.
- 21 E. Bakker and K. Chumbimuni-Torres, Modern Directions for Potentiometric Sensors, *J. Braz. Chem. Soc.*, 2008, **19**, 621–629.
- 22 E. E. Pretsch, The New Wave of Ion-Selective Electrodes, *Anal. Chem.*, 2002, **74**, 1–11.
- 23 A. Düzgün, G. a Zelada-Guillén, G. a Crespo, S. Macho, J. Riu and F. X. Rius, Nanostructured materials in potentiometry., *Anal. Bioanal. Chem.*, 2011, **399**, 171–81.
- 24 M. Novell, M. Parrilla, G. A. Crespo, F. X. Rius and F. J. Andrade, Paper-based ion-selective potentiometric sensors., *Anal. Chem.*, 2012, **84**, 4695–702.
- 25 M. Novell, T. Guinovart, P. Blondeau, F. X. Rius and F. J. Andrade, A paper-based potentiometric cell for decentralized monitoring of Li levels in whole blood., *Lab Chip*, 2014, **14**, 1308–14.
- 26 M. Cuartero, J. S. del Río, P. Blondeau, J. A. Ortuño, F. X. Rius and F. J. Andrade, Rubber-based substrates modified with carbon nanotubes inks to build flexible electrochemical sensors., *Anal. Chim. Acta*, 2014, **827**, 95–102.
- 27 C. Bieg, K. Fuchsberger and M. Stelzle, Introduction to polymer-based solid-contact ion-selective electrodes—basic concepts, practical considerations, and current research topics, *Anal. Bioanal. Chem.*, 2017, **409**, 45–61.
- 28 E. Shoji and M. S. Freund, Potentiometric sensors based on the inductive effect on the pK<sub>a</sub> of poly(aniline): A nonenzymatic glucose sensor [3], *J. Am. Chem. Soc.*, 2001, **123**, 3383–3384.
- 29 M. Parrilla, R. Cánovas and F. J. Andrade, Paper-based enzymatic electrode with enhanced potentiometric response for monitoring glucose in biological fluids., *Biosens. Bioelectron.*, 2017, **90**, 110–116.
- 30 M. Parrilla, R. Cánovas and F. J. Andrade, Enhanced Potentiometric Detection of Hydrogen Peroxide Using a Platinum Electrode Coated with Nafion, *Electroanalysis*, 2017, **29**, 223–230.

## IONSENS: A WEARABLE POTENTIOMETRIC SENSOR PATCH

---

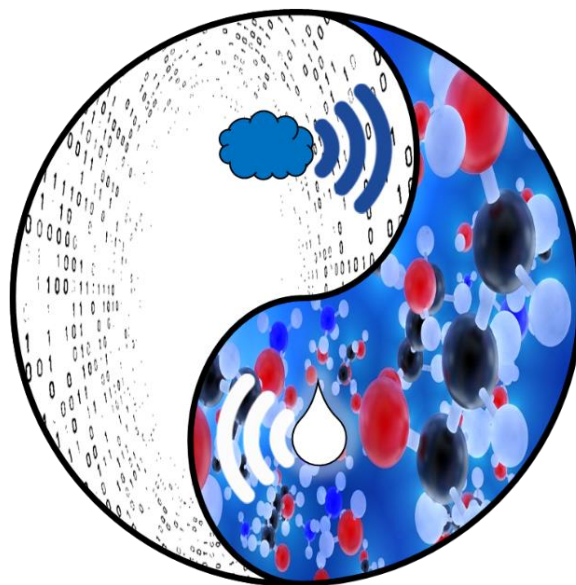
- 31 E. Grygolowicz-Pawlak, G. A. Crespo, M. Ghahraman Afshar, G. Mistlberger and E. Bakker, Potentiometric sensors with ion-exchange donnan exclusion membranes, *Anal. Chem.*, 2013, **85**, 6208–6212.
- 32 L. Y. Heng and E. A. H. Hall, Producing ‘self-plasticizing’ ion-selective membranes, *Anal. Chem.*, 2000, **72**, 42–51.
- 33 M. E. Poplawski, R. B. Brown, K. Lae Rho, S. Yong Yun, H. Jung Lee, G. Sig Cha and K. J. Paeng, One-component room temperature vulcanizing-type silicone rubber-based sodium-selective membrane electrodes, *Anal. Chim. Acta*, 1997, **355**, 249–257.
- 34 A. Michalska, S. Walkiewicz, K. Maksymiuk and E. A. H. Hall, Potentiometric responses of poly(pyrrole) films surface modified by Nafion, *Electroanalysis*, 2002, **14**, 1236–1244.
- 35 R. Cánovas, M. Parrilla, P. Blondeau and F. J. Andrade, A novel wireless paper-based potentiometric platform for monitoring glucose in blood, *Lab Chip*, 2017, **17**, 2500–2507.
- 36 T. Guinovart, G. A. Crespo, F. X. Rius and F. J. Andrade, A reference electrode based on polyvinyl butyral (PVB) polymer for decentralized chemical measurements., *Anal. Chim. Acta*, 2014, **821**, 72–80.
- 37 F. X. Rius-Ruiz, G. A. Crespo, D. Bejarano-Nosas, P. Blondeau, J. Riu and F. X. Rius, Potentiometric Strip Cell Based on Carbon Nanotubes as Transducer Layer: Toward Low-Cost Decentralized Measurements, *Anal. Chem.*, 2011, **83**, 8810–8815.
- 38 J. Hu, X. U. Zou, A. Stein and P. Bühlmann, Ion-Selective Electrodes with Colloid-Imprinted Mesoporous Carbon as Solid Contact, *Anal. Chem.*, 2014, **86**, 7111–7118.
- 39 U. Vanamo and J. Bobacka, Instrument-free control of the standard potential of potentiometric solid-contact ion-selective electrodes by short-circuiting with a conventional reference electrode, *Anal. Chem.*, 2014, **86**, 10540–10545.
- 40 V. S. Bagotsky, *Fundamentals of electrochemistry*, John Wiley & Sons, Inc., New Jersey, 2nd edn., 2006.
- 41 A. J. Bard and L. R. Faulkner, *Electrochemical methods, Fundamentals and Applications*, John Wiley & Sons, Inc., 1980.
- 42 A. Michalska, S. Walkiewicz, K. Maksymiuk and A. H. Hall, Potentiometric Responses of Poly ( pyrrole ) Films Surface Modified by Nafion, 2002, 1236–1244.
- 43 M. J. Patterson, S. D. Galloway and M. a Nimmo, Variations in regional sweat composition in normal human males., *Exp. Physiol.*, 2000, **85**, 869–875.
- 44 J. L. Matousek and K. L. Campbell, A comparative review of cutaneous pH, *Vet. Dermatol.*, 2002, **13**, 293–300.
- 45 N. A. Taylor and C. Machado-Moreira, Regional variations in transepidermal water loss, eccrine sweat gland density, sweat secretion rates and electrolyte composition in resting and exercising humans, *Extrem. Physiol. Med.*, 2013, **2**, 4.

## ***IONSENS: A WEARABLE POTENTIOMETRIC SENSOR PATCH***

---

## 10 CONCLUSIONS

---





## 10.1 A revolution in chemical sensing by design

This thesis began with a critical review of the literature concerning distributed electrochemical sensors. In this, three dominant challenges to their adoption were identified as *usability*, *affordability*, and *performance*. With varying emphasis, the subsequent chapters went on to explore the development of decentralized chemical sensors within the framework of these challenges. A common thread of emphasis was drawn throughout the work in taking a design-centred approach and ethos to the work. This shone the spotlight primarily onto the aspect of usability, the predominant weakness of distributed chemical sensing systems and an absolute necessity in order for them to flourish by finding their place in solving pressing needs.

A common trait of world-shifting technologies is that they are intuitive to use; even if we do not know *how* they work, we know *how to work them*.

Realizing functional chemical sensors has inherent complexity and requires specialized knowledge. The prototypes of the *Lab-in-a-box* exemplified the multifaceted challenge that technologists now face; to seamlessly integrate the complexity of a laboratory into something that appears as ordinary. As stated by the great science fiction writer, Arthur C. Clarke in what has become known as his third law, “*any sufficiently advanced technology is indistinguishable from magic*” [1]. Much like the now familiar technologies of the internet, the microwave, and the combustion engine- although the majority of us know how to use these, we also lack understanding of how they work. Through familiarity, the magic becomes ordinary. Similarly, through well-crafted design, the complexity of advanced technologies can appear as intuitively simple. It is hoped that chemical sensors may too traverse the divide from the magical to the ordinary, and may one day be conjured into everyday commodities. It appears that today however, they are in an intermediate stage of *advanced technology undisguised*, like an unpractised magic trick- they still require a touch of design wizardry to hide the complexity that lies beneath the hood.

The transformation that is sought, is not simply from a functional sensor to a *beautiful* functional sensor. Rather the alchemy that is required is from a drop of sweat to a personalized fitness recommendation. The transmutation that is emerging is from a morning urination, to an important call from the doctor. The revolution that is unfolding is rivers communicating with municipalities, the environment gaining a voice, and healthcare becoming individualized. While the change may be technological, the impact may be societal.

The principle conclusion of this thesis is that usability constitutes the primary barrier to the emergence of electrochemical sensing networks. As this is less of a challenge of fundamental science, and more a challenge of integrative design, it was approached and addressed as such. Both evolutionary and revolutionary directions were explored in this work, as are also being advanced by many research groups [2]. It may be that a combination of innovation and conservatism could expedite this process. As the simplest of electrochemical techniques, conductimetry and potentiometry offer conservative scientific tools well-suited to this task. The

## CONCLUSIONS

---

simplicity of these classic methods was shown to merge well with modern tools *du jour* including paper electrodes, *Arduino* microcontrollers, and 3D-printing technology.

In this age of information- in which data has become a commodity- it is striking that chemical information remains scarce in availability. Being rich in import to the critical spheres of health and environment, among others, there is a growing urgency for this information. The breaking down of the technological barriers that lock this rich information within liquids, will release a flood of new data, with unforeseeable impact. While the consequences of this are not predictable, the history of technology indicates that liberating informational types is positive, democratic, and revolutionary. This thesis strove to contribute towards this burgeoning revolution. It is hoped that the power imparted by the wealth of new chemical information may be used wisely by humans, both for their health and for the health of the planet.

We live in interesting times. May we design them to be both equitable and ecologically aware.

## CONCLUSIONS

---

### 10.2 References

- 1 A. C. Clarke, *Profiles of the future : an inquiry into the limits of the possible*, Warner Books, 1973.
- 2 C. Zuliani and D. Diamond, Opportunities and challenges of using ion-selective electrodes in environmental monitoring and wearable sensors, *Electrochim. Acta*, 2012, **84**, 29–34.

## APPENDICES

---

## Appendix 1. Scientific contributions

### Articles resulting from the thesis

- Rafael Hoekstra, Pascal Blondeau, Francisco J. Andrade  
**“Distributed electrochemical sensors: recent advances and barriers to market adoption”**  
*Analytical and Bioanalytical Chemistry*, published online 28 May 2018.
- Rafael Hoekstra, Pascal Blondeau, Francisco J. Andrade  
**“IonSens: a Wearable Potentiometric Sensor Patch for Monitoring Total Ion Content in Sweat”**  
*Electroanalysis*, published online 23 May, 2018.

### Oral Communications

- **“An Enzyme-based Potentiometric Redox Biosensor for Glucose on Paper”**  
*Nanociencia y Nanotecnología Analítica (NyNA) 2015*  
6-8 July, 2015, Salamanca, Spain
- **“Lab-In-A-Box: A Diagnostic Device for the Internet of You”**  
*IoT Solutions World Congress 2016*  
9-14 October, 2016, Barcelona, Spain

### Posters

- **“An Enzyme-based Potentiometric Redox Biosensor for Glucose on Paper”**  
*Nanociencia y Nanotecnología Analítica (NyNA) 2015*  
6-8 July, 2015, Salamanca, Spain
- **“Potentiometric flow injection determination of creatinine in biological fluids”**  
*Nanoscience, Materials and Chemical Engineering Doctoral Day 2016*  
4 May, 2016, Universitat Rovira i Virgili, Tarragona, Spain
- **“IonSens: a wearable potentiometric sensor of total ion activity”**  
*Mátrafüred 2017 International Conference on Electrochemical Sensors*  
11-16 June, 2017, Mátrafüred, Hungary

## APPENDICES

### Appendix 2. Glossary

Abbreviation	Definition
[HMIM][FAP]	[1-hexyl-3-methylimidazolium] <sup>+</sup> [tris(pentafluoroethyl)trifluorophosphate] <sup>-</sup>
3D	Three-dimensional
A	Amperes (as a unit), or Area in square metres (m <sup>2</sup> )
a	Chemical activity
AC	Alternating current
ADC	Analog-to-digital
AES	Atomic emission spectroscopy
AG	Analytical grade
aq	Aqueous
atm	Unit of pressure
BCE	Before common era
C	Concentration in moles per litre (molL <sup>-1</sup> )
C <sup>0</sup>	Signal without dispersion
C <sup>max</sup>	Signal maximum peak height
CNTs	Carbon nanotubes
CRT	Creatinine
D	Detector or dispersion coefficient
DC	Direct current
DECSs	Distributed electrochemical sensors
DIY	Do-it-yourself
DNA	Deoxyribonucleic acid
DOS	Bis-(2-ethylhexyl) sebacate
E	Electric potential in Volts (V)
e <sup>-</sup>	Electron
E <sup>'</sup> <sub>diff</sub>	Difference in potential between $E_{baseline}$ and E <sup>0</sup> in Volts (V) of the <i>establishing calibration</i>
E <sup>0</sup>	Standard electrode potential in Volts (V)
E <sup>0'</sup>	Formal potential in Volts (V)
E <sub>baseline</sub>	Baseline potential in Volts (V)
E <sub>const</sub>	Constant potential in Volts (V)
E <sub>D, Ref</sub>	Liquid-junction potential at the reference electrode in Volts (V)
E <sub>diff</sub>	Difference in potential between $E_{baseline}$ and E <sup>0</sup> in Volts (V)

## APPENDICES

---

$E_{\text{dry}}$	Electric potential of a dry potentiometric cell through a <i>capping membrane</i>
$E_{\text{el}}$	Potential generated at an electrode
$E_{\text{J}}$	Junction potential between membrane and conductor
ELISA	Enzyme-linked immunosorbent assay
$E^{\text{M}}$	Membrane potential in Volts (V)
EMF	Electromotive Force in Volts (V)
$E_{\text{PB}}$	Phase-boundary potential in Volts (V)
F	Faraday constant (96485 C mol <sup>-1</sup> )
FEP	Fluorinated ethylene propylene
FIA	Flow injection analysis
g	Acceleration due to gravity (9.8 ms <sup>-2</sup> )
h	Height in metres (m)
HMPP	2-hydroxy-2-methylpropiophenone
HOMO	Highest occupied molecular orbital
HPLC	High pressure liquid chromatography
i	Current in Amperes (A)
IDE	Integrated Development Environment
IL	Ionic liquid
IOT	Internet-of-things
ISE	Ion-selective electrode
IT	Information technology
IUPAC	International Union of Pure and Applied Chemistry
K	Cell constant in inverse metres (m <sup>-1</sup> )
kg	Kilograms
$K^{\text{pot}}_{\text{I,J}}$	Potentiometric selectivity coefficient of ion I, with respect to ion J
KTCIPB	Potassium tetrakis (4-chlorophenyl) borate
KTFPB	Potassium tetrakis-3,5-bis(trifluoromethyl)phenylborate
l	Length in metres (m)
L	Litre
LIB	Lab-in-a-box
ln	Natural logarithm
log	Logarithm to base 10
LUMO	Lowest unoccupied molecular orbital
M	Molar
M	Represents an unspecified metal ion
MBIS	N,N'-methylenebisacrylamide

## APPENDICES

---

MeOH	Methanol
MOOCs	Massive Open Online Courses
MW	Molecular weight
MWCNTs	Multi-walled carbon nanotubes
n	Number. E.g. number of charges, or numbers of replicates
NFC	Near field communication
NIST	National Institute of Standards and Technology
o-NPOE	2-nitrophenyl-octyl ether
org	organic
ORP	Oxidation-reduction potential
Ox	Oxidised form of a chemical species
PANI	Polyaniline
PET	Polyethylene terephthalate
pH	The negative logarithm of proton activity
pK <sub>a</sub>	Negative logarithm of the acid dissociation constant
POC	Point-of-care
ppm	Parts per million
PSPA	Phosphonium sulfopropylacrylate
PTFE	Polytetrafluoroethylene
PVA	Poly(vinyl alcohol)
PVB	Poly(vinyl butyral)
PVC	Poly(vinyl chloride)
R	Electrical resistance in Ohms ( $\Omega$ ), or the universal gas constant (8.314 $\text{J K}^{-1} \text{mol}^{-1}$ )
R & D	Research and development
RE	Reference electrode
Red	Reduced form of a chemical species
RF	Radio frequency
RX/TX	Receive and transmit (digital data)
S'	Sensitivity of establishing calibration (mV/dec.)
sccm	Standard cubic centimetres per minute
SFA	Segmented flow analysis
SI	International System of Units
SIA	Segmented flow analysis
T	Absolute temperature in Kelvin (K) or Celsius ( $^{\circ}\text{C}$ )
t <sub>A</sub>	Arrival time in seconds (s)
t <sub>R</sub>	Residence time in seconds (s)



## APPENDICES

---

UART	Universal asynchronous receiver-transmitter protocol
UI/UX	User interface/User experience
USB	Universal serial bus
UV	Ultraviolet
UV-Vis NIR	Ultraviolet- visible and near infrared
V	Voltage or volts in Volts (V), or volume in cubic metres (m <sup>3</sup> )
v	Velocity in metres per second (ms <sup>-1</sup> )
VC	Venture capitalist
V <sub>reactor</sub>	Reactor volume
W	Watts
WE	Working electrode or indicator electrode
wt	Weight
z	Charge number
Z	Electrical impedance in Ohms ( $\Omega$ )
$\kappa$	Conductivity in Siemens per meter (Sm <sup>-1</sup> )
$\Lambda_m$	Molar conductivity in Siemen metre squared per mole (Sm <sup>2</sup> mol <sup>-1</sup> )
$\rho$	Resistivity in Ohm-metres ( $\Omega\text{m}$ )
$\phi$	Potential drop

## Appendix 3. List of tables and figures

### *List of figures*

Figure 1.1 The branching out of sensors, biological (human) and synthetic.

Figure 1.2 Natural and synthetic electrochemical sensors; a nerve cell and a sodium-selective carbon fibre sensor (from [9]).

Figure 1.3 Advertisement from 1934 advertising the Cameron pH meter

Figure 1.4 The cycle of the design process, through iterations of analysis and synthesis (from [22])

Figure 1.5 Tools of the Maker. Left: An *Arduino Uno* microcontroller. Right: A 3D printer by *Makerbot*.

Table 2.1 Summary of electrochemical techniques used in the thesis and the associated electrical parameters

Figure 2.1 General set-up of a two-electrode conductimetric cell. An alternating voltage is applied across two platinum electrodes of area,  $A$ , separated by distance,  $l$ . By reading the voltage and current, the resistance can be determined.

Figure 2.2 A Wheatstone bridge (from [3])

Figure 2.3 A potentiometric cell

Figure 2.4 The potentials appearing between a reference electrode and a solid-state ion-selective electrode. In this example, the primary ion is positively charged. The phase-boundary potential is generated by the partitioning of this into the membrane, while the counter ion is excluded.

Figure 2.5 A: an ion-selective membrane without ions in solution. B: the ion-selective electrode membrane in contact with an aqueous solution containing a primary cation ( $J^+$ ) and counter anion ( $X^-$ ).

Figure 2.6 Representation of the Donnan equilibrium and the resulting Donnan potential generated across a semipermeable membrane. The red and green arrows represent the concentration gradients of the mobile cations and anions respectively.

Figure 2.7 The relationship between the Fermi level of a metal electrode and a single molecule in close proximity. For electron transfer to take place, the energy levels of an unoccupied molecular orbital (LUMO) would need to match the Fermi level of the metal electrode. Reproduced from [8].

Figure 2.8 Three generations of ion-selective electrodes. A: a glass membrane electrode; B: a liquid membrane ISE with inner solution; C: a solid-state ISE.

Figure 2.9 Valinomycin, the ionophore of the potassium ion. The cavity of electronegative groups optimally accommodates the potassium ion in terms of charge and ionic radius.

Figure 2.10 Reference electrodes. A: a double-junction Ag/AgCl type; B: a PBV-based Ag/AgCl type on paper; C: a PVC-based ionic liquid reference electrode on screen-printed substrate.

Figure 2.11 General setup of a flow injection analysis system. The letter D represents the detector.

## APPENDICES

---

Figure 2.12 Typical signal from flow injection analysis;  $h$  indicates peak height,  $t_A$  indicates arrival time,  $t_R$  indicates residence time.

Figure 2.13 Gold. Left: pieces of irregular size and mass. Right: the Egyptian gold Stater, perhaps the first fungible form of money.

Figure 3.1 The calix[4]pyrrole phosphonate used as ionophore for creatininium.

Figure 4.1 Major fields of application for distributed electrochemical sensors (DECSs) and the value they contribute to the field

Table 4.1 Commercialized devices for medically relevant analytes and their retail prices (Sources of prices listed are included in Appendix 4).

Figure 4.2 A: 'Sweatch' platform for sodium monitoring in sweat (from [36]) with horizontal arrangement of electronic and fluidic components consisting of 1: sweat harvesting device in 3d-printed platform base; 2: fluidic sensing chip, 3: electronic data logger and battery, and 4: 3D-printed upper casing. B: Ring-based potentiostat for threat detection (from [37]).

Figure 4.3 Decreasing size and cost of potentiostats (above) and pH electrodes (below)

Figure 4.4 A: Paper-based Li-ion battery (adapted from [69]). B: Epidermal biofuel cell for energy-harvesting from sweat (from [71]).

Figure 4.5 Timeline of major academic and commercial advances in electrochemical glucose sensors (References are included in Appendix 4).

Figure 4.6 Fully inkjet-printed paper-based potentiometric sensing device for sodium and potassium (from [90]).

Figure 5.1 Left: Cover of *Lab on a Chip* and; Right: the reality of a Lab on a Chip.

Figure 5.2 Cost-benefit analysis diagram for diagnostic sensors

Figure 5.3 Left: A schematic representation of the *Lab-in-a-box*. Right: an image of the *Lab-in-a-box* (L.I.B.) with the lid in place.

Figure 5.4 An exemplary range of the flow cells fabricated for and tested with glassy carbon and paper electrodes.

Figure 5.5 Instrumental response of the potassium-selective electrode in the *Mark I Lab-in-a-box* recorded during five consecutive determinations. The numbers indicate the logarithm of the three KCl concentrations.

Table 5.1 Sensitivities of the sensor and recoveries of a potassium solution determined on each of four consecutive days

Figure 5.6 The inside of the *Lab-in-a-box*. In this photograph, a miniature piezoelectric pump is being tested. Also, a paper-based working electrode is housed in a flow cell; the reference electrode is not shown in the image. Electronics are not visible as they are located underneath the microcontroller.

Figure 5.7 The pH breakout circuit board

Figure 5.8 Time trace of five consecutive determinations of potassium. Following an initial priming period of 90 s, the protocol selected the standard of low concentration, followed by the sample, before the standard of high concentration. Between determinations, the electrodes were washed with the blank carrier solution. Within the figure, C indicates the (blank) carrier solution, -5 indicates a standard of  $10^{-5}$  KCl, -2 indicates a standard of  $10^{-2}$  KCl, and S indicates the sample.

## APPENDICES

---

**Table 5.2** Figures of merit during five determinations of potassium in a urine sample (diluted 100x)

**Figure 5.9** The miniature peristaltic pump seen alone (left), and within the *Lab-in-a-box* (right).

**Figure 5.10** Junction potentials in a solid-contact ion-selective electrode

**Figure 5.11** The 60 minute calibration cycle repeated each hour. Times in which the pump was on are indicated by green, times in which the pump was off are indicated by red.

**Figure 5.12** Above: time trace recorded during 10 calibrations in 10 hours. Below: time trace of the first two calibrations.

**Figure 5.13** The relationship between baseline potential to standard potential during 54 hours. The dashed line passes through the point of calibration 3 and has a slope of 1. The establishing calibration at hour 3 is indicated by the black arrow. The numbers indicate the hours of calibration that were outliers to the trend.

**Figure 5.14** The  $E_{\text{diff}}$  (difference between  $E^0$  and  $E_{\text{baseline}}$ ) during 54 hours of measurements. The red line indicates the  $E_{\text{diff}}$  of the third calibration (314 mV). The inset highlights the reproducibility of the  $E_{\text{diff}}$  during hours 3 and 15.

**Figure 5.15** Accuracy of predictions of creatinine concentrations made during 54 hours. At each hour, three concentrations were tested and the accuracy of these was averaged; error bars represent one standard of deviation in the accuracy between these. The divergent accuracies of predictions when assuming the sensitivity and standard potential to be constant (black), or when predicted by the algorithm (red) are highlighted in the inset showing the first 10 hours.

**Table 5.3** The accuracies of prediction of creatinine concentration made with and without the algorithm

**Figure 5.16** The full setup of the *Lab-in-a-box*: Mark III. Fluidic system, potentiometric flow cell, microcontroller, tablet.

**Figure 5.17** Schematic representation of the Mark III *Lab-in-a-box*. S1 and S2 indicate two standard solutions. These, as well as the sample, are selectively pumped using hand-pumped dispensers through the 4-way junction point, through the flow cell, and finally collected in a waste receptacle. Check valves were located immediately before the entrance of the three input channels into the 4-way junction.

**Figure 5.18** Construction of a paper-based potassium selective potentiometric cell.

**Figure 5.19** The flow cell with four magnetic seals to sandwich a paper-based potentiometric cell between.

**Figure 5.20** The flow cell used in Mark III. Left: Open, with electrochemical cell removed. Right: Closed, with electrochemical cell inside.

**Figure 5.21** Left and center: The Mark III *Lab-in-a-Box*. Right: The *Yocto-milliVolt-Rx*.

**Figure 5.22** Calibration plot of the paper-based potassium-selective electrode (WE) and ionic liquid-based reference electrode (RE) in bulk against a common conventional reference electrode.

**Figure 5.23** Two-point calibration plot showing the reproducibility of the potentiometric cell within the flow cell. Error bars indicate one standard deviation of error between the 8 calibrations. Inset: the EMF recorded at each concentration during each of the 8 calibrations.

**Figure 5.24** Left: Time trace during the calibration of the sensor and determination of potassium in a wine sample. The three colours indicate the three stages of the analysis while the arrows indicate the time after pumping at

## APPENDICES

---

which steady-state values were considered. **Right:** Screen shot of the user-interface of the potassium sensing system during the analysis.

**Table 5.4** Key values in evaluating the recovery of potassium values in wine.

**Figure 5.25** Absorbance of light at 609 nm following the manual pumping of a blue dye (shown by blue markers), and distilled water (shown by red markers).

**Figure 6.1** Chemical structure of poly(vinyl alcohol) (PVA). The particular PVA used in this work had an average of:  $2023 < n < 2227$ .

**Figure 6.2** Graphical representation of the capping membrane concept. The electrodes of a solid-state potentiometric cell are covered and connected by overlaid membrane.

**Figure 6.3** Left: The ‘Sweatch’ platform for sodium monitoring in sweat (from [5]) with horizontal arrangement of electronic and fluidic components consisting of 1: sweat harvesting device in 3d-printed platform base; 2: fluidic sensing chip, 3: electronic data logger and battery, and 4: 3D-printed upper casing. Right: one of the screen-printed disposable potentiometric cells used in the *Sweatch* platform.

**Figure 6.4** Micrographs of the capping membrane. Left: over the electrodes. Center: after separation from the sensor. Right: capping membranes cast in water *without*  $MgCl_2$ .

**Figure 6.5** Construction of the potentiometric cell. The substrate was prepared with screen-printed electrodes, working and reference membranes were drop-cast, finally, a PVA capping membrane was applied.

**Figure 6.7** Time trace during five calibrations with NaCl from 0.1 to 100 mM NaCl. A point of 0.1 mM  $MgCl_2$  is recorded between each calibration.

**Figure 6.8** Plot of the relationship between baseline potential and standard potential for three sensors during five calibrations.

**Table 6.1** The four materials tested as capping membranes with their associated consistency and electrical impedance

**Figure 6.9** Complex impedance plot of the potentiometric cell with PVA capping membrane when dry (black markers) and when swelled with 0.1 M NaCl (red markers) (inset).

**Figure 6.10** Time trace during calibration of a capped sensor. The first 4.5 minutes while dry the sensor is dry are shown within the inset.

**Table 6.2** Sensitivity and standard potentials of six sodium sensors before and after capping with PVA

**Figure 6.11** Junction potentials appearing in the circuit of the potentiometric cell. Above: through aqueous electrolyte; Below: through PVA after a capping membrane has been applied. (RM = reference membrane: ISM = ion-selective membrane).

**Figure 6.12** Relationship between the dry potential and the standard potentials, before and after capping

**Figure 7.1** The creatinine molecule.

**Figure 7.3** Flow cells within the FIA system. A: detail of the flow cell. B: Flow cell with a single creatinine-selective membrane upon a glassy carbon electrode. Right: Flow cell with both potassium and creatinine-selective membranes upon copper wires.

**Figure 7.4** Schematic representation of the flow injection manifold.

## APPENDICES

---

**Figure 7.5** Percentage of creatinine in the protonated form (creatinium ion) as a function of pH as predicted by the Henderson-Hasselbach equation. The dashed green line indicates the  $pK_a$  of creatinine and the dashed red line indicates the working pH of the buffer.

**Figure 7.6** Calibration of the creatinine-selective electrode under flow conditions. Black: steady-state calibration. Red: flow injection calibration. Numbers indicate the logarithm of concentration.

**Figure 7.7** Calibration plots during injection of creatinine. Left: with conditioned standards. Right: with unconditioned standards. The numbers in the legend refer to flow rates, as measured in mL/minute.

**Table 7.1** Dispersion coefficients as a function of flow rate, separated into the effects of dilution and protonation. A high degree of protonation (as indicated by the green colour) is desirable, while a high degree of dilution (as indicated by the red colour) was undesirable.

**Figure 7.8** Calibration plots comparing the signals from steady-state signals during flow, with those generated by injections of 12, 22, 32 and 42  $\mu\text{L}$ . Left: injections of conditioned samples (Cond). Right: injection of unconditioned samples (Uncond). The numbers in the legends indicate the sample volumes.

**Figure 7.9** Calibration plots of conditioned (Cond) and unconditioned (Uncond) creatinine standards injected into the flow system. The numbers in the legend indicate the flow rate (mL/minute). The steady-state calibration under flow is also shown.

**Figure 7.10** Typical time trace during flow injection as detected by the creatinine ISE. The baseline is seen to rise above the initial level (indicated by the dashed line) and not recover.

**Figure 7.11** Normalised signals from both optical and potentiometric detection of creatinine (CRT) injected into the flow system.

**Figure 7.12** Superimposed peak profiles tracking injection of 1 mM of potassium and creatinine, as detected by a  $K^+$ -ISE and a creatinine-ISE. Profiles were normalized and the baselines aligned. (CRT indicates creatinine: CBN indicates calibration).

**Figure 7.13** The relationship of peak width to peak height for the creatinine and potassium selective systems in response to their primary analytes (creatinine (CRT) and potassium respectively).

**Figure 7.14** Time trace during calibration of a *blank* electrode with creatinine. The dashed line offers a guide as to the shifting of the baseline potential.

**Figure 7.15** Time trace during injection of creatinine and potassium standards, as well as 20 samples. In each calibration, the peaks sequentially increase as they represent concentrations of  $10^{-3.5}$ ,  $10^{-3}$ ,  $10^{-2.5}$ ,  $10^{-2}$ ,  $10^{-1.5}$ ,  $10^{-1}$  M.

**Figure 7.16** Plot of the creatinine-ISEs response to three injected solutions: KCl, creatinine (CRT), and both KCl and CRT together.

**Figure 7.17** Comparison between creatinine values in urine determined by the reference Jaffe method and those using the described FIA system. The line indicates a line of best fit for 13 of the samples (the 7 outliers were omitted in fitting this line).

**Figure 7.18** Comparison of the creatinine levels determined by FIA with the values of creatinine from the reference method as well as potassium and sodium levels.

**Figure 8.1** Two styles of ancient Clepsydrae (water clocks)

**Figure 8.2** Schematic representation of the Smart Toilet shown in section view. Left: full device. Right: detail of the funnel.

## APPENDICES

---

**Figure 8.3** Plot of the conductivity readings ( $\kappa$ ) of 19 urine samples validated against the readings of a commercial conductivity meter

**Figure 8.4** The Smart Toilet installed with tablet computer connected and mounted to the wall

**Figure 9.1** Illustration of the elements comprising the IonSens device. A Nafion membrane (A) and reference membrane (B) were drop-cast over carbon paper (C) and Ag/AgCl paper (D) respectively. These papers were protected by a mask (E).

**Figure 9.2** Time trace (left)) and calibration plot (right) comparing response of working electrodes based on carbon, gold and platinum papers.

**Table 9.1** Comparison of key analytical parameters between the three substrates ( $N = 3$ ).

**Figure 9.3** Ion-exchange between the solution and Nafion interface between cations,  $M^+$ , with sulfonate groups immobilized within the Nafion.

**Figure 9.4** Comparison of the working electrode's response to a series of monocations. Left: sensitivities to each cation. Right: standard potentials to each cation.

**Table 9.2** Potentiometric selectivity coefficients approximated from a separate solution method treatment of parallel calibrations of each electrolyte.

**Table 9.3** Typical sweat constitution components on the scapula [43]

**Figure 9.5** Plot validating the relationship of EMF to the logarithm of conductivity in a series of dilutions of artificial sweat. The inset is a photograph of the Ions cell.

**Figure 9.6 A:** time traces of two IonSens cells (labelled 1 and 2). Grey background indicates a calibration with artificial sweat, white background indicates a sweat sample. 'AS' indicates artificial sweat, '0.1 AS' indicates artificial sweat diluted 10x, 'M' indicates the signal maxima, 'S' indicates the signal at steady-state. The noise seen at times 15 minutes, 21 minutes, 35 minutes and 45 minutes are due to the sensor being momentarily dry between changes of solution. **B:** validation of conductivity determinations by IonSens in real sweat samples against those made by a commercial conductivity meter.

**Figure 9.7** Plot of conductivity values generated by the on-body IonSens device during 35 minutes of exercise. Subsequent on-bench measurements were made at five minute intervals and the values are superimposed at the corresponding times.

## APPENDICES

---

### *List of tables*

**Table 2.1 Summary of electrochemical techniques used in the thesis and the associated electrical parameters**

**Table 4.1 Commercialized devices for medically relevant analytes and their retail prices (Sources of prices listed are included in Appendix 4).**

**Table 5.1 Sensitivities of the sensor and recoveries of a potassium solution determined on each of four consecutive days**

**Table 5.2 Figures of merit during five determinations of potassium in a urine sample (diluted 100x)**

**Table 5.3 The accuracies of prediction of creatinine concentration made with and without the algorithm**

**Table 5.4 Key values in evaluating the recovery of potassium values in wine.**

**Table 6.1 The four materials tested as capping membranes with their associated consistency and electrical impedance**

**Table 6.2 Sensitivity and standard potentials of six sodium sensors before and after capping with PVA**

**Table 7.1 Dispersion coefficients as a function of flow rate, separated into the effects of dilution and protonation. A high degree of protonation (as indicated by the green colour) is desirable, while a high degree of dilution (as indicated by the red colour) was undesirable.**

**Table 9.1 Comparison of key analytical parameters between the three substrates (N = 3).**

**Table 9.2 Potentiometric selectivity coefficients approximated from a separate solution method treatment of parallel calibrations of each electrolyte.**

**Table 9.3 Typical sweat constitution components on the scapula [43]**

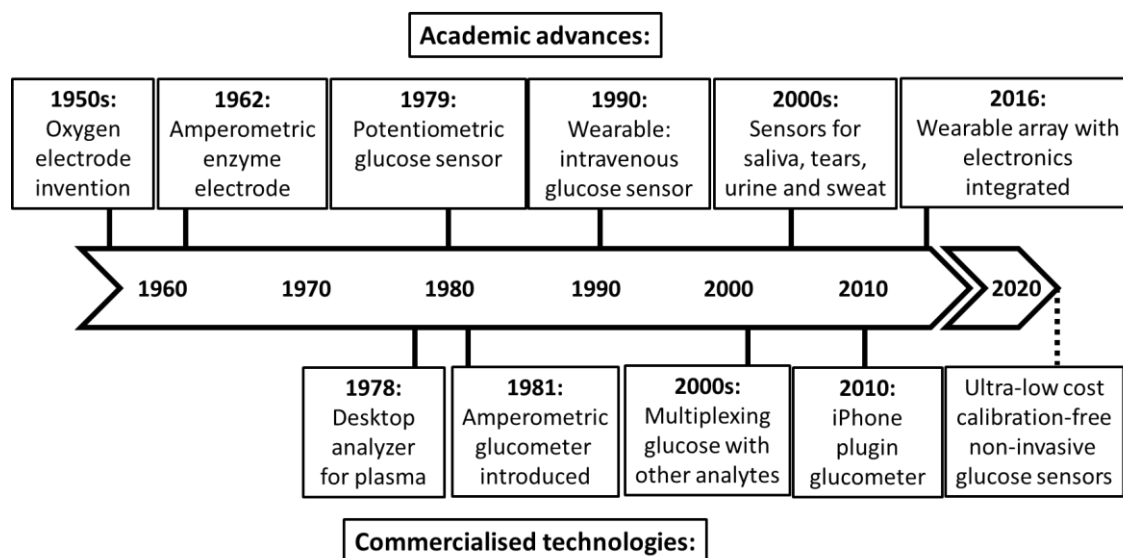


## APPENDICES

### Appendix 4. Supporting information for Chapter 4

Table of commercially available devices, the analytes they measure, and their prices. The sources for the prices are provided in the references.

Analyte	Device name	Device price	Price per test strip
Glucose	Contour Next	\$14.75	\$0.69[1]
Lactic acid	Lactate scout	\$350[2]	\$2.42[2]
Glucose, Cholesterol, Uric Acid, Haemoglobin	EasyTouch GCHb Multi Function Monitoring System	\$53.50[3]	\$0.16[4] glucose \$2.15[5] cholesterol \$0.64[6] uric acid \$0.58[7] haemoglobin
Glucose, beta ketone	Bruno Pharma Innovations MD6	\$97.99[8]	\$3.00[9] ketone \$0.60[10] glucose
Creatinine	Statsensor Analyzer XPress	\$756.04[11]	\$5.70[11]



Timeline of advances for the glucometer. References are included. 1962 amperometric enzyme electrode[12]; 1978 desktop analyser for plasma[13]; 1979 potentiometric enzyme electrode[14]; 1981 amperometric glucometer[15]; 1990 wearable intravenous glucose sensor[16], 2000s multiplexing glucose with other analytes (see Table ); 2000s sensors for saliva, tears, urine and sweat[17]; 2010 iPhone plugin glucometer[18]; 2016 wearable array with electronics integrated[19].

#### References:

## APPENDICES

---

- 1 Contour Next Test Strips Sensors (Pack of 50 Pack: 8884487: Amazon.de: Drogerie & Körperpflege, [https://www.amazon.de/Contour-Next-Sensoren-Stück-Pack/dp/B00E6722OK/ref=pd\\_bxgy\\_121\\_img\\_2?\\_encoding=UTF8&psc=1&refRID=WFEQ3D18ZPD4FPH075](https://www.amazon.de/Contour-Next-Sensoren-Stück-Pack/dp/B00E6722OK/ref=pd_bxgy_121_img_2?_encoding=UTF8&psc=1&refRID=WFEQ3D18ZPD4FPH075), (accessed 19 December 2017).
- 2 Lactate scout portable lactate test analyzer, pricing Information, [http://www.lactate.com/lr\\_prices.html](http://www.lactate.com/lr_prices.html), (accessed 7 December 2017).
- 3 EasyTouch Glucose Cholesterol Uric Acid Hemoglobin Blood Test Strips 28 G Lancet | eBay, <https://www.ebay.com/itm/EasyTouch-Glucose-Cholesterol-Uric-Acid-Hemoglobin-Blood-Test-Strips-28-G-Lancet/122806626206?hash=item1c97d8679e:g:beEAAOSwDiBZEUmM>, (accessed 7 December 2017).
- 4 Easy Touch Blood Glucose Test Strips 150 Count, Exp: 12/2017 | eBay, [https://www.ebay.com/itm/Easy-Touch-Blood-Glucose-Test-Strips-150-Count-Exp-12-2017/282165907401?\\_trkparms=aid%3D888007%26algo%3DDISC.MBE%26ao%3D1%26asc%3D41375%26meid%3D07f5eabcd84f4543bd0ceeb4b691e320%26pid%3D100009%26rk%3D1%26rkt%3D1%26sd%3D28261031100](https://www.ebay.com/itm/Easy-Touch-Blood-Glucose-Test-Strips-150-Count-Exp-12-2017/282165907401?_trkparms=aid%3D888007%26algo%3DDISC.MBE%26ao%3D1%26asc%3D41375%26meid%3D07f5eabcd84f4543bd0ceeb4b691e320%26pid%3D100009%26rk%3D1%26rkt%3D1%26sd%3D28261031100), (accessed 7 December 2017).
- 5 1 box (10 Strips) Blood Cholesterol Test Strips Easy Touch Easytouch EasyLife a | eBay, <https://www.ebay.com/itm/1-box-10-Strips-Blood-Cholesterol-Test-Strips-Easy-Touch-Easytouch-EasyLife-a/222744680020?hash=item33dc9e1654:g:VkQAAOSwHUhZ~RHs>, (accessed 7 December 2017).
- 6 25 Test Strips Easy Touch Easytouch Uric Acid Monitor Control Check Meter | eBay, [https://www.ebay.com/itm/25-Test-Strips-Easy-Touch-Easytouch-Uric-Acid-Monitor-Control-Check-Meter/282610311000?\\_trkparms=aid%3D888007%26algo%3DDISC.MBE%26ao%3D1%26asc%3D41375%26meid%3D685be7995da54ebdae084ae5f9de72cf%26pid%3D100009%26rk%3D1%26rkt%3D1%26s](https://www.ebay.com/itm/25-Test-Strips-Easy-Touch-Easytouch-Uric-Acid-Monitor-Control-Check-Meter/282610311000?_trkparms=aid%3D888007%26algo%3DDISC.MBE%26ao%3D1%26asc%3D41375%26meid%3D685be7995da54ebdae084ae5f9de72cf%26pid%3D100009%26rk%3D1%26rkt%3D1%26s), (accessed 7 December 2017).
- 7 EasyTouch Easy Touch Blood Hemoglobin (Hb) 25 Test Strips (1 Box) NEW | eBay, <https://www.ebay.com/itm/EasyTouch-Easy-Touch-Blood-Hemoglobin-Hb-25-Test-Strips-1-Box-NEW/192375043330?hash=item2cca723502:g:04QAAOSwB3BaB~Ey>, (accessed 7 December 2017).
- 8 Amazon.com: Blood Ketone Monitoring System | Track Your Ketones and Ketogenic Diet Progress | Ketosis Test Kit with Lancing Device, 10 Blood Glucose Test Strips, 10 Keto Strips + 50 Lancets by Bruno Pharma MD6: Health & Personal Care, [https://www.amazon.com/Monitoring-Ketogenic-Progress-Bruno-MD6/dp/B075DGTJCD/ref=pd\\_lpo\\_sbs\\_121\\_t\\_0?\\_encoding=UTF8&refRID=TEC1Y8WX97SJJJK3FVE4&th=1](https://www.amazon.com/Monitoring-Ketogenic-Progress-Bruno-MD6/dp/B075DGTJCD/ref=pd_lpo_sbs_121_t_0?_encoding=UTF8&refRID=TEC1Y8WX97SJJJK3FVE4&th=1), (accessed 7 December 2017).
- 9 Amazon.com: Bruno Pharma MD6 2 Boxes of 10 Ketone Test Strips to Use With Our MD6 Blood Monitoring System | Stay in Ketosis and Get the Best Results with Accurate Keto Counts While Following the Ketogenic Diet: Health & Personal Care, [https://www.amazon.com/Bruno-MD6-Monitoring-Following-Ketogenic/dp/B075F8QBFH/ref=pd\\_bxgy\\_121\\_img\\_2?\\_encoding=UTF8&pd\\_rd\\_i=B075F8QBFH&pd\\_rd\\_r=WNWCA7N1VE4BF0B6P7VP&pd\\_rd\\_w=YaFPs&pd\\_rd\\_wg=fvTH0&refRID=WNWCA7N1VE4BF0B6P7VP&th=1](https://www.amazon.com/Bruno-MD6-Monitoring-Following-Ketogenic/dp/B075F8QBFH/ref=pd_bxgy_121_img_2?_encoding=UTF8&pd_rd_i=B075F8QBFH&pd_rd_r=WNWCA7N1VE4BF0B6P7VP&pd_rd_w=YaFPs&pd_rd_wg=fvTH0&refRID=WNWCA7N1VE4BF0B6P7VP&th=1), (accessed 7 December 2017).

## APPENDICES

---

- 10 Amazon.com: Bruno Pharma MD6 Blood Glucose Test Strips (100 Count) | Fast Absorption and Accurate Results in 5 Seconds with 5-Electrode Technology | Diabetic Blood Sugar Testing Strips for MD6 Diabetes Monitor: Health & Personal Care, [https://www.amazon.com/Bruno-MD6-Absorption-5-Electrode-Technology/dp/B0711YQ9ML/ref=pd\\_bxgy\\_121\\_img\\_3?\\_encoding=UTF8&pd\\_rd\\_i=B0711YQ9ML&pd\\_rd\\_r=0D8HBMM5BPHW527FJ2FV&pd\\_rd\\_w=bUDwj&pd\\_rd\\_wg=u8Sjr&refRID=0D8HBMM5BPHW527FJ2FV&th=1](https://www.amazon.com/Bruno-MD6-Absorption-5-Electrode-Technology/dp/B0711YQ9ML/ref=pd_bxgy_121_img_3?_encoding=UTF8&pd_rd_i=B0711YQ9ML&pd_rd_r=0D8HBMM5BPHW527FJ2FV&pd_rd_w=bUDwj&pd_rd_wg=u8Sjr&refRID=0D8HBMM5BPHW527FJ2FV&th=1), (accessed 7 December 2017).
- 11 Portable Creatinine Handheld Analyzer, <https://www.cliawaived.com/cf.inventory.htm?action=showinvone&invid=3254&head=Portable+Creatinine+Handheld+Analyzer&key=Portable+Creatinine+Handheld+AnalyzerPortable+Creatinine+Handheld+Analyzer&desc=The+CardioChek+Silver+PA+Analyzer+is+portable+handheld+>, (accessed 7 December 2017).
- 12 L. C. Clark and C. Lyons, Electrode systems for continuous monitoring in cardiovascular surgery, *Ann. N. Y. Acad. Sci.*, 1962, **102**, 29–45.
- 13 K. S. Chua and I. K. Tan, Plasma glucose measurements with the Yellow Springs Glucose Analyzer, *Clin. Chem.*, 1978, **24**, 150–152.
- 14 L. B. Wingard, J. G. Schiller, S. K. Wolfson, C. C. Liu, A. L. Drash and S. J. Yao, Immobilized enzyme electrodes for the potentiometric measurement of glucose concentration: Immobilization techniques and materials, *J. Biomed. Mater. Res.*, 1979, **13**, 921–935.
- 15 Unknown, *Pittsburgh Press*, 1981, 6.
- 16 K. L. Zamzow, D. G. Schmidt, M. C. Shults, S. J. Updike, R. K. Rhodes, D. F. von Heimburg and J. O. Luebow, Development and evaluation of a wearable blood glucose monitor, *ASAIOTrans*, 1990, **36**, M588-91.
- 17 D. Bruen, C. Delaney, L. Florea and D. Diamond, Glucose sensing for diabetes monitoring: Recent developments, *Sensors*, 2017, **17**, 1–21.
- 18 A. Tenderich, Sanofi Launches First iPhone Plug-In Glucose Meter, <https://www.healthline.com/diabetesmine/newsflash-sanofi-aventis-launches-ibgstar-plug-in-glucose-meter-for-the-iphone>, (accessed 18 December 2017).
- 19 W. Gao, S. Emaminejad, H. Y. Y. Nyein, S. Challa, K. Chen, A. Peck, H. M. Fahad, H. Ota, H. Shiraki, D. Kiriya, D.-H. Lien, G. A. Brooks, R. W. Davis and A. Javey, Fully integrated wearable sensor arrays for multiplexed in situ perspiration analysis, *Nature*, 2016, **529**, 509–514.

## APPENDICES

### Appendix 5. Supporting information for Chapter 5

The accuracies of prediction of creatinine concentration made with and without the prediction algorithm described in section 5.3.4.3.

Hour	Accuracy of prediction (without algorithm)	Accuracy of prediction (with algorithm)
3	101.7 ± 3.0	101.4 ± 3.0
4	112.2 ± 5.3	102.7 ± 4.9
5	120.0 ± 5.8	100.5 ± 4.9
6	132.7 ± 5.5	100.6 ± 4.1
7	140.4 ± 6.3	100.7 ± 4.5
8	149.47 ± 7.0	100.9 ± 4.7
9	158.3 ± 6.4	102.1 ± 4.1
10	167.8 ± 6.3	104.3 ± 3.9
15	198.1 ± 11.4	99.0 ± 5.7
16	216.0 ± 46.5	93.2 ± 20.0
17	226.8 ± 14.4	94.5 ± 6.0
18	240.5 ± 23.7	106.9 ± 10.4
19	196.6 ± 37.2	90.8 ± 17.1
20	166.5 ± 12.1	82.0 ± 5.9
48	133.6 ± 8.4	84.8 ± 5.4
49	124.8 ± 5.6	77.9 ± 3.4
50	120.5 ± 4.6	85.9 ± 3.2
51	122.4 ± 5.5	85.5 ± 3.8
52	127.0 ± 8.8	83.1 ± 5.7
53	131.1 ± 5.8	83.7 ± 3.7
54	138.7 ± 5.8	83.8 ± 3.5

**APPENDICES**

**Appendix 6. Supporting information for Chapter 8**

**Results of automated analyses using the Smart Toilet for 1 month:**

<b>Date</b>	<b>Conductivity- Crison (mS/cm at 25 C)</b>	<b>Conductivity- Smart Toilet (mS/cm at 25 C)</b>	<b>Conductivity- Smart Toilet (mS/cm at 25 C) (matrix corrected)</b>	<b>Recovery (%)</b>
29/11/2017	20.90	26.73	21.43	102.55
30/11/2017	19.36	23.78	19.07	98.49
01/12/2017	14.13	19.45	15.59	110.37
	20.30	30.14	24.17	
04/12/2017	10.16	13.08	10.49	103.22
05/12/2017	4.55	5.69	4.56	100.27
06/12/2017				
07/12/2017	8.20	10.53	8.44	102.96
08/12/2017	14.92	19.60	15.72	105.33
09/12/2017	5.20	6.75	5.41	104.08
10/12/2017				
11/12/2017	25.00	36.00	28.86	115.46
12/12/2017	17.61	23.55	18.88	107.22
13/12/2017	13.28	17.33	13.90	104.63
14/12/2017	12.30	12.75	10.22	83.11
15/12/2017	15.02	19.91	15.96	106.28
16/12/2017	25.50	35.25	28.26	110.84
17/12/2017	26.60	37.55	30.11	113.19
18/12/2017	9.44	11.95	9.58	101.50
19/12/2017	9.62	12.03	9.65	100.27
20/12/2017	16.01	20.66	16.57	103.47
21/12/2017	25.60	31.10	24.94	97.41
22/12/2017	12.89	16.04	12.86	99.77
			Average	103.52
			Standard deviation	6.81

## APPENDICES

---

### Arduino code:

//The following sketch was used within the Arduino IDE in an .ino file:

```
float f_ec = 0.00;
boolean Flow = false;
boolean PreviousFlow = false;
unsigned long StartTime = 0;
unsigned long EndTime = 0;
unsigned long TotalTime = 0;
unsigned long TotalSeconds = 0;
int Volume = 0;
float Conductivity = 0;

extern volatile unsigned long timer0_millis;

// Variables for measure array
const int numReadings = 120;
float readValues[numReadings] = {0};
unsigned int i = 0;
int maxIndex = 0;

#include <SoftwareSerial.h>           //we have to include the SoftwareSerial library, or else we can't
use it
#define rx 2                         //define what pin rx is going to be
#define tx 3                         //define what pin tx is going to be

SoftwareSerial myserial(rx, tx);     //define how the soft serial port is going to work

String inputstring = "";             //a string to hold incoming data from the PC
String sensorstring = "";           //a string to hold the data from the Atlas Scientific product
boolean input_string_complete = false; //have we received all the data from the PC
boolean sensor_string_complete = false; //have we received all the data from the Atlas Scientific
product

void setup() {                       //set up the hardware
  Serial.begin(9600);                //set baud rate for the hardware serial port_0 to 9600
```

## APPENDICES

---

```
myserial.begin(9600);           //set baud rate for the software serial port to 9600
inputstring.reserve(10);       //set aside some bytes for receiving data from the PC
sensorstring.reserve(30);      //set aside some bytes for receiving data from Atlas Scientific
product
Serial.println("Smart Toilet");
}

void serialEvent() {           //if the hardware serial port_0 receives a char
  inputstring = Serial.readStringUntil(13); //read the string until we see a <CR>
  input_string_complete = true; //set the flag used to tell if we have received a completed string
  from the PC
}

void loop() {                  //here we go...

  if (input_string_complete) { //if a string from the PC has been received in its entirety
    myserial.print(inputstring); //send that string to the Atlas Scientific product
    myserial.print('\r'); //add a <CR> to the end of the string
    inputstring = ""; //clear the string
    input_string_complete = false; //reset the flag used to tell if we have received a completed string
    from the PC
  }

  if (myserial.available() > 0) { //if we see that the Atlas Scientific product has sent a character
    char inchar = (char)myserial.read(); //get the char we just received
    sensorstring += inchar; //add the char to the var called sensorstring
    if (inchar == '\r') { //if the incoming character is a <CR>
      sensor_string_complete = true; //set the flag
    }
  }
}

if (sensor_string_complete == true) { //if a string from the Atlas Scientific product has been received
  in its entirety
  if (isdigit(sensorstring[0]) == false) { //if the first character in the string is NOT a digit
    Serial.println(sensorstring); //send that string to the PC's serial monitor
  }
}
else //if the first character in the string is a digit
```

## APPENDICES

---

```
{

    print_EC_data();                // Read conductivity to f_ec (float)
    //Serial.println(f_ec);

    checkFlow();                    // Check if conductivity >2000

    // Sensor flow options: Flow and PreviousFlow keep tracking of conductivity treshold,
    // 1000 in this case. When:
    // current measure < 1000 and last measure < 1000 -> Waiting (Flow= false, PreviousFlow = false)
    // current measure > 1000 and last measure < 1000 -> Start measure (Flow=true, PreviousFlow = false)
    The sensor measure cross up the treshold
    // current measure > 1000 and last measure > 1000 -> Keep recording measures (Flow = true, PreviousFlow
    = true)
    // current measure < 1000 and last measure > 1000 -> Stop measure (Flow = false, PreviousFlow = true)
    The sensor measure cross down the treshold.

    if (Flow == true && PreviousFlow == false){
        // Starts measurement
        //Serial.println("Start measurement...");

        startCronometer();
        readOneMeasure();
        PreviousFlow = true;
    }

    if (Flow == true && PreviousFlow == true && i<numReadings){
        // Keep recording measurements
        // Serial.println("Recording data...");
        readOneMeasure();
    }

    if ((Flow == false && PreviousFlow == true) || (i>=numReadings)){
        // Stop measurement
        //Serial.println("Stop recording...");
        //Serial.println(" ");

        stopCronometer();
    }
}
```



## APPENDICES

---

```
// Look for index of max in Array measures
maxIndex = getIndexOfMaximumValue(readValues, numReadings);

Serial.print("Conductivity = ");
Serial.print(readValues[maxIndex]/1000);
Serial.println(" mS/cm at 25 C");

// Estimate Volume from measure time
checkTimeVolume();

Serial.print("Volume = ");
Serial.print(Volume);
Serial.println(" mL");

// DEBUG print all reading measures
Serial.println(" ");
//Serial.println("Array of values");
printReadings();
// Serial.println(" ");

// Clear array buffer and reset i index
memset(readValues,0,sizeof(readValues));
i = 0;

// Reset PreviousFlow
PreviousFlow = false;
}
if (Flow == false && PreviousFlow == false){
// Serial.println("Waiting...");
}
}

sensorstring = ""; //clear the string
sensor_string_complete = false; //reset the flag used to tell if we have received a completed string
from the Atlas Scientific product
}
}

// DEBUG Function to print the readValues data
```

## APPENDICES

---

```
void printReadings(){
    // Print the array content
    for (i = 0; i < numReadings; i++)
    {
        // Serial.print(readValues[i]);
        // Serial.print(", ");
    }
}

// Function to returning max value from array
// http://forum.arduino.cc/index.php?topic=41999.0
int getIndexofMaximumValue(float* array, int size) {
    int maxIndex = 0;
    float max = array[maxIndex];
    for (int j=1; j<size; j++){
        if (max<array[j]){
            max = array[j];
            maxIndex = j;
        }
    }
    return maxIndex;
}

// Read one measure and store in array readValues
void readOneMeasure(void){
    readValues[i]=f_ec;
    i = i + 1;
}

// Function to check flow
void checkFlow(void) {
    if (f_ec >= 2000) { //conductivity limit of boolean reading is 2000 uS/cm
        Flow = true;
    }
    else { Flow = false;
    }
}

void print_EC_data(void) { //this function will pars the string
```

## APPENDICES

---

```
char sensorstring_array[30];           //we make a char array
char *EC;                             //char pointer used in string parsing
char *TDS;                             //char pointer used in string parsing
char *SAL;                             //char pointer used in string parsing
char *GRAV;                            //char pointer used in string parsing
// float f_ec;                        //used to hold a floating point number that is the EC

sensorstring.toCharArray(sensorstring_array, 30); //convert the string to a char array
EC = strtok(sensorstring_array, ",");         //let's pars the array at each comma

TDS = strtok(NULL, ",");                   //let's pars the array at each comma
SAL = strtok(NULL, ",");                   //let's pars the array at each comma
GRAV = strtok(NULL, ",");                  //let's pars the array at each comma

f_ec = atof(EC);                          //uncomment this line to convert the char to a float

}

// Function to start the time recording
void startCronometer(void){
    noInterrupts (); // RESET MILLIS HACK IN THESE 3 LINES
    timer0_millis = 0;
    interrupts ();
    StartTime = millis();
}

// Function to stop the time recording
void stopCronometer(void){
    EndTime = millis();
    timer0_millis = 0;
    TotalTime = EndTime-StartTime;

    // Serial.print("Total time [s]: ");
    // Serial.println(TotalTime/1000);
}

// Funtion: Volume is estimated from total measure time
```

---

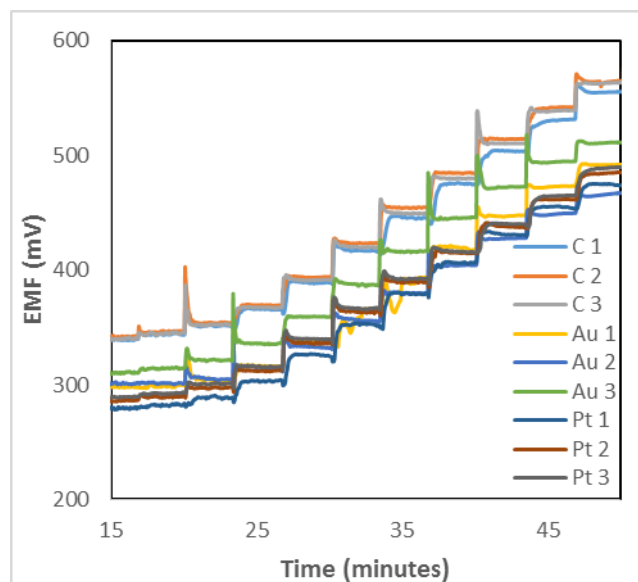
## APPENDICES

---

```
void checkTimeVolume(void){  
    if (TotalTime < 8000) {  
        Serial.println("Insufficient Volume");  
    }  
    else if (TotalTime>=8000 && TotalTime<=20900) {  
        Volume = 0.0057892 * TotalTime - 22.236;  
    }  
    else {  
        Volume = 0.0057831 * TotalTime -8.4357;  
    }  
}
```

## Appendix 7. Supporting information for Chapter 9

Carbon, gold and platinum coated papers were calibrated in triplicate. For clarity, only one of each time trace was included in Chapter 9. For completeness, all nine are included here.



Time traces of the three electrode substrates measured in triplicate

The study of reproducibility and reusability was made by calibrating five electrodes three times in succession and washing the membranes with Milli-Q water in between. The figures of merit for this are shown in the following table.

Figures of merit pertaining to three successive calibrations with NaCl against a conventional reference electrode

Calibration	1	2	3
<b>Sensitivity (mV/dec.[NaCl])</b>	56.3 ± 1.0	54.6 ± 0.8	53.4 ± 0.5
<b>Standard potential (mV)</b>	602.2 ± 5.3	604.4 ± 4.1	610.3 ± 4.4
<b>Linear range (mM)</b> (was not tested above 100 mM)	0.1 to 100	0.1 to 100	0.1 to 100
<b>Limit of detection (µmol)</b>	42.5 ± 3.4	42.5 ± 3.4	48.6 ± 4.0
<b>Maximum response time (s)</b>		42	

The conductivities measured by IonSens and by the Crison instrument are shown in the table below with the calculated recoveries and pH values included.

## APPENDICES

### Summary of data collected from eleven athletes sweat

Sample	pH	Conductivity - Crison (mS/cm at 25 °C)	Conductivity – IonSens (mS/cm at 25 °C)	Recovery (%)	n
1	7.22	47.70	49.42 ± 1.74	103.61	2
2	6.10	14.24	13.36 ± 2.06	93.84	3
3	5.98	15.01	14.22 ± 3.03	94.76	3
4	5.72	20.50	19.29 ± 0.82	94.08	3
5	7.17	32.20	29.56 ± 2.36	91.79	3
6	8.29	15.01	12.47 ± 0.97	83.08	3
7	4.94	11.93	12.18 ± 0.36	102.09	3
8	8.08	10.96	11.20 ± 3.21	102.23	3
9	8.48	30.20	27.71 ± 4.59	91.75	3
10	7.59	7.00	7.14 ± 0.33	101.98	3
11	8.18	27.40	24.19 ± 0.48	88.30	3
			Average	95.22 ± 6.60	

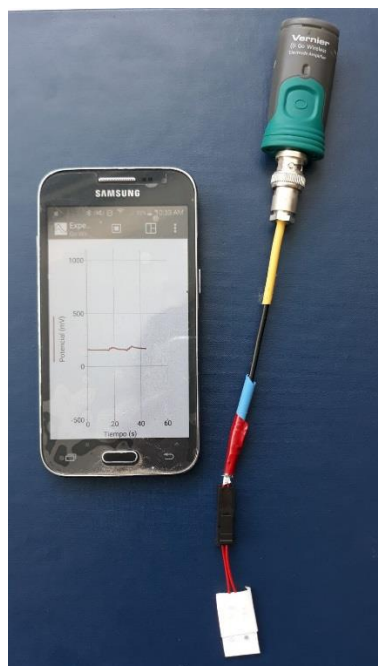


Photo of the full system for measurements: The Vernier Bluetooth potentiometer, an electrical cable, and the sensor. Also shown, the mobile phone with Vernier app used for recording data.

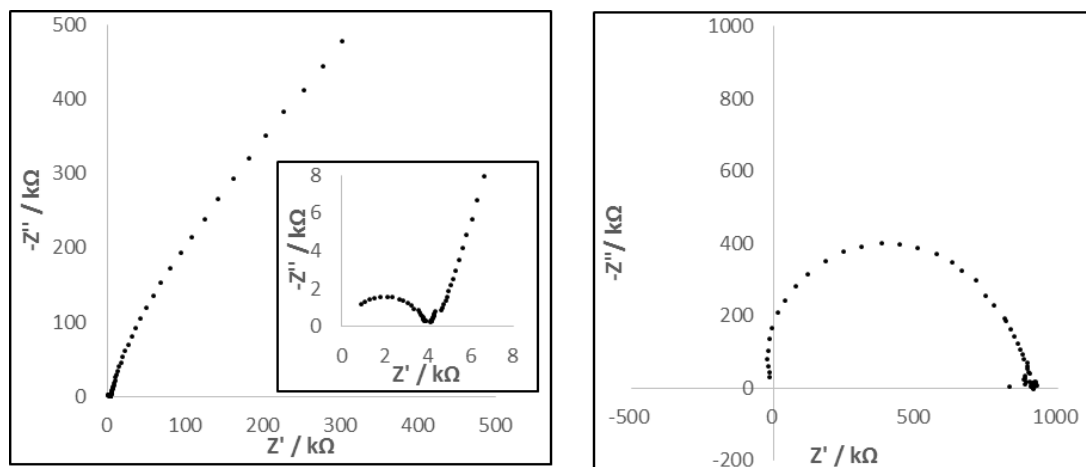
### Impedances of membranes

The working electrode as prepared (Nafion membrane on carbon ink paper) was found to have an impedance of approximately 4 k $\Omega$  (shown in the plot below). The pseudo-reference electrode as prepared was found to have an impedance of approximately 900 k $\Omega$ . By contrast, a typical PVC membrane on a glassy carbon

## APPENDICES

---

electrode has an impedance of a several M $\Omega$ . The difference is therefore some three orders of magnitude for the working electrode and one order of magnitude for the pseudo- reference electrode.



**Warburg plots of impedance. Left: measured across the working electrode (Nafion membrane upon carbon-ink coated paper). Right: measured across the pseudo-reference electrode**







